University of Southampton

Faculty of Engineering and Physical Sciences

School of Physics and Astronomy

Phenomenology of Unification-Inspired Theories of Physics Beyond the Standard Model

by

Samuel J. Rowley

Thesis for the degree of Doctor of Philosophy

October 2020

University of Southampton

Abstract

Faculty of Engineering and Physical Sciences
School of Physics and Astronomy

Thesis for the degree of Doctor of Philosophy

Phenomenology of Unification-Inspired Theories of Physics Beyond the Standard
Model
by Samuel J. Rowley

Phenomenology is a critical part of modern fundamental physics, and rigorous statistical methods are employed to ascertain the degree to which existing theories and new paradigms accurately describe nature. A collection of phenomenological analyses is presented that test novel extensions of the Standard Model inspired by unification against the latest experimental results.

We fit a minimal model of neutrino physics that employs a Type-I seesaw mechanism against data from neutrino experiments and the baryon asymmetry of the universe, with a focus on renormalisation group evolution. Such a model is an excellent fit to data, with particular combinations of numerical parameters yielding a $\chi^2 \simeq 1.5 - 2.6$ for three degrees of freedom. Through this analysis, we find that N_1-dominated leptogenesis can explain the asymmetry, which imposes strict constraints on right-handed neutrino masses. Results presented enable the Littlest Seesaw model to be tested against upcoming neutrino experiments.

We study CP-conserving non-minimal flavour violation in an $A_4 \times SU(5)$ supersymmetric grand unified theory and find that unification at high scales implies interesting correlations between flavour violating parameters across a variety of scales. By scanning over flavour violating parameters, constrained by low energy quark and lepton flavour data, we find a striking difference between results in which individual parameters are tested in isolation and those where multiple parameters are varied simultaneously.

Finally, we investigate a model with vector-like fermions and a $U(1)'$ gauge symmetry in the context of lepton flavour observables. Contributions to electron and muon anomalous magnetic moments due to Z' exchange are presented and discussed. Using analytic and numerical arguments, it is shown that such a model can explain the muon magnetic moment throughout a significant portion of the parameter space while remaining consistent with the experimental constraints from lepton flavour violating decays and neutrino trident production.

Contents

List of Figures

List of Tables

Declaration of Authorship

I, **Samuel J. Rowley**, declare that the thesis, entitled *Phenomenology of Unification-Inspired Theories of Physics Beyond the Standard Model*, and the work presented in it are both my own and have been generated by me as the result of my own original research.

I confirm that:

1. This work was done wholly or mainly while in candidature for a research degree at this University;

2. Where any part of this thesis has previously been submitted for a degree or any other qualification at this University or any other institution, this has been clearly stated;

3. Where I have consulted the published work of others, this is always clearly attributed;

4. Where I have quoted from the work of others, the source is always given. With the exception of such quotations, this thesis is entirely my own work;

5. I have acknowledged all main sources of help;

6. Where the thesis is based on work done by myself jointly with others, I have made clear exactly what was done by others and what I have contributed myself;

7. Parts of this work have been published as references [1–3].

Signed:

Date:

x

For my parents,
each success begins with you

Acknowledgements

First and foremost, I would like to thank my supervisor Steve King for his guidance and advice over the past four years. The many discussions we shared gave new meaning to our research, and my understanding of physics would not be nearly so deep without him. I am also very thankful to my collaborators; Jordan Bernigaud, Antonio Cárcamo Hernández, Adam Forster, Björn Herrmann, Simon King, Huchan Lee, Stefano Moretti, Werner Porod and Susana Molina Sedgwick for everything I have learned from them over the course of our work together. You have made me the physicist that I am today.

An aspect of PhD life that I have missed in recent times is working in an office with a diverse class of colleagues. There are many of my peers without whom my time in Southampton would not have been the same, but I wish to mention especially Ciara Byers, Azaria Coupe, Billy Ford, Jack Foster, Ross Glew, Matt Kellet, Andrew Lawson, Dan Locke, Alex Mitchell, Elena Perdomo, James Richings, Ronnie Rodgers and Matt Russell. You made it a joy to come into the office every single day, and your contributions to this work are more significant than you might think. Thank you.

I would also like to mention those outside the physics community at Southampton and back in Shropshire during my master's degree and PhD. You've all helped me along the way with food, debates serious and otherwise, games and the occasional beer or three, and I am grateful to all of you.

Finally, I'd like to thank my steadfast parents and long-suffering brother Lee. Be in no doubt that nothing presented here would have been possible without your consistent encouragement and support. You will forever have my gratitude.

List of Abbreviations

BAU	Baryon Asymmetry of the Universe
BSM	Beyond the Standard Model
CKM	Cabbibo-Kobayashi-Maskawa
CP	Charge-Parity
CSD	Constrained Sequential Dominance
DM	Dark Matter
EFT	Effective Field Theory
EW	Electroweak
EWSB	Electroweak Symmetry Breaking
FCNC	Flavour-Changing Neutral Current
GIM	Glashow-Iliopoulos-Maiani
GUT	Grand Unified Theory
IO	Inverted Ordering
LS	Littlest Seesaw
LFV	Lepton Flavour Violation
LUV	Lepton Universality Violation
LH	Left-Handed
LHC	Large Hadron Collider
LSP	Lightest Supersymmetric Partner
MFV	Minimal Flavour Violation
MSSM	Minimal Supersymmetric Standard Model
NMFV	Non-Minimal Flavour Violation
NO	Normal Ordering
PMNS	Pontecorvo-Maki-Nakagawa-Sakata
QCD	Quantum Chromodynamics
QED	Quantum Electrodynamics
RGE	Renormalisation Group Evolution
RH	Right-Handed
SM	Standard Model
SSB	Spontaneous Symmetry Breaking
SUSY	Supersymmetry
VEV	Vacuum Expectation Value

Chapter 1

Motivation

Particle phenomenology is a critical part of fundamental physics. Both before and since the discovery of the Higgs boson by ATLAS and CMS in 2012 [4, 5], a plethora of theories have been developed that utilise new mechanisms to solve some of the Standard Model's (SM) many problems. Such issues include, but are not limited to; the nature of dark matter, predicting the Higgs mass and its hierarchy of scales, the flavour puzzle concerning the origin of fermion masses and mixings, the generation of neutrino masses and associated oscillation patterns, and various magnetic moment anomalies.

The ability to confront models with experimental data, and compare them with other theories, therefore remains of paramount importance; without rigorous analysis, we cannot know if a theory is capable of describing nature accurately. Phenomenology is not carried out in isolation, and there is a certain amount of feedback to model builders discussing which theories are considered viable and merit further development. There are several approaches to building new scenarios including effective theories, simplified models, and ultraviolet-complete models at high scales, all of which deserve investigation. Unified theories and simplified models can direct experimentalists as to signatures of potential particles, and study of anomalies in effective field theories can uncover relevant operators and propose new particles that are ultimately responsible for non-standard physics.

Studying high energy models may seem far removed from the low-scale physics of experiments, but heavy fields leave distinct physical imprints that can persist at low scales after renormalisation group evolution, and can participate in quantum corrections to physical observables and incite flavour mixing across generations of Standard Model fermions. In this thesis, we investigate several concrete scenarios that incorporate Beyond the Standard Model (BSM) physics and are inspired by unified scenarios manifest at some high scale. By performing phenomenological analyses, we determine their viability as explanations for some of the Standard Model's shortcomings. In-depth investigations of different models are presented in separate chapters, corresponding to work carried out by the author during their research candidature.

Chapter 2 reviews the Standard Model, including its symmetries and idiosyncrasies,

focusing on electroweak theory and the Higgs mechanism. In the latter part of this chapter, shortcomings of the Standard Model are discussed in detail to properly motivate the need for physics beyond this well-established paradigm. Chapter 3 extends the Standard Model in a variety of ways intended to improve the current understanding of theoretical physics by solving some combination of problems present in the Standard Model. Concepts introduced here include the Type-I seesaw mechanism, supersymmetry and the Minimal Supersymmetric Standard Model, vector-like fermions and Grand Unified Theories. Later chapters detail original research.

Chapter 4 presents an analysis of the Littlest Seesaw model of neutrino physics. This model adds two new fields to Standard Model content in the form of gauge singlet right-handed neutrinos that explain the observed smallness of neutrino masses through a simple Type-I seesaw mechanism. Such a model can also explain the predominance of matter over antimatter in the universe through a mechanism of leptogenesis involving asymmetric decay of heavy right-handed neutrinos. This minimal and well-motivated theory is investigated through a statistical fit including renormalisation group evolution effects. The model is found to be a good candidate to explain the most recent data from various neutrino experiments and the observed baryon asymmetry of the universe.

The flavour implications of supersymmetry-breaking in a Minimal Supersymmetric Standard Model that originates from an $A_4 \times SU(5)$ flavoured theory are discussed in Chapter 5. Such a model is readily able to accommodate the anomalous muon magnetic moment and dark matter phenomenology. Due to grand unification and renormalisation group evolution effects, interesting correlations occur whereby hadronic parameters are constrained by leptonic constraints along with other curious effects. The interplay discussed provides signposts for physicists building flavoured models based on unified theories in the future. This work also shows that correlations between leptonic and hadronic flavour observables, if seen at experiments, give hints for grand unification at high scales.

The phenomenology of vector-like quarks has received much attention in the past ten years, and recently model builders have been considering whether vector-like fermions are responsible for the observed deviations from lepton universality in meson decays. Chapter 6 studies a model of vector-like fermions and $U(1)'$ symmetry originally intended to resolve such tensions. We discuss the possibility for such a model to explain the long-standing anomalous muon magnetic moment and the more recent deviation seen in the magnetic dipole moment of the electron. A relevant region of parameter space for these two observables is explored, and we find that non-observation of the flavour violating decay $\mu \to e\gamma$ and trident production of neutrinos impose strict constraints on this space.

Chapter 7 concludes with remarks on presented results in the broader context of particle physics.

Chapter 2

The Standard Model

2.1 A quantum theory of fields and symmetries

The Standard Model is a predictive theory of physics that continues to be an excellent description of nature sixty years after its conception, and the scientific community is yet to develop a more successful model of physics at the fundamental level. It is a quantum theory of fields and symmetries based on the Glashow-Weinberg-Salam model of the weak force [6–8], Gell-Mann's non-Abelian vision of the strong force [9–12], and the Higgs-Brout-Englert mechanism[1] of spontaneous symmetry breaking [13–15]. The vast majority of data obtained from the LHC at CERN conforms to well-known, exhaustively studied SM predictions. There is no quantum theory of gravity included in the Standard Model, and we do not consider any quantum formulation of gravity in this thesis.

Three gauge symmetries formulate Quantum Chromodyanmics (QCD) and Electroweak (EW) theory that together form the Standard Model (SM). The combination of symmetries is given in Equation (2.1).

$$G_{\text{SM}} = SU(3)_C \times SU(2)_L \times U(1)_Y \tag{2.1}$$

The subscript 'C' is for colour, 'L' denotes that $SU(2)_L$ acts on fermions of left-handed chirality and antifermions of right-handed chirality[2], and 'Y' denotes the so-called weak hypercharge quantum number. The field content of the model includes three generations of chiral fermions (who only differ by their respective masses), gauge fields for the symmetries and a single scalar (denoted ϕ) that breaks electroweak symmetry. All such fields are detailed in Table 2.1. Note that because quarks transform as triplets under $SU(3)$, they also have QCD indices which have been suppressed here for brevity. The fields in Table 2.1a are expressed in the standard notation of their $SU(2)$ doublets;

---

[1]Commonly referred to as the Higgs mechanism

[2]Sometimes, this is disambiguated by denoting $SU(2)_L$ as $SU(2)_W$, where W represents the weak force. We adopt the more common notation of $SU(2)_L$ in this thesis. In principle, additional right-handed fermions could be charged under $SU(2)_L$.

Field	Representation/charge		
	$SU(3)_C$	$SU(2)_L$	$U(1)_Y$
Q_{Li}	**3**	**2**	$1/6$
u_{Ri}	**3**	**1**	$2/3$
d_{Ri}	**3**	**1**	$-1/3$
L_{Li}	**1**	**2**	$-1/2$
e_{Ri}	**1**	**1**	-1

(a) Chiral fermions, $i = 1, 2, 3$ for different generations.

Field	Representation/charge		
	$SU(3)_C$	$SU(2)_L$	$U(1)_Y$
G^a	**8**	**1**	0
W^b	**1**	**3**	0
B	**1**	**1**	0
ϕ	**1**	**2**	$1/2$

(b) Gauge boson and scalar fields, $a = 1, ..8$, $b = 1, 2, 3$.

Table 2.1: Standard Model field content

$Q_{Li} = (u_{Li}, d_{Li})^T$, $L_i = (e_{Li}, \nu_{Li})^T$. ν denotes the SM neutrino fields, of which there only exist the left-handed (LH) chirality in the SM and such neutrinos are massless. The final particle in Table 2.1b is the Higgs doublet of the SM; $\phi = (\Phi^+, \Phi^0)^T$. Fermions exist in the trivial or fundamental representations of the gauge groups, and gauge bosons inhabit the adjoint representation [16]. In Table 2.2, we expand the family indices and $SU(2)_L$ doublets, showing the six flavours of quark and three charged leptons and neutrinos. Naming conventions for SM fermions are given in Table 2.3. From here,

Family Index	Quark Flavour	Lepton Flavour
$i = 1$	$Q_{L1} = (u_L, d_L)^T$, $u_{R1} = u_R$, $d_{R1} = d_R$	$L_{L1} = (\nu_{eL}, e_L)^T$, $e_{R1} = e_R$
$i = 2$	$Q_{L2} = (c_L, s_L)^T$, $u_{R2} = c_R$, $d_{R2} = s_R$	$L_{L2} = (\nu_{\mu L}, \mu_L)^T$, $e_{R2} = \mu_R$
$i = 3$	$Q_{L3} = (t_L, b_L)^T$, $u_{R3} = t_R$, $d_{R3} = b_R$	$L_{L3} = (\nu_{\tau L}, \tau_L)^T$, $e_{R3} = \tau_R$

Table 2.2: Expansion of fermion $SU(2)_L$ doublets in the SM

Family Index	Quark Symbol	Quark Name	Lepton Symbol	Lepton Name
$i = 1$	u	up quark	e	electron
	d	down quark	ν_e	electron neutrino
$i = 2$	c	charm quark	μ	muon
	s	strange quark	ν_μ	muon neutrino
$i = 3$	t	top quark	τ	tau
	b	bottom quark	ν_τ	tau neutrino

Table 2.3: Fermion nomenclature

we explore gauge transformations and symmetries in more detail, and following this we discuss the symmetry-breaking mechanism behind mass generation in the SM. This chapter closes with an in-depth discussion of problems with the SM and convincing motivation for physics beyond the Standard Model.

4

2.2 Gauge transformations

The SM conforms to several gauge symmetries and is invariant under the associated gauge transformations. Gauge transformations are local and therefore space-time dependent. Take a fermion field $\psi(x)$ and a small transformation parameter of an Abelian symmetry $\alpha(x)$. The action of an infinitessimal transformation on such a field is given in Equation (2.2).

$$\psi(x) \rightarrow e^{-i\alpha(x)}\psi(x) \tag{2.2}$$

The kinetic term of the Dirac equation for $\psi(x)$ will experience this transformation thus:

$$i\overline{\psi}\slashed{\partial}\psi \rightarrow i\overline{\psi}\slashed{\partial}\psi + \left(\overline{\psi}\gamma^\mu\psi\right)\left(\partial_\mu\alpha(x)\right) \tag{2.3}$$

For the Lagrangian to be locally invariant under the gauge symmetry, we introduce the gauge field $A_\mu(x)$ into the covariant derivative and assign to it appropriate transformation properties detailed in Equations (2.4) and (2.5).

$$D_\mu\psi(x) = \left(\partial_\mu - igA_\mu(x)\right)\psi(x) \tag{2.4}$$

$$A_\mu(x) \rightarrow A_\mu(x) + \frac{1}{g}\partial_\mu\alpha(x) \tag{2.5}$$

g is the gauge coupling, a parameter that is not predicted by the theory and must be determined experimentally. Generalisation of the above to non-Abelian theory is simple; the transformation on $\psi(x)$ becomes that in Equation (2.6), where t^a denotes a non-Abelian generator and $\theta^a(x)$ is some small transformation parameter.

$$\psi(x) \rightarrow \exp\left(-it^a\theta^a(x)\right)\psi(x) \tag{2.6}$$

Contraction of the gauge index a denotes an implicit sum. The covariant derivative has a similar form to the Abelian version in Equation (2.4):

$$D_\mu\psi(x) = \left(\partial_\mu - igA_\mu^a(x)t^a\right)\psi(x) \tag{2.7}$$

Generators satisfy $\left[t^a, t^b\right] = if^{abc}t^c$ with structure constants f^{abc} that are unique for each distinct Lie group, and the non-Abelian gauge field transforms as per Equation (2.8), leaving the Lagrangian invariant under the local transformation.

$$A_\mu^a(x) \rightarrow A_\mu^a(x) + \frac{1}{g}\partial_\mu\theta^a(x) + f^{bca}A_\mu^b(x)\theta^c(x) \tag{2.8}$$

The SM conforms to a number of Abelian and non-Abelian symmetries as per Equation (2.1). It should be noted that mass terms for gauge bosons inserted by hand into a

gauge theory such as $\frac{1}{2}M_B^2 B_\mu B^\mu$ (for an Abelian symmetry) are not gauge invariant, and so true gauge invariance requires the associated bosons to be necessarily massless.

2.3   Quantum chromodynamics

The $SU(3)$-based theory that describes the strong force is quantum chromodynamics (QCD), through this theory the hadronic spectrum of combined quark states is fully determined. Gell-Mann's famous 8-fold way of creating compound states of quarks and gluons forms the basis for the theory [9–12]. $SU(3)$ is a non-Abelian Lie algebra and in an associated gauge theory multi-boson scattering is not prohibited. The Lagrangian for QCD and its coupling to SM quarks is given in Equation (2.9), all leptons are singlets under $SU(3)_C$.

$$\mathcal{L}_{\text{QCD}} = -\frac{1}{4}G_{\mu\nu}^a G^{a\ \mu\nu} + \bar{q}_L \left(i\slashed{D}\right) q_R \tag{2.9}$$

q can be one of any six flavours of quark as per the second column of Table 2.3. All quark indices have been suppressed for readability, and their are no cross-generational fermion interactions in QCD. The index $a = 1, ..., 8$ as QCD gauge bosons (gluons) G_μ^a reside in the adjoint representation of $SU(3)_C$. $G_{\mu\nu}^a$ represents the gauge field strength tensor, and is expanded in Equation (2.10). Due to the gauge coupling of QCD g_s being large and non-perturbative at low energies, QCD is a confining theory and free quarks are not seen in experiments. Instead one observes hadrons, bound states of either two or three quarks called mesons and baryons respectively. This incites much rich phenomenology that is the subject of a vast swathe of research in particle physics, but this topic is not discussed in detail here.

$$\begin{aligned} D_\mu &= \partial_\mu - ig_s G_\mu^a T^a \\ G_{\mu\nu}^a &= \partial_\mu G_\nu^a - \partial_\nu G_\mu^a + ig_s f^{abc} G_\mu^b G_\nu^c \end{aligned} \tag{2.10}$$

f^{abc} denotes the $SU(3)$ structure constants, T^a are generators of $SU(3)$ rotations and are proportional to the Gell-Mann matrices $T^a = \lambda^a/2$. The final term in the second line of Equation (2.10) describes multi-boson scattering, which is a feature of non-Abelian gauge theories[3].

2.4   Electroweak theory

In the SM, electromagnetism and the weak force are described by electroweak theory. The corresponding symmetry group is $SU(2)_L \times U(1)_Y$, and there are several

---

[3]The three- and four-point gluon scattering vertices in QCD make perturbative calculations in high-scale QCD quite difficult.

components to the Lagrangian of this joint description as per Equation (2.11).

$$\mathcal{L}_{EW} = \mathcal{L}_{kinetic} + \mathcal{L}_{Yukawa} + \mathcal{L}_{Higgs} \tag{2.11}$$

We explore each of these parts separately: The kinetic part contains information about fermion couplings to the EW gauge bosons and the propagating information of the adjoint representation degrees of freedom.

$$\mathcal{L}_{kinetic} = i\overline{\psi}\slashed{D}\psi - \frac{1}{4}W^b_{\mu\nu}W^{b\;\mu\nu} - \frac{1}{4}B_{\mu\nu}B^{\mu\nu} \tag{2.12}$$

ψ represents any fermion fields which are allowed by gauge invariance, Lorentz symmetry and renormalisability. $W^b_{\mu\nu}$ is the $SU(2)_L$ field strength tensor, with b representing $SU(2)_L$ indices, and similarly for $B_{\mu\nu}$ with $U(1)_Y$ where no index is required as the $U(1)$ algebra has only a single generator.

$$W^b_{\mu\nu} = \partial_\mu W^b_\nu - \partial_\nu W^b_\mu + g\epsilon^{bcd}W^c_\mu W^d_\nu \tag{2.13}$$

W^b_μ represents the three $SU(2)_L$ gauge degrees of freedom, and ϵ^{bcd} is the totally antisymmetric $SU(2)_L$ tensor, the Levi-Civita symbol. An analogue for Equation (2.13) can be written for $B_{\mu\nu}$, where the last term vanishes as $U(1)_Y$ is Abelian. Interactions between gauge bosons are described in the final term in Equation (2.13). The covariant derivative that appears in the fermionic part of Equation (2.12) is expanded in the usual way for fermion-gauge interactions. This is provided in all detail in Equation (2.14).

$$D_\mu = \partial_\mu - ig'B_\mu\mathcal{Y} - igW^b_\mu\mathcal{T}^b \tag{2.14}$$

$\mathcal{Y}$ denotes the generator of hypercharge rotations, $\mathcal{T}^b$ generates $SU(2)_L$ transformations, and g, g' refer to the gauge coupling constants of $SU(2)_L$ and $U(1)_Y$ respectively, which are parameters of the theory. $SU(2)_L$ generators are related to the Pauli matrices as $\mathcal{T}^b = \sigma^b/2$. The second part of the Lagrangian, $\mathcal{L}_{Yukawa}$, couples the scalar Higgs field to the fermionic degrees of freedom through dimensionless[4] 'Yukawa couplings' given in Equation (2.15).

$$\mathcal{L}_{Yukawa} = (Y_u)_{ij}\overline{Q}_{Li}\widetilde{\phi}u_{Rj} + (Y_d)_{ij}\overline{Q}_{Li}\phi d_{Rj} + (Y_e)_{ij}\overline{L}_i\phi e_{Rj} + H.c. \tag{2.15}$$

As usual, $i, j = 1, 2, 3$ for the three generations fermions, meaning that the couplings Y_u, Y_d, Y_e are 3×3 matrices in the space of fermion flavour. $\widetilde{\phi} = i\sigma^2\phi^*$, with σ^2 being the second Pauli matrix. $\widetilde{\phi}$ is allowed in the Yukawa coupling term for up-type quarks because it transforms as a $\overline{\mathbf{2}}$ under $SU(2)_L$, which has equivalent transformation properties as the fundamental $\mathbf{2}$ representation. The final part of the $SU(2)_L \times U(1)_Y$ Lagrangian is that which contains the Higgs potential and is responsible for the sym-

---

[4]Without mass dimension. Throughout this work we assume $c = \hbar = 1$.

metry breaking and fermion mass generation in the SM.

$$\mathcal{L}_{Higgs} = (D_\mu \phi)^\dagger D^\mu \phi - V(\phi) \tag{2.16}$$

The covariant derivative is identical to Equation (2.14), and the scalar potential $V(\phi)$ has a structure fully determined by the requirements for gauge invariance and renormalisability:

$$V(\phi) = \mu^2 \phi^\dagger \phi + \lambda(\phi^\dagger \phi)^2 \tag{2.17}$$

The breaking of the symmetry is ultimately controlled by the two parameters μ and λ, and their values determine both the shape of the potential and the scale at which symmetry breaking-occurs.

2.4.1   Spontanteous symmetry breaking and the Higgs mechanism

At scales accessible to colliders, the SM is not whole as at high energies but instead conforms to a broken subgroup of $SU(3)_C \times U(1)_{QED}$, where $U(1)_{QED}$ emerges precisely as the unbroken subgroup of $SU(2)_L \times U(1)_Y$, which is broken by the Higgs field. We express the Higgs $SU(2)_L$ doublet in terms of its weak isospin components:

$$\phi \equiv \begin{pmatrix} \Phi_+ \\ \Phi_0 \end{pmatrix} \equiv \frac{1}{\sqrt{2}} \begin{pmatrix} \phi_1 + i\phi_2 \\ \phi_3 + i\phi_4 \end{pmatrix} \tag{2.18}$$

$\phi_{1,2..4}$ are the four real degrees of freedom of the Higgs in the unbroken $SU(2)_L$ phase. For a potential that is properly bounded from below, λ must always be positive. Normalisation of the $SU(2)_L$ doublet is chosen such that the kinetic Lagrangian piece has the correct prefactor. At high temperatures or early in the universe's life, μ^2 is positive and the potential in Equation (2.17) has a minimum at $|\phi| = \sqrt{\phi^\dagger \phi} = 0$, corresponding to an unbroken symmetry where all generators of $SU(2)_L \times U(1)_Y$ are preserved. This is because each of those generators acting on the vacuum state $\phi = 0$ do not change the state; the vaccuum state is invariant under the symmetry transformations. The potential in this phase is shown in Figure 2.1a. As time progresses and the universe cools, eventually μ^2 is driven negative, resulting in the well-known 'wine bottle' potential shape, which has a minimum away from zero seen in Figure 2.1b as the ring of blue. The minimum of this potential is no longer situated at $|\phi| = 0$, but is instead at v, which is known as the vacuum expectation value or 'VEV'. Because there is an $O(4)$ symmetry between the degrees of freedom in the Higgs field $\phi_{1,2,3,4}$, one of these components can be chosen to take the VEV, rather than some combination of such fields. Without loss of generality we choose $\langle \phi_3 \rangle = v, \langle \phi_{1,2,4} \rangle = 0$ in terms of field components. We define a new scalar field $h(x)$, required to have zero vacuum expectation value, such that $\phi_3 = v + h(x)$ [17]. The number of degrees of freedom has not changed, and we
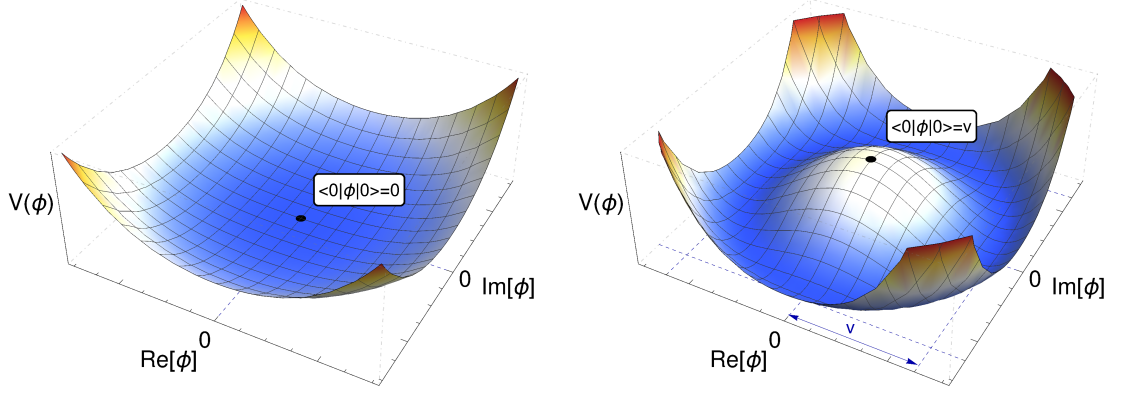
(a) Unbroken symmetry (high temperature)   (b) Broken symmetry (low temperature)

Figure 2.1: SM Higgs potential $V(\phi) = \mu^2\phi^\dagger\phi + \lambda(\phi^\dagger\phi)^2$ in the unbroken phase (left, $\mu^2 > 0$) and the broken phase after spontaneous symmetry breaking (right, $\mu^2 < 0$). In the broken phase, the minimum of the potential lies at $\phi = v/\sqrt{2} = 174$ GeV.

can now re-express the Higgs field in terms of these components as per Equation (2.19).

$$\phi = \frac{1}{\sqrt{2}}\begin{pmatrix} \phi_1 + i\phi_2 \\ v + h(x) + i\phi_4 \end{pmatrix} \tag{2.19}$$

We theoretically infer the value of v by probing the Higgs vacuum and studying the Higgs potential. We calculate the one-point function of the field as per Equation (2.20), where $|0\rangle$ denotes the vacuum quantum state.

$$\langle 0|\phi|0\rangle \equiv \phi_0 = \frac{1}{\sqrt{2}}\begin{pmatrix} 0 \\ v \end{pmatrix}, \qquad v = \frac{|\mu|}{\sqrt{\lambda}} = 246 \,\text{GeV} \tag{2.20}$$

The numerical value for v is determined from experimental measurements of weak force gauge boson properties. If we expand the potential in terms of the constants and scalar fields seen in Equation (2.19), then the following terms become apparent:

$$V(\phi) = C + 0 \cdot \phi_1^2 + 0 \cdot \phi_2^2 + \lambda v^2 h(x)^2 + 0 \cdot \phi_4^2 + \mathcal{O}(\phi^3) \tag{2.21}$$

C represents some constant term and higher order terms that are cubic or greater in the scalar fields are neglected. ϕ_1, ϕ_2 and ϕ_4 are massles scalars and $h(x)$ is a scalar with mass $m_h = \sqrt{2\lambda v^2}$ [17]. Experimentally, $h(x)$ is the scalar boson of mass 125GeV seen at the ATLAS and CMS detectors in 2012 [4, 5]. We can write ϕ in the form of Equation (2.22), provided that $\xi^1 = \phi_2, \xi^2 = \phi_1, \xi^3 = -\phi_4$.

$$\phi = \frac{1}{\sqrt{2}}\exp\left(\frac{i\xi^a\sigma^a}{v}\right)\begin{pmatrix} 0 \\ v + h(x) \end{pmatrix} \tag{2.22}$$

σ^a are the Pauli matrices and the implicit sum is over $a = 1, 2, 3$. Such a description is physically equivalent to Equation (2.19). Now we perform a $SU(2)_L$ gauge transformation on the Higgs field:

$$\phi \to \exp\left(i\beta^a(x)\frac{\sigma^a}{2}\right)\phi \tag{2.23}$$

Fixing the gauge $\beta^a(x) = -2\xi^a/v$ for each point in the spacetime manifold moves the theory into unitary gauge. The Higgs field in this gauge is represented by Equation (2.24), where we have 'gauged away' the fields ξ^a, which is equivalent to eliminating the massless modes $\phi_{1,2,4}$.

$$\phi(x) = \phi_0 + h(x) = \frac{1}{\sqrt{2}}\begin{pmatrix} 0 \\ v + h(x) \end{pmatrix} \tag{2.24}$$

Three of the four degrees of freedom shown in Equation (2.18) have been removed, and the only degree of freedom left is the physical Higgs field $h(x)$, which represents radial fluctuations around the minimum of $V(\phi)$. The symmetry that remains is a relic $U(1)_{QED}$ represented by a continuous rotational symmetry of the minimum in Figure 2.1b.

In the language of group theory, spontaneous symmetry breaking (SSB) breaks three generators of $SU(2)_L \times U(1)_Y$, leaving a single unbroken generator that corresponds to the $U(1)_{QED}$ rotation, i.e. the unbroken generator describes rotations in the angular direction of the circular minimum in Figure 2.1b. We summarise the implications of spontaneous symmetry breaking for the Higgs field and SM symmetries in Equation (2.25):

$$\frac{1}{\sqrt{2}}\begin{pmatrix} \phi_1 + i\phi_2 \\ \phi_3 + i\phi_4 \end{pmatrix} \xrightarrow{SSB} \frac{1}{\sqrt{2}}\begin{pmatrix} 0 \\ v + h(x) \end{pmatrix},$$

$$SU(2)_L \times U(1)_Y \xrightarrow{SSB} U(1)_{QED} \tag{2.25}$$

Note that because each point on the circular minimum of Figure 2.1b is physically equivalent, the vacuum state ϕ_0 is invariant under $U(1)_{QED}$ transformations.

2.4.2 Massive gauge bosons

The degrees of freedom that are eliminated by spontaneous symmetry breaking cannot simply disappear. From Goldstone's theorem, we know that there exists a Goldstone boson (scalar degree of freedom) for each of the three broken generators that the vacuum is no longer invariant under after spontaneous symmetry breaking [18]. These massless modes ($\phi_{1,2,4}$ from Equation (2.19)) are transmitted into longitudinal gauge boson degrees of freedom, and three $SU(2)_L \times U(1)_Y$ gauge bosons gain masses in this

manner[5]. This phenomenon is best seen by diagonalising the kinetic term in the Higgs Lagrangian from Equation (2.16) after breaking electroweak symmetry.

$$(D_\mu\phi)^\dagger D^\mu\phi \supset \frac{1}{2}\Big(0, v + h(x)\Big)\big(i\frac{g'}{2}B_\mu + igW_\mu^b\mathcal{T}^b\big)\cdot$$
$$\big(-i\frac{g'}{2}B^\mu - igW^{b\,\mu}\mathcal{T}^b\big)\begin{pmatrix} 0 \\ v + h(x) \end{pmatrix} \tag{2.26}$$

$$= \frac{1}{2}(v + h(x))^2\Big(g^2(W^1)^2 + g^2(W^2)^2 + (-gW^3 + \frac{g'}{2}B)^2\Big) \tag{2.27}$$

Pieces of Equation (2.27) that contain $h(x)$ describe couplings between the SM Higgs and gauge bosons such as $hWW, hhWW, hZZ$ and $hhZZ$. We define four mass eigenstate gauge bosons and derive their masses directly from this Lagrangian:

$$W_\mu^\pm \equiv \frac{1}{\sqrt{2}}\big(W_\mu^1 \mp iW_\mu^2\big) \tag{2.28}$$

$$Z_\mu \equiv \frac{1}{\sqrt{g^2 + g'^2}}\big(gW_\mu^3 - g'B_\mu\big) \tag{2.29}$$

$$A_\mu \equiv \frac{1}{\sqrt{g^2 + g'^2}}\big(g'W_\mu^3 + gB_\mu\big) \tag{2.30}$$

These are precisely the $W^\pm$, Z bosons and electromagnetic photon field (A) that are observed in experiments. The Weinberg weak mixing angle, θ_W, parameterises the mismatch between gauge boson fields in the different bases described in Equations (2.27) and Equations (2.28) through (2.30) respectively.

$$\begin{pmatrix} Z_\mu \\ A_\mu \end{pmatrix} = \begin{pmatrix} \cos\theta_W & -\sin\theta_W \\ \sin\theta_W & \cos\theta_W \end{pmatrix}\begin{pmatrix} W_\mu^3 \\ B_\mu \end{pmatrix} \tag{2.31}$$

From studying terms in Equations (2.27) that do not contain the propagating Higgs field $h(x)$ after the definitions in Equations (2.28) to (2.30), one can extract masses for the gauge bosons, given in Equation (2.32).

$$M_W = gv/2$$
$$M_Z = \sqrt{g^2 + g'^2}(v/2) \tag{2.32}$$

A simple expression then becomes apparent for the Weinberg angle, $\cos\theta_W = M_W/M_Z$. M_W and g are both well-measured, and this allows us to determine the Higgs VEV to be $v = 246$ GeV. The photon state is orthogonal to the Z, and does not obtain a longitudinal degree of freedom as it doesn't couple to the Higgs field, and therefore the photon remains massless. One can now write the covariant derivative of electroweak

---

[5]It is sometimes said that the Goldstone bosons are 'eaten' by the gauge bosons

theory in terms of the mass eigenstate gauge boson fields. In Equation (2.33), we define a linear combination of $SU(2)_L$ generators; $\mathcal{T}^{\pm} \equiv \mathcal{T}^1 \pm i\mathcal{T}^2$.

$$D_\mu \xrightarrow{SSB} \partial_\mu - \frac{ig}{\sqrt{2}}\left(W_\mu^+ \mathcal{T}^+ + W_\mu^- \mathcal{T}^-\right) - \frac{igZ_\mu}{\sqrt{2}\cos\theta_W}\left(\cos^2\theta_W \mathcal{T}^3 - \sin^2\theta_W \mathcal{Y}\right)$$
$$- ig\sin\theta_W A_\mu\left(\mathcal{T}^3 + \mathcal{Y}\right) \tag{2.33}$$

Because we identify A_μ as the photon field, we express the magnitude of a unit electric charge and the generator for $U(1)_{QED}$ in terms of primordial $SU(2)_L \times U(1)_Y$ parameters:

$$\mathcal{Q} = \mathcal{T}^3 + \mathcal{Y} \tag{2.34}$$

$$|e| = g\sin\theta_W \tag{2.35}$$

One can now write down a gauge transformation for the relic $U(1)_{QED}$ and show that the Higgs vacuum in the broken electroweak phase is still invariant under such a transformation:

$$\phi_0 \to e^{-iq_{h_0}e\mathcal{Y}(x)}\phi_0 = \phi_0 \tag{2.36}$$

This is clear as the physical Higgs is not charged under $U(1)_{QED}$, i.e. $q_{h_0} = 0$, evident from its charges under SM gauge groups.

2.4.3 Masses for fermions and CKM mixing

To study how quarks acquire masses through the Higgs mechanism, we need to re-examine the Yukawa couplings between SM fermions and the Higgs boson field. If we study Equation (2.15) and expand each term after electroweak symmetry breaking (EWSB), we will be left with mass terms for the fermions, and terms that couple the physical Higgs state to the fermions of the SM. These are expressed in Equation (2.37).

$$\mathcal{L}_{Yukawa} \xrightarrow{SSB} \frac{1}{\sqrt{2}}\left[(Y_u)_{ij}\overline{u_{Li}}h(x)u_{Rj} + (Y_d)_{ij}\overline{d_{Li}}h(x)d_{Rj} + (Y_e)_{ij}\overline{e_{Li}}h(x)e_{Rj} + H.c.\right]$$
$$+ (m_u)_{ij}\overline{u_{Li}}u_{Rj} + (m_d)_{ij}\overline{d_{Li}}d_{Rj} + (m_e)_{ij}\overline{e_{Li}}e_{Rj} \tag{2.37}$$

The subscript $i,j = 1,2,3$ for fermion flavour as before. This Lagrangian lacks a coupling between the Higgs and neutrinos because there are no right-handed (RH) neutrinos in the SM, and in the Standard Model this makes them necessarily massless. Fermion mass matrices are defined as the following:

$$(m_u)_{ij} = \frac{v}{\sqrt{2}}(Y_u)_{ij}, \quad (m_d)_{ij} = \frac{v}{\sqrt{2}}(Y_d)_{ij}, \quad (m_e)_{ij} = \frac{v}{\sqrt{2}}(Y_e)_{ij} \tag{2.38}$$

There is no requirement for such matrices to be diagonal by gauge or Lorentz invariance. In all generality they are off-diagonal, and there is a misalignment between the flavour basis of pure interacting states and the mass eigenbasis of propagating physical fields. This mismatch emerges as mixing between flavours of quarks in the mass basis, through flavour-changing charged currents. Posed another way, quark mass eigenstates are linear combinations of states in the flavour eigenbasis. To determine the quark mass eigenvalues, we need to diagonalise the Yukawa matrices at low scales. We perform a unitary transformation on the quark fields as per Equation (2.39).

$$u_{Li} \to u'_{Li} = \left(U_{uL}\right)_{ij} u_{Lj}, \quad u_R \to u'_{Ri} = \left(U_{uR}\right)_{ij} u_{Rj},$$

$$d_{Li} \to d'_{Li} = \left(U_{dL}\right)_{ij} d_{Lj}, \quad d_R \to d'_{Ri} = \left(U_{dR}\right)_{ij} d_{Rj}, \tag{2.39}$$

$$e_{Li} \to e'_{Li} = \left(U_{eL}\right)_{ij} e_{Lj}, \quad e_R \to e'_{Ri} = \left(U_{eR}\right)_{ij} e_{Rj},$$

Note that $u_{Li} = \left(u_L, c_L, t_L\right)^T$ and similarly for the down-type quarks and charged leptons. These field transformations arrive with commensurate bi-unitary rotations on the Yukawa coupling matrices, which will ensure that the eigenvalues are real and positive. Matrix indices have been dropped in Equation (2.40) for simplicity.

$$Y_u \to Y'_u = U_{uL} Y_u \left(U_{uR}\right)^\dagger = \begin{pmatrix} y_u & 0 & 0 \\ 0 & y_c & 0 \\ 0 & 0 & y_t \end{pmatrix}$$

$$Y_d \to Y'_d = U_{dL} Y_d \left(U_{dR}\right)^\dagger = \begin{pmatrix} y_d & 0 & 0 \\ 0 & y_s & 0 \\ 0 & 0 & y_b \end{pmatrix} \tag{2.40}$$

$$Y_e \to Y'_e = U_{eL} Y_e \left(U_{eR}\right)^\dagger = \begin{pmatrix} y_e & 0 & 0 \\ 0 & y_\mu & 0 \\ 0 & 0 & y_\tau \end{pmatrix}$$

From these diagonalised matrices, we can extract the Yukawa eigenvalues and physical masses of the SM fermions. A summary of these is given in Table 2.4. It is convenient to parameterise all quark mixing in terms of a unitary matrix. We can do this by combining the transformations used to diagonalise the Yukawa couplings into the famous Cabbibo-Kobayashi-Maskawa (CKM) matrix [19, 20] as detailed in Equation (2.41).

$$\left(U_{uL}\right)^\dagger U_{dL} = V_{\text{CKM}} = \begin{pmatrix} V_{ud} & V_{us} & V_{ub} \\ V_{cd} & V_{cs} & V_{cb} \\ V_{td} & V_{ts} & V_{tb} \end{pmatrix} \tag{2.41}$$

SM theory does not predict values for CKM matrix elements, and instead these must be determined experimentally. Practically speaking, the parameterisation of the CKM

Species		Mass	Species		Mass
	u	$m_u = y_u \frac{v}{\sqrt{2}}$		e	$m_e = y_e \frac{v}{\sqrt{2}}$
	d	$m_d = y_d \frac{v}{\sqrt{2}}$		ν_e	$m_{\nu_e} = 0$
	c	$m_c = y_c \frac{v}{\sqrt{2}}$		μ	$m_\mu = y_\mu \frac{v}{\sqrt{2}}$
Quarks	s	$m_s = y_s \frac{v}{\sqrt{2}}$	Leptons	ν_μ	$m_{\nu_\mu} = 0$
	b	$m_b = y_b \frac{v}{\sqrt{2}}$		τ	$m_\tau = y_\tau \frac{v}{\sqrt{2}}$
	t	$m_t = y_t \frac{v}{\sqrt{2}}$		ν_τ	$m_{\nu_\tau} = 0$

Table 2.4: Mass eigenstate Standard Model fermions

matrix given in Equation (2.41) does not give much intuition into quark mixing, as there are nine complex parameters in this matrix, but the number of parameters can be reduced in the following way: The CKM matrix is unitary by defintion, providing nine constraints, which leaves nine real, independent parameters. A further five inputs can be eliminated through rephasing the six quark fields, leaving four real parameters that can be expressed in the angular parameterisation in Equation (2.42).

$$
V_{\mathrm{CKM}} = \begin{pmatrix} 1 & 0 & 0 \\ 0 & \cos\theta_{23} & \sin\theta_{23} \\ 0 & -\sin\theta_{23} & \cos\theta_{23} \end{pmatrix} \begin{pmatrix} \cos\theta_{13} & 0 & \sin\theta_{13}e^{-i\delta_Q} \\ 0 & 1 & 0 \\ -\sin\theta_{13}e^{i\delta_Q} & 0 & \cos\theta_{13} \end{pmatrix} \begin{pmatrix} \cos\theta_{12} & \sin\theta_{12} & 0 \\ -\sin\theta_{12} & \cos\theta_{12} & 0 \\ 0 & 0 & 1 \end{pmatrix}
$$
(2.42)

The off-diagonal elements of the CKM matrix are what give rise to flavour-changing charged currents in the SM, which amounts to charged weak bosons coupling inter-generationally in the quark sector. This essentially boils down to couplings that are proportional to the mixing angles in the mass basis quark Lagrangian ($\propto \sin\theta_{12}W^+ c_L d_R$). Schematically, the arrangement of how these angles appear in Feynman vertices is shown in Figure 2.2. Thus far, we have discussed only flavour-chainging charged currents.
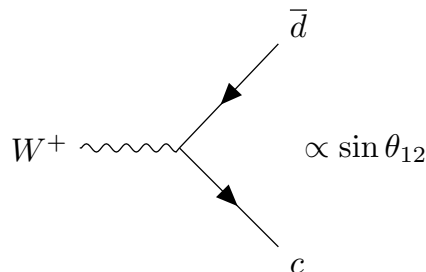
Figure 2.2: Flavour-changing charged current induced by quark flavour-mass basis misalignment in the SM. Mixing angles are small, making inter-generational couplings smaller than those within the same generation.

Flavour-changing neutral currents (FCNCs) are forbidden at tree-level in the SM, as Z boson interactions are flavour conserving. There is the possibility to introduce FCNCs at the loop level through exchanging two W bosons, but these come suppressed by the so-called Glashow-Iliopoulos-Malani (GIM) mechanism. This mechanism not only explains why there are negligible FCNCs in the SM, but also postulated the existence of the charm quark, as only the up, down and strange had been discovered at the time of its conception. Let us assume that there exist only two flavours of down-type quark. From Equation (2.39), we then recover the following:

$$d'_{Li} = \sum_{j=1,2} (V_{CKM})_{ij} d_{Li} \tag{2.43}$$

Here, we have choosen that $d_{L1} = d_L, d_{L2} = s_L$ flavour eigenstates, and that primed fields denote mass eigenstates. Therefore, for a unitary V_{CKM}:

$$\sum_i \overline{d'_{Li}} \gamma^\mu d'_{Li} = \sum_{ijk} \overline{d_{Lj}} (V_{CKM})^\dagger_{ji} \gamma^\mu (V_{CKM})_{ik} d_{Lk} = \sum_i \overline{d_{Li}} \gamma^\mu d_{Li} \tag{2.44}$$

As such, any electrically neutral coupling between two flavour eigenstates is identical to one between two mass eigenstates, and electrically neutral inter-generational couplings between quarks are forbidden at tree-level.

2.5 Discrete symmetries

Electroweak theory is said to be *chiral*, it couples to only to left-handed fermions and right-handed antifermions. This has important consequences for discrete symmetries that the SM is (mostly) invariant under. Here, we will review these symmetries in detail and their implications for the SM.

2.5.1 Parity (P)

Parity is a symmetry under the transformation of which spatial co-ordinates are reversed as per Equation (2.45). Predictions of the SM should be invariant under such a transformation.

$$x^\mu \to \hat{P} x^\mu = (x_0, -\vec{x}) \tag{2.45}$$

Dirac fermions and bosons should therefore transform with an intrinsic parity that dictates how such fields transform under a parity rotation. This is detailed in Equation (2.46).

$$\begin{aligned} \psi(x) &\to \eta^P_\psi \psi^P(x) = \eta^P_\psi \gamma^0 \psi(x_0, -\vec{x}) \\ \phi(x) &\to \eta^P_\phi \phi^P(x_0, -\vec{x}) \end{aligned} \tag{2.46}$$

It is trivial to see that two parity transformations will return a co-ordinate system to its original state $\hat{P}(\hat{P}x^\mu) = x^\mu$, so intrinsic parity values for scalars are restricted, $|\eta_\phi^P| = 1$. For a Dirac fermion field ψ, the transformation on the co-ordinates comes with an additional gamma matrix, γ^0, as the transformed field must still satisfy the Dirac equation.

2.5.2 Charge conjugation (C)

Under a charge conjugation transformation, particles are converted to antiparticles and vice versa, which changes the sign of its charge under $U(1)_{QED}$. As such, a theory that has a Lagrangian invariant under C will treat particles and antiparticles on equal footing. Similarly to a parity transformation, fermions and scalars have an intrinsic property under charge conjugation.

$$
\begin{aligned}
\psi(x) &\to \eta_\psi^C \psi^C(x) = \eta_\psi^C \hat{C}\gamma^0 \psi^*(x) \\
\phi(x) &\to \eta_\phi^C \phi^C(x) = \eta_\phi^C \phi^*(x)
\end{aligned}
\tag{2.47}
$$

ψ^* is the complex conjugate (antifermion) of the fermion field ψ and C is 4-dimensional charge conjugation matrix for Dirac fermions which is given in Equation (2.48), σ_2 is the second Pauli matrix. ϕ^* is the complex conjugate of the scalar field.

$$
\hat{C} = \begin{pmatrix} i\sigma_2 & 0 \\ 0 & -i\sigma_2 \end{pmatrix}
\tag{2.48}
$$

The matrix $\hat{C}$ is required to be that in Equation (2.48) such that $\hat{C}\gamma^0\psi^*(x)$ satisfies the Dirac equation. For any real field, its intrinsic property under charge conjugation must be $\eta^C = \pm 1$. This has physical significance; the photon field must obey the following;

$$
\hat{C} A_\mu(x) \hat{C}^{-1} = -A_\mu(x)
\tag{2.49}
$$

such that its interactions with fermions are C-invariant (the photon should treat fermions and antifermions in the same way). Hence, a particle with $\eta^C = 1$ such as the neutral pion π_0 cannot decay into an odd number of photons.

2.5.3 Time-reversal (T)

A theory that has an invariant Lagrangian under time-reversal symmetry is one that treats time running forwards and backwards equally: Time-reversal is the time analogue of parity.

$$
x^\mu \to x_T^\mu = (-x_0, \vec{x})
\tag{2.50}
$$

16

Scalars and fermions once more have specific transformation rules under such symmetries:

$$
\begin{aligned}
\psi(x) &\rightarrow \eta_\psi^T \psi^T(x) = \eta_\psi^T \hat{B} \psi^*(x_T) \\
\phi(x) &\rightarrow \eta_\phi^T \phi^T(x) = \eta_\phi^T \phi^*(x_T)
\end{aligned}
\tag{2.51}
$$

x_T is defined in Equation (2.50) and $\hat{B}$ represents the 4-dimensional time reversal transformation matrix in Dirac notation, given in Equation (2.52).

$$
\hat{B} = \begin{pmatrix} i\sigma_2 & 0 \\ 0 & i\sigma_2 \end{pmatrix}
\tag{2.52}
$$

Physical quantities for a theory should be invariant under T transformations, for example, S-matrix elements for forward and backward processes (such as production or decay Feynman diagrams for a given particle) are equivalent under exchange of initial and final state particles.

2.5.4 The CPT theorem

We have discussed the consequences of each of the C, P and T transformations separately, and it is now important to discuss compound transformations of these three. The CPT theorem states that a Lagrangian that is invariant under transformations of the proper Lorentz group should also be invariant under the product of C, P and T transformations [21, 22]. Such a theory should not distinguish between left-handed particles travelling forwards in time and right-handed antiparticles propagating backwards in time.

$$
\hat{\Theta} = \hat{C}\hat{P}\hat{T}
\tag{2.53}
$$

The effect of $\hat{\Theta}$ on the Standard Model Lagrangian is displayed in Equation (2.54).

$$
\hat{\Theta}\mathcal{L}_{SM}(x_\mu)\hat{\Theta}^{-1} = \mathcal{L}_{SM}(-x_\mu)
\tag{2.54}
$$

CP-violation

In the interaction of the weak force and quarks, the compound transformation symmetry of CP is violated. This means that weak interactions do not treat left-handed quarks and right-handed antiquarks on equal footings. In the Standard Model, this CP-violation manifests in the CKM matrix as the single irreducible complex phase δ_Q. The presence of CP-violation in the SM therefore *requires* three generations of quarks; with only two generations, a complex phase can be eliminated using the CKM unitarity and quark field redefinitions. The CKM phase appears in mixing between some neutral hadrons such as $K^0 - \overline{K^0}$ mixing and the decays of some hadrons, showing that CP-violation is visible in experiments. CP-violation also turns out to be crucial for studying

the early universe and the open question of why we live in a matter-dominated universe [23].

2.6 Renormalisation group running

Renormalisation redefines parameters in a Lagrangian to absorb unphysical infinities from quantum corrections, and ensures that physical observables are always finite. The physically relevant, renormalised parameters of a Lagrangian are the ones that can be determined from experimentally measured observables.

A consequence of renormalisation is that physical couplings such as gauge and Yukawa couplings vary (or 'run') with energy scale. The renormalisation group (RG) is a theoretical apparatus that provides information on coupling running with scale once we know its beta function, which we can determine using the Feynman diagrams of a relevant process, truncated at a chosen loop order. The beta function of the QCD gauge coupling g_s means that although quark confinement is present at low scales, the coupling decreases with energy scale and at very high energies free quarks participate in hard scattering processes. RG running is a crucial piece of the phenomenological puzzle of any theory, and in this section running in SM gauge couplings is discussed.

We demonstrate running gauge couplings in the SM using beta functions, truncating at one-loop order for simplicity. There are higher-order corrections that will alter the beta functions, but such corrections become smaller and smaller as the loop order increases, provided that relevant couplings remain perturbative. Therefore, in the approximation of small couplings, one-loop beta functions encode the majority of RG running. When discussing gauge coupling RG effects, it is useful to define α_1 for $U(1)_Y$, α_2 for $SU(2)_L$ and α_3 for QCD.

$$\alpha_1 = \frac{5}{3}\frac{g'^2}{4\pi}, \qquad \alpha_2 = \frac{g^2}{4\pi}, \qquad \alpha_3 = \frac{g_s^2}{4\pi} \tag{2.55}$$

The normalisations here are somewhat arbitrary but allow for nice comparison later on. The variation of these couplings with renormalisation scale defines the beta functions:

$$\mu^2 \frac{d^2}{d\mu^2}\frac{\alpha_i}{\pi} = \beta_i\big(\{\alpha_j\}, \epsilon\big) \tag{2.56}$$

$i, j = 1, 2, 3$, and ϵ is the small perturbation to the number of dimensions in dimensional regularisation, μ represents the renormalisation scale. This scale is a probe that we use to investigate running. At some point, we must also have some cut-off scale. We postulate that above such a scale, the theory is no longer valid and another model takes over, with appropriate matching at the transition scale. For example, it is well known that the SM can only valid up to the Planck scale $\Lambda_P = 10^{19}$GeV, where using current RG knowledge and assuming no new physics, gravity becomes non-perturbative.

In the example scenario, we renormalise in the modified minimal subtraction ($\overline{\text{MS}}$)

scheme[6], and calculate the beta functions displayed in Equations (2.57), (2.58) and (2.59), where N_g represents the number of fermion generations that participate in Feynman diagrams for one-loop corrections [24].

$$\beta_1 = \frac{\alpha_1^2}{4\pi^2}\left(\frac{2}{5} + \frac{16N_g}{3}\right) \tag{2.57}$$

$$\beta_2 = \frac{\alpha_2^2}{4\pi^2}\left(-\frac{86}{3} + \frac{16N_g}{3}\right) \tag{2.58}$$

$$\beta_3 = \frac{\alpha_3^2}{4\pi^2}\left(-44 + \frac{16N_g}{3}\right) \tag{2.59}$$

From the differential equation with respect to renormalisation scale given in Equation
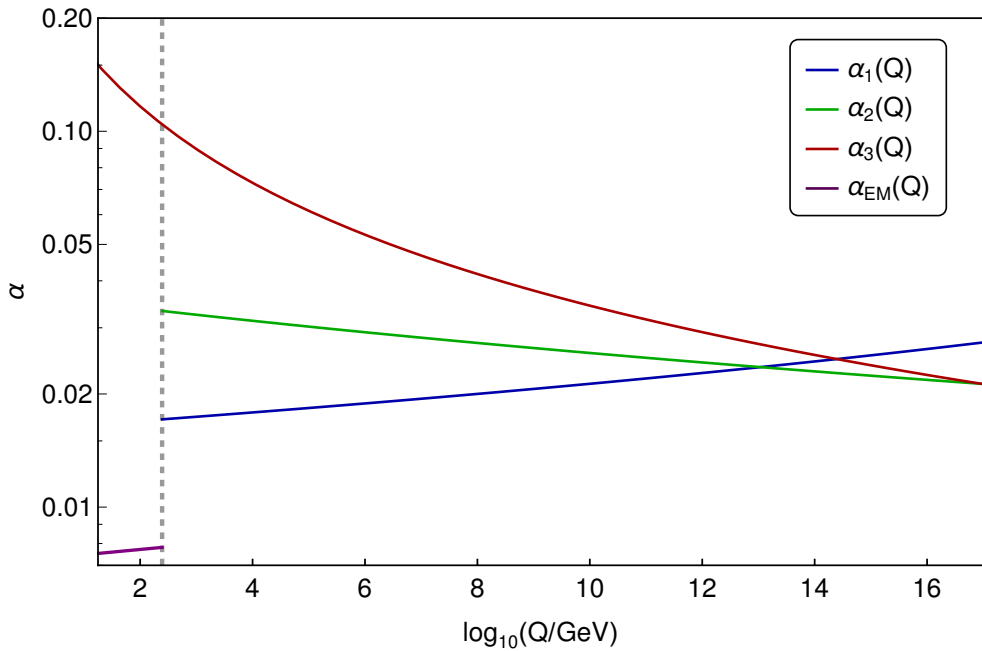
Figure 2.3: Gauge coupling running in the Standard Model. EW scale shown as a dashed line. $SU(2)_L \times U(1)_Y$ broken to $U(1)_{QED}$ at the EW scale, whilst QCD remains a conserved symmetry throughout. One can clearly see the QCD coupling increasing at lower energy scales.

(2.56) and the beta functions above, we derive how the gauge couplings run with energy scale in the SM. This is given in Figure 2.3, where we include the electroweak breaking scale and subsequent running below the EW scale when only $SU(3)_C$ and $U(1)_{\mathrm{EM}}$ are present.

The Yukawa couplings in the SM also run above the electroweak scale, and one can perform an analogous derivation for their beta functions. Running couplings and masses have an important consequence for phenomenology; when comparing predictions to

---

[6]At the one-loop level, beta functions are independent of renormalisation scheme and all schemes are physically identical.

measured quantities, it is important that observables predicted by a model are derived at the appropriate scale, else comparisons drawn between theory and data will not be valid. In this way, a deep understanding of RG effects is a critical component of any phenomenological analysis.

2.7 Limitations and shortcomings

Although the SM is incredibly predictive and forms the best theory of fundamental physics that is yet known, there are also various phenomena that we know the SM has no way of explaining. Here, we list a subset of such phenomena and review the problems that each poses.

2.7.1 Dark matter

There are several pieces of evidence that point toward a species of matter that is not predicted by the SM and interacts only gravitationally called dark matter (DM). Another idea, that of modifying Newtonian gravity has also been proposed as a solution to some of this evidence but has been found lacking compared to the dark matter scenario as it cannot explain all of the evidence simultaneously.

Galactic rotation curves

Throughout the 1970's it was found that spiral galaxies such as Andromeda had rotation curves that could not be accounted for by their measured mass distributions, instead, something was smoothing the curves out at large radii [25, 26]. As an example, in
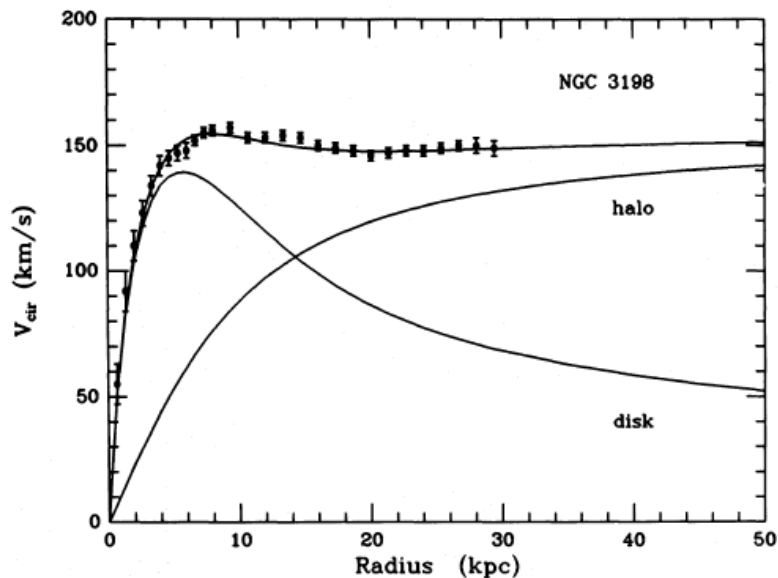
Figure 2.4: Rotation curve of galaxy NGC 3198 [27]. 'disk' portion is the rotation curve one would obtain using only the SM matter in the galaxy, the curve with datapoints is the observed rotation curve. 'Halo' denotes the theorised dark matter component.

20

Figure 2.4, we show the rotation curve for the nearby spiral galaxy NGC 3198. This galaxy exhibits the behaviour of interest; the 'disk' curve shows the rotation curve expected from the distribution of visible, Standard Model matter in the galaxy, derived using Newtonian physics. The line labelled 'NGC 3198' is the observed rotation curve of the galaxy. Beyond even 5 kiloparsecs from the galactic centre, the observed rotation curve deviates significantly from the astrophysical prediction which uses matter visible to telescopes.

A spherical 'halo' of invisible matter that interacts with the SM content only gravitationally could explain the measured rotation curve. The rotational curve of the theorised dark matter halo is also shown in Figure 2.4. Combination of the visible galaxy and this dark matter distribution can be responsible for the measured rotation curve.

The Bullet cluster

Collisions of galaxy clusters are influenced by any matter that interacts gravitationally. The most famous example of galactic collisions is the 'Bullet Cluster', in which two clusters have passed through one other. The distributions of visible matter after this collision do not conform to the gravitational influence of only the visible matter colliding. Instead, baryonic matter appears to be distributed as though much additional mass was also involved in the collision, postulated to be dark matter. The false colour
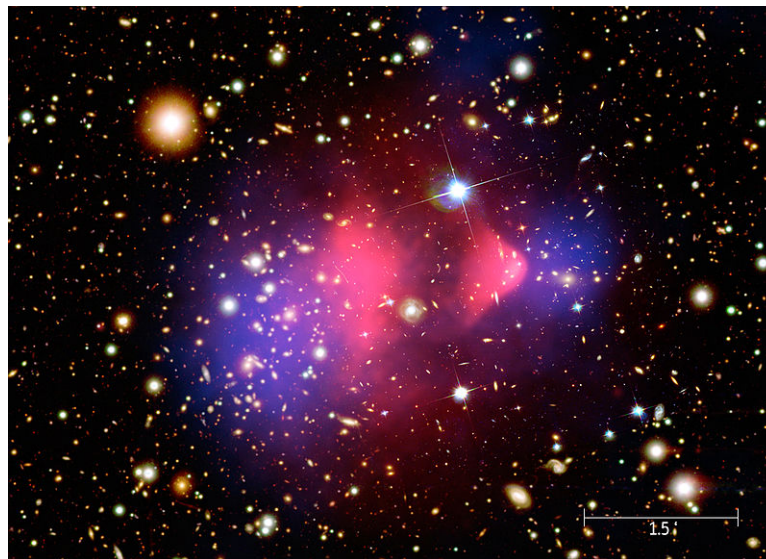
Figure 2.5: False-colour image of the Bullet cluster from the Chandra X-Ray Observatory [28, 29]. Pink shows distribution of visible matter, blue denotes theorised dark matter components of the clusters. Scale in bottom-right is in MegaParsecs (MPc).

in Figure 2.5 denotes the following; pink is the distribution of baryonic matter after the cluster collision[7], and blue outlines the theorised dark matter portion of the clusters.

---

[7]The prominent bullet-shaped concentration of visible matter in pink on the right is what gives the cluster its distinctive name.

In short, only in the presence of the blue, should the pink appear as it is observed. The Bullet cluster image is seen by many as definitive proof of dark matter's existence.

From a fundamental perspective then, a theory which solves the problem of dark matter must predict a stable, electrically neutral particle that is 'cold' (slowly travelling, as a large free-streaming length could spoil the ordinary matter distribution in a given galaxy). Various mechanisms can be used to produce dark matter thermally in the early universe, but the consensus is that there must a leftover or 'relic' density of the particle species at current times. The quantity of interest that a theory must predict to propose experimentally viable cold dark matter is the so-called relic density, which was measured experimentally by the Planck satellite in 2018 [30] under the assumption that dark matter explains these gravitational anomalies. The observed value is given in Equation (2.60) in dimensionless units (with h being the usual Planck constant).

$$\Omega_{DM}h^2 = 0.1200 \pm 0.0012 \tag{2.60}$$

2.7.2 The flavour puzzle

The Standard Model doesn't require three generations of fermion, nor does it predict the structure of Yukawa matrices or their eigenvalues, and hence physical quark and lepton masses. This is a theoretical problem with the SM; from an experimental point of view there are three generations and they are all measurable, but the question of *why* there are three generations can only be answered with a theoretical explanation. In Figure 2.6,
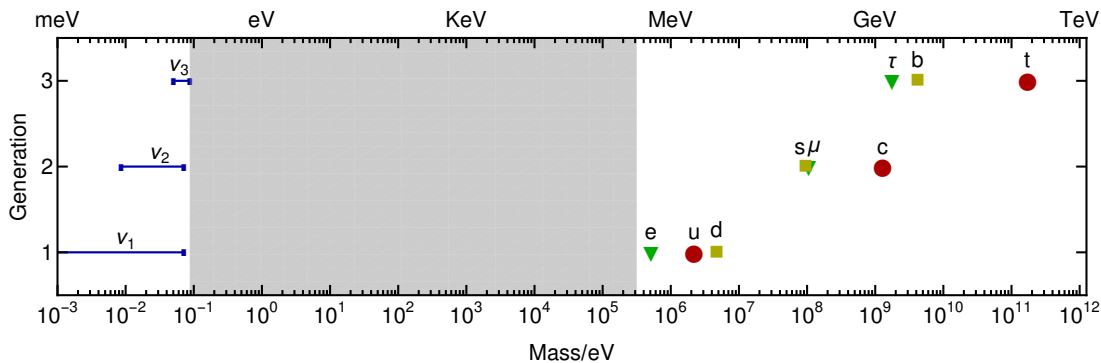
Figure 2.6: Graphic of fermion mass distribution (inspired by [31]). Neutrino mass ranges in context of most-recent data. Hierarchy clearly visible on the log scale; leptons in green, down-type quarks in yellow, up-type quarks in red and neutrinos in blue. ν_1, ν_2, ν_3 correspond to the neutrino mass eigenstates in order of increasing mass in the 'normal ordering' paradigm. Grey region represents desert between neutrino masses and charged fermion masses.

the hierarchy of fermion masses is shown in detail. Neutrino masses are shown as ranges because the absolute scale of neutrino masses is yet to be determined experimentally[8].

---

[8]Due to the difficulties associated with measuring neutrino properties, the mass differences squared are measured.

Previously, the flavour puzzle has been posed as a set of open theoretical questions that are closely related [32]:

- Why are the quark and lepton masses hierarchical?

- Why are there three generations of fermions in the SM?

- What is the origin of lepton and quark mixings, and why are they different?

- What is the theory behind neutrino mass generation?

The last point is also part of neutrino physics problems that we discuss in more detail later, but we list the idea here as it may well be closely related to the flavour puzzle. It is not yet known if there is a concrete mechanism that addresses all of these problems, but various solutions to the flavour puzzle have been proposed that utilise discrete symmetries such as S_4 and A_4 [33, 34], or modular symmetries [35].

2.7.3 Higgs mass hierarchy

The Higgs mass in the Standard Model was determined experimentally in 2012 [4, 5] to be close to 125 GeV, close to the W and Z boson masses as one expects from EW theory. However, theoretically speaking, the mass is very sensitive to new physics above the EW scale because it is not protected by any symmetry from acquiring large corrections. Many solutions to problems put forward in this section expect to see new physics somewhere between the TeV scale and the Planck scale ($10^3 - 10^{19}$GeV) and should this new physics appear then we would expect the SM Higgs mass to be around the same scale. In the SM, the particle which contributed the largest loop correction to the Higgs mass propagator is the top quark, as it has the largest Yukawa coupling. The possible correction to the Higgs mass due to a new fermion is given in Equation (2.61), where Λ_{NP} is the RG scale at which the new physics becomes apparent, m_f is the fermion's mass, and λ_f is its coupling to the Higgs. The hierarchy problem is *not* with the unphysical regulator Λ_{UV} but is instead parameterised Higgs mass-squared parameter being quadratically sensitive to the new particle's mass m_f. However, if this is the case, then we should not see the Higgs at 125 GeV, this is the core issue of the hierarchy problem.

$$\Delta m_h^2 = -\frac{|\lambda_f|^2}{8\pi^2}\left[\Lambda_{NP}^2 + 24m_f^2 \ln\left(\frac{\Lambda_{UV}}{m_f}\right) + \dots\right] \tag{2.61}$$

This problem has been studied in much detail and many possible solutions are available. Indeed, to this day the Higgs mass hierarchy problem and its solution in supersymmetry present one of the most attractive hints at the Minimal Supersymmetric Standard Model (MSSM) [36] which is discussed in more detail later. Well-motivated solutions that rely on extra dimensions are also possible [37, 38]. There are also other solutions that rely on compositeness etc., but here we make the assumption that the Higgs is a

fundamental scalar, and therefore its mass is not protected from large corrections due to new physics.

2.7.4 Neutrino masses and mixing

The absence of neutrino mass terms in the SM Lagrangian is one of the most glaring pieces of evidence that the SM is incomplete; the SM contains neutrinos that are massless due to the absence of Yukawa couplings, however, it has long been observed that neutrinos have very small masses with recent data supporting this [39, 40]. Though quark mixing in the CKM matrix is very small, analogous mixing in the neutrino sector is very large. This can be seen pictorially in Figure 2.7, where each of the colours represents a different flavour eigenstate of the LH neutrinos, and each colours' size represents how much of each flavour eigenstate is present in the presented m_1, m_2 and m_3 mass eigenstates. Note that the ν_3 state that has mass m_3 does contain a small admixture of ν_e. The absolute neutrino mass scale is not known, and experimentally,
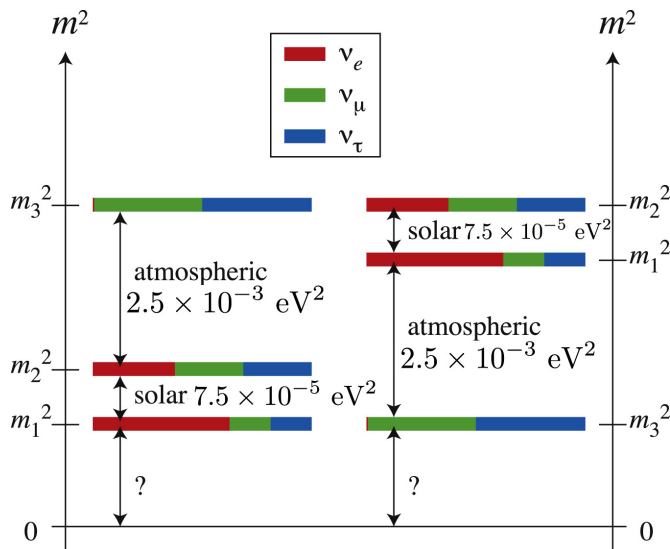
Figure 2.7: Light, left-handed neutrino masses and mixing by proportion. So-called 'normal ordering' of masses displayed on the left, with 'inverted ordering' on the right. Coloured bars show the proportions of each flavour eigenstate contained within the mass eigenstates. '?' signifies that the absolute scale neutrino mass is not known.

we measure the mass-squared differences detailed in Equation (2.62). Neutrino masses are said to be 'normally ordered' (NO) if these differences are both positive, i.e. the heaviest eigenstate contains the greatest fraction of ν_τ, analogously to the tau being the heaviest charged lepton. Ordering that has m_3 as the smallest neutrino mass, which is still possible in the context of current data, is called 'inverted ordering' (IO). Normal ordering is slightly preferred by the current global fit to neutrino data [39]. The definition of the neutrino mass-squared differences that are measured by neutrino

experiments are given in Equation (2.62).

$$\Delta m_{21}^2 = m_2^2 - m_1^2$$
$$\Delta m_{31}^2 = m_3^2 - m_1^2$$

(2.62)

There is also a cosmological limit on the neutrino mass sum from structure formation, though this limit does come along with a small dependence on the assumed cosmological model [40]:

$$\sum_{i=1,2,3} m_i < 0.23\text{eV}$$

(2.63)

The leptonic mixing given as coloured bars in Figure 2.7 is independent of ordering, but if we were to construct a leptonic mixing matrix here analogous to that for the quarks, then the mixing angles would depend on whether we assume NO or IO for our neutrinos. Through the advent of the seesaw mechanism which can be used to explain neutrino masses, it is also thought that there is a possible role for neutral leptons to play in Big Bang Baryogensis, and this will be discussed in much detail in a subsequent chapter.

2.7.5   Lepton magnetic moments

Any fundamental particle charged under electromagnetism will have a magnetic dipole moment along the direction of its spin. Magnetic moments of leptons are derived by considering their interactions with magnetic fields. For such spin-1/2 particles, this will be of the following form:

$$\vec{\mu} = g_{\vec{s}} \left(\frac{q}{2m} \right) \vec{s}$$

(2.64)

$g_{\vec{s}}$ is the dimensionless Landé g-factor, $\vec{\mu}$ is the magnetic moment vector and $\vec{s}$ is the particle's spin. The classical result of tree-level QED Feynman diagrams is that $g_{\vec{s}} = 2$, resulting in the so-called 'Dirac' magnetic moment. Quantum corrections to this result differ for muons and electrons, and deviate from the tree-level result by fractions of a percent. Deviations from the Dirac moment are called anomalous magnetic moments as defined in Equation (2.65).

$$\vec{\mu} = \left(1 + a \right) \left(\frac{q}{2m} \right) \vec{s}, \qquad a = \frac{g_{\vec{s}} - 2}{2}$$

(2.65)

The first term in $\vec{\mu}$ is the Dirac part, and the second piece is the anomalous Pauli magnetic moment, with the dimensionless a commonly referred to as the anomaly, which shows up as a purely quantum correction. a is also commonly represented as $(g-2)_\mu$.

Anomalous muon moment

(a) Dirac contribution   (b) Schwinger contribution
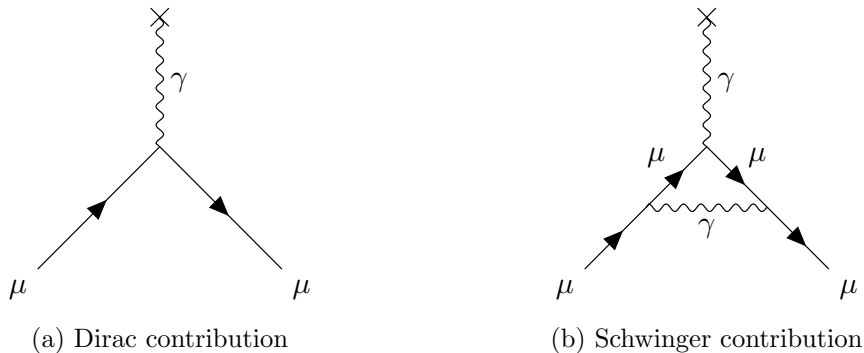
Figure 2.8: Feynman diagrams that contribute to the muon $g_{\vec{s}}$ factor.

For the magnetic moment of the muon, Feynman diagrams that contribute at leading and next-to-leading order are given in Figure 2.8, where 2.8a shows the famous Dirac contribution which gives $g_{\vec{s}} = 2$, and 2.8b is the lowest-order radiative correction first calculated (for the electron) by Schwinger [41]. The most-recent SM prediction of the anomalous muon moment takes into account QED calculations at high loop orders and QCD corrections below the confinement scale from lattice simulations [42–60]. Such incredibly precise calculations lead to an expression for the muon anomaly that is accurate to one part in 10^{10} as per Equation (2.66).

$$a_\mu^{SM} = 2.00116591810(43) \tag{2.66}$$

That being said, the experimental measurement of $(g-2)_\mu$ is just as precise, and for some time there has been a discrepancy between the theoretical calculation and experimental data below the per-mille level [60, 61]. We express the difference between experimental results and SM predictions as Δa_μ [42–65]:

$$\Delta a_\mu = a_\mu^{\text{exp}} - a_\mu^{\text{SM}} = (26.1 \pm 8.0) \times 10^{-10} \tag{2.67}$$

After the recent theoretical consensus [60], this unresolved tension circa 3σ persists.

Anomalous electron moment

More recently, a discrepancy has been seen in precision data from the electron magnetic moment, which was calculated from a measurement of the fine-structure constant of electromagnetism made with Caesium nuclei [66], which shows a 2.5σ deviation from the very precise SM prediction [67–69]. This discrepancy is summarised by Δa_e as shown in Equation (2.68).

$$\Delta a_e = a_e^{\text{exp}} - a_e^{\text{SM}} = \left(-0.88 \pm 0.36 \right) \times 10^{-12} \tag{2.68}$$

From a theoretical side, it would be aesthetically pleasing to find a joint solution which is able to explain both the electron and muon magnetic moments simultaneously, but the deviations being in opposing directions make this difficult.

2.8   Moving beyond

It is clear from the issues discussed that the SM is not complete, and must be an effective theory that originates from some more complete theory manifest at high scales. Any new paradigm that supersedes the SM must reduce to it at low scales to reproduce the swathe of phenomena that the SM correctly predicts. In the next chapter, we introduce and discuss theories of physics beyond the SM; these are models that aim to explain one or more of the aforementioned issues, and may have other desirable qualities. Phenomenology is needed to determine whether these novel and optimistic theories are better candidates to explain nature at the fundamental level.

Chapter 3

Beyond the Standard Model Physics

It is clear, due to evidence discussed in the previous chapter, that we need to move beyond the Standard Model, with the intent to construct a complete theory of physics that can explain some of the open questions in fundamental physics. In this chapter, we review some such models that attempt to solve some problems by introducing new fields and symmetries.

3.1   Approaches to BSM physics

Any experimentally viable theory that one constructs must somehow incorporate the SM, and must reproduce the observed low-scale physics that we attribute to the SM. There are two philosophies to investigating new theories of physics at the fundamental level:

- Bottom-up: Using effective operators that could originate from a range of different high-energy particles, commonly referred to as effective field theories (EFTs). Higher mass dimension (> 4) operators [70, 71] describe non-renormalisable interactions that originate from new degrees of freedom at high scales. An example EFT is the Fermi theory of weak interactions where W and Z bosons are integrated out to provide a schematic picture of low-scale physics.

- Top-down: Creating and investigating concrete models of ultra-violet physics that can be reduced to an effective Standard Model at low scales through symmetry-breaking or integrating out particles with large masses e.g. Minimal Supersymmetric Standard Model (MSSM), Grand Unified Theories etc.

There is much interesting physics to be discussed concerning effective field theories and the bottom-up approach, but for the remainder of this thesis, we concern ourselves with the top-down paradigm. Unified theories, which combine symmetries and representations of SM fields at high scales, fall into this category. Studying the phenomenology of

such theories allows one to make firm statements about the viability of a given theory, and can inform research into related models and emerging fields. The remainder of this chapter is organised as follows: Section 3.2 details the seesaw mechanism of neutrino mass generation, Section 3.3 is an introduction to vector-like fermions, Section 3.4 discusses Supersymmetry, then Section 3.5 details the most minimal viable supersymmetric model; the Minimal Supersymmetric Standard Model, and finally Section 3.6 introduces the concept of a unified high-scale theory.

3.2 The seesaw mechanism

Charged leptons in the SM acquire masses through the usual Yukawa coupling that couples a left-handed lepton to a right-handed lepton through the Higgs. Such a term cannot be constructed for the neutral leptons. A simple way to introduce neutrino mass terms is to add one or more right-handed neutrinos, enabling Dirac Yukawa coupling terms for neutral leptons [72, 73]. By themselves, these Yukawa couplings are sufficient to explain the masses of LH neutrinos, however, to do so would require couplings $\mathcal{O}(10^{-11})$, considered theoretically unnatural as this is much smaller than the smallest Yukawa in the SM, that of the electron which is $\mathcal{O}(10^{-6})$.

The new RH neutrinos are gauge singlets and are Majorana fermions, their own antiparticles. Since they are singlets under the SM gauge group and are not protected by other symmetries, these Majorana particles can be arbitrarily heavy, with their masses being free parameters of the theory.

Through the interplay between Dirac Yukawa couplings and RH neutrino Majorana masses, the left-handed SM neutrinos acquire small effective Majorana masses via the seesaw mechanism, of which there are a number of variations. The Type-I seesaw was the first to be created [72–76], and others such as Type-II [77, 78], Type-III [79, 80] and the Inverse Seesaw [81–83] have also been proposed. For simplicity and relevance to the work presented in later chapters, we concentrate exclusively on the Type-I seesaw mechanism here. Note that in this section, we will utilise Weyl notation for fermions, as it allows us to more easily distinguish between left- and right-handed fields. A detailed description of the differences between Weyl notation and the Dirac interpretation is presented in Appendix A.

3.2.1 Type-I seesaw

With the addition of n RH neutrinos, N_R, extra terms become apparent in the Lagrangian. Such terms are given in Equation (3.1), and are collected into the neutrino mass Lagrangian; $\mathcal{L}_\nu$.

$$\mathcal{L}_\nu = -(Y_\nu)_{ij} \overline{L}_{Li} \widetilde{\phi} N_{Rj} - \frac{1}{2}(M_R)_{ij} \overline{N_{Ri}^c} N_{Rj} + H.c. \tag{3.1}$$

M_R is an $n \times n$ matrix and Y_ν has dimensions $3 \times n$, with i, j flavour indices as appropriate, $\widetilde{\phi} = i\sigma_2\phi^*$, and σ_2 is the second Pauli matrix. A superscript c on a field denotes the CP-conjugate of said field. The first term in Equation (3.1) is a Dirac Yukawa coupling analogous to the charged leptons, which is promoted to a mass term once electroweak symmetry is broken and ϕ has acquired a VEV, i.e. $m_D = Y_\nu v/\sqrt{2}$. The second term is the so-called Majorana mass term [84], explicitly available for the RH neutrinos only. The eigenvalues of M_R can live at the Planck scale since they are not protected by any symmetry.

From the Dirac and Majorana mass terms in Equation (3.1), we can construct a mass term in the neutrino Lagrangian involving both the left- and right-handed neutrinos as per Equation (3.2), where the full neutrino mass matrix is sandwiched by the fermion fields, and flavour indices are omitted for brevity.

$$M_\nu = \begin{pmatrix} \overline{\nu_L} & \overline{N_R^c} \end{pmatrix} \begin{pmatrix} 0 & m_D \\ (m_D)^T & M_R \end{pmatrix} \begin{pmatrix} \nu_L^c \\ N_R \end{pmatrix} \tag{3.2}$$

The expression in Equation (3.2) applies at high scales when the RH neutrinos are present in the theory. In this regime, there is no mass term which couples together the LH neutrinos; the first element of the full matrix is a texture zero. When the theory is carried to low scales through RG running, the RH neutrinos must be integrated out and a Majorana mass term for LH neutrinos is generated effectively. The light masses are determined by diagonalising the full mass matrix under the assumption that $M_R \gg m_D$[1]. This diagonalisation gives an expression for the light neutrino masses (Equation (3.3)) known as the 'seesaw formula'.

$$m_\nu = v^2 Y_\nu^T (M_R)^{-1} Y_\nu \tag{3.3}$$

Where the light neutrino masses are precisely eigenvalues of the matrix m_ν. If, as in the Type-I seesaw, the RH neutrinos are very heavy[2], the LH neutrino masses are suppressed by this high scale, providing a natural explanation for the smallness of neutrino masses in the Standard Model. The seesaw formula is represented by the Feynman graph in Figure 3.1. The diagram in its entirety represents for LH neutrinos what the centre section does for RH neutrinos; once the heavy fermions have been integrated out and the Higgs acquires its vacuum expectation value, the diagram becomes an effective Majorana mass insertion for the SM neutrinos. For the Type-I seesaw to be phenomenologically viable, the number of RH neutrinos n must be at least two. A minimal model with two Majorana fermions can reproduce neutrino phenomenology and comes along with one eigenvalue of m_ν being zero, which corresponds to a vanishing mass for the lightest SM neutrino. This is still allowed with respect to current data

---

[1]This assumption is reasonable if we require natural Yukawa couplings i.e. that the eigenvalues of Y_ν are $\mathcal{O}(1)$.

[2]The RH neutrino masses are well approximated as the eigenvalues of M_R, as $m_D \ll M_R$.
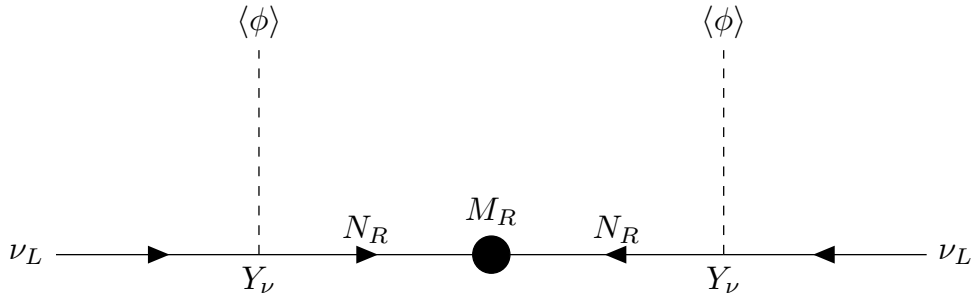
Figure 3.1: Feynman diagram representation of how LH neutrinos acquire masses in the Type-I seesaw mechanism. The dot in the centre represents the mass-insertion of the RH Majorana mass, which is only possible when N_R is a Majorana fermion.

[39]. A scenario where all LH neutral leptons are massive requires three RH Majorana neutrinos.

3.2.2 Leptonic mixing

Yukawa couplings in the neutrino sector can give rise to leptonic mixing in the same way that quark mixing arises because up- and down-type quark Yukawa matrices cannot be diagonalised simultaneously by a single unitary transformation. The charged lepton Yukawa and light neutrino mass matrices are diagonalised in Equation (3.4):

$$Y'_e = (U_{eL})^\dagger Y_e U_{eL} \,, \qquad m'_\nu = (U_{\nu L})^T m_\nu U_{\nu L} \tag{3.4}$$

Where primed matrices are diagonal. Analogously to the quark sector, the mixing in the leptonic sector is described by a unitary matrix composed of a product of these basis transformations. For the lepton sector, this is the Pontecorvo-Maki-Nakagawa-Sakata (PMNS) matrix [85, 86].

$$U_{\mathrm{PMNS}} = (U_{eL})^\dagger U_{\nu L} \tag{3.5}$$

In the basis that has a diagonal charged lepton Yukawa matrix, the PMNS matrix details how to transform from the flavour basis (of pure interacting states) to the mass eigenbasis and hence parameterises neutral lepton mixing. A representation of this basis mismatch is given in Equation (3.6).

$$|\nu_\alpha\rangle = \sum_i (U_{\mathrm{PMNS}})_{\alpha i} |\nu_i\rangle \tag{3.6}$$

Where $\alpha = 1, 2, 3$, $i = e, \mu, \tau$, ν_α denotes a neutrino in the mass eigenbasis and ν_i represents fields in the flavour basis. The PMNS matrix can be fully determined by three angles and a further three phases, and similarly to the CKM matrix, it can be

decomposed to make this description apparent.

$$U_{\text{PMNS}} = \begin{pmatrix} 1 & 0 & 0 \\ 0 & \cos\theta_{23}^L & \sin\theta_{23}^L \\ 0 & -\sin\theta_{23}^L & \cos\theta_{23}^L \end{pmatrix} \begin{pmatrix} \cos\theta_{13}^L & 0 & \sin\theta_{13}^L e^{i\delta_L} \\ 0 & 1 & 0 \\ -\sin\theta_{13}^L e^{i\delta_L} & 0 & \cos\theta_{13}^L \end{pmatrix} \begin{pmatrix} \cos\theta_{12}^L & \sin\theta_{12}^L & 0 \\ -\sin\theta_{12}^L & \cos\theta_{12}^L & 0 \\ 0 & 0 & 1 \end{pmatrix}$$

$$\times \text{Diag}\left(1, e^{i\alpha_{21}/2}, e^{i\alpha_{31}/2}\right)$$

$$(3.7)$$

The irreducible phases shown in the second line of Equation (3.7) are the so-called 'Majorana phases' and vanish in the case that neutrino masses are purely explained by Dirac Yukawa couplings. The δ_L phase is analogous to the CP-violating phase present in the CKM matrix. Because new physics is needed to explain the observed patterns of the PMNS matrix, neutrino mixing forms compelling evidence for physics beyond the SM. Using a given neutrino Yukawa matrix and the Type-I seesaw mechanism, one can predict the mixing patterns parameterised by the PMNS matrix.

To summarise, the Type-I seesaw mechanism can readily accommodate the observed masses and mixings of neutrinos through the introduction of a small number of gauge singlet right-handed neutrinos. It can be incorporated easily into more complete theories and is a minimal, well-motivated extension of the Standard Model.

3.3   Vector-like fermions

The flavour puzzle in the SM could also lead one to question why are there *only* three families of quarks and leptons in the SM. Adding a chiral fourth family of fermions to the Standard Model is constrained through four avenues:

- Direct searches via production at hadron colliders

- Flavour observables affected by the introduction of new fields into loop diagrams

- Electroweak precision observables are affected by new particles entering into loop processes

- Indirect searches through Higgs production and decay processes that can proceed via fermion loops (eg. $gg \to h$)

In a recent review of the SM with a fourth, chiral family of fermions, it is concluded that this paradigm is excluded by around five standard deviations, due to numerous of the reasons alluded to above [87].

However, it is possible to construct a theory with so-called 'vector-like' fermions that do not suffer from the majority of these constraints, although they are still subject to collider searches. Left- and right-handed components of a vector-like fermion couple identically to SM gauge groups. In Table 3.1, we introduce an example vector-like quark

Field	Representation/Charge		
	$SU(3)_C$	$SU(2)_L$	$U(1)_Y$
$Q_4 = \left(t', b'\right)^T$	**3**	**2**	$+1/3$
$\widetilde{Q}_4 = \left(\widetilde{t'}, \widetilde{b'}\right)^T$	**3**	**2**	$+1/3$

Table 3.1: Example vector-like quark $SU(2)_L$ doublet

$SU(2)_L$ doublet to the SM: Q_4 and $\widetilde{Q}_4$ transform like doublets under $SU(2)_L$, just like the doublet of left-handed top and bottom quarks. In this simple example, the new vector-like states acquire only a vector-like mass: $M_{Q_4}\overline{Q}_4\widetilde{Q}_4$. Note that Lagrangian mass term respects SM symmetries and is renormalisable, but cannot originate from coupling with the Higgs field due to the requirement for gauge invariance. Because this mass term is not protected by any symmetry, M_{Q_4} can be large without causing issues. Since these mass terms are gauge invariant and do not require coupling to the SM Higgs, instead we may take such masses to be free parameters.

It is possible for vector-like fermions to mix with their SM counterparts, provided they have the same quantum numbers. Such mixing can contribute to flavour observables and induce flavour-violating lepton decays[3] like $\mu \to e\gamma$, which are severely constrained by null results from various experiments [88], and the phenomenology of vector-like fermions has been the subject of much recent work [89–92]. Some possibilities for vector-like fermions are presented in Chapter 6.

3.4 Supersymmetry

The concept of supersymmetry (SUSY) has been a topic of much research for the past 50 years and is still considered to be a promising avenue for BSM physics. In this section, we build up to a phenomenological model of SUSY by first outlining the core concept, then considering the Minimal Supersymmetric Standard Model (MSSM), the most compact viable SUSY extension of the SM. Today, the main motivation for pursuing phenomenological SUSY is the elegant solution that the framework presents to the Higgs mass hierarchy problem, but originally, SUSY was proposed as a purely theoretical mechanism [93, 94].

3.4.1 An extension of spacetime symmetries

At its core, supersymmetry is a symmetry that relates fields with integer spin quantum numbers to half-integer spin fields and vice versa. It is the maximal extension of the Poincaré algebra of spacetime symmetries, and the generators $\hat{Q}, \hat{Q}^\dagger$ of supersymmetry

---

[3]Provided we also allow for vector-like leptons along with the quarks considered in the simple example.

are themselves anti-commuting spinors [36].

$$\hat{Q}|\psi\rangle = |\varphi\rangle \,, \qquad \hat{Q}|\varphi\rangle = |\psi\rangle \tag{3.8}$$

φ denotes a scalar and ψ is a fermion. For the generators to interact properly with other spacetime symmetries, they must obey the following rules put forward by the Coleman-Mandula theorem and its extensions [95, 96], where $\hat{P}^\mu$ is the generator of four-momentum spacetime transformations[4]:

$$\{\hat{Q}, \hat{Q}^\dagger\} = \hat{P}^\mu \,, \tag{3.9}$$

$$\{\hat{Q}, \hat{Q}\} = \{\hat{Q}^\dagger, \hat{Q}^\dagger\} = 0 \,, \tag{3.10}$$

$$[\hat{P}^\mu, \hat{Q}] = [\hat{P}^\mu, \hat{Q}^\dagger] = 0 \tag{3.11}$$

Spinor indices on the generators and fields are suppressed here for simplicity. Single-particle states of a SUSY theory reside in irreducible representations of the SUSY algebra called supermultiplets, and each supermultiplet contains both integer spin, and half-integer spin degrees of freedom which are described as one another's superpartners [36]. Because $\hat{Q}, \hat{Q}^\dagger$ commute with gauge symmetry transformation generators, members of the same supermultiplet must reside in the same representation of any gauge symmetry groups of the theory, regardless of their differing spin quantum numbers. It can be shown that any given supermultiplet must contain the same number of integer spin and half-integer spin degrees of freedom. The most minimal supermultiplet that can be constructed consists of a single Weyl fermion (with two helicity states) and a complex scalar field (with two real degrees of freedom);

$$\widehat{\Phi} = \begin{pmatrix} \varphi \\ \widetilde{\varphi} \end{pmatrix} = \begin{pmatrix} \varphi \\ \psi \end{pmatrix} \tag{3.12}$$

where $\widetilde{\varphi}$ denotes the superpartner of φ. Supermultiplets are generally represented by a hatted field, and Equation (3.12) describes a chiral supermultiplet. Another SUSY field that we consider is the vector[5] supermultiplet, which is composed of a massless spin-1 vector gauge boson with two helicity states and its superpartner; a massless Weyl fermion, again with two possibilities for its helicity. These so-called gauginos must also transform in the adjoint representations of gauge symmetries, just as the massless vector bosons do.

$$\widehat{V} = \begin{pmatrix} V \\ \widetilde{V} \end{pmatrix} \tag{3.13}$$

---

[4]A consequence of the Coleman-Mandula theorem is that one cannot non-trivially extend the Poincaré group with Lie groups.

[5]Also known as a 'gauge supermultiplet' in some literature

We represent the gauge boson by V and the gaugino by $\widetilde{V}$. There are possibilities for other supermultiplets in a renormalisable theory, however, these can always be constructed from linear combinations of chiral and vector supermultiplets. The SUSY format we present here, composed of only one set of SUSY generators $\hat{Q}, \hat{Q}^\dagger$, and which has only chiral and vector supermultiplets is known as '$\mathcal{N} = 1$ supersymmetry', with $\mathcal{N}$ denoting the number of supersymmetries. Extended SUSY with $\mathcal{N} > 1$ and copies of the generators $\hat{Q}$ and $\hat{Q}^\dagger$ are theoretically well-known, but not relevant to the content of this thesis. A more complete theoretical overview of supersymmetry is included in Martin's primer [36].

3.4.2 Revisiting the Higgs hierarchy

We have already seen that the Higgs boson mass-squared (m_h^2) receives quantum corrections from every field that couples in some way to the Higgs field. This makes the introduction of any new heavy particles that couple to the Higgs theoretically undesirable; why is the Higgs VEV so small if it gives mass to very heavy fields? This problem is resolved in a SUSY theory when we introduce a chiral supermultiplet (for example), in an elegant way. The one-loop correction due to a Dirac fermion of mass m_f and

(a) Fermion correction

(b) Scalar correction
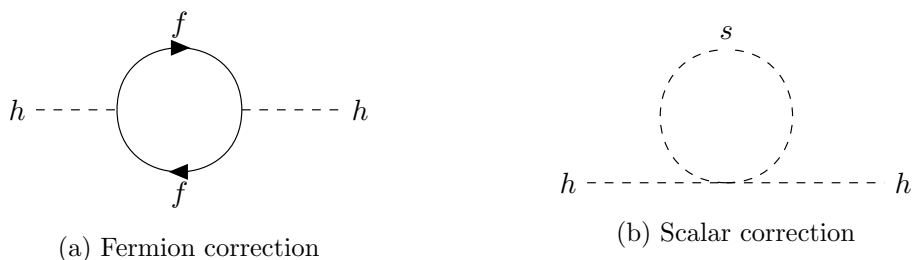
Figure 3.2: Corrections to the SM Higgs two-point function from massive fermions and scalars. In principle, these particles could be superpartners and reside together in a chiral supermultiplet.

Yukawa coupling to the Higgs of y_f yields a correction to the SM Higgs mass-squared as per Equation (2.61), as represented by Figure 3.2a. The corresponding correction due to a new scalar particle (such as a superpartner of the fermion f) is given in Equation (3.14) and is displayed pictorially in Figure 3.2b. Ellipses represent smaller terms that enter at higher orders.

$$\Delta m_h^2\big|_s = +\frac{\lambda_s}{16\pi^2}\left[\Lambda_{NP}^2 - 2m_s^2 \ln\left(\frac{\Lambda_{UV}}{m_s}\right) + \dots\right] \tag{3.14}$$

One can postulate that Λ_{NP} is an unphysical regulator that can be eliminated by dimensional regularisation, however the pieces proportional to m_s^2 and m_f^2 cannot be eliminated in a similar manner. Note that this problem can also arise even if the Higgs does not couple directly to the new fields but instead interacts with the Higgs via another particle. If the Higgs is truly a fundamental scalar and new physics is present

above the EW scale, either none of this new physics couples to the Higgs or some striking cancellation is required.

Supersymmetry provides a very elegant solution to this problem: In a SUSY extension of the SM, there exist two complex scalars for each fermionic degree of freedom. Because these fermions and scalars reside in chiral supermultiplets, their Higgs couplings obey the relationship $\lambda_s = |\lambda_f|^2$, and hence contributions to the Higgs mass-squared from Equations (2.61) and (3.14) necessarily cancel [97–100]. In fact, SUSY ensures cancellations of all such contributions to m_h^2 beyond one-loop order; incredibly, this means that in a BSM theory where SUSY is respected, this theoretical problem is resolved and the Higgs mass is correctly predicted. This provides a striking motivation for incorporating SUSY into a BSM theory; any new field introduced at or above the TeV scale will also come with a superpartner, and the Higgs mass will remain stable.

3.5   The Minimal Supersymmetric Standard Model

The way in which we construct a viable SUSY model is different to adding extra fields and symmetries as in a typical BSM scenario; in any SUSY extension of the SM, every fundamental field resides in either a chiral or vector supermultiplet. It is also clear that left- and right-handed chiralities of fermion must reside in different supermultiplets as they transform differently under electroweak theory $SU(2)_L \times U(1)_Y$. Because they exist in chiral supermultiplets, bosonic partners of the fermions must be spin-0 scalars rather than vector bosons.

Quark superpartners are called 'squarks', for leptons they are 'sleptons' and the collective term for fermion superpartners is 'sfermions'. Furthermore, the partner for a left-handed quark is not the same field as the partner for a right-handed quark of the same flavour: For example, the left-handed up quark's (u_L) partner is the left-handed up squark $\widetilde{u}_L$, where the handedness refers not to the spin-0 squark but to its SM partner. Note that because the quarks and squarks live in the same supermultiplet, their gauge interactions are identical.

It is also clear that the Higgs must reside in a chiral supermultiplet as it is spin-0, however, if we have just one supermultiplet for the Higgs sector this would come along with an electroweak gauge anomaly. Conditions for EW gauge anomalies to vanish include $\mathrm{Tr}[T_3^2 Y] = \mathrm{Tr}[Y^3] = 0$, which is miraculously satisfied in the SM[6]. However, if we introduce a fermionic superpartner for the complex Higgs field this condition is spoiled: Traces in the condition run over all Weyl fermions in the theory, and the new 'Higgsino' superpartner must be an $SU(2)_L$ doublet with $Y = 1/2$ or $Y = -1/2$ hypercharge; for either scenario, a non-zero contribution will be made and the cancellation condition will no longer hold. This unfortunate circumstance can be

---

[6]T_3 is the third component of isospin, i.e. the eigenvalue of the third transformation matrix generator of $SU(2)_L$ for a given field. Y is the $U(1)_Y$ hypercharge. The trace runs over all Weyl fermion degrees of freedom in the theory.

avoided with the addition of a second doublet, with the opposite hypercharge to the first. The chiral supermultiplets and their components in the MSSM, along with their transformation properties under the SM gauge groups, are listed in Table 3.2. Family indices are omitted for simplicity on the quarks and leptons. Due to their vector nature,

Fields		Components		Representation/Charge		
		Spin-0	Spin-1/2	$SU(3)_C$	$SU(2)_L$	$U(1)_Y$
squarks, quarks	$\widehat{Q}$	$(\widetilde{u}_L, \widetilde{d}_L)$	(u_L, d_L)	**3**	**2**	1/6
	$\widehat{U}$	$\widetilde{u}_R$	u_R	**3**	**1**	$-2/3$
	$\widehat{D}$	$\widetilde{d}_R$	d_R	**3**	**1**	1/3
sleptons, leptons	$\widehat{L}$	$(\widetilde{e}_L, \widetilde{\nu}_L)$	(e_L, ν_L)	**1**	**2**	$-1/2$
	$\widehat{E}$	$\widetilde{e}_R$	e_R	**1**	**1**	1
Higgs, higgsinos	$\widehat{H}_u$	(H_u^+, H_u^0)	$(\widetilde{H}_u^+, \widetilde{H}_u^0)$	**1**	**2**	1/2
	$\widehat{H}_d$	(H_d^0, H_d^-)	$(\widetilde{H}_d^0, \widetilde{H}_d^-)$	**1**	**2**	$-1/2$

Table 3.2: Chiral supermultiplets in the MSSM. Spin-0 components are complex scalars and spin-1/2 fields are two-component Weyl fermions.

the gauge bosons of the SM are now promoted to reside in vector supermultiplets. These supermultiplets are detailed in Table 3.3. These two sets of supermultiplets form the

Fields		Components		Representation/Charge		
		Spin-1	Spin-1/2	$SU(3)_C$	$SU(2)_L$	$U(1)_Y$
gluon, gluino	$\widehat{G}$	g	$\widetilde{g}$	**8**	**1**	0
W bosons, winos	$\widehat{W}$	(W^1, W^2, W^3)	$(\widetilde{W}^1, \widetilde{W}^2, \widetilde{W}^3)$	**1**	**3**	0
B boson, binos	$\widehat{B}$	B^0	$\widetilde{B}^0$	**1**	**1**	0

Table 3.3: Vector supermultiplets in the MSSM; spin-1 fields are vector bosons and spin-1/2 particles are Weyl fermions known as 'gauginos'.

entirety of the MSSM's field content. From this construction we can already infer that if SUSY exists in nature, it *must* be broken: Fields that reside in the same supermultiplet will have identical masses in a theory where supersymmetry is preserved, hence we would expect to see not just fermions but also scalars at the various quark and lepton masses. This is not the case as we do not observe scalar particles at these masses in collider experiments. Therefore, SUSY in the MSSM must be somehow broken. SUSY-breaking in the MSSM is discussed in Section 3.5.2.

3.5.1 The MSSM superpotential

The superpotential of a SUSY theory contains all of the non-kinetic terms of the theory's Lagrangian, and parameterises Yukawa couplings and interactions between Higgs doublets of the theory. The superpotential of the MSSM is given in Equation (3.15).

$$W_{\mathrm{MSSM}} = Y_u \widehat{\overline{U}} \widehat{Q} \widehat{H}_u - Y_d \widehat{\overline{D}} \widehat{Q} \widehat{H}_d - Y_l \widehat{\overline{E}} \widehat{L} \widehat{H}_d + \mu \widehat{H}_u \widehat{H}_d \qquad (3.15)$$

All hatted objects here are chiral superfields as per Table 3.2. Such a superpotential could be expanded in terms of the fields that inhabit the supermultiplets, and an analogue of the above equation could be easily written for just the scalar components. The final, so-called 'μ term' in Equation (3.15) is a Higgs boson mass term analogue. It is unique as other terms that couple together $\widehat{H}_u$ and $\widehat{H}_d$ are forbidden by requiring that the superpotential be holomorphic in scalar fields (and hence the chiral supermultiplets presented in Equation (3.15)). Yukawa couplings will determine the masses of Standard Model fermions at low scales and also will contribute toward sfermion masses, though the vast majority of superpartner mass is derived from SUSY-breaking terms in the soft-breaking Lagrangian.

3.5.2 Soft SUSY-breaking

If we break supersymmetry dynamically, then the masses of scalars in the theory will receive large quantum corrections at the breaking scale. Dynamical breaking will also give rise to colour- and charge-breaking vacua. Therefore we must break SUSY 'softly' [98], i.e. rather than introducing VEVs for some of the scalars or fermionic states forming a condensate, instead one simply introduces terms which break the symmetry by hand, and ensures that such terms only have positive mass dimension [36]. Many mechanisms of SUSY-breaking are known including, but not limited to gauge-mediated [101], gravity-mediated [102, 103] and anomaly-mediated SUSY-breaking [104, 105]. An advantage of the MSSM is that a particular breaking mechanism is not assumed, but rather the Lagrangian includes all terms that hold to gauge invariance and renormalisability, but do not necessarily respect SUSY. This soft-breaking Lagrangian is used as a method of parameterising ignorance in the breaking mechanism, and in this way we introduce SUSY-breaking terms explicitly[7]. We can split MSSM Lagrangian into terms which respect supersymmetry ($\mathcal{L}_{\mathrm{SUSY}}$) and those that do not ($\mathcal{L}_{\mathrm{soft}}$):

$$\mathcal{L} = \mathcal{L}_{\mathrm{SUSY}} + \mathcal{L}_{\mathrm{soft}} \qquad (3.16)$$

If the largest scalar mass is of the scale m_{soft}, then all additional corrections to Higgs mass-squared parameters from SUSY-breaking must vanish in the limit $m_{\mathrm{soft}} \to 0$.

---

[7]The MSSM still needs $\lambda_s = |\lambda_f|^2$ to provide a solution to the Higgs hierarchy problem.

These additional corrections are of the form given in Equation (3.17).

$$\Delta m_h^2|_{\text{soft}} = m_{\text{soft}} \left[\frac{\lambda}{16\pi^2} \ln\left(\frac{\Lambda_{NP}}{m_{\text{soft}}}\right) + \dots \right] \tag{3.17}$$

λ here represents a generic dimensionless coupling and ellipses represent smaller, higher-order corrections. The SUSY spectrum is then determined through a combination of SM masses and soft masses, but it should be noted that soft masses cannot be too large according to Equation (3.17) lest we encounter a new hierarchy problem. The measured SM Higgs mass points toward an MSSM with superpartner masses around the TeV scale, and so soft mass parameters should also be close to this scale. The soft-breaking Lagrangian includes the following terms, where tildes denote superpartners of SM fields:

$$\begin{aligned}
\mathcal{L}_{\text{soft}} = &-\frac{1}{2}\left(M_3\widetilde{g}\widetilde{g} + M_2\widetilde{W}\widetilde{W} + M_1\widetilde{B}\widetilde{B} + c.c.\right) \\
&-\left(A_u\widetilde{\overline{U}}\widetilde{Q}H_u - A_d\widetilde{\overline{D}}\widetilde{Q}H_d - A_e\widetilde{\overline{E}}\widetilde{L}H_d + c.c.\right) \\
&-M_Q^2\widetilde{Q}^\dagger\widetilde{Q} - M_L^2\widetilde{L}^\dagger\widetilde{L} - M_U^2\widetilde{\overline{U}}\widetilde{\overline{U}}^\dagger - M_D^2\widetilde{\overline{D}}\widetilde{\overline{D}}^\dagger - M_E^2\widetilde{\overline{E}}\widetilde{\overline{E}}^\dagger \\
&-M_{H_u}^2 H_u^* H_u - M_{H_d}^2 H_d^* H_d - \left(bH_uH_d + c.c.\right)
\end{aligned} \tag{3.18}$$

Gauge indices have been suppressed here for simplicity. M_1, M_2 and M_3 are the gluino, wino and bino masses respectively. A_u, A_d and A_e are 3×3 scalar trilinear coupling matrices with canonical mass dimension of 1, these are SUSY-breaking as we cannot construct analogous terms for SM fermions. Each of the M^2 matrices is 3×3 with dimensions of mass-squared, and the final line is the SUSY-breaking terms for the two Higgs doublets present in the model. Many parameters are introduced here, which come with a large degree of arbitrarity, but none of these parameters should be much more than 10^3GeV or 10^6GeV^2, whichever is relevant. The large number of parameters can to some extent be reduced using the concept of Grand Unified Theories (GUTs) which we touch on in Section 3.6.

Electroweak symmetry-breaking in the MSSM

EWSB must be altered in the MSSM due to the additional Higgs doublet, but the theory should still predict a neutral scalar around 125 GeV to conform with the results seen at the LHC in 2012 [4, 5]. The scalar potential of the theory is in principle quite complicated but we can ignore terms from all sfermions and concentrate only on the scalars from $\widehat{H}_u$ and $\widehat{H}_d$ that acquire VEVs. For electromagnetism to remain an unbroken symmetry we must require that the charged components of the $SU(2)_L$ doublets have zero VEVs; $\langle H_u^+ \rangle = \langle H_d^- \rangle = 0$. The scalar potential under examination

is given in Equation (3.19).

$$V = \left(\mu^2 + M_{H_u}^2\right)|H_u^0|^2 + \left(\mu^2 + M_{H_d}^2\right)|H_d^0|^2 - \left(bH_u^0 H_d^0 + c.c.\right)$$
$$+ \frac{1}{8}\left(g^2 + g'^2\right)\left(|H_u^0|^2 - |H_u^0|^2\right)^2 \tag{3.19}$$

Knowing that what we predict in the MSSM must match EWSB observables in the SM, we define $v_u = \langle H_u^0 \rangle$ and $v_d = \langle H_d^0 \rangle$. Such VEVs must then conform to the Z boson mass constraint.

$$v_u^2 + v_d^2 = v^2 = \frac{2M_Z^2}{g^2 + g'^2} \simeq (246\text{GeV})^2 \tag{3.20}$$

The ratio $\tan\beta = v_u/v_d$ is usually taken as a parameter of the MSSM, this ratio is not fixed by experiment but is heavily dependent on the mass spectrum. More information on EWSB in the MSSM is given in Martin's complete introduction [36].

3.5.3 R-parity

New interactions between SM fields and their SUSY counterparts can give rise to proton decay on very short lifetimes, due to their violating baryon (B) and lepton (L) quantum numbers. Therefore in the MSSM, we must introduce a new symmetry to curb these interactions, but allow the SUSY-preserving and SUSY-breaking couplings that we have discussed previously. This is 'R-parity' and the conserved quantum number is defined for each particle in the theory as per Equation (3.21), where s is the spin quantum number of the field under test. It is clear then, that particles within the same supermultiplet do not have the same R-parity due to their half-integer differences in their spin.

$$P_R = \left(-1\right)^{3(B-L)+2s} \tag{3.21}$$

R-parity is a discrete $\mathcal{Z}_2$ symmetry, under which all SM particles and Higgs bosons are said to be 'even'; $\left(P_R = +1\right)$ whilst all superpartners have 'odd' intrinsic R-parity $\left(P_R = -1\right)$. If this new symmetry is exactly preserved, only certain couplings are allowed between SM fields and their SUSY counterparts, and a single SUSY partner cannot decay into only SM particles. There are three important consequences of this [36]:

1. Lightest SUSY partner (LSP) must be stable. LSPs that are neutral under QED then appear to interact only gravitationally with SM particle content and hence make excellent candidates for cold dark matter [106, 107].

2. Every sparticle other than the LSP must eventually decay into a state with an odd number of LSPs (usually one).

3. At colliders such as the LHC, SUSY partners of SM fields can only be produced in even numbers.

We require that the MSSM conforms to exact R-parity conservation. This is an ad-hoc requirement from a theoretical standpoint but is well-motivated by experimental evidence and the postulation that dark matter is the LSP.

3.5.4 Gauge coupling running

Due to additional particles present starting at the TeV scale, the running of gauge couplings in the SM will be altered once superpartners become present in loops. This amendment can result in the unification of gauge couplings at some high-scale, perhaps hinting at the possibility that SM gauge symmetries originate from the breaking of a single symmetry that was conserved in the early universe. Running inverse gauge couplings (α^{-1}) are given in Figure 3.3[8]. A 'SUSY-scale', where all superpartners enter
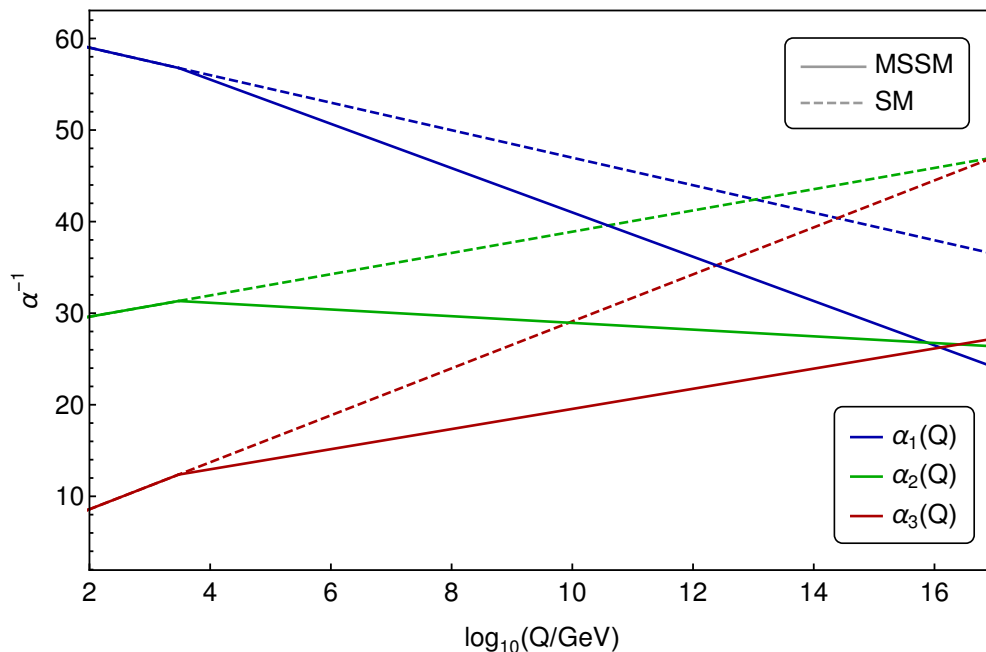
Figure 3.3: Inverse gauge coupling running in the SM and MSSM, denoted by dashed and solid lines respectively. Couplings in the MSSM unify almost exactly circa 10^{16}GeV. A common SUSY scale of 3 TeV is assumed, at which the new superpartners are assumed to enter into beta functions for the gauge couplings.

into the theory on-shell, is assumed to be 3 TeV. Modifying this scale between 1 and 10 TeV does not much alter the approximate intersection of the couplings at around 10^{16} GeV. If we assume that more new physics enters at roughly this scale, threshold corrections (which we do not consider for SUSY at this stage) can easily bend the gauge couplings to intersect exactly at some scale close to 10^{16} GeV. This could hint at something remarkable; what if our three fundamental quantum symmetries originate

---

[8]The inverse couplings are plotted for ease of comparison between the two theories.

from a single force at high scales, just as electroweak symmetry is broken at the EW scale from $SU(2)_L \times U(1)_Y$ to $U(1)_{\text{QED}}$? If some other Lie algebra can successfully accommodate the SM gauge groups and spontaneously be broken around $10^{16}\,\text{GeV}$, then such a unification of forces could be manifest.

3.6 Grand unification

A Grand Unified Theory (GUT) takes the idea of force unification at high scales and runs with it, unifying SM fields into representations of a Lie group that contains the subgroup $SU(3) \times SU(2) \times U(1)$.

$$G_{\text{GUT}} \supset SU(3)_C \times SU(2)_L \times U(1)_Y \tag{3.22}$$

GUTs aim to explain a variety of phenomena including the miraculous cancellation between electron and proton charges. They were originally were developed outside of a supersymmetric framework, though most modern interpretations that are still phenomenologically viable include some form of SUSY. The original Grand Unified Theories were the Georgi-Glashow model [108], based on $SU(5)$ symmetry, and the Pati-Salam model [109], based on $SU(4)_C \times SU(2)_L \times SU(2)_R$, where the $SU(2)_R$ is a copy of the $SU(2)_L$ in the SM that couples only to right-handed fermions, and leptons are the fourth 'colour' of $SU(4)_C$. There are also GUTs based on the larger Lie group of $SO(10)$ [110, 111], which is usually broken to $SU(5)$ or the Pati-Salam gauge group.

The charge quantisation problem of the SM (why protons have charge e and electrons have charge $-e$) is addressed in GUTs by quarks and leptons cohabiting in the same representation of G_{GUT}. The gauge group in Equation (3.22) must be rank four or greater to contain a sufficient number of degrees of freedom to encapsulate the SM gauge group. Exceptional Lie groups can also form the basis for Grand Unified Theories, but here we consider only $SU(5)$ in detail, as it is the simplest gauge group and the subject of some research presented in this thesis. The scale at which gauge coupling unification takes place is known as the Grand Unification scale, M_{GUT}.

3.6.1 SU(5)

The rank 4 gauge group of $SU(5)$ is arguably the most minimal choice for a Grand Unified Theory. It has 24 gauge bosons which reside in the **24** (adjoint) representation. The entirety of SM gauge boson content is accomodated in this representation of $SU(5)$. In the fundamental representation **5**, generators of $SU(3)_C$ and $SU(2)_L$ gauge groups are accomodated as the upper left 3×3 and lower 2×2 blocks respectively of the 5×5 $SU(5)$ generator matrices, which must be traceless. $U(1)_Y$ generators are recovered by their commutation relations with the other SM gauge groups, and the resulting arrangement is a diagonal matrix in the $SU(5)$ space: $\text{diag}(-1/3, -1/3, -1/3, 1/2, 1/2)$.

An entire generation of LH Weyl fermions in the SM transform as a $\overline{\mathbf{5}} \bigoplus \mathbf{10}$ of $SU(5)$:

$$\overline{\mathbf{5}} = \begin{pmatrix} d_r^c \\ d_b^c \\ d_g^c \\ e \\ -\nu_e \end{pmatrix}_L \qquad \mathbf{10} = \begin{pmatrix} 0 & u_g^c & -u_b^c & -u_r & -d_r \\ -u_g^c & 0 & u_r^c & -u_b & -d_b \\ u_b^c & -u_r^c & 0 & -u_g & -g_d \\ u_r & u_b & u_g & 0 & -e^c \\ d_r & d_b & d_g & e^c & 0 \end{pmatrix}_L \qquad (3.23)$$

A superscript c denotes a CP-conjugated fermion[9], and r, g and b are the different QCD colours for quarks. The sum of quantum numbers for Q, T_3 and Y, the generators of QED charge, the third component of weak isospin and weak hypercharge respectively, must vanish as the trace of any such operators acting on the $\overline{\mathbf{5}}$ and $\mathbf{10}$ must vanish. This fixes the charges of up- and down-type quarks to be what we observe in the SM, and hence provides an elegant solution to the charge quantisation issue.

In a GUT theory that reduces to the SM at low scales, the SM Higgs that breaks EW symmetry at low scales is accomodated in a $\mathbf{5}$ representation of $SU(5)$. In a SUSY GUT based on $SU(5)$ and the MSSM, the H_u doublet lives in a $\mathbf{5}$ and the other, H_d doublet resides in a $\overline{\mathbf{5}}$ representation. Along with usual $SU(2)_L$ doublets, these $SU(5)$ fields also come along with $SU(3)_C$ colour triplet scalar fields. Such colour triplets will induce proton decay as they violate both B and L quantum numbers, and we must require that they have masses around the unification scale $\mathcal{O}(M_{\text{GUT}})$ such that nucleons have acceptably long lifetimes that conform to the lack of observed proton decays at experiments. This is the so-called 'doublet-triplet splitting problem'; we need the $SU(2)_L$ doublet parts of the 5-plet to have masses around the EW scale for correct EWSB, but we also impose that the $SU(3)_C$ triplet components have masses at the GUT scale. But because these fields all live within the $SU(5)$ 5-plet, we would expect their masses to be of the same scale. This is an ongoing theoretical question in Grand Unified Theories.

The $\mathbf{24}$ representation also contains new gauge bosons that we label X and Y from the 12 additional degrees of freedom surplus to the 8+3+1 from SM gauge content. Such new gauge fields will also induce nucleon decays, and the lifetime for any proton decay in an $SU(5)$ theory must be very long indeed, hence matrix elements of Feynman diagrams that contribute to such a decay must be very suppressed. In order to reproduce the observed pattern of SM gauge groups at low scales, $SU(5)$ must be broken to the SM gauge group. This can be done in a one-stage breaking by a new Higgs field in the $\mathbf{24}$ representation, which must acquire a VEV in a direction which leaves the $SU(3) \times SU(2) \times U(1)$ subgroup of $SU(5)$ intact. In this way, the breaking of $SU(5)$ symmetry gives mass to the new X and Y gauge bosons near the GUT scale, and leaves the $SU(2)$ doublet components of the Higgs $\overline{\mathbf{5}}, \mathbf{5}$ representations untouched, ensuring

---

[9]Recall that for a LH Weyl fermion u_L, the CP-conjugate u_L^c transforms like a RH fermion.

that the precise orientation of Higgs masses needed to break EW symmetry at the appropriate scale persists.

Turning to the issue of fast nucleon decays, we must ensure that any interactions in a GUT theory which can give contributions to nucleon decay are not unacceptably large. The effective interactions which are responsible for such decays can be represented by Lagrangian terms like $lqqq/\Lambda$, where l refers to a lepton, q denotes a quark of any flavour and Λ is the characteristic energy scale. The current lower limit on Λ set from non-observation of a proton decaying into a pion-positron pair ($P \rightarrow e^+\pi^0$) is around 10^{15} GeV [112]. The GUT theories that are based on the MSSM have a unification scale M_{GUT} around 2×10^{16} GeV. The breaking scale of $SU(5)$ must be here, hence the masses of $\mathbf{24}$ Higgs fields and X, Y gauge bosons should also be at this scale and the theory is safe from nucleon decay constraints. Another reason to have fields at these chosen scales is that additional content charged under the SM gauge groups will further modify the RG equations of the gauge couplings and could spoil the unification achieved with the MSSM. We therefore expect a 'desert' between 10^3 to 10^{16} GeV, to preserve the delicate balance of RG running needed to achieve unification of forces. The remaining content of this thesis is composed of original research conducted during the author's candidature.

Chapter 4

Right-Handed Neutrinos in the Littlest Seesaw

4.1 Introduction

Neutrino oscillation experiments continue to provide solid evidence for new physics in the form of neutrino mass and mixing [113]. We commented in Section 2.7 that the theoretical origin of neutrino mass generation and lepton flavour mixing remains unknown [114, 115]. In addition, large statistical uncertainties remain in measurements for the mixing parameters; for example, the atmospheric angle's (θ_{23}^L) octant is not yet determined, and its precise value is constrained only loosely. While the T2K experiment has long preferred close to 'maximal atmospheric mixing' angle [116] $(\theta_{23}^L \simeq \pi/4)$, the NO$\nu$A experiment originally excluded maximal mixing at a significance of 2.6σ [117], though the latest analysis with more data is now consistent with maximal mixing [118–120]. Furthermore, the CP-violating phase relevant for oscillations has only very loose bounds. The leading candidate for a theoretical explanation of neutrino mass and mixing remains the original Type-I seesaw mechanism [72–76, 121] which utilises heavy right-handed neutrinos.

Although the Type-I seesaw mechanism provides an attractive paradigm for understanding the smallness of neutrino masses, in its most general form it comes with a large number of free parameters. In the so-called flavour basis, where the charged lepton mass matrix and the right-handed neutrino mass matrix are both diagonal, there are typically a larger number of undetermined Yukawa couplings and phases than low energy observables, with the precise number depending on the multiplicity of right-handed neutrinos [76]. This means that it is not possible to uniquely determine the high-energy parameters of the theory from low-energy neutrino data for the general model. If right-handed neutrino masses are above the TeV scale, then such a model is also difficult to test directly. This motivates the study of minimal seesaw models with fewer input parameters.

One approach to reducing the number of parameters is to consider a minimal sce-

nario involving either one [122] or two right-handed neutrinos [123, 124]. The original model [122] - with one texture zero and two right handed neutrinos - predicted normal ordering (NO, $m_3 > m_2 > m_1$) with the lightest neutrino being massless, $m_1 = 0$. Subsequently, a similar model was proposed [125] with two texture zeros in the Dirac neutrino Yukawa matrix, consistent with cosmological leptogenesis [126–134]. However, such a model with two texture zeros is only compatible with an inverted ordering (IO $m_3 < m_1 < m_2$) of neutrino masses [132, 133]. Present data slightly favours normal ordering, and thus the two RH neutrino model with one texture zero as originally proposed [123, 124].

To increase predictivity further, a constrained form of the Yukawa matrix called constrained sequential dominance (CSD) was later proposed, which led to approximate bimaximal mixing [135] known as tri-bimaximal mixing. Following the measurement of a non-zero reactor angle, generalised forms of such a constrained Yukawa matrix in the flavour basis were proposed, called CSD(n), once more leading to highly predictive schemes [34, 136–148]. The most successful of these was CSD(3), with Yukawa columns in the flavour basis proportional to $(0, 1, 1)$ and $(1, 3, 1)$ or $(1, 1, 3)$, with real constants of proportionality together with a relative phase between these columns of $\mp\pi/3$ [137].

The successful CSD(3) scheme [137] was later dubbed the Littlest Seesaw (LS) [143], to emphasise its status as the most minimal seesaw model which can explain current data with the smallest number of parameters; two right-handed neutrino masses and real coefficients of the two column vectors comprising the Yukawa matrix, in the flavour basis. It was later shown that the LS model could be obtained from S_4 family symmetry together with other discrete symmetries [144, 146] often used in GUT model building. Recently it has been shown that the LS model has (approximate) accidental mu-tau reflection symmetry, which accounts for its predictions of maximal atmospheric mixing and maximal CP-violation [148]. The prospects of testing such predictions at future experiments has also been studied [145], assuming minimal RG running.

Renormalisation group corrections to the LS model have been considered in [149], including a comprehensive χ^2 analysis of the low energy masses and mixing angles for various right-handed neutrino mass regimes and orderings, both with and without supersymmetry [150]. In particular, it was shown that the heavier RH neutrino mass strongly affects RG corrections in such models. Leptogenesis allows us to explain the observed disparity between matter and antimatter in the universe at current times through the decay of heavy neutral leptons (such as RH neutrinos in this class of models), but was not considered in these previous analyses. Since, in scenarios similar to this, the baryon asymmetry of the universe is mainly controlled by the lighter RH neutrino [142], we are motivated in this work to include leptogenesis in the global fit to fix the heavy neutrino masses. This enables both the high-energy mass parameters and the Yukawa coupling constants a, b to be fixed by low-energy neutrino data and leptogenesis for the first time in any seesaw model.

In this chapter we show that the four high-energy LS parameters in the flavour

basis - two real Yukawa couplings a, b plus the two right-handed neutrino masses - can be determined by a fit to the seven currently constrained observables of low-energy neutrino data and leptogenesis. Although there are in effect ten observables (the baryon asymmetry of the Universe, three low energy neutrino masses, three physical lepton mixing angles, one Dirac CP phase and two Majorana CP phases), the lightest physical neutrino mass is predicted to vanish, while the two Majorana phases are unconstrained (one vanishes), leaving seven observables currently constrained by data. Taking into account RG corrections, we estimate $\chi^2 \simeq 1.5 - 2.6$ for the three d.o.f., depending on the high-energy scale and type of Littlest Seesaw model under test. We extract allowed ranges of neutrino parameters from our fit data, including the approximate mu-tau symmetric predictions $\theta_{23} = 45^o \pm 1^o$ and $\delta = -90^o \pm 5^o$, which, together with a normal mass ordering with $m_1 = 0$, will enable LS models to be tested in future neutrino experiments.

4.2   The Littlest Seesaw

The seesaw mechanism [72–75, 121] extends the SM with a number of right-handed neutrino singlets N_{iR}. The mass Lagrangian of such a theory is detailed in Equation (4.1).

$$-\mathcal{L}_m = Y_\nu \overline{L_L} \widetilde{\phi} N_R + \frac{1}{2} M_R \overline{N_R^c} N_R + \text{h.c.} \tag{4.1}$$

where L_L and $\widetilde{\phi} \equiv i\sigma_2 \phi^*$ stand respectively for the left-handed lepton and Higgs doublets, E_R and N_R are the right-handed charged lepton and neutrino singlets, λ_l and Y_ν are the charged lepton and Dirac neutrino Yukawa coupling matrices, and M_R is the Majorana mass matrix of right-handed neutrino singlets. Physical light effective neutrino masses are generated via the seesaw mechanism, resulting in the light left-handed Majorana neutrino mass matrix Equation (4.2).

$$m_\nu = -v^2 Y_\nu M_R^{-1} Y_\nu^T . \tag{4.2}$$

The RH masses are denoted M_{atm} and M_{sol}. In addition, we consider some family symmetry broken by triplet flavons $\varphi_{\text{atm}}, \varphi_{\text{sol}}$, whose vacuum alignment will control the Yukawa coupling matrix's shape. Operators that correspond to such structure are given in Equation (4.3).

$$\frac{1}{\Lambda_f} \widetilde{\phi}(\overline{L} \cdot \varphi_{\text{atm}}) N_{\text{atm}} + \frac{1}{\Lambda_f} \widetilde{\phi}(\overline{L} \cdot \varphi_{\text{sol}}) N_{\text{sol}}, \tag{4.3}$$

where L combines the SU(2) lepton doublets, such that it transforms as a triplet under the family symmetry, while $N_{\text{atm}}, N_{\text{sol}}$ are the right-handed neutrinos N_R and ϕ is the usual EW Higgs doublet, the latter two being family symmetry singlets but dis-

tinguished by some additional quantum numbers. Λ_f is the scale at which the family symmetry is broken. The right-handed neutrino Majorana potential is typically chosen to give a diagonal mass matrix as per Equation (4.4).

$$M_R = \text{diag}(M_{\text{atm}}, M_{\text{sol}}) \qquad (4.4)$$

CSD(n) emerges from the alignments of VEVs in effective operators involving scalar fields φ_{atm} and φ_{sol} which are triplets under the flavour symmetry and acquire vacuum expectation values that break said discrete group ($\langle\varphi_{\text{atm}}\rangle,\langle\varphi_{\text{sol}}\rangle$). The subscript 'atm' and 'sol' are noted such because φ_{atm} is largely responsibe for the atmospheric neutrino mass m_3, and φ_{sol} gives rise to the solar neutrino mass m_2. CSD(n) corresponds the choice of vacuum alignments given in Equation (4.5).

$$\langle\varphi_{\text{atm}}\rangle = v_{\text{atm}} \begin{pmatrix} 0 \\ 1 \\ 1 \end{pmatrix}, \quad \langle\varphi_{\text{sol}}\rangle = v_{\text{sol}} \begin{pmatrix} 1 \\ n \\ (n-2) \end{pmatrix} \textbf{ or } \langle\varphi_{\text{sol}}\rangle = v_{\text{sol}} \begin{pmatrix} 1 \\ (n-2) \\ n \end{pmatrix} \qquad (4.5)$$

where n is some positive integer, and phases are allowed only in overall proportionality constants. Such vacuum alignments are discussed in [144]. In the flavour basis, where the charged leptons and right-handed neutrino are their $SU(2)$ weak eigenstates, Cases A, B are defined by the mass hierarchy $M_{\text{atm}} \ll M_{\text{sol}}$, hence $M_R = \text{diag}(M_{\text{atm}}, M_{\text{sol}})$, and the corresponding Yukawa matrix structure is given in Equation (4.6):

$$\text{Case A}: \ Y_\nu^A = \begin{pmatrix} 0 & be^{i\eta/2} \\ a & nbe^{i\eta/2} \\ a & (n-2)be^{i\eta/2} \end{pmatrix} \quad \text{or} \quad \text{Case B}: \ Y_\nu^B = \begin{pmatrix} 0 & be^{i\eta/2} \\ a & (n-2)be^{i\eta/2} \\ a & nbe^{i\eta/2} \end{pmatrix} \qquad (4.6)$$

with a, b, η being three real parameters and n the integer for CSD(n). These scenarios were analysed previously [149, 150] with heavy neutrino masses of $M_{\text{atm}} = M_1 = 10^{12}$GeV and $M_{\text{sol}} = M_2 = 10^{15}$GeV. Conversely, Cases C and D consider an alternative mass ordering of the heavy neutrinos, $M_{\text{atm}} \gg M_{\text{sol}}$, and consequently $M_R = \text{diag}(M_{\text{sol}}, M_{\text{atm}})$, the two columns of Y_ν in Equation (4.6) must be exchanged.

$$\text{Case C}: Y_\nu^C = \begin{pmatrix} be^{i\eta/2} & 0 \\ nbe^{i\eta/2} & a \\ (n-2)be^{i\eta/2} & a \end{pmatrix} \quad \text{or} \quad \text{Case D}: Y_\nu^D = \begin{pmatrix} be^{i\eta/2} & 0 \\ (n-2)be^{i\eta/2} & a \\ nbe^{i\eta/2} & a \end{pmatrix}, \ (4.7)$$

The well-defined cases of $M_{\text{atm}} = M_2 = 10^{15}$GeV and $M_{\text{sol}} = M_1 = 10^{12}$GeV have been studied previously [149, 150]. Below the RH neutrino mass scales, one can apply the seesaw formula in Equation (4.2), for Cases A, B, C and D using the Yukawa coupling matrices $Y_\nu^{A,B}$ in Equation (4.6) with $M_R^{A,B} = \text{diag}(M_{\text{atm}}, M_{\text{sol}})$ and $Y_\nu^{C,D}$ in Equation (4.6) with $M_R^{C,D} = \text{diag}(M_{\text{sol}}, M_{\text{atm}})$, to give (after rephasing) the light neutrino mass matrices in terms of the real parameters $m_a = a^2v^2/2M_{\text{atm}}$, $m_b = b^2v^2/2M_{\text{sol}}$ with

$v = 246\text{GeV}$. The full light neutrino mass matrices for each case are outlined below:

$$m_\nu^{A,C} = m_a \begin{pmatrix} 0 & 0 & 0 \\ 0 & 1 & 1 \\ 0 & 1 & 1 \end{pmatrix} + m_b \mathrm{e}^{\mathrm{i}\eta} \begin{pmatrix} 1 & n & (n-2) \\ n & n^2 & n(n-2) \\ (n-2) & n(n-2) & (n-2)^2 \end{pmatrix} \qquad (4.8)$$

$$m_\nu^{B,D} = m_a \begin{pmatrix} 0 & 0 & 0 \\ 0 & 1 & 1 \\ 0 & 1 & 1 \end{pmatrix} + m_b \mathrm{e}^{\mathrm{i}\eta} \begin{pmatrix} 1 & (n-2) & n \\ (n-2) & (n-2)^2 & n(n-2) \\ n & n(n-2) & n^2 \end{pmatrix} \qquad (4.9)$$

Note the degeneracy in light neutrino masses of Cases A, C and Cases B, D. Studies which ignore RG effects do not distinguish between these degenerate cases. In this study, the degeneracy is resolved and we must deal with the four physically distinct cases. The neutrino masses and lepton flavour mixing parameters at the electroweak scale $\Lambda_{\mathrm{EW}} \sim \mathcal{O}(1000\text{GeV})$ can be derived by diagonalising the effective neutrino mass matrix via

$$U_{\nu L} m_\nu U_{\nu L}^T = \mathrm{diag}(m_1, m_2, m_3) \qquad (4.10)$$

From a neutrino mass matrix as given in Equations (4.8) and (4.9), one immediately obtains normal ordering with $m_1 = 0$. Furthermore, these scenarios only provide one physical Majorana phase σ_M. As a consequence of parameterising our theory in the flavour basis, the PMNS matrix is given by $U_{\mathrm{PMNS}} = U_{\nu L}^\dagger$. We use the standard parametrisation for the mixing angles and the CP-violating phase δ, the standard Particle Data Group Majorana phase φ_1 vanishes and $-\varphi_2/2 = \sigma_M$. The low-energy phenomenology of Case A has been studied in detail both analytically [143] and numerically [137, 141], where it was found that the best fit to experimental data of neutrino oscillations is obtained for $n = 3$ when $\eta \approx 2\pi/3$, while for Case B the preferred choice is $n = 3$ and $\eta \approx -2\pi/3$ [137, 144]. Due to the degeneracy of Cases A, C and Cases B, D at tree level, the preferred choice for n and η carries over. The prediction for baryon asymmetry through leptogenesis within Case A has also been studied [142], where it was shown that Case C predicts the CP-violating phase to be $\delta \approx 90^o$ which is disfavoured by current global fits to neutrino oscillation data [120]. It is straightforward to show that Case B is disfavoured for a similar reason. Therefore, taking into account the positive sign of the observed baryon asymmetry and the present experimentally favoured prediction of $\delta \approx -90^o$, we study two cases of interest here; Case A with $\eta = 2\pi/3$ and Case D with $\eta = -2\pi/3$, fixing $n = 3$ for both. These successful

scenarios are summarised in Equations (4.11) and (4.12):

$$\text{Case A}: \quad Y_\nu^A = \begin{pmatrix} 0 & be^{i\pi/3} \\ a & 3be^{i\pi/3} \\ a & be^{i\pi/3} \end{pmatrix} \quad \text{with} \quad M_R = \text{diag}(M_{\text{atm}}, M_{\text{sol}}) \tag{4.11}$$

$$\text{Case D}: \quad Y_\nu^D = \begin{pmatrix} be^{-i\pi/3} & 0 \\ be^{-i\pi/3} & a \\ 3be^{-i\pi/3} & a \end{pmatrix} \quad \text{with} \quad M_R = \text{diag}(M_{\text{sol}}, M_{\text{atm}}) \tag{4.12}$$

Columns are ordered so that the lighter right-handed neutrino of mass M_1 is in the first column and the heavier right-handed neutrino of mass M_2 is in the second column. In both layouts normal hierarchy is predicted with $m_1 = 0$ and the physical atmospheric neutrino mass m_3 is dominantly controlled by the combination $m_a = a^2v^2/2M_{\text{atm}}$, while the solar neutrino mass m_2 is dominantly controlled by the combination $m_b = b^2v^2/2M_{\text{sol}}$. These two setups form the focus of this numerical study.

4.3   Renormalisation group evolution

We suppose that the seesaw theory is defined at the grand unification or GUT scale, denoted by Λ_{GUT}, and typically close to 2.0×10^{16} GeV. The theory is susceptible to large corrections from RG running; as such, it is necessary to correctly evolve predictions from the model at Λ_{GUT} to a scale at which experimental data is available for testing. To achieve this, the relevant renormalisation group equations (RGEs) must be known to some loop order, which is only possible in a concrete model such as the LS, where RGEs follow the SM with modifications in the lepton sector arising from the right-handed neutrinos. As a consequence of approximations made in leptogenesis calculations, we always consider hierarchical Majorana masses. Each RH neutrino must then be integrated out separately to obtain accurate predictions. We make use of effective field theories below the scale at which the heaviest RH neutrino is integrated out, taking care to ensure matching between each EFT at the appropriate scale [151]:

$$M_Z \ll M_1 \ll M_2 \ll \Lambda_{\text{GUT}} \tag{4.13}$$

Below, we outline mass matrix calculation in the three distinct regions relevant to our model. For a given renormalisation scale μ, calculation of the light neutrino mass matrix is given for each of the RG regimes that we consider:

4.3.1 $\mu > M_2$

In this regime, RG effects are due to running of the Yukawa coupling and Majorana mass matrices only, and light neutrino masses are calculated as per Equation (4.2).

4.3.2 $M_1 < \mu < M_2$

In the intermediate EFT that is valid between the scales of the RH neutrinos, light neutrino masses are given by:

$$m_\nu^{(2)} = -v^2 \left[\kappa^{(2)} + Y_\nu^{(2)} M_1^{-1} (Y_\nu^{(2)})^T \right]$$

(4.14)

The superscript (2) in Equation (4.14) denotes a matrix that has been altered by integrating out the heaviest RH neutrino. For instance, the matrix $\kappa^{(2)} \propto Y_\nu M_2^{-1} Y_\nu^T$ is the correction for this intermediate EFT, which represents the heavier RH neutrino contribution to the mass matrix, once it has been integrated out.

4.3.3 $\mu > M_1$

Below $\mu = M_1$, the theory reduces to the SM with a five-dimensional Weinberg operator modification to the Lagrangian as per Equation (4.15):

$$\mathcal{L}_m(\mu < M_1) = \frac{1}{2} \kappa^{(1)} \left(\overline{L_L} \widetilde{H} \right) \left(\widetilde{H}^T \overline{L_L^c} \right) + \text{h.c.}$$

(4.15)

In this analysis, the one-loop RGEs for the LS are numerically solved from the GUT scale to M_Z using the REAP Mathematica package [151], which ensures correct matching between effective theories and allows us to calculate the light neutrino masses and PMNS mixing parameters in each EFT. More complete discussions of RG running in scenarios such as this are given in [149–151].

4.4 Leptogenesis

The predominance of matter over antimatter present in the observable Universe is thought to have arisen in the early evolution of our local region. The hypothetical out-of-equilibrium process in the expanding Universe through which the number of baryons and antibaryons was effectively fixed is known as Big Bang Baryogenesis [152, 153]. Traditional SM calculations of this thermal freeze-out of baryons predict equal number densities of particles and antiparticles in contrast to observation, which has measured the so-called Baryon Asymmetry of the Universe (BAU) (normalised to entropy density) to be [40]:

$$Y_B = \frac{n_B - n_{\overline{B}}}{s} = 0.87 \pm 0.01 \times 10^{-10}, \qquad s = \frac{S}{V}$$

(4.16)

In order for matter and antimatter to be produced at different rates, baryon-generating interactions in the early universe must satisfy the three Sakharov conditions [23]:

- baryon number (B) violation
- charge (C) and charge-parity conjugation (CP) violation

- interactions that depart from thermal equillibirum

The SM allows for C violation in weak interactions of quarks and leptons via the irreducible complex phases in the CKM matrix. CP-violation has been intensively studied in the quark sector - specifically, in the neutral kaon and B-meson systems - but is yet to be definitively observed in the neutrino sector, though tantalising hints persist [39].

Despite the absence of concrete evidence, this has led to the suggestion that, at an early and higher-temperature era of the universe, CP was violated in the lepton sector leading to a lepton-antilepton asymmetry, such a mechanism is known as leptogenesis [126]. The lepton asymmetry is then communicated to the baryon sector as the universe evolved via SM electroweak sphaleron processes that violate conservation of baryon (B) and lepton (L) number but conserve the difference (B-L). The discovery of neutrino oscillations has opened up the possibility of relating the BAU to neutrino properties, perhaps providing an elegant explanation for the matter-antimatter asymmetry. In models such as the Littlest Seesaw, the lepton asymmetry is generated by the preferential decays of heavy RH neutrinos. In particular, the simplest version of leptogenesis sees it largely dominated by the interactions and decay of the lighter RH neutrino [154]. As such, imposing a requirement of successful baryogenesis yields constraints on masses of both light and heavy neutrinos, and provides a means of fixing the lightest RH neutrino mass in the LS. A positive Y_B corresponds to a negative lepton asymmetry as per Equation (4.17):

$$Y_B = -\frac{12}{37} \sum_\alpha Y_{\Delta\alpha} \qquad (4.17)$$

where α index denotes flavour ($\alpha = e, \mu, \tau$) and 12/37 is the fraction of B-L asymmetry converted into baryo inbalance through sphaleron processes [155]. The lepton asymmetry $Y_{\Delta\alpha}$ can be parametrised as [156]:

$$Y_{\Delta\alpha} = \eta_\alpha \epsilon_{1,\alpha} Y_{N1}^{eq}(z \ll 1) \qquad (4.18)$$

where η_α is an efficiency factor, $\epsilon_{1,\alpha}$ is the decay asymmetry of the lightest right-handed neutrino into lepton flavour α, derived through calculating the relevant Feynman diagrams. $Y_{N1}^{eq}(z \ll 1)$ is the number density of the same neutrino at temperature $T \gg M_1$ if it was in thermal equilibrium, normalised to entropy density. The dimensionless quantity z denotes a ratio of the lighter RH neutrino mass over temperature $z = M_1/T$. It should be noted that in previous works [131], analysis limited the possible range of masses for the lightest RH neutrino to $10^9 \leq M_1 \leq 10^{12}$ GeV, to enforce the condition of successful leptogenesis in a Littlest Seesaw setup. As such, it is necessary to work in the two-flavour basis, where the tauon Yukawa interactions are in thermal equilibrium, and there will be two eigenstates, for the tauon flavour and linear combination of muon

and electron flavours, respectively. Thus, Equation (4.18) will become:

$$Y_{\Delta\alpha} = Y_{N1}^{\text{eq}}(z \ll 1) \left[\eta_\tau \epsilon_{1,\tau} + \eta_2 \left(\epsilon_{1,e} + \epsilon_{1,\mu}\right)\right] \tag{4.19}$$

where η_2 is the efficiency factor corresponding to this linear combination of e and μ flavours but it is not simply the sum of these factors i.e. $\eta_2 \neq \eta_e + \eta_\mu$. This efficiency factor is outlined in Equation 4.27. In the Boltzmann approximation, the number density in Equation (4.19) is given by [156]:

$$Y_{N1}^{\text{eq}}(z \ll 1) \approx \frac{45}{\pi^4 g_*} \tag{4.20}$$

g_* is the number of effective degrees of freedom, which in the SM is 106.75. The decay asymmetry into Higgs and left-handed leptons is defined as [156]:

$$\epsilon_{1,\alpha} = \frac{\Gamma_{N_1 l_\alpha} - \Gamma_{N_1 \bar{l}_\alpha}}{\sum_\alpha (\Gamma_{N_1 l_\alpha} + \Gamma_{N_1 \bar{l}_\alpha})} \tag{4.21}$$

where $\Gamma_{N_1 l_\alpha} = \Gamma(N_1 \to H + l_\alpha)$ and $\Gamma_{N_1 \bar{l}_\alpha} = \Gamma(N_1 \to H^* + \bar{l}_\alpha)$ are the decay rates of the heavy neutrino into particles and antiparticles, respectively. The decay asymmetry arises beginning at the 1-loop level [157] and is given in Equation (4.22):

$$\epsilon_{1,\alpha} = \frac{1}{8\pi} \frac{\sum_{J=2,3} \text{Im}[(Y_\nu^\dagger)_{1\alpha} [Y_\nu^\dagger Y_\nu]_{1J} (Y_\nu^T)_{J\alpha}]}{(Y_\nu^\dagger Y_\nu)_{11}} g^{\text{SM}} \left(\frac{M_J^2}{M_1^2}\right) \tag{4.22}$$

Y_ν denotes the Yukawa matrix and the loop function g in the SM is given by [156]:

$$g^{\text{SM}}(x) = \sqrt{x} \left[\frac{1}{1-x} + 1 - (1+x) \ln \frac{1+x}{x}\right] \tag{4.23}$$

In addition, for the Littlest Seesaw, the sum running over $J = 2, 3$ can be simplified to J_2, as only two RH neutrinos are present in the model. It should be noted the factor J_2 will always appear due to the fact that the heavier RH neutrino field N_2 can participate in the loop diagram for N_1's decay [157]. As such, there will be some sensitivity in our leptogenesis calculation to the heavier RH neutrino mass. However, the dominant contribution will come from the lighter RH neutrino: Under the assumption of a hierarchical limit $M_1 \ll M_2$, Equation (4.23) can be approximated[1] as $g^{\text{SM}}(x) \simeq -3/2\sqrt{x}$. Then, for the Case A Yukawa matrix given in Equation (4.6),

---

[1]It should be noted that in the numerical analysis we use the full expression for g^{SM} given in Equation (4.23) and also include the RG running effects on leptogenesis down to M_2. The approximations discussed here are purely for the purposes of illustrating the respective contributions of M_1 and M_2.

individual flavour-dependent asymmetries at Λ_{GUT} reduce to:

$$\epsilon_{1,e}^A = 0$$

$$\epsilon_{1,\mu}^A \simeq -\frac{3}{16\pi}\frac{M_1}{M_2}n(n-1)b^2\sin\eta \tag{4.24}$$

$$\epsilon_{1,\tau}^A \simeq -\frac{3}{16\pi}\frac{M_1}{M_2}(n-1)(n-2)b^2\sin\eta$$

As stated in Section 4.2, the quantity b^2/M_2 is proportional to m_b - in our analysis, this is kept to within an order of magnitude for Case A to obtain favourable neutrino observables at low energies. Thus, the lighter RH neutrino of mass M_1 will have a larger effect in the decay asymmetries in Equation (4.24), and the BAU will have the intended effect of constraining this mass. Analogously, the asymmetries in Case D reduce to the following:

$$\epsilon_{1,e}^D = 0$$

$$\epsilon_{1,\mu}^D \simeq \frac{3}{8\pi}\frac{M_1}{M_2}\frac{(n-1)(n-2)}{(2n^2-4n+5)}a^2\sin\eta \tag{4.25}$$

$$\epsilon_{1,\tau}^D \simeq \frac{3}{8\pi}\frac{M_1}{M_2}\frac{n(n-1)}{(2n^2-4n+5)}a^2\sin\eta$$

In this case a^2/M_2 is kept approximately fixed; hence M_1 will still be the most sensitive parameter with respect to the decay asymmetry. We assume that there is a vanishing initial abundance very early in the universe's life ($N_{N_1}^{in} = 0$), hence the efficiency factor will be composed of two contributions [154, 158];

$$\eta_\alpha = \eta_-(K_\alpha, P_{1\alpha}^0) + \eta_+(K_\alpha, P_{1\alpha}^0) \tag{4.26}$$

with decay parameters K_α and tree-level branching fractions $P_{1\alpha}^0$. As before, when working in the two-flavour basis, the above expression is treated separately for each of the two eigenstates:

$$\eta_\tau = \eta_-(K_\tau, P_{1\tau}^0) + \eta_+(K_\tau, P_{1\tau}^0)$$
$$\eta_2 = \eta_-(K_2, P_{12}^0) + \eta_+(K_2, P_{12}^0) \tag{4.27}$$

The negative contribution comes from an initial stage where $N_{N_1} \leq N_{N_1}^{\text{eq}}$ and $z \leq z_{\text{eq}}$. It is approximated by [158]:

$$\eta_-(K_\alpha, P_{1\alpha}^0) \simeq -\frac{2}{P_{1\alpha}^0}e^{\left[-\frac{3\pi K_\alpha}{8}\right]}\left(e^{\left[\frac{P_{1\alpha}^0}{2}N_{N_1}(z_{eq})\right]} - 1\right) \tag{4.28}$$

where, in the above expression:

- The N_1 abundance at z_{eq} is defined as [158]:

$$N_{N_1}(z_{eq}) \simeq \overline{N}(K_\alpha) \equiv \frac{N(K_\alpha)}{\left(1 + \sqrt{N(K_\alpha)}\right)^2} \qquad (4.29)$$

and $N(K_\alpha) = \frac{3\pi}{4}K_\alpha$, where K_α is the decay parameter [159]. For the flavour-dependent case this will become K_2, combining the e and μ parameters. For each flavour, the individual parameter will be given by:

$$K_\alpha = (Y_\nu^\dagger)_{1\alpha}(Y_\nu)_{\alpha 1}\frac{v^2}{m_{SM}^* M_1} \qquad (4.30)$$

where $m_{\text{SM}}^* \simeq 1.08 * 10^{-3}\text{eV}$ is the equilibrium neutrino mass [154] and v is the SM Higgs vacuum expectation value ($\left[v = 246/\sqrt{2}\right]\text{GeV}$). Thus, K_2 is simply the sum of e and μ pieces.

- The tree-level branching ratios are given by:

$$P_{1\alpha}^0 \simeq \frac{|(Y_\nu)_{\alpha 1}|^2}{[(Y_\nu)^\dagger(Y_\nu)]_{11}} \qquad (4.31)$$

and similarly, P_{12}^0 in Equation (4.27) refers to $P_{12}^0 = \sum_{\alpha=e,\mu} P_{1\alpha}^0$ in our two-flavour basis.

The positive contribution corresponds to the stage when $N_{N_1} \geq N_{N_1}^{\text{eq}}$ and $z \geq z_{\text{eq}}$. It is approximated by [158]:

$$\eta_+(K_\alpha, P_{1\alpha}^0) \simeq \frac{2}{z_B(K_\alpha)K_\alpha}\left(1 - e^{\left[-\frac{K_\alpha z_B(K_\alpha)N_{N_1}(z_{eq})}{2}\right]}\right) \qquad (4.32)$$

where the same definitions hold as for the negative contribution and in addition the freeze-out parameter is given by $z_B(K_\alpha) \simeq 2 + 4K_\alpha^{0.13}e^{-\frac{2.5}{K_\alpha}}$ [160]. In this way, all of the necessary terms can be determined to calculate a prediction of the BAU for a given parameter point. The inclusion of leptogenesis in this analysis immediately invalidates Cases B and C. A general seesaw mechanism in $\text{CSD}(n)$ assuming two right-handed neutrinos will involve a single phase η, which provides the link between the neutrino oscillation phase and the CP-violating phenomenon responsible for satisfying a Sakharov condition in leptogenesis[2] [161]. Following the derivation set out in [156], this relation can be seen as $Y_B \propto \pm \sin\eta$, where the positive sign will correspond to the scenario in which $M_{\text{atm}} \ll M_{\text{sol}}$ (here, Cases A and B) and the negative sign

---

[2]This phase is not to be confused with the efficiency factor η included in the above calculations.

scenario to $M_{\rm sol} \ll M_{\rm atm}$ (Cases C and D). As the resulting BAU observed is required to be positive, η must therefore be positive in the first category and negative in the second. However, as discussed in Section 4.2, the phenomenology of each LS case has been studied extensively, and Case B has been shown to prefer a value of $\eta \approx -2\pi/3$, corresponding to the current experimental hint for $\delta_{CP} \sim -\pi/2$, while Case C prefers $\eta \approx 2\pi/3$ for similar reasons. Given the required positive BAU, we see therefore that B and C are in conflict with current hints for $\delta_{CP} \sim -\pi/2$. Thus, when leptogenesis calculations are included in the analysis, we consider only Cases A and D which result in a positive final baryon asymmetry.

4.5 Fitting procedure

As discussed in previous sections, we focus exclusively on Cases A and D as defined in Equations (4.6) and (4.7). Each of these cases involves just four real free parameters at high energies which predict the entire neutrino sector and the BAU from leptogenesis - two Yukawa parameters a and b and two masses $M_{\rm atm}$ and $M_{\rm sol}$. In this chapter, we determine optimal RH neutrino masses and Yukawa parameters through a fit to low-scale experimental data, using the χ^2 statistic defined in Equation (4.33) as a goodness-of-fit measure.

$$\chi^2 = \sum_{i=1}^{N} \left(\frac{P_i(x) - \mu_i}{\sigma^i} \right)^2 \tag{4.33}$$

Low-energy predictions of the model denoted $P_i(x)$ are fully determined by our set of four parameters, collectively labelled x.

$$x = (a, b, M_{\rm atm}, M_{\rm sol}) \tag{4.34}$$

$$\mu_i = (\sin^2 \theta_{12}, \sin^2 \theta_{13}, \sin^2 \theta_{23}, \Delta m_{12}^2, \Delta m_{13}^2, \delta, Y_B) \tag{4.35}$$

The model predictions are tested against the global fit of neutrino data from NuFit3.2 [120] and the measured value of the BAU from Planck satellite's 2015 dataset [40]. σ_i in Equation 4.33 corresponds to the 1σ bounds for each of the experimentally measured values μ_i. If the data follows a Gaussian distribution, these bounds are simply the standard deviations of such data. We calculate the reduced χ^2 for each parameter point:

$$\chi_\nu^2 = \frac{\chi^2}{n_{\rm d.o.f.}} \tag{4.36}$$

where $n_{\rm d.o.f.}$ is the number of degrees of freedom - the number of observables minus the number of parameters in our analysis. A model is said to be a good fit to data if $\chi_\nu^2 \simeq 1$ and any model that deviates significantly from this we accept to be a poor fit.

Observable	NuFit3.2($\pm 1\sigma$)	Assumed Values($\pm 1\sigma$)
$\theta_{12}/^\circ$	$33.62^{+0.78}_{-0.76}$	$33.62^{+0.76}_{-0.76}$
$\theta_{13}/^\circ$	$8.54^{+0.15}_{-0.15}$	$8.54^{+0.15}_{-0.15}$
$\theta_{23}/^\circ$	$47.2^{+1.9}_{-3.6}$	$46.4^{+2.8}_{-2.8}$
$\delta/^\circ$	-126^{+43}_{-31}	-120^{+37}_{-37}
$\Delta m^2_{12}/\text{eV}^2$	$7.40^{+0.21}_{-0.20} \times 10^{-5}$	$7.40^{+0.20}_{-0.20} \times 10^{-5}$
$\Delta m^2_{13}/\text{eV}^2$	$2.494^{+0.033}_{-0.031} \times 10^{-3}$	$2.494^{+0.031}_{-0.031} \times 10^{-3}$
Y_B	$0.87^{+0.01}_{-0.01} \times 10^{-10}$	$0.87^{+0.01}_{-0.01} \times 10^{-10}$

Table 4.1: Global fit values from NuFit3.2 [120] in the case of normal ordering, along with latest 1σ bounds on Y_B from Planck satellite [40].

In Table 4.1, we see that distributions for some experimentally measured observables are asymmetric; hence, to keep the analysis clean and simple, we approximate the χ^2 for each parameter point in the following manner: We assume that the observables conform to a symmetric Gaussian distribution, where the central value are those given in the table and we use the smaller of the quoted uncertainties in our calculations for all constraints except θ_{23} and δ. For these two observables, we approximate the distribution as Gaussian with its central value located in the arithmetic centre of the quoted 1σ range from Table 4.1. Thus, the modifications from the true experimental values stated in the table are as follows: $\theta_{23} = 46.35^{\circ}{}^{+2.75^\circ}_{-2.75^\circ}$, $\delta = 120^{\circ}{}^{+37^\circ}_{-37^\circ}$.

In this way, the 1σ range is preserved and we do not vastly overestimate the χ^2 contributions from these observables relative to others. However, it is important to note that this method will always underestimate the χ^2 slightly. The procedure used to test each parameter point is outlined in Figure 4.1. We scan over the four input parameters with a predefined step for each one, with ranges inspired by previous analysis of the LS [150]. A four-dimensional grid is created, and at each point of this grid - corresponding to a particular combination of parameters - the values for each parameter are inserted into the relevant matrices to define a single parameter point at the GUT scale. The Yukawa matrices and Majorana mass matrix are run down from the GUT scale to M_Z, using the Mathematica program REAP [151], to integrate out the RH neutrinos and ensure that the relevant EFTs are correctly matched at appropriate scales (see Section 4.3). We extract neutrino and leptogenesis predictions and calculate the χ^2 statistic. After each full run of the grid scan, we reduce the tested bounds of every input parameter, iteratively scanning more finely in all parameters to find the best-fit point with a stable minimum χ^2. It is worth noting here that the conventions used by REAP differ from those given here and in other literature. We have defined our Yukawa matrices in Section 4.2 as per left-right (LR) convention. This means that the matrix is defined with the LH SU(2) lepton doublet on the left-hand side of the Lagrangian term. Conversely, REAP takes only matrices defined in RL convention. Standard PDG
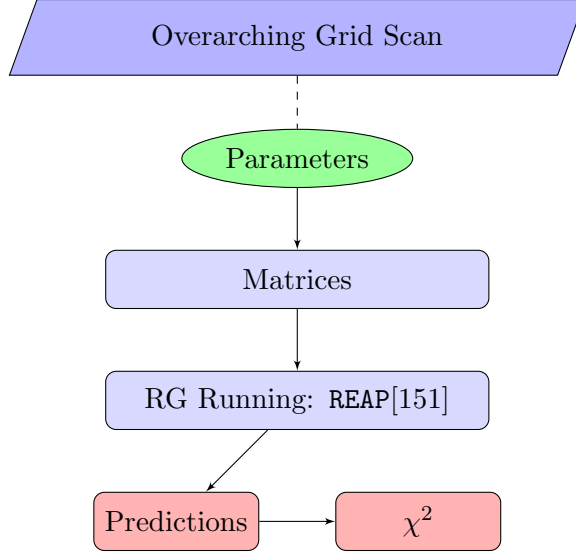
Figure 4.1: Parameter scan and data flow for a single scanned point.

parametrisation is used for the mixing angles and the CP-violating phase in the neutrino Yukawa matrix. The convention for the Yukawa matrix can be summarised in Equation (4.37), where Y_ν refers to any Littlest Seesaw Yukawa matrix already defined in this chapter.

$$(Y_\nu)_{\texttt{REAP}} = Y_\nu^\dagger \qquad (4.37)$$

4.6 Results

Following the method outlined in Section 4.5, core results are summarised in Table 4.2, in which the best fit points for each case are outlined, for a selection of assumed GUT scales. Case A1 (A2) refers to the benchmark point obtained from a full fit of Case

	Case A1	Case D1	Case A2	Case D2
$\Lambda_{\mathrm{GUT}}/\mathrm{GeV}$	1.0×10^{16}	1.0×10^{16}	2.0×10^{16}	2.0×10^{16}
$M_{\mathrm{atm}}/\mathrm{GeV}$	5.10×10^{10}	1.59×10^{12}	5.05×10^{10}	1.36×10^{13}
$M_{\mathrm{sol}}/\mathrm{GeV}$	3.28×10^{14}	1.08×10^{10}	5.07×10^{13}	1.06×10^{10}
a	0.00817	0.0456	0.00806	0.135
b	0.215	0.00117	0.0830	0.00116
$\chi^2/\mathrm{d.o.f.}$	1.51/3	2.64/3	1.75/3	2.07/3

Table 4.2: Benchmark points

A with the GUT scale fixed at 1.0×10^{16} GeV (2.0×10^{16} GeV), and analogously for Case D. From these points we can conclude that both cases of the LS give excellent fits to the experimental data, and also that the $\chi^2/\mathrm{d.o.f.}$ for each benchmark point are

near-degenerate and we cannot determine a preference for one case over another here. We remind the reader that due to the approximations in our method (of particular relevance for the atmospheric angle) the χ^2 is always somewhat underestimated. However, although the treatment of asymmetric errors is beyond the scope of our analysis, our method does respect one-sigma ranges of all the observables (see assumed values in Table 4.1), and so uncertainties in our method should be within one-sigma accuracy.

4.6.1 Observables and χ^2 contributions

To explore these results in more detail we take the benchmark points from Table 4.2 and examine predictions for experimental observables made by each of them. The

	Case A1	Case D1	Case A2	Case D2	Experiment[40, 120]
$\theta_{12}/°$	34.20	34.32	34.30	34.33	$33.62^{+0.78}_{-0.76}$
$\theta_{13}/°$	8.58	8.64	8.59	8.59	$8.54^{+0.15}_{-0.15}$
$\theta_{23}/°$	45.33	44.24	45.62	44.24	$47.2^{+1.9}_{-3.6}$
$\Delta m_{21}{}^2/10^{-5}\text{eV}^2$	7.43	7.33	7.36	7.34	$7.40^{+0.21}_{-0.20}$
$\Delta m_{31}{}^2/10^{-3}\text{eV}^2$	2.49	2.48	2.50	2.50	$2.494^{+0.033}_{-0.031}$
$\delta/°$	−89.0	−93.2	−87.4	−93.0	-126^{+43}_{-31}
$Y_B/10^{-10}$	0.860	0.860	0.860	0.861	$0.87^{+0.01}_{-0.01}$
$\chi^2/\text{d.o.f.}$	1.51/3	2.64/3	1.76/3	2.07/3	-

Table 4.3: Benchmark point observables.

predictions for θ_{23} and δ are particularly interesting. Regardless of case studied, the LS yields close to maximal atmospheric mixing. Likewise, the CP-violating phase is consistently predicted to be in the vicinity of $-\pi/2$. In order to be concise, we concentrate on Case A2 and D2 for the remainder of results shown. Figure 4.2 depicts contributions made to the total χ^2 by each observable. θ_{12} exerts a large pull over the data for both cases. This observable is always fixed close to $33° - 34°$, resulting from a sum rule that can be derived from the model:

$$\tan\theta_{12} = \frac{1}{\sqrt{2}}\sqrt{1 - 3\sin^2\theta_{13}} \tag{4.38}$$

A more complete discussion of analytic predictions for the Littlest Seesaw is given in [143, 144].

4.6.2 RG Effects in benchmark points

We take the best fit points from Table 4.2 and study the RG running in detail, paying particular attention to the variation of neutrino mass eigenstates and PMNS angles: Consider Case A2 from Table 4.2, the RGE running from the GUT scale down to the
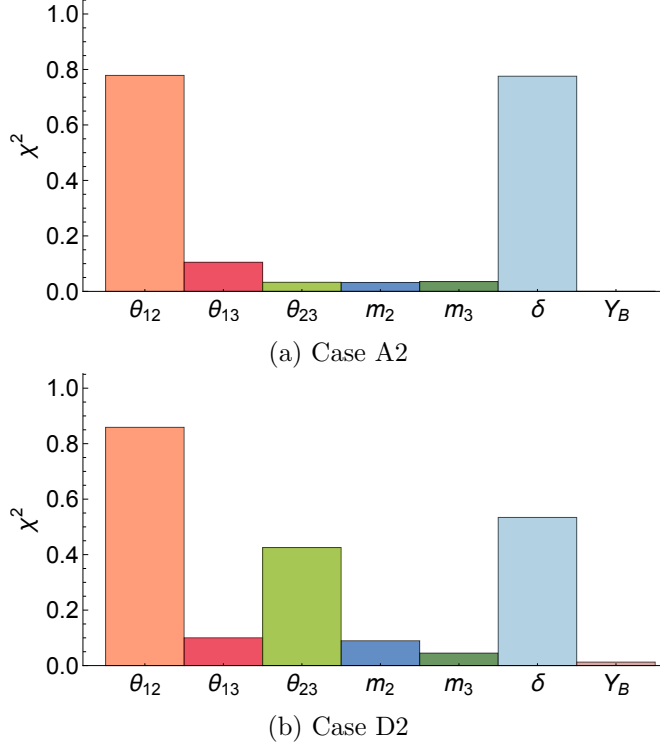
Figure 4.2: χ^2 contribution of each observable for best fit points.

electroweak (EW) scale of neutrino predictions arising from this benchmark point is presented on the left-hand side of Figure 4.3. It can be seen that RGE effects on the mass eigenstates become very apparent below the lightest seesaw scale when the model reduces to the SM extended by a five-dimensional Weinberg operator. However, for the PMNS angles, it is a different story. For both θ_{13} and θ_{23}, RGE effects are manifest to some degree in the EFT between seesaw scales; however, both above and below these scales there is very little running to be seen.

In short, RGE effects are more significant in mass eigenstates than in mixing angles, but the scales at which these effects occur are vastly different between the various observables that we extract from the model. Case D2, shown on the right-hand side of Figure 4.3, exhibits much the same behaviour as Case A2; large running in the mass eigenstates and small but non-negligible running in the mixing angles. The ratio of masses is also plotted for each case, to better understand the effects of running in both masses simultaneously. We see identical running for the light masses below the lowest seesaw scale for both cases, as the ratio of masses is constant below this scale. It is the running apparent between M_2 and M_1 that allows us to make a concrete prediction for the heavy RH neutrino mass, the lighter already being severely constrained by leptogenesis. Note that the bounds on Δm_{21}^2 are not any less precise than those on Δm_{31}^2, but the mass eigenstates are shown on a logarithmic scale. There is a particularly large 1σ range for θ_{23}.
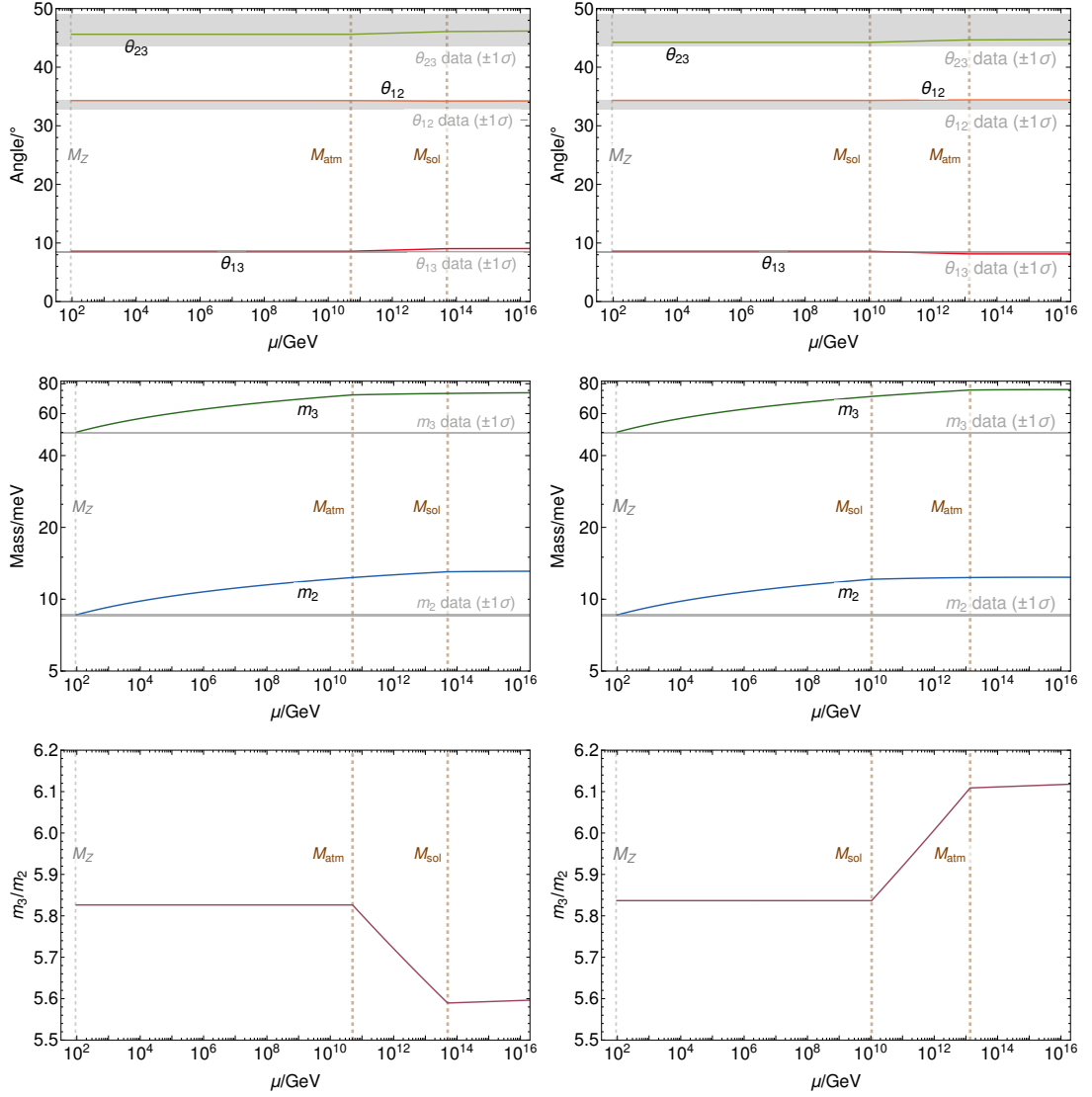
Figure 4.3: Running of neutrino observables. Case A2 on the left, Case D2 on the right.

4.6.3 Perturbations around best fit points

We vary input parameters around the benchmark points in both one and two dimensions, and we see that perturbations in parameter space yield variations around smooth, stable minima. Figure 4.4 shows heat maps representing increases in χ^2 as one moves away from the benchmark points, for variations in a, b or $M_{\mathrm{atm}}, M_{\mathrm{sol}}$ parameter space, respectively. Note the resulting shape is never an exact circle, as there is some small correlation between parameters. We vary each parameter individually around the best
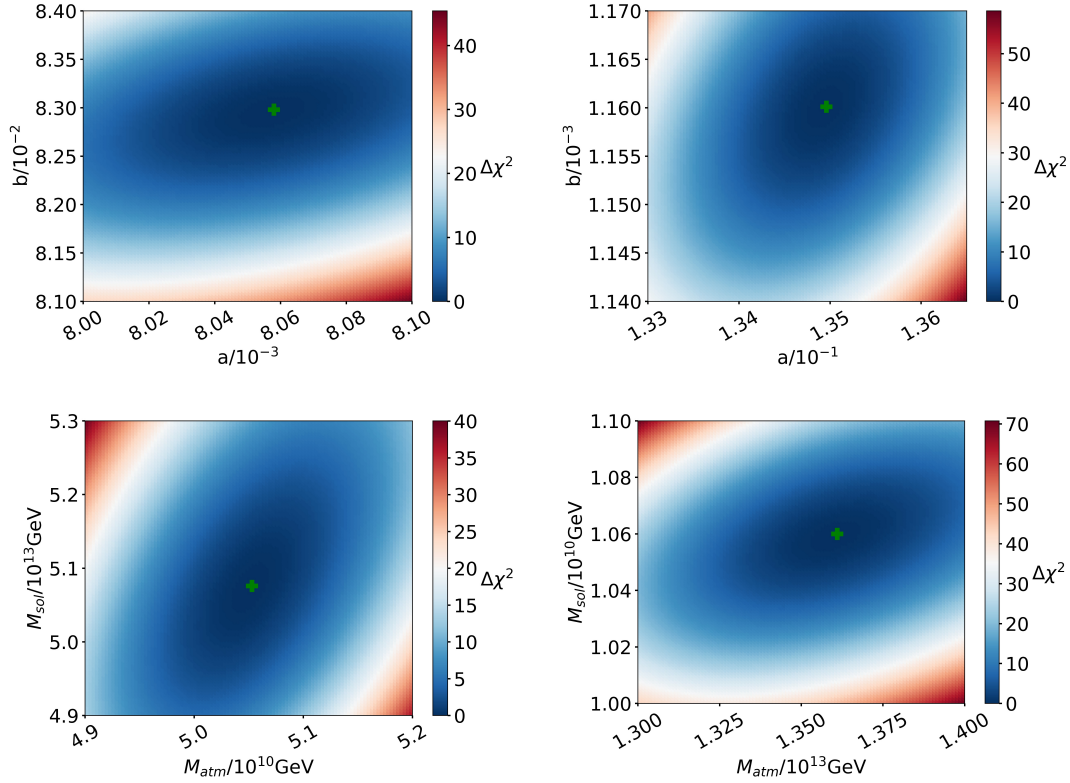
Figure 4.4: Perturbations around Case A2 on the left, Case D2 on the right. Green cross marks benchmark point.

fit points given in Cases A2 and D2, whilst keeping the other three parameters fixed - Figure 4.5 shows such perturbations. On the vertical axes, $\Delta\chi^2$ is the deviation from minimum χ^2; the stationary point thus shows a vanishing $\Delta\chi^2$ corresponding to the benchmark point itself.

4.6.4 Future tests of the Littlest Seesaw

Given the constantly evolving nature of particle physics and the rapid technological advances being made in neutrino experiments, it is to be expected that the precision of PMNS parameter measurements will improve considerably in the coming years. With this in mind, it is pertinent to discuss the range of values of each observable for which this analysis method of the LS remains a relevant and viable test of neutrino masses

Figure 4.5: Perturbations around Case A2 benchmark point shown on the left, those for Case D2 on the right.

and properties. Table 4.4 below shows 1σ, 2σ and 3σ ranges for each of the observables predicted by Case A2. The same ranges are shown for Case D2 in Table 4.5. It

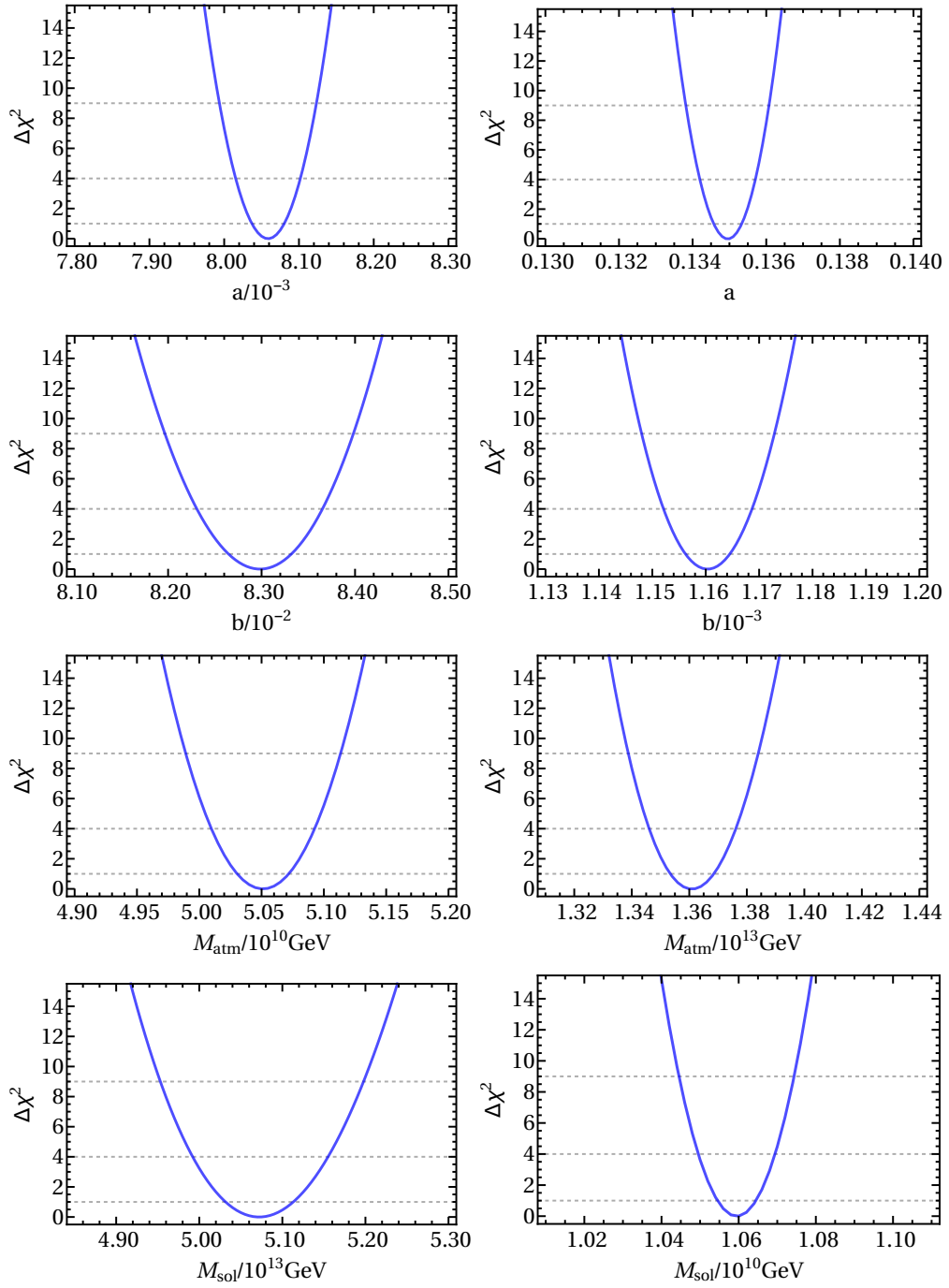|	1σ range	2σ range	3σ range
$\theta_{12}/°$	$34.254 \rightarrow 34.350$	$34.236 \rightarrow 34.365$	$34.217 \rightarrow 34.383$
$\theta_{13}/°$	$8.370 \rightarrow 8.803$	$8.300 \rightarrow 8.878$	$8.218 \rightarrow 8.959$
$\theta_{23}/°$	$45.405 \rightarrow 45.834$	$45.343 \rightarrow 45.910$	$45.269 \rightarrow 45.996$
$\Delta m_{12}^2/10^{-5}\mathrm{eV}^2$	$7.030 \rightarrow 7.673$	$6.930 \rightarrow 7.805$	$6.788 \rightarrow 7.952$
$\Delta m_{31}^2/10^{-3}\mathrm{eV}^2$	$2.434 \rightarrow 2.561$	$2.407 \rightarrow 2.587$	$2.377 \rightarrow 2.616$
$\delta/°$	$-88.284 \rightarrow -86.568$	$-88.546 \rightarrow -86.287$	$-88.864 \rightarrow -85.966$
$Y_B/10^{-10}$	$0.839 \rightarrow 0.881$	$0.831 \rightarrow 0.889$	$0.822 \rightarrow 0.898$

Table 4.4: Ranges of observables for Case A2.

is interesting to note that for Case D, the values of θ_{23} favoured by the model are slightly lower than in Case A, as are the predicted values of δ. In other words, if

	1σ range	2σ range	3σ range
$\theta_{12}/°$	$34.291 \rightarrow 34.379$	$34.278 \rightarrow 34.391$	$34.264 \rightarrow 34.404$
$\theta_{13}/°$	$8.384 \rightarrow 8.784$	$8.329 \rightarrow 8.838$	$8.268 \rightarrow 8.902$
$\theta_{23}/°$	$44.044 \rightarrow 44.434$	$43.991 \rightarrow 44.484$	$43.925 \rightarrow 44.539$
$\Delta m_{12}^2/10^{-5}\mathrm{eV}^2$	$7.058 \rightarrow 7.615$	$6.966 \rightarrow 7.688$	$6.875 \rightarrow 7.787$
$\Delta m_{31}^2/10^{-3}\mathrm{eV}^2$	$2.435 \rightarrow 2.562$	$2.407 \rightarrow 2.590$	$2.373 \rightarrow 2.624$
$\delta/°$	$-93.708 \rightarrow -92.180$	$-93.919 \rightarrow -91.964$	$-94.160 \rightarrow -91.730$
$Y_B/10^{-10}$	$0.838 \rightarrow 0.881$	$0.827 \rightarrow 0.893$	$0.820 \rightarrow 0.899$

Table 4.5: Case D2 ranges for observables.

future neutrino experiments were to precisely measure these values as well outside these ranges, this would be a way to disqualify this method of testing the LS. This statement is of particular relevance when it comes to θ_{23}, as it can be seen that any experimentally measured departure from close to maximal mixing would come in direct contradiction with a feature intrinsic to the model. It is also interesting to note once again the case of δ - although the experimental uncertainty on this parameter is at present extremely large, the fits performed in this analysis provided a suggestion for $\delta \sim -90°$, which is consistent with recent hints from global fits. However, the ranges stated above are purely indicative and should not be taken as absolute. The method used to obtain them incurs limitations, as it was not possible to analyse the range of each observable separately here. The χ^2 values used to define ranges studied were made up of contributions from all seven observables at the same time, which explains why the final valid ranges of observables are rather narrow (as the effect of, for instance, Y_B

will be more dominant on the total χ^2 than that of the mixing angles).

As an additional test of the model, we hypothesised a possible future experimental sensitivity on θ_{23}, based on the work of [145]. Taking the current measured central value of $\theta_{23} = 47.2°$ with its expected future 1σ precision of $\pm 0.66°$ - based on a combined sensitivity analysis of DUNE and T2HK - we perform a new scan to see whether this measurement would greatly alter the χ^2 and thus invalidate the LS. Results for both Case A and D - denoted by A2' and D2' respectively - are shown in Table 4.6 and compared to the results obtained previously. It can be seen that the χ^2 of Case D2

	Case A2	Case A2'	Case D2	Case D2'
χ^2/d.o.f.	1.749/3	7.49/3	2.070/3	21.80/3

Table 4.6: Best fit point χ^2 for hypothetical θ_{23}.

suffers a very large increase for this new hypothetical experimental value of θ_{23}, which would seem to rule out this case as a viable test of the model. However, Case A2 would only see its χ^2 pushed to a value of 2.49 per d.o.f., which could possibly be improved with additional testing. We can therefore conclude that if this observable were indeed measured very precisely to be its current value, the LS could potentially continue to be a valid model, in spite of a departure from close to maximal mixing.

4.7 Summary

The Littlest Seesaw model remains the most minimal seesaw model which can explain current data. It involves two right-handed neutrino masses and two real coefficients a, b of the column vectors proportional to $(0, 1, 1)$ and $(1, 3, 1)$ or $(1, 1, 3)$, comprising the Yukawa matrix in the flavour basis, with a fixed relative phase between these columns of $\pi/3$. In this chapter, we fitted the LS model to low-energy neutrino data and leptogenesis taking into account RG corrections. The four high-energy LS parameters in the flavour basis, namely two real Yukawa couplings a, b and two right-handed neutrino masses were determined by an excellent fit to the seven currently constrained observables of low-energy neutrino data and leptogenesis.

For Case A corresponding to Yukawa columns $a(0, 1, 1)$ and $b(1, 3, 1)$, we fit the respective right-handed neutrino masses to be $M_{\mathrm{atm}} \simeq 5 \times 10^{10}$ GeV and $M_{\mathrm{sol}} \simeq 0.5 - 3 \times 10^{14}$ GeV, depending on the GUT scale. For Case D corresponding to Yukawa columns $b(1, 1, 3)$ and $a(0, 1, 1)$, we fit the respective right-handed neutrino masses to be $M_{\mathrm{sol}} \simeq 1 \times 10^{10}$ GeV and $M_{\mathrm{atm}} \simeq 1.6 - 14 \times 10^{12}$ GeV. We estimate $\chi^2 \simeq 1.5 - 1.75$ for the three d.o.f. for Case A, and $\chi^2 \simeq 2.1 - 2.6$ for the three d.o.f. for Case D. Both are excellent fits, regardless of the assumed unification scale. We extract allowed ranges of neutrino parameters from our fit data, including $\theta_{23} = 45.3^o - 46.0^o$ and $\delta = -87^o \pm 2^o$ for Case A and $\theta_{23} = 44.0^o - 44.5^o$ and $\delta = -93^o \pm 2^o$ for Case D. These results enable the Littlest Seesaw to be tested in future neutrino experiments.

The Littlest Seesaw continues to be a relevant, highly consistent model that provides an outstanding fit to data. It is predictive, with just four high-energy parameters resulting in seven observables apparent at low scales. Taking into account RG corrections, this enables both the high-energy RH neutrino masses and the Yukawa coupling constants a, b to be fixed by low-energy neutrino data and leptogenesis, for the first time in any seesaw model. In turn, the resulting fit gives restricted ranges of low-energy observables, where these predictions will be confronted by data emerging in a few years. Within this framework, future neutrino experiments will allow a window into the GUT scale parameters of the most minimal seesaw model, providing insight into physics at the highest scales.

Chapter 5

Non-Minimal Flavour Violation from Unification in the MSSM

5.1 Introduction

Despite the absence of direct experimental evidence, supersymmetric extensions continue to provide attractive solutions to shortcomings of the SM. Phenomenologically, they provide viable dark matter candidates and can readily accommodate seesaw explanations for neutrino masses, such as that introduced in Chapter 4. From a theoretical point of view, they cure the Higgs mass correction hierarchy problem and lead to precise gauge-coupling unification as discussed in Chapter 3. This last point can be seen as a hint towards Grand Unified Theories.

The fact that predicted superpartners have not been observed so far may be moderated by the argument that current direct searches rely on specific assumptions, for example, that scalar masses are assumed to be degenerate at the GUT scale where gauge couplings unify. Moreover, as superpartner mass limits creep ever higher, the assumption of Minimal Flavour Violation (MFV), postulating that the flavour structure of the theory is identical to the SM (all flavour-violating interactions are related to the CKM and PMNS matrices only), may be relaxed without violating experimental limits. Relaxing this assumption and allowing for additional sources of flavour violation leads to modification of decay patterns, for example in squark searches. As a further consequence, mass limits in this sector may be considerably weakened [162–164]. In addition, it appears that a considerable region of the parameter space of the TeV scale MSSM can accommodate such Non-Minimal Flavour Violation (NMFV) in the squark sector with respect to current experimental and theoretical constraints [165–167].

In recent years, the possibility of NMFV has received considerable attention in the context of TeV scale physics studies [168], mainly concerning collider signatures [169–182], dark-matter-related aspects [183–186] and precision [187–190]. Moreover, a considerable amount of work has been realized on flavour violation aspects within ultraviolet frameworks [191–207]. In a GUT framework, the flavour structure may

be generated at the high scale, perhaps through flavour symmetries. Within a SUSY theory, imposing such symmetries can yield a pattern of soft-breaking terms which accomodate flavour violating terms at the unification scale. Renormalisation group running then generates the corresponding terms at the TeV scale, which enter the phenomenology at low scales.

The link between NMFV terms at the TeV scale and the GUT scale is important from both phenomenological and model-building points of view. First, although they may be numerically rather different, flavour violating interactions in the squark and slepton sectors are linked if a unifying symmetry is present. The same source of flavour violation may therefore be challenged by experimental data from both sectors. Second, uncovering information on the flavour structure of a new physics framework at the TeV-scale may give valuable hints towards unification and related flavour symmetries. The work presented in this chapter is a first step in this direction.

In a recent paper [208], a scenario was discussed in the framework of an $SU(5)$ GUT combined with A_4 family symmetry[1]. The idea was that three $\overline{\mathbf{5}}$ representations form a single triplet of the family symmetry with a unified soft mass m_F, while the three $\mathbf{10}$ representations are singlets under the family symmetry with independent soft masses m_{T_1}, m_{T_2}, m_{T_3}. Assuming MFV, it was shown that to account for the muon anomalous magnetic moment $(g-2)_\mu$, dark matter and LHC data simultaneously, non-universal gaugino masses M_i $(i=1,2,3)$ at the unification scale are required. This work focussed on a region of parameter space that has not before been studied in detail characterised by low higgsino mass $\mu \simeq -300$ GeV. The scenario also required a right-handed smuon $\tilde{\mu}_R$ with a mass around 100 GeV, and a neutralino $\tilde{\chi}_1^0$ several GeV lighter which allows successful dark matter. The LHC will be able to fully test this scenario with the upgraded luminosity via muon dominated tri- and di-lepton signatures resulting from higgsino dominated $\tilde{\chi}_1^\pm \tilde{\chi}_2^0$ and $\tilde{\chi}_1^+ \tilde{\chi}_1^-$ production, along with direct smuon searches in the same kinematic region.

The above study [208] was concerned with the implications of a flavoured GUT model for the superpartner spectrum consistent with $(g-2)_\mu$ and the dark matter relic density. However, it was assumed that there was no flavour violation at the GUT scale, whereas it is well known that such flavour violation is expected in these models [209–211]. The goal of this investigation was to extend this work to the NMFV framework by introducing off-diagonal squark and slepton mass-squared terms at the GUT scale. Here, we take a phenomenological approach, and simply introduce flavour violating terms at high energy by hand, to explore their effect on observables. To this end two MFV 'reference points' are considered, one of which is inspired by the findings of past work [208] and involves a very light smuon capable of accounting for $(g-2)_\mu$, and the other with a heavier smuon, harder to discover at the LHC, but not able to account for $(g-2)_\mu$. In both cases, we perturb around these points, switching on off-diagonal

---

[1]Note that the A_4 may be replaced by S_4 or $SO(3)$ or indeed any family symmetry which contains both triplet and singlet representations.

mass terms, consistently with $SU(5)$, which we assume arise from A_4 breaking effects. We find interesting correlations between flavour violating parameters at the GUT scale consistent with the stringent lepton flavour violating processes $\mu \to e\gamma$.

5.2 Non-Minimal Flavour Violation in SUSY GUTs

The model under consideration in this chapter is presented here, namely the MSSM based on $SU(5)$ unification, including A_4 flavour symmetry entailing NMFV terms present at the GUT scale.

5.2.1 SUSY-breaking in the MSSM

Although the exact breaking mechanism is not completely understood, it is well known that for SUSY to be a viable symmetry of nature, it must be broken to some degree. The associated SUSY-breaking Lagrangian contains all terms which do not necessarily respect SUSY but hold to gauge symmetries and renormalisability. In the MSSM, the most general SUSY-breaking Lagrangian reads as per Equation (5.1).

$$
\begin{aligned}
\mathcal{L}_{\text{soft}}^{MSSM} = &-\frac{1}{2}\Big(M_3\widetilde{g}\widetilde{g} + M_2\widetilde{W}\widetilde{W} + M_1\widetilde{B}\widetilde{B} + c.c.\Big) \\
&- M_Q^2\widetilde{Q}^\dagger\widetilde{Q} - M_L^2\widetilde{L}^\dagger\widetilde{L} - M_U^2\widetilde{\overline{U}}\widetilde{\overline{U}}^\dagger - M_D^2\widetilde{\overline{D}}\widetilde{\overline{D}}^\dagger - M_E^2\widetilde{\overline{E}}\widetilde{\overline{E}}^\dagger \\
&- \Big(A_u\widetilde{\overline{U}}\widetilde{Q}H_u - A_d\widetilde{\overline{D}}\widetilde{Q}H_d - A_e\widetilde{\overline{E}}\widetilde{L}H_d + c.c.\Big) \\
&- M_{H_u}^2 H_u^* H_u - M_{H_d}^2 H_d^* H_d - \big(bH_uH_d + c.c.\big)
\end{aligned}
\tag{5.1}
$$

While the soft mass and trilinear parameters appearing in Equation (5.1) are assumed diagonal matrices in flavour space within the MFV framework, they may comprise non-diagonal entries when relaxing this hypothesis and considering an NMFV scenario. It should be noted that generic SUSY models do not possess any symmetry preventing large off-diagonal elements in soft-SUSY parameters. The soft mass-squared parameters

are defined in the Super-CKM (SCKM) basis[2] and are detailed in Equation (5.2):

$$
M_Q^2 = \begin{pmatrix} (M_Q)_{11}^2 & (\Delta_{12}^Q)^2 & (\Delta_{13}^Q)^2 \\ \cdot & (M_Q)_{22}^2 & (\Delta_{23}^Q)^2 \\ \cdot & \cdot & (M_Q)_{33}^2 \end{pmatrix},
$$

$$
M_U^2 = \begin{pmatrix} (M_U)_{11}^2 & (\Delta_{12}^U)^2 & (\Delta_{13}^U)^2 \\ \cdot & (M_U)_{22}^2 & (\Delta_{23}^U)^2 \\ \cdot & \cdot & (M_U)_{33}^2 \end{pmatrix}, \qquad M_D^2 = \begin{pmatrix} (M_D)_{11}^2 & (\Delta_{12}^D)^2 & (\Delta_{13}^D)^2 \\ \cdot & (M_D)_{22}^2 & (\Delta_{23}^D)^2 \\ \cdot & \cdot & (M_D)_{33}^2 \end{pmatrix},
$$

$$
M_L^2 = \begin{pmatrix} (M_L)_{11}^2 & (\Delta_{12}^L)^2 & (\Delta_{13}^L)^2 \\ \cdot & (M_L)_{22}^2 & (\Delta_{23}^L)^2 \\ \cdot & \cdot & (M_L)_{33}^2 \end{pmatrix}, \qquad M_E^2 = \begin{pmatrix} (M_E)_{11}^2 & (\Delta_{12}^E)^2 & (\Delta_{13}^E)^2 \\ \cdot & (M_E)_{22}^2 & (\Delta_{23}^E)^2 \\ \cdot & \cdot & (M_E)_{33}^2 \end{pmatrix}
$$

$$(5.2)$$

Such matrices are associated with the left-handed squarks, right-handed up- and down-type squarks, left-handed sleptons and sneutrinos, and right-handed sleptons, respectively. In addition, Equation (5.3) shows the full trilinear coupling matrices.

$$
A_U = \begin{pmatrix} (A_U)_{11} & \Delta_{12}^{AU} & \Delta_{13}^{AU} \\ \Delta_{21}^{AU} & (A_U)_{22} & \Delta_{23}^{AU} \\ \Delta_{31}^{AU} & \Delta_{32}^{AU} & (A_U)_{33} \end{pmatrix}, \quad A_D = \begin{pmatrix} (A_D)_{11} & \Delta_{12}^{AD} & \Delta_{13}^{AD} \\ \Delta_{21}^{AD} & (A_D)_{22} & \Delta_{23}^{AD} \\ \Delta_{31}^{AD} & \Delta_{32}^{AD} & (A_D)_{33} \end{pmatrix},
$$

$$
A_E = \begin{pmatrix} (A_E)_{11} & \Delta_{12}^{AE} & \Delta_{13}^{AE} \\ \Delta_{21}^{AE} & (A_E)_{22} & \Delta_{23}^{AE} \\ \Delta_{31}^{AE} & \Delta_{32}^{AE} & (A_E)_{33} \end{pmatrix}
$$

$$(5.3)$$

Detailed expressions for diagonal elements of the matrices given in Equations (5.3) and (5.3) can be found in Martin's famous primer [36]. Note that the soft mass matrices in Equation (5.3) are symmetric due to the requirement for hermiticity. It is convenient to parametrize the off-diagonal and hence flavour violating elements of the above matrices in a dimensionless manner by normalizing them to the respective diagonal entries of sfermion mass matrices. In the SCKM basis, one can recover the following parameterisation [200];

$$
(\delta_{LL}^Q)_{ij} = \frac{(\Delta_{ij}^Q)^2}{(M_Q)_{ii}(M_Q)_{jj}}, \quad (\delta_{RR}^U)_{ij} = \frac{(\Delta_{ij}^U)^2}{(M_U)_{ii}(M_U)_{jj}}, \quad (\delta_{RR}^D)_{ij} = \frac{(\Delta_{ij}^D)^2}{(M_D)_{ii}(M_D)_{jj}},
$$

$$
(\delta_{RL}^U)_{ij} = \frac{v_u}{\sqrt{2}} \frac{\Delta_{ij}^{AU}}{(M_Q)_{ii}(M_U)_{jj}}, \quad (\delta_{RL}^D)_{ij} = \frac{v_d}{\sqrt{2}} \frac{\Delta_{ij}^{AD}}{(M_Q)_{ii}(M_D)_{jj}}, \tag{5.4}
$$

$$
(\delta_{LL}^L)_{ij} = \frac{(\Delta_{ij}^L)^2}{(M_L)_{ii}(M_L)_{jj}}, \quad (\delta_{RR}^E)_{ij} = \frac{(\Delta_{ij}^E)^2}{(M_E)_{ii}(M_E)_{jj}}, \quad (\delta_{RL}^E)_{ij} = \frac{v_d}{\sqrt{2}} \frac{\Delta_{ij}^{AE}}{(M_L)_{ii}(M_E)_{jj}}
$$

---

[2]The super-CKM basis is the one in which the up- and down-type SM quark Yukawa couplings are diagonal matrices.

In Equation (5.4), v_u and v_d denote vacuum expectation values of the up- and down-type Higgs doublets. Note that these definitions hold at any scale, but in particular here we are interested in the GUT and TeV scales. Moreover, the situation where all off-diagonal NMFV parameters defined in Equation (5.4) vanish corresponds to a scenario with very minimal flavour violation.

5.2.2 SU(5) unification

The full model under consideration is based on the gauge group $SU(5)$, which accomodates its matter fields in the $F = \overline{\mathbf{5}}$ and $T = \mathbf{10}$ representations according to Equation (5.5).

$$
F = \overline{\mathbf{5}} = \begin{pmatrix} d_r^c \\ d_b^c \\ d_g^c \\ e \\ -\nu_e \end{pmatrix}_L , \qquad
T = \mathbf{10} = \begin{pmatrix} 0 & u_g^c & -u_b^c & u_r & d_r \\ . & 0 & u_r^c & u_b & d_b \\ . & . & 0 & u_g & d_g \\ . & . & . & 0 & e^c \\ . & . & . & . & 0 \end{pmatrix}_L , \qquad (5.5)
$$

Everything is written as a left-handed Weyl fermion. The Higgs doublets H_u and H_d which break the electroweak symmetry may arise from $SU(5)$ multiplets $H_{\mathbf{5}}$ and $H_{\overline{\mathbf{5}}}$, provided colour triplet components are heavy. The $SU(5)$ gauge group may be broken by an additional Higgs multiplet in the $\mathbf{24}$ representation developing a vacuum expectation value, the breaking pattern of the symmetry is shown in Equation (5.6).

$$
SU(5) \ \to \ SU(3)_C \times SU(2)_L \times U(1)_Y \tag{5.6}
$$

Complete SM quark and lepton families (Q, u^c, d^c, L, e^c) can be readily accomodated into $SU(5)$ representations.

$$
\begin{aligned}
F(\overline{\mathbf{5}}) &= d^c(\overline{\mathbf{3}}, \mathbf{1}, 1/3) \oplus L(\mathbf{1}, \overline{\mathbf{2}}, -1/2), \\
T(\mathbf{10}) &= u^c(\overline{\mathbf{3}}, \mathbf{1}, -2/3) \oplus Q(\mathbf{3}, \mathbf{2}, 1/6) \oplus e^c(\mathbf{1}, \mathbf{1}, 1)
\end{aligned} \tag{5.7}
$$

In a supersymmetric framework $SU(5)$ symmetry provides relationships between the soft terms belonging to supermultiplets within a given representation. For the MSSM under consideration, we express the soft-breaking Lagrangian in terms of $SU(5)$ fields:

$$
\begin{aligned}
\mathcal{L}_{\mathrm{soft}}^{\mathrm{SU(5)MSSM}} = &-\frac{1}{2}\left(M_1 \widetilde{B}\widetilde{B} + M_2 \widetilde{W}\widetilde{W} + M_3 \widetilde{g}\widetilde{g} + \mathrm{h.c.}\right) \\
&- M_F^2 \widetilde{F}^\dagger \widetilde{F} - M_T^2 \widetilde{T}^\dagger \widetilde{T} \\
&- \left(A_{TT}\widetilde{T}^* H_u \widetilde{T} + A_{FT}\widetilde{F}^* H_d \widetilde{T} + \mathrm{h.c.}\right) \\
&- m_{H_u}^2 H_u^* H_u - m_{H_d}^2 H_d^* H_d - \left(b H_u^* H_d + \mathrm{h.c.}\right).
\end{aligned} \tag{5.8}
$$

where $\widetilde{F}$ and $\widetilde{T}$ are the superpartner fields of F and T given in Equation (5.5). Comparing this with Equation (5.1) leads to relations as per Equation (5.9).

$$
\begin{aligned}
M_Q^2 \;=\; M_U^2 \;=\; M_E^2 \;&\equiv\; M_T^2 \,, \\
M_D^2 \;=\; M_L^2 \;&\equiv\; M_F^2 \,, \\
A_D \;=\; (A_E)^T \;&\equiv\; A_{FT} \,, \\
A_U \;&\equiv\; A_{TT} \,,
\end{aligned}
\tag{5.9}
$$

Such definitions hold only at the GUT scale as renormalisation group evolution towards lower scales will spoil these relations.

5.2.3 The $\mathbf{A_4 \times SU(5)}$ model

In addition to $SU(5)$ grand unification, we impose an A_4 (alternating group of order 4) flavour symmetry on our model content. To this end we unify the three families of $F = \bar{\mathbf{5}} = (d^c, L)$ into the triplet of A_4 leading to a unified soft mass parameter m_F for the three generations. The three sets of $T_i = \mathbf{10}_i = (Q, u^c, e^c)_i$ are singlets under A_4, i.e. the three generations may have independent soft mass parameters m_{T_1}, m_{T_2}, m_{T_3} [34, 209, 212–214]. Through breaking the discrete symmetry, we induce flavour violation in soft parameters. We express this primordial flavour violation as the matrices M_T^2, M_F^2, A_{FT}, and A_{TT} analogously to Equation (5.2) in the flavour basis of A_4, before rotation to the SCKM:

$$
M_T^2 = \begin{pmatrix} m_{T_1}^2 & (\Delta_{12}^T)^2 & (\Delta_{13}^T)^2 \\ \cdot & m_{T_2}^2 & (\Delta_{23}^T)^2 \\ \cdot & \cdot & m_{T_3}^2 \end{pmatrix} , \qquad
M_F^2 = \begin{pmatrix} m_F^2 & (\Delta_{12}^F)^2 & (\Delta_{13}^F)^2 \\ \cdot & m_F^2 & (\Delta_{23}^F)^2 \\ \cdot & \cdot & m_F^2 \end{pmatrix} ,
$$

$$
A_{FT} = \begin{pmatrix} (A_{FT})_{11} & \Delta_{12}^{FT} & \Delta_{13}^{FT} \\ \Delta_{21}^{FT} & (A_{FT})_{22} & \Delta_{23}^{FT} \\ \Delta_{31}^{FT} & \Delta_{32}^{FT} & (A_{FT})_{33} \end{pmatrix} , \qquad
A_{TT} = \begin{pmatrix} (A_{TT})_{11} & \Delta_{12}^{TT} & \Delta_{13}^{TT} \\ \Delta_{21}^{TT} & (A_{TT})_{22} & \Delta_{23}^{TT} \\ \Delta_{31}^{TT} & \Delta_{32}^{TT} & (A_{TT})_{33} \end{pmatrix}
\tag{5.10}
$$

Note that the breaking of A_4 around the GUT scale enforces off-diagonal elements of matrices in Equation (5.10) to be smaller than diagonal entries, giving theoretical motivation for small-but-non-zero flavour violation in such a class of models. $SU(5)$ gives the following relationships between the dimensionless NMFV parameters in the

basis before rotation to the SCKM (as denoted by the subscript '0'):

$$
\begin{aligned}
\delta_{LL}^{Q_0} &= \delta_{RR}^{U_0} = \delta_{RR}^{E_0} \equiv \delta_T, \\
\delta_{RR}^{D_0} &= \delta_{LL}^{L_0} \equiv \delta_F, \\
\delta_{RL}^{D_0} &= (\delta_{RL}^{E_0})^T \equiv \delta_{FT}, \\
\delta_{RL}^{U_0} &\equiv \delta_{TT}
\end{aligned}
\tag{5.11}
$$

These four matrices parameterise flavour violation in the $A_4 \times SU(5)$ setup. Note that δ_T, δ_F and δ_{TT} are necessarily symmetric whereas δ_{FT} is not (see Equations (5.8) and (5.10)) leading to a total of 15 NMFV parameters at the GUT scale. It is apparent that we have flavour violation at phenomenological scales from two distinct sources: The presence of off-diagonal elements in various coupling matrices at the GUT scale due to A_4 breaking and further effects induced by RGE running.

5.3   Setup and tools

We assessed the impact of flavour violating parameters introduced at the GUT scale on low-energy physics. In order to work with a concrete framework, we focus on the model based on $A_4 \times SU(5)$ presented in Section 5.2. The high-scale model is tested against the dark matter relic density along with leptonic and hadronic flavour changing observables and the observed Higgs boson mass.

5.3.1   MFV reference points

We begin by choosing suitable reference scenarios respecting the MFV paradigm. From previous work [208] it is apparent that successfully imposing the dark matter relic density as well as the anomalous magnetic moment of the muon on the $A_4 \times SU(5)$ framework requires specific numeric configurations. More precisely, the corresponding parameter points feature a physical spectrum where the "right-handed" smuon is light and almost mass-degenerate with the lightest neutralino, which is bino-like. This specific setup simultaneously satisfies the $(g-2)_\mu$ and relic density constraints [40, 215]. For our study, we choose two fixed MFV reference scenarios that we will not alter based on this previous investigation, which are summarized in Table 5.1. The first reference point of our choice corresponds to the scenario labelled 'BP4' in the past investigation by other authors [208]. Due to the practicalities of including NMFV terms at the GUT scale, we do not make use of the same version of the spectrum generator SPheno. In consequence, effects from renormalization group running differ slightly, and we have adapted the input parameters of the original BP4 reference scenario to the ones given in Table 5.1. Note that although there is a small deviation for the TeV scale parameters as compared to BP4, the phenomenological aspects of our reference scenario at the TeV scale are unchanged. Recall that the rather low smuon mass parameter, $m_{T_2} = 200$

	Parameter/Observable	Scenario 1	Scenario 2
MFV Parameters at GUT scale	m_F	5000	5000
	m_{T_1}	5000	5000
	m_{T_2}	200	233.2
	m_{T_3}	2995	2995
	$(A_{TT})_{33}$	-940	-940
	$(A_{FT})_{33}$	-1966	-1966
	M_1	250.0	600.0
	M_2	415.2	415.2
	M_3	2551.6	2551.6
	m_{H_u}	4242.6	4242.6
	m_{H_d}	4242.6	4242.6
	$\tan\beta$	30	30
	μ	-2163.1	-2246.8
Physical masses	m_h	126.7	127.3
	$m_{\widetilde{g}}$	5570.5	5625.7
	$m_{\widetilde{\mu}_L}$	4996.7	4997.5
	$m_{\widetilde{\mu}_R}$	102.1	254.4
	$m_{\widetilde{\chi}_1^0}$	94.6	250.4
	$m_{\widetilde{\chi}_2^0}$	323.6	322.0
	$m_{\widetilde{\chi}_3^0}$	2248.8	2331.1
	$m_{\widetilde{\chi}_4^0}$	2248.8	2331.2
	$m_{\widetilde{\chi}_1^\pm}$	323.8	322.2
	$m_{\widetilde{\chi}_2^\pm}$	2249.8	2332.2
	$\Omega_{\widetilde{\chi}_1^0}h^2$	0.116	0.120
	$\sigma_{\mathrm{SI}}^{\mathrm{proton}}/10^{-14}\,\mathrm{pb}$	2.987	1.055
	$\sigma_{\mathrm{SI}}^{\mathrm{neutron}}/10^{-14}\,\mathrm{pb}$	3.249	0.986

Table 5.1: GUT scale inputs together with selected physical masses for MFV reference scenarios. First- and second-generation trilinear couplings set to zero. Unless otherwise stated, dimensionful quantities are given in GeV. DM direct detection cross-sections given for protons and neutrons.

GeV, which leads to the physical mass $m_{\tilde{\mu}_R} = 102.1$ GeV, is required in order to satisfy simultaneously the $(g-2)_\mu$ and relic density constraints as discussed in previous investigations [208]. The choice for m_{T_2} is an assumption in this work.

While current limits on "right-handed" smuons still allow masses as low as about 100 GeV [216], Scenario 1 will be directly probed by ongoing LHC searches. For this reason, we choose to include a second reference point which is inspired by the first but features heavier smuons and neutralinos. Such a scenario can still satisfy the relic density constraint due to efficient co-annihilation and avoids LHC limits to be published in the near future. Note that the higher smuon mass $m_{\tilde{\mu}_R} \sim 250$ GeV does not resolve the tension between the measured value of $(g-2)_\mu$ and SM prediction. Let us emphasize that both reference scenarios capture the essential results of previous studies [208], namely almost mass-degenerate "right-handed" smuon and a bino-like neutralino, while all other MSSM states are essentially decoupled.

In both reference scenarios, the required neutralino relic density is achieved by efficient co-annihilation with smuons and even smuon pair annihilation. All (co)annihilation contributions are summarised in Table 5.2. Neutralino pair annihilation mainly proceeds through t- and u-channel smuon exchange, while smuon pair annihilation proceeds through t- or u-channel neutralino exchange. Moreover, the relative importance of the co-annihilation and smuon pair annihilation with respect to the neutralino pair annihilation is governed by the Boltzmann factor involving the mass difference of the two particles [217]. The smuon mass therefore plays a central role for dark matter predictions. Considering NMFV, the off-diagonal elements of the matrices in Equations (5.2) and (5.3) not only violate flavour but can in addition have a significant impact on the smuon mass and thus on the relic density. provided they are comparable to the diagonal elements at some scale.

Annihilation channel	Relative contribution to $\Omega_{\tilde{\chi}_1^0} h^2$	
	Scenario 1	Scenario 2
$\tilde{\chi}_1^0 \tilde{\chi}_1^0 \to \mu \bar{\mu}$	27%	2%
$\tilde{\chi}_1^0 \tilde{\mu}_R \to \mu \gamma$	45%	31%
$\tilde{\chi}_1^0 \tilde{\mu}_R \to \mu Z^0$	8%	8%
$\tilde{\mu}_R \tilde{\mu}_R \to \mu \mu$	10%	37%
$\tilde{\mu}_R \tilde{\mu}_R^* \to \gamma \gamma$	3%	11%

Table 5.2: Dominant annihilation channels contributing to the annihilation cross-section and the neutralino relic density in two MFV reference scenarios.

5.3.2 Introducing NMFV

Starting from the two MFV reference points, we study the impact of flavour violating soft terms by perturbing around these scenarios. Keeping normal MSSM parameters

fixed at the values given in Table 5.1, we perform a random scan on the flavour violating parameters introduced in Equation (5.11) at the GUT scale using flat prior distributions. We vary the NMFV parameters both independently and as part of a multi-dimensional scan over all parameters simultaneously. We subsequently study the impact of experimental data detailed in Table 5.3. We require the Higgs boson mass

Observable	Constraint	Remarks	Refs.
m_h	(125.2 ± 2.5) GeV	(SPheno th.)	[218–220]
$\mathrm{BR}(\mu \to e\gamma)$	$< 4.2 \times 10^{-13}$	90% (exp.)	[218]
$\mathrm{BR}(\mu \to 3e)$	$< 1.0 \times 10^{-12}$	90% (exp.)	[218]
$\mathrm{BR}(\tau \to e\gamma)$	$< 3.3 \times 10^{-8}$	90% (exp.)	[218]
$\mathrm{BR}(\tau \to \mu\gamma)$	$< 4.4 \times 10^{-8}$	90% (exp.)	[218]
$\mathrm{BR}(\tau \to 3e)$	$< 2.7 \times 10^{-8}$	90% (exp.)	[218]
$\mathrm{BR}(\tau \to 3\mu)$	$< 2.1 \times 10^{-8}$	90% (exp.)	[218]
$\mathrm{BR}(\tau \to e^-\mu\mu)$	$< 2.7 \times 10^{-8}$	90% (exp.)	[218]
$\mathrm{BR}(\tau \to e^+\mu\mu)$	$< 1.7 \times 10^{-8}$	90% (exp.)	[218]
$\mathrm{BR}(\tau \to \mu^-ee)$	$< 1.8 \times 10^{-8}$	90% (exp.)	[218]
$\mathrm{BR}(\tau \to \mu^+ee)$	$< 1.5 \times 10^{-8}$	90% (exp.)	[218]
$\mathrm{BR}(B \to X_s\gamma)$	$(3.32 \pm 0.18) \times 10^{-4}$	2σ (exp.)	[221]
$\mathrm{BR}(B_s \to \mu\mu)$	$(2.7 \pm 1.2) \times 10^{-9}$	2σ (exp.)	[218]
ΔM_{B_s}	$(17.757 \pm 0.042 \pm 2.7)$ ps^{-1}	2σ (exp.), (th.)	[218, 222]
ΔM_K	$(3.1 \pm 1.2) \times 10^{-15}$ GeV	2σ (th.)	[218, 223]
ϵ_K	2.228 ± 0.29	2σ (th.)	[218, 223]
$\Omega_{\mathrm{DM}}h^2$	0.1198 ± 0.0042	2σ (exp.), 1% (th.)	[40, 224–226]

Table 5.3: Experimental constraints imposed on the $A_4 \times SU(5)$ MSSM parameter space in our study. Upper limits are given at the 90% confidence level, two-sided limits given at 2σ.

to be reasonably close to the observed value of about 125 GeV, where we account for a theory uncertainty of 2.5 GeV from the SPheno calculation. For the B_s meson oscillation, we take the experimental value $\Delta M_{B_s} = (17.757 \pm 0.021)$ ps^{-1} [215] and add a theory uncertainty of 1.35ps^{-1} [222] from lattice calculations which dominates the total error. For the neutralino relic density, we require that the lightest neutralino accounts for the totality of observed dark matter. The error given by the Planck collaboration is augmented to take into account the 1% accuracy of the theoretical calculation of the relic density by micrOMEGAs. Finally, note that although the reference scenarios defined in Table 5.1 have been obtained considering the anomalous magnetic moment of the muon as a key observable [208], we do not discuss this process in this work. Since

$(g-2)_\mu$ is a flavour-conserving process, we do not expect sizeable effects from NMFV terms on this observable within the ranges allowed from other data.

For numerical evaluation, we make use of the spectrum generator `SPheno 4.0.3` [219, 220], where we utilise the MSSM with general flavour mixing from the `Mathematica` package `SARAH 4.12.3` [227–230]. From the resulting code `SPhenoMSSM` we obtain two-loop renormalization group equations for the soft-breaking parameters and the physical mass spectrum at the TeV scale, along with numerical predictions for flavour observables listed in Table 5.3. The neutralino relic density $\Omega_{\tilde\chi_1^0}h^2$ is computed using `micrOMEGAs 4.3.5` [224–226]. Again, we have used `SARAH` to obtain the `CalcHEP` model files necessary to accomodate NFMV effects in the calculation. Our computational setup is summarized in Figure 5.1. The mass spectrum obtained from `SPhenoMSSM` is handed to `micrOMEGAs` by making use of the *SUSY Les Houches Accord 2* [231]. Note that, since the spin-independent scattering cross-sections related to direct dark matter detection given in Table 5.1 are relatively low as compared to the corresponding experimental limits, such cross-sections are not explicitly evaluated in the numerical analysis. Before running `SPheno`, we first need to perform a CKM transformation to certain GUT scale matrices to comply with the basis that `SPheno` requires for the input parameters (see Appendix B). Let us note that, for typical values of Yukawa parameters inserted into our MFV reference points, CKM matrix running between the GUT and TeV scales is negligible. We therefore assume that the CKM matrix is identical across all scales. In the full multi-dimensional scan, the studied range for each parameter is set empirically to give reasonable computational efficiency as informed by one-dimensional[3] scans over individual parameters. The obtained ranges have been increased slightly to study whether correlations between the different NMFV parameters result in larger allowed ranges compared to one-dimensional scans. The applied limiting values for each MFV scenario under consideration and for each NMFV parameter are given in Table 5.4. From the individual scans, it becomes apparent that for certain NMFV parameters, especially in the case of Scenario 1, small deviations from the MFV case can induce either a charged dark matter candidate (the smuon in this case) or tachyonic mass spectra. We therefore set

$$(\delta_T)_{23} = (\delta_{FT})_{21} = (\delta_{FT})_{32} = 0 \qquad (5.12)$$

throughout the analysis of Scenario 1, and scan over the remaining 12 NMFV parameters according to Table 5.4. This situation does not occur for Scenario 2, where we vary all 15 NMFV parameters. Starting from the GUT scale, we test each point against the observables listed in Table 5.3. Points which do not satisfy all the imposed constraints within the associated uncertainties are collected in the prior distribution only, while those which comply with all constraints are recorded as part of the posterior distribution. In examining the latter, we obtain allowed ranges for each of the NMFV

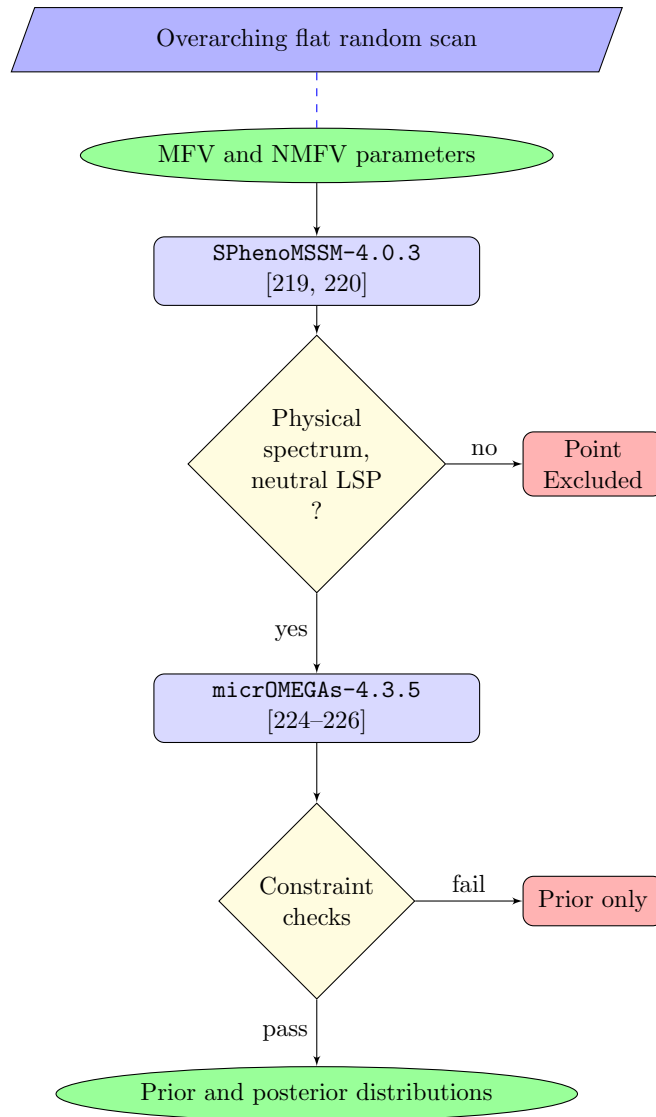[3] one-dimensional here refers to scanning over one parameter at a time

Figure 5.1: Illustration of the computational procedure applied to each point of the parameter scan.

Parameters	Scenario 1	Scenario 2
$(\delta_T)_{12}$	$[-2.00, 2.00] \times 10^{-2}$	$[-5.57, 5.15] \times 10^{-2}$
$(\delta_T)_{13}$	$[-8.01, 8.01] \times 10^{-2}$	$[-0.267, 0.301]$
$(\delta_T)_{23}$	0.0	$[-5.73, 5.73] \times 10^{-2}$
$(\delta_F)_{12}$	$[-8.00, 8.00] \times 10^{-3}$	$[-8.00, 8.00] \times 10^{-3}$
$(\delta_F)_{13}$	$[-1.00, 1.00] \times 10^{-2}$	$[-8.00, 8.00] \times 10^{-2}$
$(\delta_F)_{23}$	$[-1.60, 1.60] \times 10^{-2}$	$[-8.00, 8.00] \times 10^{-2}$
$(\delta_{TT})_{12}$	$[-8.69, 10.43] \times 10^{-4}$	$[-7.46, 8.95] \times 10^{-4}$
$(\delta_{TT})_{13}$	$[-1.74, 1.74] \times 10^{-3}$	$[-3.48, 1.74] \times 10^{-3}$
$(\delta_{TT})_{23}$	$[-0.0174, 0.145]$	$[-0.0871, 0.124]$
$(\delta_{FT})_{12}$	$[-4.64, 4.64] \times 10^{-5}$	$[-5.47, 5.47] \times 10^{-5}$
$(\delta_{FT})_{13}$	$[-7.74, 7.74] \times 10^{-5}$	$[-3.87, 3.87] \times 10^{-4}$
$(\delta_{FT})_{21}$	0.0	$[-1.04, 1.04] \times 10^{-4}$
$(\delta_{FT})_{23}$	$[-1.16, 1.16] \times 10^{-4}$	$[-2.32, 2.32] \times 10^{-4}$
$(\delta_{FT})_{31}$	$[-1.39, 1.39] \times 10^{-5}$	$[-8.81, 8.81] \times 10^{-5}$
$(\delta_{FT})_{32}$	0.0	$[-1.49, 1.49] \times 10^{-4}$

Table 5.4: Ranges of the NMFV parameters defined at the GUT scale for the multi-dimensional scan around reference scenarios. Parameters given as 0.0 have been switched off since even small variations lead to tachyonic mass spectra and/or charged dark matter candidates.

parameters. In addition, by comparing the prior and posterior distributions, and taking into account posterior distributions based on a single constraint, we identify the most important constraints among those listed in Table 5.3 for each NMFV parameter.

5.4   Results

Here we collect results of the analysis. To begin, the general aspects and the obtained limits on the NMFV parameters are presented in Table 5.5. Ultimately, we perform two different kinds of scan on the parameter space: "individual" scans, where only a single δ is varied and all others are set to zero, and "simultaneous" scans where all of the NMFV parameters are varied at the same time according to the ranges given in Table 5.4. From the multi-dimensional scan, we conclude that for the majority of

Parameters	Scenario 1	Most constraining obs. 1	Scenario 2	Constraining obs. 2
$(\delta^T)_{12}$	[-0.015, 0.015]	$\mu \to 3e$, $\mu \to e\gamma$, $\Omega_{\tilde{\chi}_1^0}h^2$	[-0.12, 0.12]†	$\Omega_{\tilde{\chi}_1^0}h^2$, $\mu \to e\gamma$
$(\delta^T)_{13}$	]-0.06, 0.06[	$\Omega_{\tilde{\chi}_1^0}h^2$	[-0.3, 0.3]†	$\Omega_{\tilde{\chi}_1^0}h^2$
$(\delta^T)_{23}$	[0,0]*	$\Omega_{\tilde{\chi}_1^0}h^2$, $\mu \to 3e$, $\mu \to e\gamma$	[-0.1, 0.1]†	$\Omega_{\tilde{\chi}_1^0}h^2$, $\mu \to 3e$, $\mu \to e\gamma$,
$(\delta^F)_{12}$	[-0.008, 0.008]	$\mu \to 3e$, $\mu \to e\gamma$	[-0.015, 0.015]†	$\mu \to 3e$, $\mu \to e\gamma$
$(\delta^F)_{13}$	]-0.01, 0.01[	$\mu \to e\gamma$	[-0.15, 0.15]†	$\mu \to 3e$, $\mu \to e\gamma$
$(\delta^F)_{23}$	]-0.015, 0.015[	$\mu \to e\gamma$, $\Omega_{\tilde{\chi}_1^0}h^2$	[-0.15, 0.15]†	$\Omega_{\tilde{\chi}_1^0}h^2$, $\mu \to e\gamma$, $\mu \to 3e$
$(\delta^{TT})_{12}$	[-3, 3.5] $\times10^{-5}$	prior	[-1, 1.5]† $\times10^{-3}$	prior, $\Omega_{\tilde{\chi}_1^0}h^2$
$(\delta^{TT})_{13}$	]-6, 7[$\times10^{-5}$	prior, $\Omega_{\tilde{\chi}_1^0}h^2$	[-4, 2.5]† $\times10^{-3}$	prior, $\Omega_{\tilde{\chi}_1^0}h^2$
$(\delta^{TT})_{23}$	]-0.5, 4[$\times10^{-5}$	prior, $\Omega_{\tilde{\chi}_1^0}h^2$	[-0.25, 0.2]†	prior, $\Omega_{\tilde{\chi}_1^0}h^2$
$(\delta^{FT})_{12}$	[-0.0015, 0.0015]	$\Omega_{\tilde{\chi}_1^0}h^2$	[-1.2, 1.2]† $\times10^{-4}$	$\mu \to 3e$, $\Omega_{\tilde{\chi}_1^0}h^2$, $\mu \to e\gamma$
$(\delta^{FT})_{13}$	]-0.002, 0.002[	$\Omega_{\tilde{\chi}_1^0}h^2$	[-5, 5] $\times10^{-4}$	$\Omega_{\tilde{\chi}_1^0}h^2$, $\mu \to 3e$, $\mu \to e\gamma$
$(\delta^{FT})_{21}$	[0,0]*	prior	[-1.2, 1.2]† $\times10^{-4}$	$\Omega_{\tilde{\chi}_1^0}h^2$, prior
$(\delta^{FT})_{23}$	]-0.0022, 0.0022[	$\Omega_{\tilde{\chi}_1^0}h^2$	[-6, 6]† $\times10^{-4}$	$\mu \to 3e$, $\Omega_{\tilde{\chi}_1^0}h^2$, $\mu \to e\gamma$
$(\delta^{FT})_{31}$	]-0.0004, 0.0004[	$\Omega_{\tilde{\chi}_1^0}h^2$	[-2, 2]† $\times10^{-4}$	$\Omega_{\tilde{\chi}_1^0}h^2$
$(\delta^{FT})_{32}$	[0,0]*	prior	[-1.5, 1.5] $\times10^{-4}$	$\Omega_{\tilde{\chi}_1^0}h^2$

Table 5.5: Estimated allowed GUT scale flavour violation for both reference scenarios and impactful constraints ordered from most to least constraining. Where square brackets are shown open, we scan up to these values but even if there was some impact from constraints on the relevant distribution, it seems that the allowed region can be larger and extrapolation to concrete limits is not straightforward. * denotes parameters fixed to 0 in order to satisfy LSP and physical mass spectrum requirements. † represents extrapolated ranges; the posterior does not drop to 0 but extrapolation to a limit is reasonable. A parameter that is constrained by the 'prior' is limited by LSP and physical mass requirements.

NMFV parameters, the most sensitive observables are the branching ratios $\mu \to e\gamma$ and $\mu \to 3e$, along with the neutralino relic density $\Omega_{\tilde{\chi}_1^0}h^2$. As discussed in Section 5.3, the impact of the relic density can be attributed to the small mass difference between the smuon and neutralino, which depends strongly on the off-diagonal elements in

the slepton mass matrix. Since both our reference scenario exhibit a relatively small value of $(m_T)_{22}$, very small flavour violating elements can be excluded by current data. Although the experimental limit is more stringent (by about a factor of two) for the decay $\mu \to e\gamma$, the $\mu \to 3e$ decay has similar constraining power and is in certain cases the dominant constraint. This is explained as follows: The amplitude of $\mu \to e\gamma$ is helicity-suppressed and therefore contains a suppression factor m_e/m_μ. While this is also the case for $\mu \to 3e$ diagrams related to those of $\mu \to e\gamma$, there are additional four-point diagrams, where the helicity suppression is lifted since an SM photon is not involved in such topologies. Despite the additional gauge coupling factor and the greater degree of loop suppression, these diagrams are numerically competitive to those of $\mu \to e\gamma$.

One can see that NMFV parameters mixing the first or second generation with the third are constrained by decays $\mu \to e\gamma$ and $\mu \to 3e$ rather than by the corresponding τ decays. This can be traced to the better experimental precision of the muonic decay measurements with respect to the analogous tau decays. Even though NMFV parameters mediating $e - \tau$ or $\mu - \tau$ transitions provide dominant contributions of the tau decays, these parameters also enter into the muon decay amplitudes. For example, if the $\mu \to e\gamma$ process includes a stau in the loop, the corresponding amplitude is proportional to terms including products of the type $(\delta)_{23}(\delta)_{13}$. See Figure 5.2 for a diagrammatic representation. Since muon decay limits are stronger than tau decays by four to five orders of magnitude, the $e - \tau$ and $\mu - \tau$ mixing parameters are constrained by the $e - \mu$ processes first. We have explicitly checked this by artificially lowering the bounds on tau decays. In this case, the tau decay becomes the dominant constraint for the $(\delta)_{13}$ and $(\delta)_{23}$ parameters. Finally, we observe that the constraints coming
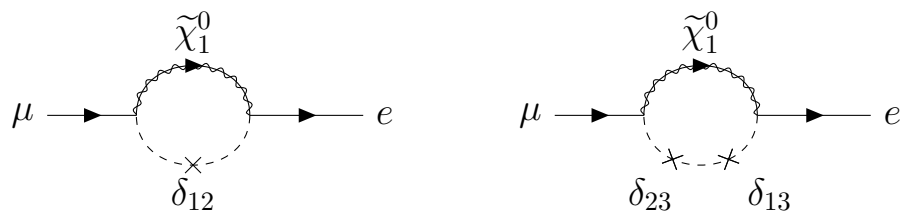

Figure 5.2: Diagrams that contribute to $\mu \to e\gamma$, dashed line represents a slepton and δ denotes a mass insertion. Photon emitted from any particle charged under QED.

from the hadronic sector, such as the $B \to X_s\gamma$ or $B_s \to \mu^+\mu^-$ decays, which are dominant in the case of NMFV in the squark sector alone [167], are not competitive compared to the leptonic constraints in a unified setup. This can be traced to the greater experimental precision of dedicated leptonic measurements compared to meson decays.

All constraints [individual]

a)

probability density

$\left(\delta^F\right)_{12} / 10^{-2}$

All constraints [simultaneous]

b)

probability density
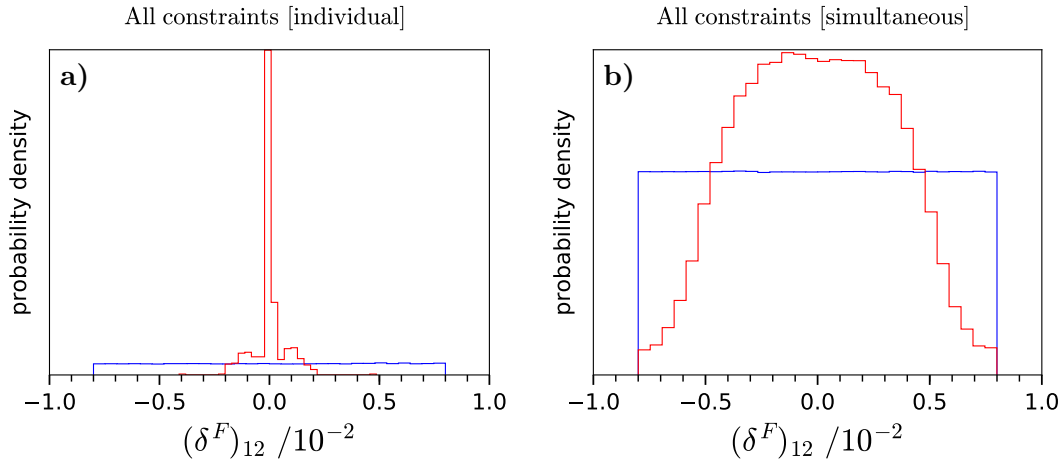
$\left(\delta^F\right)_{12} / 10^{-2}$

Figure 5.3: Comparison of individual (panel a) vs. simultaneous (panel b) scan of the NMFV parameter $(\delta_F)_{12}$ around Scenario 1. Panels show the prior (blue) together with the posterior (red) distributions. All probability densities integrate to unity as required.

All constraints [simultaneous]

a)

probability density

$\left(\delta^F\right)_{12} / 10^{-2}$

BR($\mu \to 3e$) [simultaneous]

b)

probability density
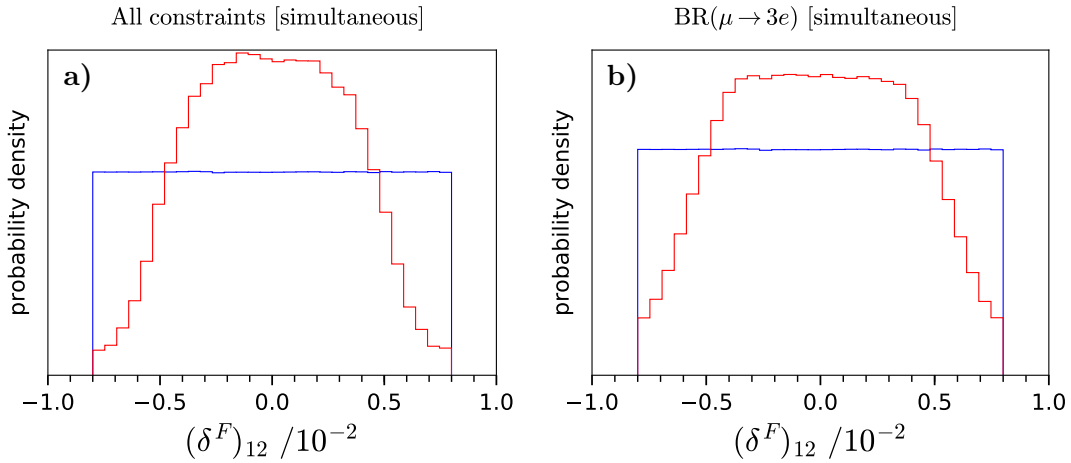
$\left(\delta^F\right)_{12} / 10^{-2}$

Figure 5.4: Dominant constraints on the parameter $(\delta_F)_{12}$ from simultaneous scan around Scenario 1. Prior distributions are given in blue, posterior in red.

5.4.1 Scan around Scenario 1

MFV parameters are fixed at values given in Table 5.1, while we scan over the NMFV parameters according to the ranges given in Table 5.4, either individually, or simultaneously. For each scan, we record the prior distribution containing all points featuring a physical mass spectrum and neutralino dark matter candidate (see also Figure 5.1) along with posterior distribution obtained when imposing either one or all constraints summarised in Table 5.3. Figure 5.3 shows the prior and posterior distributions for the NMFV parameter $(\delta_F)_{12}$. The viable region for this parameter with respect to the imposed constraints is much larger for the case of simultaneous scanning as compared to the individual scan. Indeed, more than one NMFV parameter may enter the calculation of one or more observables. In such a case, interference betwee contributions induced by different NMFV parameters can occur. As a consequence, simultaneous scans can give rise to viable regions of parameter space that would not be fully explored when varying each parameter in isolation. This is seen quantitatively as a broadening of posterior distributions when comparing a simultaneous scan result against one from an individual scan. This feature is present for several of the flavour violating parameters under consideration.

Figure 5.4, panel b) shows the action of a single observable, $\mathrm{BR}(\mu \to 3e)$, on the same parameter $(\delta_F)_{12}$ for simulultaneous scan, and can thus be directly compared to Figure 5.3 [4]. Since the single-constraint posterior shape almost matches the distribution obtained imposing all constraints, we conclude that this parameter is mainly limited by the $\mu \to 3e$ flavour violating decay. The $\mu \to e\gamma$ observable is less important in this case (see Table 5.5, corresponding posterior not shown). Considering $(\delta_T)_{12}$ shown in Figure 5.5 including all constraints, note that the obtained viable interval is again broadened when comparing the individual scan, leading to $|(\delta_T)_{12}| \leq 0.2 \times 10^{-2}$, with the simultaneous scan yielding $|(\delta_T)_{12}| \leq 1.6 \times 10^{-2}$. For the same NMFV parameter $(\delta_T)_{12}$, we detail in Figure 5.6 the effect of three important constraints. The $\mu \to e\gamma$ constraint can be seen to admit the scanned region in its entirety when considering the simultaneous scan, whereas it is by far the most stringent constraint in the individual scan (see Figure 5.5). In addition, Figure 5.6 illustrates how the posterior distribution is constrained by observables.

$(\delta_T)_{13}$ is given in Figure 5.7. It is constrained only by the neutralino relic density, and flavour constraints have no effect. This gives insight on the unexpected shape of the posterior distribution: As we have seen for two previous examples, other NMFV parameters are allowed under flavour constraints to shift significantly away from zero. This gives a marked reduction in superpartner masses which are determined by diagonalising the mass-squared matrices from Equation (5.2). Of particular note is the right-handed smuon, as the initial smallness of m_{T_2} means that small NMFV parameters can reduce the smuon mass with relative ease. As a consequence, the relic density

---

[4] Note that panel b) of Figure 5.3 is identical to panel a) in Figure 5.4.

is reduced due to the smaller mass difference between smuon and neutralino, which can spoil the delicate interplay of co-annihilation which is utilised to obtain a reasonable relic density. The smuon mass also is influenced by $(\delta_T)_{13}$, which by virtue of being unconstrained by flavour observables, may be significant. This parameter increases the lightest smuon mass as a result of specific hierarchies in the slepton mass matrix. $(\delta_T)_{13}$ approximately re-establishes the initial mass difference between the smuon and neutralino allowing the relic density to stay within Planck limits [40]. If one relaxes the assumption that the neutralino $\tilde{\chi}_1^0$ accounts for the totality of relic dark matter, i.e. relax the lower limit on the relic density, then the caracteristic shape observed for $(\delta_T)_{13}$ in Figure 5.7 disappears.

Any NMFV parameters among those listed in Table 5.4 whose distributions are not detailed here do not have much in the way of interesting phenomenona associated with the imposed constraints, therefore the reader can deduce the full effect and resulting ranges from Table 5.5. Recall that for this scenario, the parameters $(\delta_T)_{13}$, $(\delta_{FT})_{21}$, and $(\delta_{FT})_{32}$ have been set to zero resulting from requirements for a physical spectrum and neutral LSP. For all δ_{TT} parameters, these two requirements form the most stringent constraints, hence we comment that the *prior* distribution dominantes over flavour observables. Finally, we do not discuss the δ_{FT} parameters as the corresponding results are much the same as for the scan around Scenario 2 presented below. From the discussed results related to reference Scenario 1, it is clear that varying the NMFV parameters individually is not sufficient to properly explore the entirety of parameter space. For this reason, we do not discuss individual variations any further.

5.4.2 Scan around Scenario 2

We discuss selected results of the simultaneous scan around Scenario 2. NMFV parameters are varied according to the ranges given in Table 5.4, while the MFV parameters are fixed to the values given in Table 5.1. Note that the change of ordinary MSSM inputs compared to Scenario 1 allows the variation of all 15 NMFV parameters. This yields limits on the full range of flavour violation allowed in Scenario 2. Prior and posterior distributions for $(\delta_T)_{13}$ are presented in Figure 5.8, we observe the same feature as for Scenario 1 (see Figure 5.7), however the constraints' effects are more pronounced. Once more, slightly positive or negative values for $(\delta_T)_{23}$ counteract the effects of other NMFV parameters on the neutralino relic density. For $(\delta_F)_{13}$, Figure 5.9 shows that, rather than a single observable having a clear effect, cumulatively $\mu \to e\gamma$, $\mu \to 3e$, and $\Omega_{\tilde{\chi}_1^0}h^2$ constrain the parameter together. Here, we see the effect of flavour violating muon decays on $(\delta)_{13}$ parameters as elaborated upon at the beginning of Section 5.4. Similarly to Scenario 1, all δ_{TT} parameters are constrained by the requirement for a physical mass spectrum and neutral dark matter candidate, and flavour observables have a negligible effect (see Table 5.5). The posterior distribution of $(\delta_{FT})_{13}$ is shown in Figure 5.10, this parameter is practically only constrained by the relic density, as
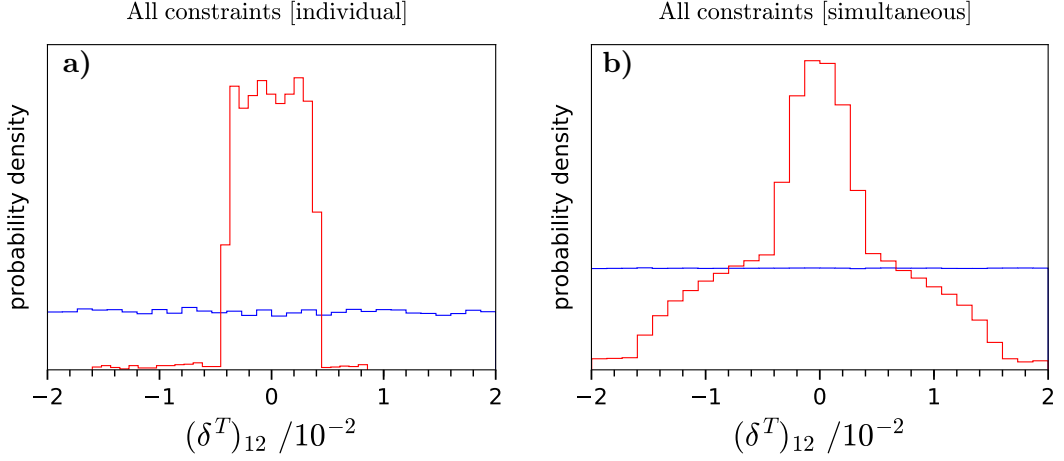
Figure 5.5: Comparison of individual (left) vs. simultaneous (right) scan of $(\delta_T)_{12}$ for Scenario 1. Each panel shows the prior (blue) together with the posterior (red) distributions.
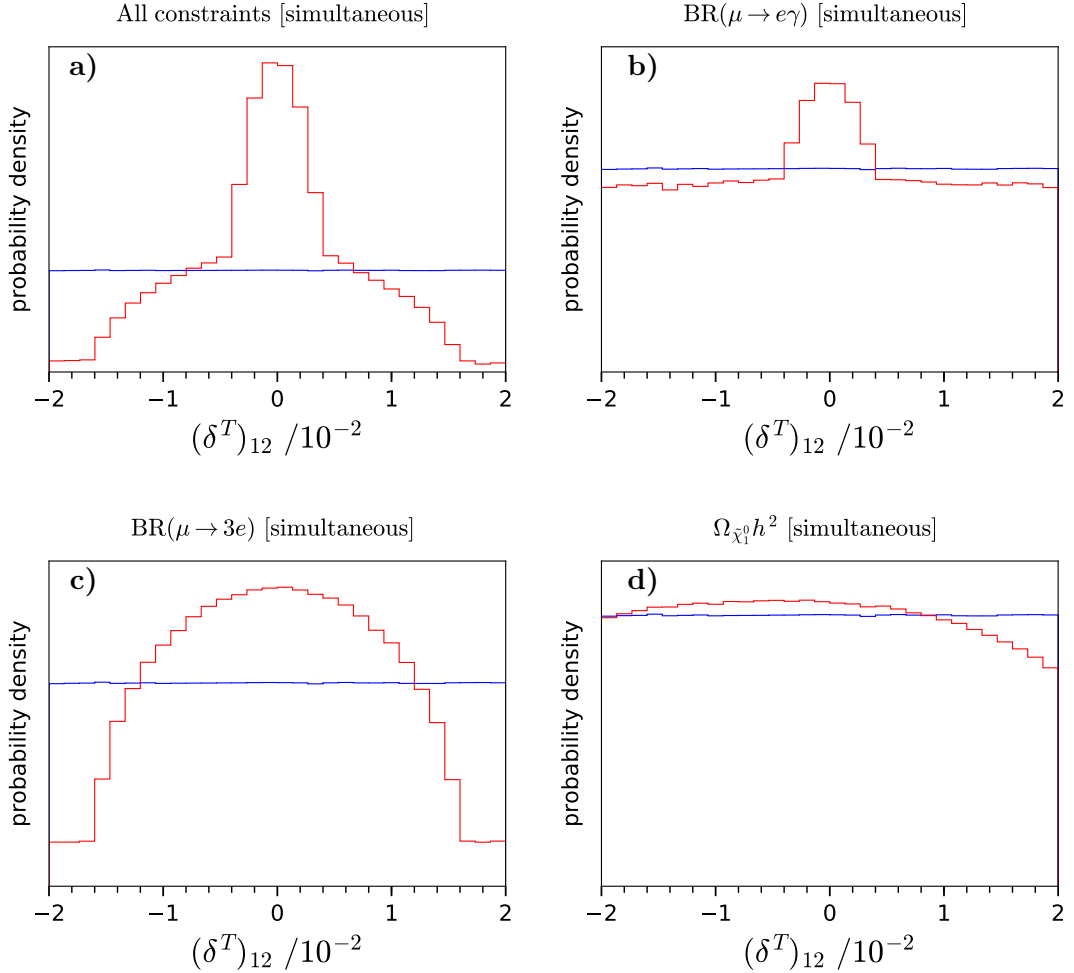

Figure 5.6: Dominant constraints on the parameter $(\delta_T)_{12}$ from simultaneous scan around Scenario 1. Prior distributions are given in blue and posterior distribution in red.
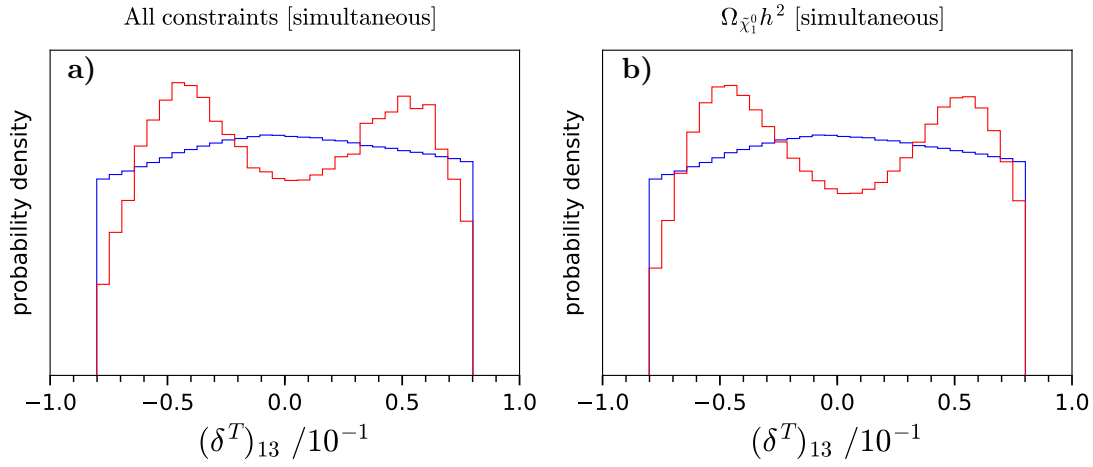
Figure 5.7: Dominant constraints on the parameter $(\delta_T)_{13}$ from simultaneous scan around Scenario 1. Prior distributions are given in blue and posterior distribution are given in red.
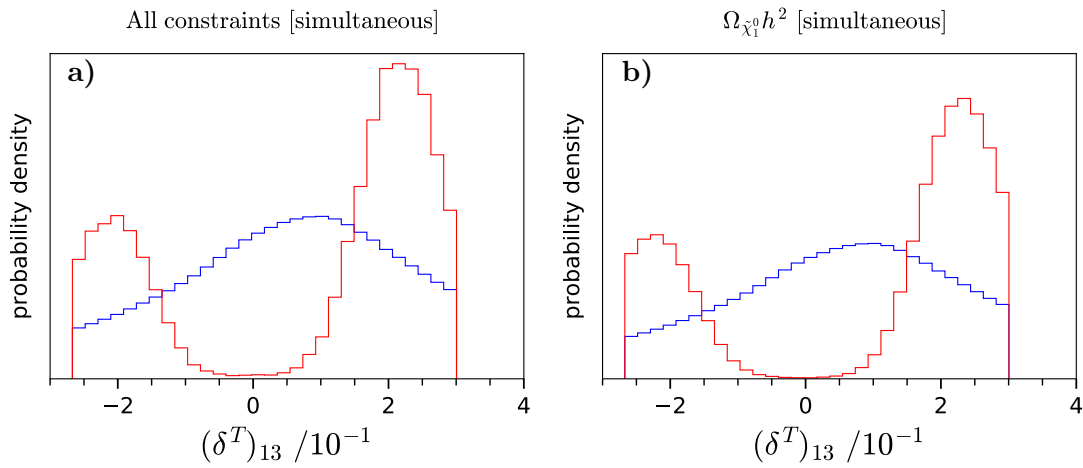

Figure 5.8: Dominant constraints on the parameter $(\delta_T)_{13}$ from simultaneous scan around Scenario 2.
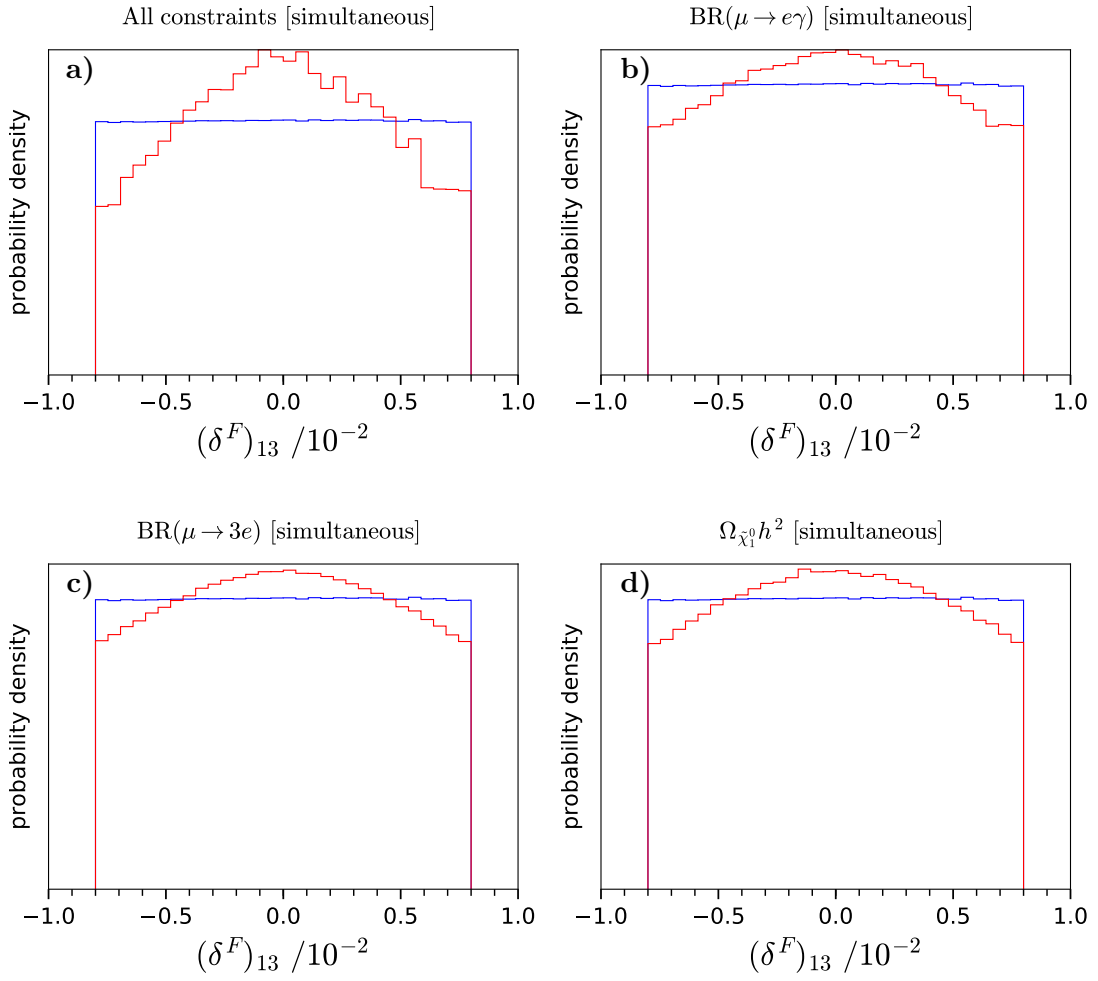
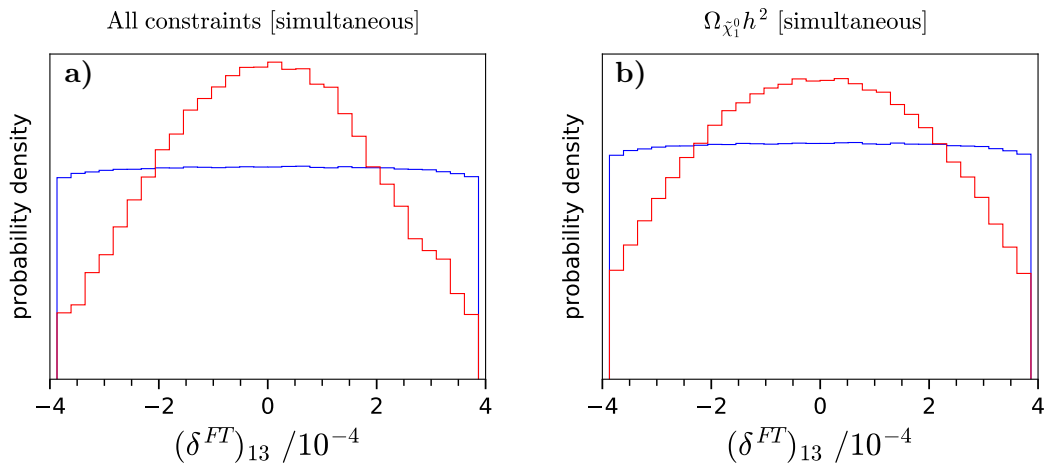Figure 5.9: Dominant constraints on the parameter $(\delta_F)_{13}$ from simultaneous scan around Scenario 2.

Figure 5.10: Dominant constraints on the parameter $(\delta_{FT})_{13}$ from simultaneous scan around Scenario 2.

can be seen in the panels' similarity. Complete information on limits and dominant constraints of all NMFV parameters associated with Scenario 2 is provided in Table 5.5.

5.4.3 SUSY-scale NMFV parameters for Scenario 2

While from the model-building point of view it is useful to explore the allowed level of flavour violation at the GUT scale, it is equally important to explore the resulting physics at the SUSY scale. Renormalisation group running from the GUT scale to the SUSY scale breaks the delicate unification conditions from Equation (5.9) and consequently those in Equation (5.11). The fact that these relations are not valid below the GUT scale is a consequence of the symmetry breaking at that scale. This section is devoted to highlighting selected results related to the NMFV parameters obtained at the SUSY scale. In Figure 5.11 we show the example of $(\delta_F)_{12}$, defined at the GUT scale, and the two resulting SUSY scale parameters $(\delta_{LL}^L)_{12}$ and $(\delta_{RR}^D)_{12}$, which originate from that GUT scale parameter through RG evolution. First, we see that the prior distribution is altered by the renormalisation group effects between the GUT scale in panel a) and the SUSY scale distributions in panels b) and c). The imposed flat priors at the GUT scale are transformed into very different distributions at the SUSY scale. Studying the corresponding posteriors, the SUSY scale distributions seem more peaked than the corresponding GUT scale histograms. One should note that, at the SUSY scale, the allowed range for the hadronic parameter $(\delta_{RR}^D)_{12}$ is wider than that for the related leptonic parameter $(\delta_{LL}^L)_{12}$. This behaviour is somewhat unexpected since gluino running, which is flavour blind, drives the diagonal squark mass parameters higher, while it leaves leptonic ones unaffected. In turn, this is expected to reduce the squark NMFV parameters once normalized as per Equation (5.4) [200]. We find that this behaviour is identical for all NMFV parameters stemming from *individual* scans (see examples in Figure 5.11 panels d) and e)), agreeing with the results presented in previous analyses [200]. However, for the δ_F parameters, the reverse is true when considering the *simultaneous* scan. We suspect that strong RG effects are the cause of this feature, since multiple NMFV parameters interact with each other during evolution from the GUT scale to the SUSY scale.

5.4.4 Parameter correlations

We examine correlations between NMFV parameters, these being the reason that scanning over all inputs simultaneously is ultimately required. The key point is that cancellations may exist between certain parameters in the calculation of a given observable. Dealing with analytical results for the different experimental constraints is difficult and beyond the scope of this work. Instead, we choose to take advantage of the numerical results, showing posterior distributions of several parameters together. The first panel in Figure 5.12 shows viable parameter sets that have an increased density of points
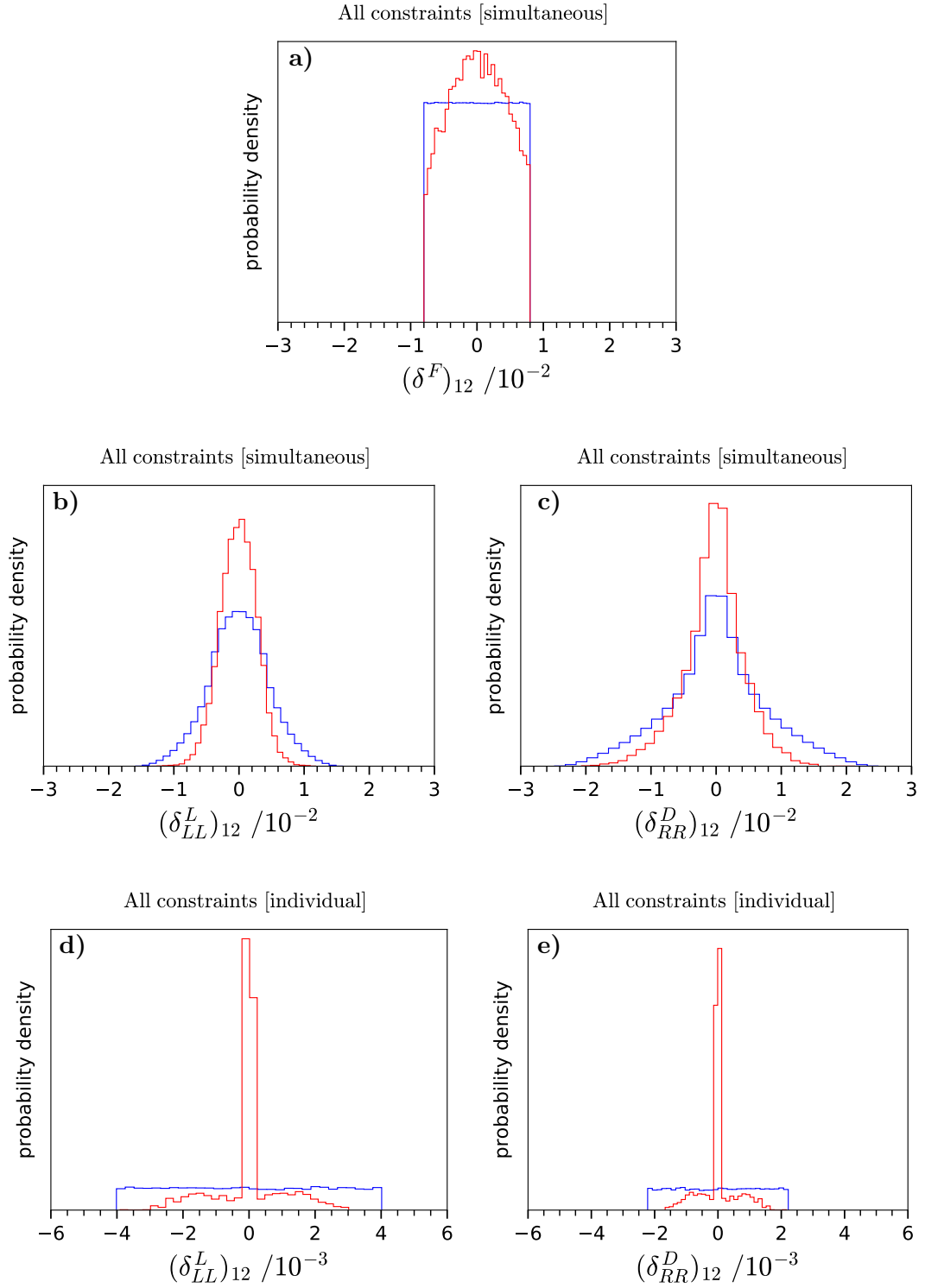
Figure 5.11: Distributions for the GUT-scale parameter $(\delta_F)_{12}$ and associated SUSY-scale $(\delta^L_{LL})_{12}$ and $(\delta^D_{RR})_{12}$ from simultaneous (b) and c)) and individual (d) and e)) scan around Scenario 2.

Figure 5.12: Correlation of GUT-scale parameters $(\delta^F)_{12}$ and $(\delta^{FT})_{12}$ (left panel) and associated correlation of the SUSY-scale parameters $(\delta^L_{LL})_{12}$ and $(\delta^E_{RL})_{12}$ (right panel) for Scenario 1. While the first plot shows the results for the full scan, the second one shows only the surviving points once the constraints of Table 5.3 are applied.

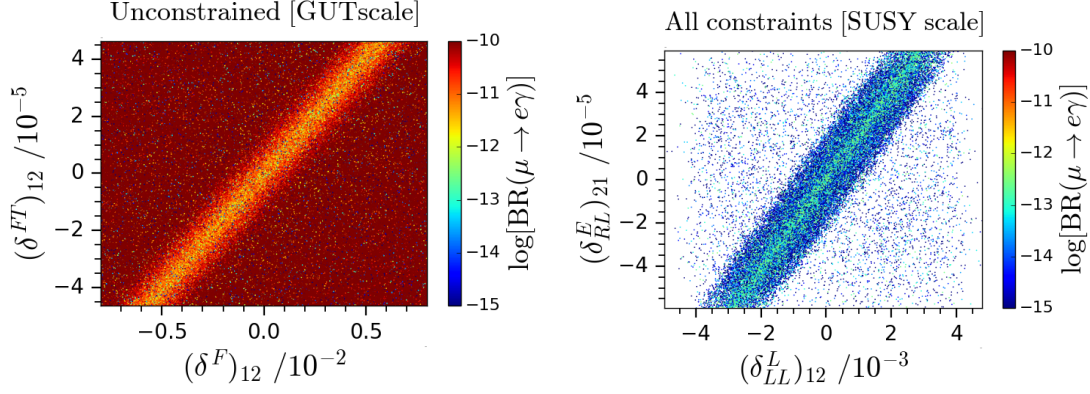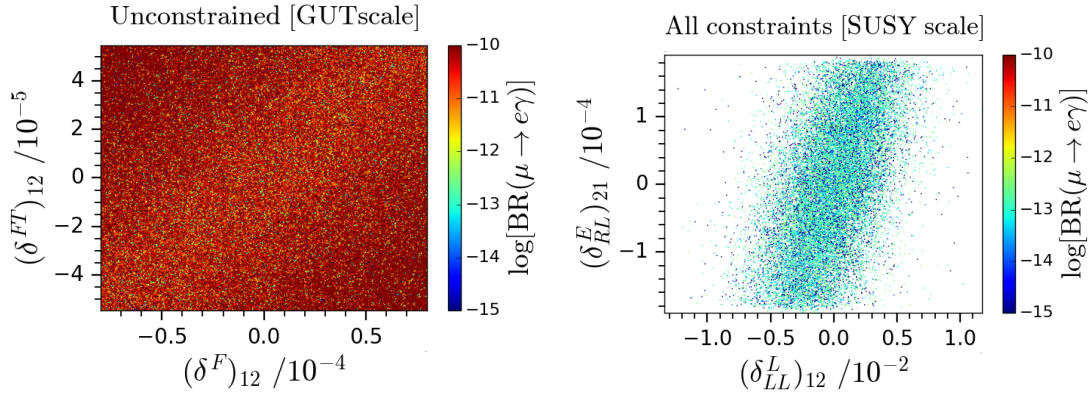
Figure 5.13: Correlation of the GUT-scale parameters $(\delta^F)_{12}$ and $(\delta^{FT})_{12}$ (left panel) and associated correlation of the SUSY-scale parameters $(\delta^L_{LL})_{12}$ and $(\delta^E_{RL})_{12}$ (right panel) for Scenario 2. While the first plot shows the results for the full scan, the second one shows only the surviving points once the constraints of Table 5.3 are applied.

concentrated around a linear relationship between the GUT scale parameters $(\delta_F)_{12}$ and $(\delta_{FT})_{12}$. Indeed, the impact of $\mathrm{BR}(\mu \to e\gamma)$ is suppressed along this line due to cancellation between the two parameters in the analytic expression for this observable. One can also see this in the right panel, only those points lying close to or along the line are consistent with the experimental limit. Said correlation could provide an interesting hint for future SUSY GUT model building. The analytic expression for the decay rate of $\mu \to e\gamma$ can be written as per Equation (5.13) [200].

$$\frac{\mathrm{BR}(\ell_i \to \ell_j \gamma)}{\mathrm{BR}(\ell_i \to \ell_j \nu_i \nu_j)} \;=\; \frac{48\pi^3 \alpha}{G_F^2} \left(|F_L^{ij}|^2 + |F_R^{ij}|^2 \right) \tag{5.13}$$

The branching ratio of the decay $\ell_i \to \ell_j \nu_i \nu_j$ is a constant with respect to the NMFV parameters under consideration in the present work. For real NMFV parameters, the form factors $F_{L,R}$ are related to the flavour violating parameters at the SUSY scale according to Equation (5.14).

$$\begin{aligned} F_L^{ij} &= c_1 (\delta_{LL}^L)_{ij} + c_2 (\delta_{RL}^E)_{ij}\,, \\ F_R^{ij} &= c_3 (\delta_{RR}^L)_{ij} + c_4 (\delta_{RL}^E)_{ji} \end{aligned} \tag{5.14}$$

The coefficients c_i ($i = 1, \ldots, 4$) are combinations of loop factors, masses, and other numerical inputs which can be assumed constant in our analysis. Minimising the form factors $F_{L,R}$ in Equation (5.14) to yield small $\mu \to e\gamma$ branching ratios and hence satisfy the experimental constraint leads to relations of the form given in Equation (5.15).

$$(\delta_{LL}^L)_{ij} \;=\; -\frac{2c_2}{c_1} (\delta_{RL}^E)_{ij} \tag{5.15}$$

Such a relationship corresponds to the observed lines in Figures 5.12 and 5.13. As such, the "golden line" that we recover purely from our numerical analysis is consistent with the analytic formulae for this lepton flavour-violating decay.

5.5 Summary

In this chapter we considered CP-conserving non-minimal flavour violation in $A_4 \times SU(5)$ inspired Supersymmetric Grand Unified Theories, focussing on regions of parameter space where dark matter is successfully accommodated due to a light right-handed smuon a few GeV heavier than the lightest neutralino dark matter candidate. Such regions of parameter space are obtained by choosing part of the second generation (the T_2 rep. of $SU(5)$) to have a light soft mass, while the heavy gluino mass ensures that squarks in this multiplet are heavy after RG running to low energy. We considered two scenarios along such lines, one with a light right-handed smuon which is capable of being discovered or excluded by the LHC soon, but which can account for the $(g-2)_\mu$ results, and another scenario with a somewhat heavier smuon. In such regions

we found that some flavour violating parameters, in particular, $(\delta^T)_{13}$ and $(\delta^{FT})_{32}$, are constrained by the requirement of dark matter relic density, due to delicate interplay between the smuon and neutralino masses.

By scanning over many GUT scale flavour violating parameters, constrained by low energy quark and lepton flavour violating observables, we discovered a striking difference between the results where individual parameters are varied to those where multiple parameters are scanned simultaneously, where the latter relaxes the constraints on flavour violating parameters due to cancellations and/or correlations. Since charged lepton flavour violation provides the strongest constraints within a GUT framework, due to relationships between quark and lepton flavour violation, we examined a prominent correlation between parameters $(\delta^F)_{12}$ and $(\delta^{FT})_{12}$ at the GUT scale consistent with $\mu \to e\gamma$. By switching on both flavour violating parameters together, we have seen that much more flavour violation is allowed than if only one parameter were scanned at a time. We have examined this correlation also in terms of the resulting low energy flavour violating parameters in the quark and lepton sectors, and have provided some analytic estimates to aid understanding of the observed correlation.

Precision flavour physics measurements could present challenges to this work and warrant further attention. Particularly, situations such as this often predict small-but-non-zero branching ratios for the LFV decays $\mu \to e\gamma$ and $\mu \to 3e$, and stricter bounds on such processes will further limit the NMFV allowed in such scenarios. Figures 5.12 and 5.13 are purely data-driven and show the regions that experimental data prefers; any model which predicts such a correlation could allow reasonable flavour violation and hence be preferred over other, similar theories.

In general, we have examined the relation between GUT scale and low scale flavour violating parameters and shown how expected results give way to new data-driven phenomena. We presented results in the framework of non-minimal flavour violation in $A_4 \times SU(5)$ inspired Supersymmetric Grand Unified Theories, with smuon assisted dark matter. Such a framework is interesting since it provides the smoking gun prediction of a light right-handed smuon accessible at LHC energies. Results presented here can inform flavoured GUT model building, and further motivate study of the MSSM outside of the normally-assumed MFV paradigm.

Chapter 6

Lepton Flavour Violation and Magnetic Moments in a Model of Vector-Like Leptons

6.1 Introduction

The Standard Model provides an excellent explanation of all experimental data, apart from neutrino mass and lepton mixing. Yet there are a few possible anomalies in the flavour sector that may indicate new physics beyond the SM. For example, recently, there have been hints of universality violation in the charged lepton sector from $B \to K^{(*)}l^+l^-$ decays by the LHCb collaboration [232–234]. Specifically, the R_K [235] and R_{K^*} [236] ratios of $\mu^+\mu^-$ to e^+e^- final states in the $B \to K^{(*)}l^+l^-$ decays are observed to be about 70% of their expected values with a roughly 2.5σ deviation from the Standard Model in each channel. Following the recent measurement of R_{K^*} [236], a number of phenomenological analyses have been presented [237–243] that favour a new effective field theory physics operator of the $C_{9\mu}^{NP} = -C_{10\mu}^{NP}$ form [244–246]. The most recent global fit of this operator combination yields $C_9 = (34.0\,\mathrm{TeV})^{-2}$ [246], though other well-motivated solutions are also possible [247].

In previous works [244], it has been suggested that definitive observations of charged lepton universality violation (LUV) must be accompanied by charged lepton flavour violation (LFV), however, such a link cannot be established in a model-independent way because low-energy effective operators for each class of processes are different. Nevertheless, in concrete models the connection is often manifest, which motivates the study of such a breed of theory. For example, studies of LFV in B-decays using generic Z' models (published before the R_{K^*} measurement but compatible with it) have been studied [248]. A concise review of BSM scenarios that aim to explain LUV and possible connections to dark matter is provided by Vicente [249]. Other theoretical explanations for universality violation in the lepton sector have been discussed in various works [91,

244, 248, 250–270].

Independently of B-anomalies, for some time now, it has been known that the experimentally measured anomalous magnetic moments of both the muon and electron observe a discrepancy of a few standard deviations with respect to SM predictions. The longstanding non-compliance of $(g-2)_\mu$ with SM predictions was first observed by the Brookhaven E821 experiment at BNL [61]. Following a recent measurement of the fine structure constant [66], a discrepancy with the predicted and observed values of the electron magnetic moment has been revealed. The different magnitudes and opposing signs of the electron and muon deviations make it difficult to explain these anomalies simultaneously in any model. All existing simultaneous explanations involve new scalars [190, 271–278] or conformal extended technicolour [279]. This study is one of the first to discuss both anomalies in a Z' model. A possible reason is that the LFV process $\mu \to e\gamma$ is very constraining. Neutrino phenomena do give rise to LFV but in the most minimal extensions, this would occur at a very low rate in the charged sector, making it practically unobservable. Given the considerable resources committed to looking for LFV, it is critical to study relevant, well-motivated BSM scenarios which allow for LFV at potentially observable rates. For example, such decays can be enhanced by several orders of magnitude if one considers extensions of the SM with an extra $U(1)'$ gauge symmetry spontaneously broken at the TeV scale. To summarise, although such extensions are able to successfully accommodate the experimental value of the muon magnetic moment [90, 91, 269, 280, 281], until the advent of this work there was no study of a Z' model which discussed both the electron and muon magnetic moments, while including constraints from well-measured lepton flavour violating observables.

In this chapter, we study the possibility of explaining the anomalous muon and electron magnetic moments in a Z' model. Such a study is difficult to undertake in general, since there are many possible Z' models. We consider a model in which the Z' only has couplings to the electron and muon and their associated neutrinos, arising from mixing with a vector-like fourth family of leptons, thereby eliminating quark couplings and allowing us to focus on the connection between LUV, LFV and the lepton $g-2$ anomalies. Such a renormalisable and gauge-invariant model is possible within a $U(1)'$ gauge extension of the SM augmented by a fourth, vector-like family of fermions and right-handed neutrinos as proposed in [253]. In a fermiophobic version of this model [253], only the fourth family carries $U(1)'$ charges, with the three chiral families not coupling to the Z', except through mixing. This allows controlled couplings of the Z' to only the electron and muon of the kind needed for contributions to magnetic moments. Such a model allows charged lepton universality violation at tree-level with LFV and contributions to the electron and muon magnetic moments at loop level. Within such a model we attempt to explain the anomalous magnetic moments of both the muon and electron within the relevant parameter space of the model, while avoiding overlarge contributions to $\mathrm{BR}(\mu \to e\gamma)$ and neutrino trident production. Using both analytic and numerical arguments, we find that it is not possible to simultaneously explain the

electron and muon magnetic moment results consistent with these constraints.

The remainder of this article is organised as follows; in Section 6.2 we outline the renormalisable and gauge-invariant fermiophobic model in which the Z' couples only to a vector-like fourth family. In Section 6.3, we show how it is possible to switch on the couplings of the Z' to the electron and muon and their associated neutrinos, eliminating all unnecessary couplings and allowing us to focus on the connection between LUV, LFV and the electron and muon anomalies. A simplified analytical analysis of LFV and the lepton magnetic moments in the fermiophobic Z' model is presented in Section 6.4. In Section 6.5, we analyse the parameter space numerically, presenting detailed predictions for each of the examined leptonic phenomena. Section 6.6 concludes this chapter with a summary of the investigation.

6.2 Vector-like fermions and $U(1)'$ symmetry

Consider an extension of the SM with a $U(1)'$ gauge symmetry, where fermion content is expanded by right-handed neutrinos and a fourth, vector-like family. The scalar sector is augmented by gauge singlet fields with non-trivial charge assignments under the new symmetry. The basic framework for such a theory is defined in [253]. Henceforth we consider the case where SM fermions in our model are uncharged under the additional symmetry, whereas vector-like fermions are charged under $U(1)'$, corresponding to a "fermiophobic Z'" model. The field content and charge assignments are given in Table 6.1. Note that such a theory is anomaly free; left- and right-handed fields of the vector-like fermion family have identical charges under $U(1)'$, and hence chiral anomalies necessarily cancel. Although the Z' couples only to the vector-like fourth family to

Field	Q_{4L}	$\widetilde{Q}_{4R}$	$\widetilde{u}_{4L}$	u_{4R}	$\widetilde{d}_{4L}$	d_{4R}	L_{4L}	$\widetilde{L}_{4R}$	$\widetilde{E}_{4L}$	E_{4R}	ν_{4R}	$\widetilde{\nu}_{4L}$	ϕ_f
$SU(3)_c$	**3**	**3**	**3**	**3**	**3**	**3**	**1**	**1**	**1**	**1**	**1**	**1**	**1**
$SU(2)_L$	**2**	**2**	**1**	**1**	**1**	**1**	**2**	**2**	**1**	**1**	**1**	**1**	**1**
$U(1)_Y$	$\frac{1}{6}$	$\frac{1}{6}$	$\frac{2}{3}$	$\frac{2}{3}$	$-\frac{1}{3}$	$-\frac{1}{3}$	$-\frac{1}{2}$	$-\frac{1}{2}$	-1	-1	0	0	0
$U(1)'$	q_{Q_4}	q_{Q_4}	q_{u_4}	q_{u_4}	q_{d_4}	q_{d_4}	q_{L_4}	q_{L_4}	q_{e_4}	q_{e_4}	q_{ν_4}	q_{ν_4}	$-q_{f_4}$

Table 6.1: Particle assigments for fields additional to SM under $SU(3)_c \times SU(2)_L \times U(1)_Y \times U(1)'$ gauge symmetry. $i = 1, 2, 3$. The SM singlet scalars ϕ_f ($f = Q, u, d, L, e$) have $U(1)'$ charges $-q_{f_4} = -q_{Q_4, u_4, d_4, L_4, e_4}$.

start with, due to the mixing between SM fermions and those of the fourth vector-like family the Z' will get induced couplings to chiral SM fermions. After mixing, the model can allow for a viable dark matter candidate and operators crucial for explaining the R_K and R_{K^*} flavour anomalies [91]. This setup can also generate LFV signatures such as $\mu \to e\gamma$ and accommodate the experimental value of the anomalous muon and electron magnetic dipole moments. With the particle content, symmetries and charge assignments in Table 6.1, the following renormalisable Lagrangian terms are available,

in addition to the Standard Model:

$$\mathcal{L}_Y = \sum_{i=1}^{3}\sum_{j=1}^{3} y_{ij}^{(u)}\overline{Q}_{iL}\widetilde{H}u_{jR} + \sum_{i=1}^{3}\sum_{j=1}^{3} y_{ij}^{(d)}\overline{Q}_{iL}Hd_{jR} + \sum_{i=1}^{3}\sum_{j=1}^{3} y_{ij}^{(e)}\overline{L}_{iL}He_{jR} + \sum_{i=1}^{3}\sum_{j=1}^{3} y_{ij}^{(\nu)}\overline{L}_{iL}\widetilde{H}\nu_{jR}$$

$$+ y_4^{(u)}\overline{Q}_{4L}\widetilde{H}u_{4R} + y_4^{(d)}\overline{Q}_{4L}Hd_{4R} + y_4^{(e)}\overline{L}_{4L}HE_{4R} + y_4^{(\nu)}\overline{L}_{4L}\widetilde{H}\nu_{4R}$$

$$+ \sum_{i=1}^{3} x_i^{(Q)}\phi_Q\overline{Q}_{Li}\widetilde{Q}_{4R} + \sum_{i=1}^{3} x_i^{(u)}\phi_u\overline{\widetilde{u}}_{4L}u_{Ri} + \sum_{i=1}^{3} x_i^{(d)}\phi_d\overline{\widetilde{d}}_{4L}d_{Ri} + \sum_{i=1}^{3} x_i^{(L)}\phi_L\overline{L}_{Li}\widetilde{L}_{4R} + \sum_{i=1}^{3} x_i^{(e)}\phi_e\overline{\widetilde{E}}_{4L}e_{Ri}$$

$$+ M_4^Q\overline{Q}_{4L}\widetilde{Q}_{4R} + M_4^u\overline{\widetilde{u}}_{4L}u_{4R} + M_4^d\overline{\widetilde{d}}_{4L}d_{4R} + M_4^L\overline{L}_{4L}\widetilde{L}_{4R} + M_4^E\overline{\widetilde{E}}_{4L}E_{4R} + M_4^\nu\overline{\widetilde{\nu}}_{4L}\nu_{4R} + H.c.$$

$$(6.1)$$

where the requirement of $U(1)'$ invariance of the Yukawa interactions involving the fourth family yields the following constraints on the $U(1)'$ charges of fourth fermion families:

$$q_{Q_4} = q_{u_4} = q_{d_4} \qquad q_{L_4} = q_{e_4} = q_{\nu_4} \qquad (6.2)$$

It is clear from Equation (6.1) that fields in the vector-like family obtain masses from two sources; firstly, Yukawa terms involving the SM Higgs field such as $y_4^{(e)}\overline{L}_{4L}He_{4R}$, which get promoted to chirality-flipping fourth family mass terms M_4^C once the Higgs acquires a VEV, and secondly from vector-like mass terms like $M_4^L\overline{L}_{4L}\widetilde{L}_{4R}$ (these terms appear in lines 2 and 4 of Equation (6.1) respectively). For clarity, we treat M_4^C and M_4^L as independent masses in the analysis of physical quantities, rather than constructing a full mass matrix for the vector-like fermions and diagonalising it, since many quantities of interest rely on a chirality flip and are sensitive to M_4^C rather than the vector-like mass. Spontaneous breaking of $U(1)'$ by the scalars ϕ_i spontaneously acquiring VEVs gives rise to a massive Z' boson featuring couplings with the chiral and vector-like fermion fields. In the interaction basis such terms will be diagonal and of the following form:

$$\mathcal{L}_{Z'}^{gauge} = g'Z'_\mu(\overline{Q}_L D_Q\gamma^\mu Q_L + \overline{u}_R D_u\gamma^\mu u_R + \overline{d}_R D_d\gamma^\mu d_R + \overline{L}_L D_L\gamma^\mu L_L + \overline{e}_R D_e\gamma^\mu e_R + \overline{\nu}_R D_\nu\gamma^\mu \nu_R)$$

$$(6.3)$$

Here, g' is the 'pure' gauge coupling of $U(1)'$ and each of the 'D's are 4x4 matrices. Only the fourth family has non-vanishing $U(1)'$ charges as per Table 6.1 and hence these matrices are given by:

$$D_Q = \text{diag}(0,0,0,q_{Q_4}), \quad D_u = \text{diag}(0,0,0,q_{u_4}), \quad D_d = \text{diag}(0,0,0,q_{d_4}),$$
$$D_L = \text{diag}(0,0,0,q_{L_4}), \quad D_e = \text{diag}(0,0,0,q_{e_4}), \quad D_\nu = \text{diag}(0,0,0,q_{\nu_4})$$

$$(6.4)$$

At this stage, the SM quarks and leptons do not couple to the Z'. However, the Yukawa couplings detailed in Equation (6.1) have no requirement to be diagonal. Before we can determine the full masses of the propagating vector-like states and SM fermions, we need to transform the field content of the model such that the Yukawa couplings become diagonal. Therefore, fermions in the mass basis (denoted by primed fields) are

related to particles in the interaction basis by the following unitary transformations:

$$Q'_L = V_{Q_L} Q_L, \quad u'_R = V_{u_R} u_R, \quad d'_R = V_{d_R} d_R, \quad L'_L = V_{L_L} L_L, \quad e'_R = V_{e_R} e_R, \quad \nu'_R = V_{\nu_R} \nu_R$$
(6.5)

Mixing then induces couplings of SM mass eigenstate fermions to the massive Z' which can be expressed as per Equation 6.6.

$$D'_Q = V_{Q_L} D_Q V_{Q_L}^\dagger, \quad D'_u = V_{u_R} D_u V_{u_R}^\dagger, \quad D'_d = V_{d_R} D_d V_{d_R}^\dagger,$$
$$D'_L = V_{L_L} D_L V_{L_L}^\dagger, \quad D'_e = V_{e_R} D_e V_{e_R}^\dagger, \quad D'_\nu = V_{\nu_R} D_\nu V_{\nu_R}^\dagger$$
(6.6)

Thus far, all discussion of interactions and couplings has been general. In Sections 6.3 and 6.5, mixing is prohibited in some sectors to simplify our phenomenological analysis. In particular, we shall only consider induced Z' couplings to the electron and muon.

6.3 Lepton flavour and universality violation

We take a minimal scenario and consider mixing only between first and second families of charged leptons, and ignore all quark and neutrino mixing, leading to a leptophillic Z' model, in which the Z' couples only to the electron, muon and their associated neutrinos. Therefore, only V_{L_L} and V_{e_R} will be non-diagonal, and LHC results will not constrain the Z' mass as there is no direct coupling between SM quarks and the new vector boson, nor mixing between SM and vector-like quarks. Among the LFV processes, we will focus on $\mu \to e\gamma$, which is much more constraining than the $\tau \to \mu\gamma$ and $\tau \to e\gamma$ decays. To simplify the parameter space, we also forbid the third family fermions from mixing with any other fermionic content. As such, mixing at low energies can be fully expressed as per Equation (6.7).

$$V_{L_L, e_R} = \begin{pmatrix} \cos\theta_{12}^{L,R} & \sin\theta_{12}^{L,R} & 0 & 0 \\ -\sin\theta_{12}^{L,R} & \cos\theta_{12}^{L,R} & 0 & 0 \\ 0 & 0 & 1 & 0 \\ 0 & 0 & 0 & 1 \end{pmatrix} \begin{pmatrix} \cos\theta_{14}^{L,R} & 0 & 0 & \sin\theta_{14}^{L,R} \\ 0 & 1 & 0 & 0 \\ 0 & 0 & 1 & 0 \\ -\sin\theta_{14}^{L,R} & 0 & 0 & \cos\theta_{14}^{L,R} \end{pmatrix} \begin{pmatrix} 1 & 0 & 0 & 0 \\ 0 & \cos\theta_{24}^{L,R} & 0 & \sin\theta_{24}^{L,R} \\ 0 & 0 & 1 & 0 \\ 0 & -\sin\theta_{24}^{L,R} & 0 & \cos\theta_{24}^{L,R} \end{pmatrix}$$
(6.7)

The angles defined here take the theory from the interaction basis in Equation (6.1) to the mass eigenbasis of primed fields introduced with Equation (6.5). They directly parameterise the mixing between the vector-like family and the usual three chiral families of SM fermions. Such mixing parameters will cause the D' matrices from Equation (6.6) to become off-diagonal. This incites couplings between the massive Z' vector boson and the SM leptons, suppressed by the mixing angles. These angles can be expressed in terms of parameters from the Lagrangian (Equation (6.1)), as per Equation (6.8) [253].

$$\tan\theta_{14}^L = \frac{x_1^{(L)}\langle\phi_L\rangle}{M_4^L}, \qquad \tan\theta_{24}^L = \frac{x_2^{(L)}\langle\phi_L\rangle}{\sqrt{\left(x_1^{(L)}\langle\phi_L\rangle\right)^2 + \left(M_4^L\right)^2}}$$
(6.8)

With the restrictions defined in Equation (6.7) and above, all of the relevant couplings between the massive Z' and fermions in the mass basis of propagating fields can be described thus:

$$\mathcal{L}_{Z'}^{gauge} = Z'_\mu \bar{l}_{L,R}(g_{L,R})_{ll'}\gamma^\mu l'_{L,R} \qquad (6.9)$$

where $l, l' = e, \mu, E$ are the mass eigenstate electron, muon and vector-like lepton respectively with couplings to the Z' as per Equations (6.10) to (6.15).

$$(g_{L,R})_{\mu\mu} = g' q_{L_4,e_4}\Big(\cos\theta_{12}^{L,R}\sin\theta_{24}^{L,R} - \cos\theta_{24}^{L,R}\sin\theta_{12}^{L,R}\sin\theta_{14}^{L,R} \Big)^2 \qquad (6.10)$$

$$(g_{L,R})_{ee} = g' q_{L_4,e_4}\Big(\sin\theta_{12}^{L,R}\sin\theta_{24}^{L,R} + \cos\theta_{12}^{L,R}\cos\theta_{24}^{L,R}\sin\theta_{14}^{L,R} \Big)^2 \qquad (6.11)$$

$$(g_{L,R})_{EE} = g' q_{L_4,e_4}\Big(\cos\theta_{14}^{L,R} \Big)^2 \Big(\cos\theta_{24}^{L,R} \Big)^2 \qquad (6.12)$$

$$(g_{L,R})_{eE} = g' q_{L_4,e_4}\cos\theta_{14}^{L,R}\cos\theta_{24}^{L,R}\Big(\sin\theta_{12}^{L,R}\sin\theta_{24}^{L,R} + \cos\theta_{12}^{L,R}\cos\theta_{24}^{L,R}\sin\theta_{14}^{L,R} \Big) \qquad (6.13)$$

$$(g_{L,R})_{\mu E} = g' q_{L_4,e_4}\cos\theta_{14}^{L,R}\cos\theta_{24}^{L,R}\Big(\cos\theta_{12}^{L,R}\sin\theta_{24}^{L,R} - \cos\theta_{24}^{L,R}\sin\theta_{12}^{L,R}\sin\theta_{14}^{L,R} \Big) \qquad (6.14)$$

$$(g_{L,R})_{\mu e} = g' q_{L_4,e_4}\Big(\sin\theta_{12}^{L,R}\sin\theta_{24}^{L,R} + \cos\theta_{12}^{L,R}\cos\theta_{24}^{L,R}\sin\theta_{14}^{L,R} \Big)$$
$$\times \Big(\cos\theta_{12}^{L,R}\sin\theta_{24}^{L,R} - \cos\theta_{24}^{L,R}\sin\theta_{12}^{L,R}\sin\theta_{14}^{L,R} \Big) \qquad (6.15)$$

It is important to note that only the first and second family of SM leptons couple to the massive Z', with their non-universal and flavour changing couplings controlled by the mixing angles $\theta_{14}^{L,R}, \theta_{24}^{L,R}$. Throughout the remainder of this work, we assume that $g' q_{L4,e4} = 1$ for simplicity.

6.3.1 Flavour violating muon decay

We study charged lepton flavour violating process $\mu \to e\gamma$ in the context of this BSM scenario. It is worth mentioning that a future observation of the $\mu \to e\gamma$ decay will be indisputable evidence of physics beyond currently accepted knowledge. The SM does predict non-zero branching ratios for $\mu \to e\gamma$, $\tau \to \mu\gamma$ and $\tau \to e\gamma$, but such predictions are several orders of magnitude below experimental sensitivities [282, 283]. In this paradigm, the $\mu \to e\gamma$ decay rate is enhanced with respect to the SM by additional contributions due to virtual Z' and charged vector-like lepton exchange at the one-loop level. General $l_i \to l_j\gamma$ decay can be described by the following effective operator [282]:

$$\mathcal{L}_{EFT} = \frac{\mu_{ij}^M}{2}\bar{l}_i\sigma^{\mu\nu}l_j F_{\mu\nu} + \frac{\mu_{ij}^E}{2}i\bar{l}_i\gamma^5\sigma^{\mu\nu}l_j F_{\mu\nu} \qquad (6.16)$$

where $F_{\mu\nu}$ denotes the electromagnetic field strength tensor, μ_{ij}^E and μ_{ij}^M are the transition electric and magnetic moments, respectively and $i, j = 1, 2, 3$ denote family indices for the electron, muon and tau respectively. Diagonal elements in the transition magnetic moment μ_{ij}^M give rise to the magnetic dipole moments $\Delta a_l = \frac{1}{2}(g_l - 2)$ of leptons, whilst off-diagonal elements in the transition moments contribute to the generic $l_i \to l_j \gamma$ decay amplitude. Based on the effective Lagrangian in Equation (6.16), the amplitude for a generic lepton decay $f_1 \to f_2 \gamma$ has the form [284]:

$$\mathcal{A} = e\varepsilon_\mu^*(q)\overline{v}_2(p_2)\left[i\sigma^{\mu\nu}q_\nu(\sigma_L P_L + \sigma_R P_R)\right]u_1(p_1) \tag{6.17}$$

where σ_L and σ_R are numerical quantities with dimension of inverse mass that can be expressed in terms of loop integrals [284]. u_1 and v_2 are spinors with momenta p_1 and p_2 respectively, and ϵ_μ denotes the polarisation four-vector of the photon. Other quantities are defined in Equation (6.18).

$$\sigma^{\mu\nu} = \frac{i}{2}\left[\gamma^\mu, \gamma^\nu\right], \qquad P_{L,R} = \frac{1}{2}(1 \mp \gamma_5), \qquad q = p_1 - p_2 \tag{6.18}$$

γ denote Dirac matrices that conform to the Clifford algebra as usual. In this case, the decay rate for $\mu \to e\gamma$ in this model can be expressed in the following way [90, 282, 284, 285]:

$$\Gamma(\mu \to e\gamma) = \frac{\alpha_{em}}{1024\pi^4}\frac{m_\mu^5}{M_{Z'}^4}(|\widetilde{\sigma}_L|^2 + |\widetilde{\sigma}_R|^2) \tag{6.19}$$

where $\widetilde{\sigma}_L$ and $\widetilde{\sigma}_R$ are given by:

$$\begin{aligned}
\widetilde{\sigma}_L &= \sum_{a=e,\mu,E}\left[(g_L)_{ea}(g_L)_{a\mu}F(x_a) + \frac{m_a}{m_\mu}(g_L)_{ea}(g_R)_{a\mu}G(x_a)\right], \\
\widetilde{\sigma}_R &= \sum_{a=e,\mu,E}\left[(g_R)_{ea}(g_R)_{a\mu}F(x_a) + \frac{m_a}{m_\mu}(g_R)_{ea}(g_L)_{a\mu}G(x_a)\right], \qquad x_a = \frac{m_a^2}{M_{Z'}^2}
\end{aligned} \tag{6.20}$$

$F(x)$ and $G(x)$ are loop functions related to the Feynman diagrams for $\mu \to e\gamma$ as per Figure 6.1, and have the functional form given in Equation (6.21). $g_{L,R}$ are couplings in the fermion mass basis, as detailed in Equations (6.10) through (6.15). When $a = E$, m_a here corresponds to the full propagating mass of the vector-like partners. In the approximation where the vector like mass M_4^L is always much greater than the chirality-flipping mass M_4^C ($M_4^L \gg M_4^C$) that we adopt here, this full propagating mass is well-approximated by the vector-like mass. Therefore when $a = E$, we approximate $m_E \simeq M_4^L$. Loop functions are given in Equation (6.21) [90]:

$$\begin{aligned}
F(x) &= \frac{5x^4 - 14x^3 + 39x^2 - 38x - 18x^2\ln x + 8}{12(1 - x)^4}, \\
G(x) &= \frac{x^3 + 3x - 6x\ln x - 4}{2(1 - x)^3}
\end{aligned} \tag{6.21}$$

Equation (6.19) has some generic features; the loop function $F(x)$ varies between 0.51 and 0.67 when x is varied in the range $10^{-3} \leq x \leq 2$, whilst in the same region, $G(x)$ varies between -1.98 and -0.84. Consequently, in the case of charged fermions running in loops, contributions proportional to $G(x)$ will likely dominate over those proportional to $F(x)$. The dominant contributions involve left-right and right-left Z' couplings, whereas the subleading ones include either left-left or right-right couplings. Dividing Equation (6.19) by the known decay rate of the muon yields a prediction for the $\mu \to e\gamma$ branching fraction [90, 282, 284, 285]:

$$
\begin{aligned}
\mathrm{BR}(\mu \to e\gamma) = & \frac{\alpha}{1024\pi^4} \frac{m_\mu^5}{M_{Z'}^4 \Gamma_\mu} \Bigg[\Big| (g_L)_{\mu\mu}(g_L)_{\mu e} F(x_\mu) + (g_L)_{\mu E}(g_L)_{eE} F(x_E) + (g_L)_{\mu e}(g_L)_{ee} F(x_e) \\
& + \frac{m_\mu}{m_\mu}(g_L)_{\mu e}(g_R)_{\mu\mu} G(x_\mu) + \frac{M_4^C}{m_\mu}(g_L)_{eE}(g_R)_{\mu E} G(x_E) + \frac{m_e}{m_\mu}(g_L)_{ee}(g_R)_{\mu e} G(x_e) \Big|^2 \\
& + \Big| (g_R)_{\mu\mu}(g_R)_{\mu e} F(x_\mu) + (g_R)_{\mu E}(g_R)_{eE} F(x_E) + (g_R)_{\mu e}(g_R)_{ee} F(x_e) \\
& + \frac{m_\mu}{m_\mu}(g_R)_{\mu e}(g_L)_{\mu\mu} G(x_\mu) + \frac{M_4^C}{m_\mu}(g_R)_{eE}(g_L)_{\mu E} G(x_E) + \frac{m_e}{m_\mu}(g_R)_{ee}(g_L)_{\mu e} G(x_e) \Big|^2 \Bigg]
\end{aligned}
$$

(6.22)

where the total muon decay width is $\Gamma_\mu = \frac{G_F^2 m_\mu^5}{192\pi^3} = 3 \times 10^{-19}$ GeV. The mass M_4^C that appears in the Feynman diagrams with a chirality flip on the vector-like fermions E_4 (Figure 6.1, 5th and 11th diagrams) is *not* the vector-like mass, but instead arises from the Yukawa-like couplings from Equation (6.1), $M_4^C = y_{44}^{(e)} v$, where v is the vacuum expectation value of the SM Higgs field, which acquires a VEV and spontaneously breaks electroweak symmetry in the established manner. Under the assumption that $M_4^C > m_\mu$, such terms proportional to M_4^C in Equation (6.22) give by far the largest contributions to $\mu \to e\gamma$. The experimental limit on $\mathrm{BR}(\mu \to e\gamma)$ is determined from non-observation at the MEG experiment at the 90% confidence level [88, 218]:

$$
\mathrm{BR}(\mu \to e\gamma) < 4.2 \times 10^{-13}
$$

(6.23)

Equation (6.22), as with all other observables, is expanded in terms of mixing angles between generations of leptons in Appendix C.

6.3.2 Anomalous magnetic moment of the muon

In this subsection, the muon anomalous magnetic moment in the context of our BSM scenario is derived. Feynman diagrams for $\mu \to e\gamma$ are easily modified to give contributions to the anomalous magnetic moment of the muon as per Figure 6.2. The prediction
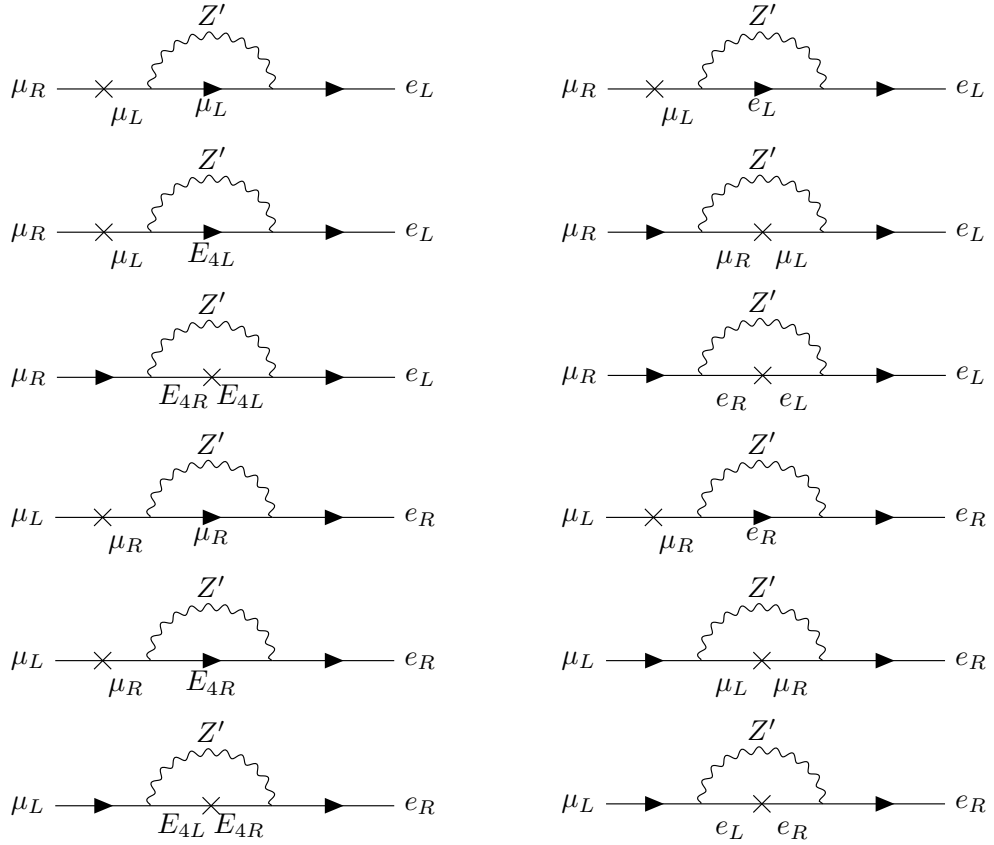
Figure 6.1: Feynman diagrams contributing to the $\mu \to e\gamma$ decay. Note that these diagrams all rely on a chirality flip. Where the chirality flip involves the fourth family, the relevant mass is M_4^C.
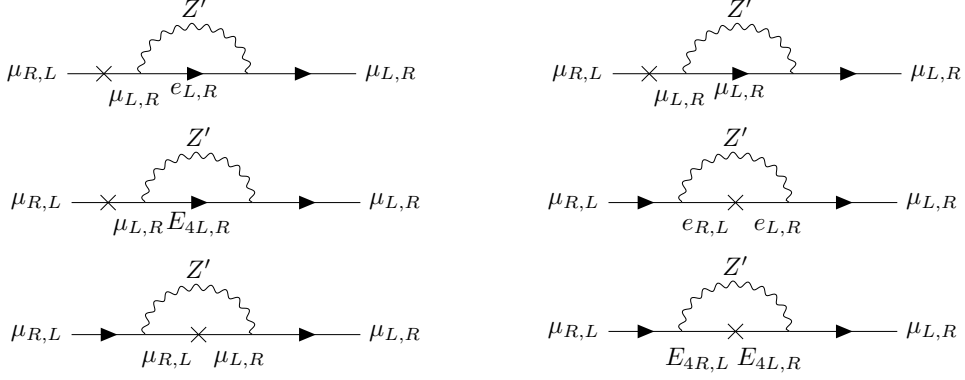
Figure 6.2: Feynman diagrams contributing to $(g-2)_\mu$

for such an observable in our model therefore takes the form of Equation (6.24) [90].

$$\Delta a_\mu^{Z'} = -\frac{m_\mu^2}{8\pi^2 M_{Z'}^2}\Bigg[\left(|(g_L)_{\mu\mu}|^2 + |(g_R)_{\mu\mu}|^2\right)F(x_\mu) + \left(|(g_L)_{\mu E}|^2 + |(g_R)_{\mu E}|^2\right)F(x_E)$$

$$+ \left(|(g_L)_{\mu e}|^2 + |(g_R)_{\mu e}|^2\right)F(x_e) + \mathrm{Re}\left((g_L)_{\mu\mu}(g_R^*)_{\mu\mu}\right)G(x_\mu)$$

$$+ \mathrm{Re}\left((g_L)_{\mu E}(g_R^*)_{\mu E}\right)\frac{M_4^C}{m_\mu}G(x_E) + \mathrm{Re}\left((g_L)_{\mu e}(g_R^*)_{\mu e}\right)\frac{m_e}{m_\mu}G(x_e)\Bigg]$$

(6.24)

Once more, dominant terms will be those proportional to the enhancement factor of $\frac{M_4^C}{m_\mu}$, corresponding to the final diagram in Figure 6.2, provided $M_4^C > m_\mu$. Recent experimental evidence has shown that the magnetic moment as measured by the E821 experiment is at around a 3.5σ deviation from the SM prediction [42, 46, 61–65].

$$(\Delta a_\mu)_{\mathrm{exp}} = (26.1 \pm 8.0) \times 10^{-10} \tag{6.25}$$

6.3.3 Anomalous magnetic moment of the electron

Analogously to the muon, there is an amendment to $(g-2)_e$ in this scenario, from Feynman diagrams given in Figure 6.3. The analytic expression for Δa_e is the following [90]:

$$\Delta a_e^{Z'} = -\frac{m_e^2}{8\pi^2 M_{Z'}^2}\Bigg[\left(|(g_L)_{ee}|^2 + |(g_R)_{ee}|^2\right)F(x_e) + \left(|(g_L)_{e\mu}|^2 + |(g_R)_{e\mu}|^2\right)F(x_\mu)$$

$$+ \left(|(g_L)_{eE}|^2 + |(g_R)_{eE}|^2\right)F(x_E) + \mathrm{Re}\left((g_L)_{ee}(g_R^*)_{ee}\right)\frac{m_e}{m_e}G(x_e)$$

$$+ \mathrm{Re}\left((g_L)_{e\mu}(g_R^*)_{e\mu}\right)\frac{m_\mu}{m_e}G(x_\mu) + \mathrm{Re}\left((g_L)_{eE}(g_R^*)_{eE}\right)\frac{M_4^C}{m_e}G(x_E)\Bigg]$$

(6.26)

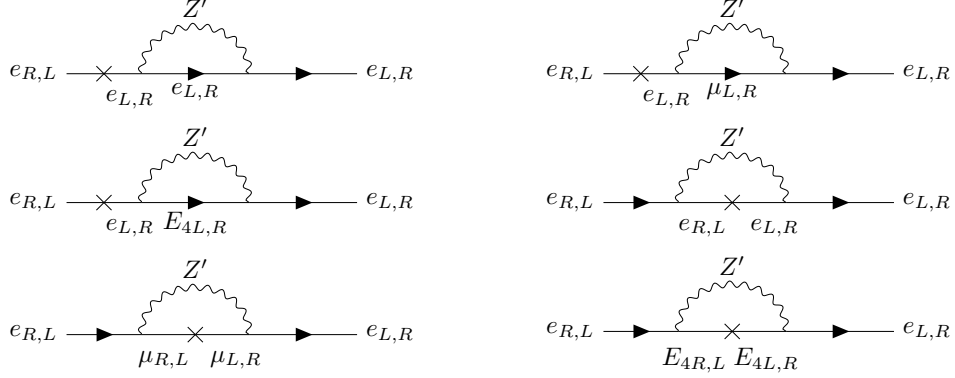As per the muon moment, if $M_4^C > m_\mu$ the largest contribution to the electron moment

Figure 6.3: Feynman diagrams contributing to $(g-2)_e$

will be the final term in Equation (6.26), corresponding to the last diagram in Figure 6.3. The most recent experimental result of $(g-2)_e$, obtained from measurement of the fine structure constant of QED, shows a 2.5σ deviation from the SM [66] as per Equation 6.27.

$$(\Delta a_e)_{\exp} = (-0.88 \pm 0.36) \times 10^{-12} \tag{6.27}$$

Note that Equations (6.25) and (6.27) have deviations from the SM in opposite directions, and explaining both phenomena simultaneously can be difficult.

6.3.4 Neutrino trident production

So-called 'trident production' of neutrinos through the process $\nu_\mu \gamma^* \to \nu_\mu \mu^+ \mu^-$ is also relevant in this setup. The Feynamn diagram contributing to neutrino trident production in this model is shown in Figure 6.4. This process constrains the following effective four lepton interaction, which in this scenario arises from leptonic Z' interactions [286–288]:

$$\Delta \mathcal{L}_{eff} \supset -\frac{(g_L)^2_{\mu\mu}}{2M^2_{Z'}}(\overline{\mu}_L \gamma^\lambda \mu_L)(\overline{\nu}_{\mu L}\, \gamma_\lambda\, \nu_{\mu L}) - \frac{(g_R)_{\mu\mu}(g_L)_{\mu\mu}}{2M^2_{Z'}}(\overline{\mu}_R \gamma^\lambda \mu_R)(\overline{\nu}_{\mu L}\, \gamma_\lambda\, \nu_{\mu L}) \tag{6.28}$$

This coupling is constrained as in the $SU(2)_L$ symmetric SM, left-handed muons and muon neutrinos couple identically to the Z' vector boson. Experimental data on neutrino trident production $\nu_\mu \gamma^* \to \nu_\mu \mu^+ \mu^-$ yields the constraint on the couplings given in Equation (6.29) at 95% CL [289].

$$-\frac{1}{(390\text{GeV})^2} \leq \frac{(g_L)^2_{\mu\mu} + (g_L)_{\mu\mu}(g_R)_{\mu\mu}}{M^2_{Z'}} \leq \frac{1}{(370\text{GeV})^2} \tag{6.29}$$

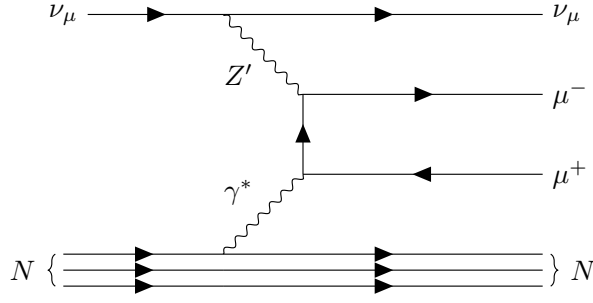This limit can be applied to the fermion-Z' couplings directly.

Figure 6.4: Feynman diagram contributing to neutrino trident production, N denotes a nucleus.

6.3.5 LEP-II Z' production

When couplings are apparent between Standard Model electrons and a new Z' vector boson, this allows for such a boson to potentially be observed at lepton colliders via s-channel production (if the decay products of the Z' are electrons, this can also proceed through t- and u-channel exchanges). This proceeds through a Feynman diagram such as Figure 6.5. Z' gauge bosons were never observed at LEP [112, 290, 291], and so
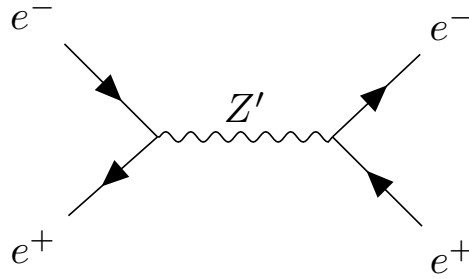
Figure 6.5: Potential Z' production mode at the LEP-II lepton collider.

this places a bound on either the coupling between electrons and the Z' boson in this model, or the mass of the boson itself.

$$(g_{L,R})_{ee} \leq 10^{-2}, \qquad M_{Z'} \leq 209 \text{GeV} \tag{6.30}$$

Therefore, one or other of the bounds detailed in Equation (6.30) must always be respected in these investigations.

A combined constraint can also be derived when the Z' couples to both muons and electrons. This originates from a diagram analogous to Figure 6.30, where the final state electrons are replaced by muons. The bound is summarised as per Equation (6.31), where we take the most strict bound possible from LEP-II [292–294], to be conservative.

$$\frac{(g_{L,R})_{ee}(g_{L,R})_{\mu\mu}}{4\pi M_{Z'}^2} \geq \frac{1}{\left(6.8 \, \text{TeV}\right)^2} \tag{6.31}$$

This constraint is valid for any $M_{Z'} < 209$ GeV when the Z' couples to electrons and

muons.

6.4 Analytic discussion

In order to gain an analytic understanding of the interplay between $(g-2)_\mu$, $(g-2)_e$ and $\mathrm{BR}(\mu \to e\gamma)$, in this section we make assumptions about the parameters appearing in Equations (6.24), (6.26) and (6.22). If we assume large fourth family chirality-flipping masses $M_4^C \gg m_\mu$, then the expressions for these phenomena reduce to a minimal number of terms, all proportional to M_4^C. Furthermore, we assume that left- and right-handed couplings are related by some real, positive constants k_1 and k_2 defined thus:

$$
\begin{aligned}
(g_L)_{\mu E} &= g_{\mu E}, &\quad (g_R)_{\mu E} &= k_1 g_{\mu E}, \\
(g_L)_{eE} &= g_{eE}, &\quad (g_R)_{eE} &= -k_2 g_{eE}
\end{aligned}
\tag{6.32}
$$

The final coupling in Equation (6.32) is defined with a sign convention such that, seeing as it is known numerically that the 'G' loop function is always negative, the correct sign is automatically recovered for all observables. We also define the following prefactor constants to further simplify the expressions:

$$
C_1 = \frac{\alpha}{1024\pi^2} \frac{m_\mu^5}{M_{Z'}^4 \Gamma_\mu} \;, \quad C_2 = \frac{m_\mu^2}{8\pi^2 M_{Z'}^2} \;, \quad C_3 = \frac{m_e^2}{8\pi^2 M_{Z'}^2}
\tag{6.33}
$$

Under such assumptions, Equations (6.24), (6.26) and (6.22) reduce to the following:

$$
\mathrm{BR}(\mu \to e\gamma) = C_1 \left(\left| \frac{M_4^C}{m_\mu} k_1 g_{eE} g_{\mu E} G(x_E) \right|^2 + \left| \frac{M_4^C}{m_\mu} k_2 g_{eE} g_{\mu E} G(x_E) \right|^2 \right)
\tag{6.34}
$$

$$
|\Delta a_\mu| = C_2 k_1 g_{\mu E}^2 \frac{M_4^C}{m_\mu} |G(x_E)|
\tag{6.35}
$$

$$
|\Delta a_e| = C_3 k_2 g_{eE}^2 \frac{M_4^C}{m_e} |G(x_E)|
\tag{6.36}
$$

We can then invert Equations (6.35) and (6.36) to obtain expressions for the couplings in terms of the observables as per Equation (6.37).

$$
g_{\mu E} = \sqrt{\frac{|\Delta a_\mu|}{C_2 k_1} \frac{1}{|G(x_E)|} \frac{m_\mu}{M_4^C}} \;, \qquad g_{eE} = \sqrt{\frac{|\Delta a_e|}{C_3 k_2} \frac{1}{|G(x_E)|} \frac{m_e}{M_4^C}}
\tag{6.37}
$$

Substituting into the flavour violating muon decay in Equation (6.34) and expanding the constants defined earlier yields Equation (6.38).

$$
\mathrm{BR}(\mu \to e\gamma) = \frac{\alpha\pi^2}{16} \frac{(k_1^2 + k_2^2)}{k_1 k_2} |\Delta a_\mu| |\Delta a_e| \frac{m_\mu^2}{\Gamma_\mu m_e}
\tag{6.38}
$$

Independently of $M_{Z'}$ and M_4^C which cancel. Rearranging Equation 6.38 and setting the physical quantities $|\Delta a_\mu|$, $|\Delta a_e|$ equal to their central values, yields a simple condition on $r = k_1/k_2$ in order to satisfy the bound on $\text{BR}(\mu \to e\gamma)$:

$$\|r + \frac{1}{r}\| < 5.57 \times 10^{-10} \tag{6.39}$$

Since the left hand side is minimised for $r = 1$, the bound on $\text{BR}(\mu \to e\gamma)$ can never be satisfied while accounting for $(g-2)_\mu$, $(g-2)_e$ (although clearly, it is possible to satisfy it with either $(g-2)_\mu$ or $(g-2)_e$ but not both). However, this conclusion is based on the assumption that physical quantities are dominated by the diagrams involving the mass $M_4^C \gg m_\mu$. To relax this assumption, a more complete analysis of the parameter space is required, one that considers all relevant terms in our expressions for observables in a numerical exploration of the parameter space. Such investigations are detailed in Section 6.5.

6.5 Numerical analysis

Given the expressions for observables outlined above, these phenomena are used to constrain the parameter space of the model. As mentioned, a minimal parameter space is considered here, limiting mixing to the lepton sector and omitting the third chiral family from any mixing. From coupling expressions in Section 6.3, angular mixing parameters such as θ_{24L} and particle masses form a minimal parameter space for this model. We set direct mixing between the electron and muon ($\theta_{12L,R}$) to be vanishing for all tests, as even small $\theta_{12L,R}$ easily violates the strict MEG constraint on $\text{BR}(\mu \to e\gamma)$.

6.5.1 Muon magnetic moment

Initially, we focus on the long-standing muon magnetic moment anomaly. A simple parameter space is utilised as we only require mixing between the muon and vector-like lepton fields. To keep the analysis in a region potentially testable by upcoming future experiments, we take a vector-like fourth family lepton mass of $M_4^L = 1\,\text{TeV}$ and a chirality-flipping fourth family mass of $M_4^C = 200\,\text{GeV}$ (we make a distinction between these two sources of mass). The smaller value of M_4^C is well motivated by the need for perturbativity in Yukawa couplings, since M_4^C is proportional to the Higgs VEV and the Yukawa coupling. For this investigation the region of parameter space under test is detailed in Table 6.2. Within this region, expressions for observables under test are simplified considerably, and with fixed M_4^C and M_4^L we constrain the space in terms of three variables; $\sin^2 \theta_{24L}$, $\sin^2 \theta_{24R}$ and $M_{Z'}$, shown in Figure 6.6. Note that, as $\theta_{12L,R}$ and $\theta_{14L,R}$ are set vanishing, contributions to $(g-2)_e$ and $\text{BR}(\mu \to e\gamma)$ are necessarily vanishing, which can be readily seen from Equations (6.26) and (6.22). The dominant contribution to $(g-2)_\mu$ under these assumptions is shown in the final Feynman diagram in Figure 6.2 which has an enhancement factor of M_4^C/m_μ. The legend in Figure 6.6

Parameter	Value/Scanned Region
$M_{Z'}$	$50 \rightarrow 1000$ GeV
M_4^C	200 GeV
M_4^L	1000 GeV
$\sin^2 \theta_{12L,R}$	0.0
$\sin^2 \theta_{14L}$	0.0
$\sin^2 \theta_{14R}$	0.0
$\sin^2 \theta_{24L,R}$	$0.0 \rightarrow 1.0$

Table 6.2: Explored parameter space for $(g-2)_\mu$ test.
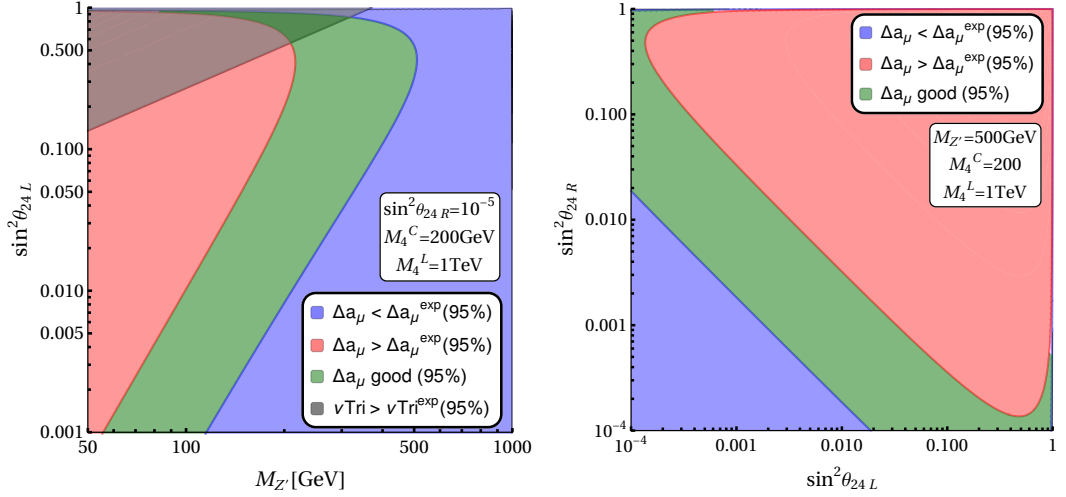
(a) Trident exclusion and regions of Δa_μ, with a fixed $\sin^2 \theta_{24R}$.

(b) Δa_μ in angular parameter space with fixed Z' mass

Figure 6.6: Constraints in the $M_{Z'}$, $\sin^2 \theta_{24L}$ and $\sin^2 \theta_{24R}$ parameter space, when mixing between the electron and vector-like lepton is switched off.

shows the constraint from neutrino trident production as 'νTri' for brevity. Using only mixing between the muon and vector-like lepton, it is not possible to predict a value for the electron $(g-2)$ consistent with the observed value as the electron-Z' coupling does not exist. In this way, constraints from the LEP experiment do not apply to this region of the parameter space.

6.5.2 Electron magnetic moment

To test the electron magnetic moment in isolation, we investigate only mixing between the electron and vector-like lepton, and ignore muon mixing contributions. The region of parameter space under test is given in Table 6.3, note that mixing with the right-handed electron field is not required to obtain a good prediction. In Figure 6.7, we

Parameter	Value/Scanned Region
$M_{Z'}$	$50 \rightarrow 1000$ GeV
M_4^C	200 GeV
M_4^L	1000 GeV
$\sin^2 \theta_{12L,R}$	0.0
$\sin^2 \theta_{14L}$	$0.0 \rightarrow 1.0$
$\sin^2 \theta_{14R}$	0.0
$\sin^2 \theta_{24L,R}$	0.0

Table 6.3: Explored parameter space for $(g-2)_e$ test.

colour $(g-2)_e$ being greater than the observed value (i.e. 'less negative' than the experimental data) as the blue region, as such values are more SM-like. Blue regions, therefore, ameliorate the SM's tension with the experimental data but do not fully resolve it. Similarly to the preceding section, because there are no couplings between electron and muon (even at loop level), there are no contributions to the LFV decay $\mu \rightarrow e\gamma$. Similarly, there are no amendments to the SM expressions for neutrino trident decay. Unfortunately, the entirety of the region which can nicely explain the electron magnetic moment comes with both large mixing between the vector-like lepton and small Z' masses, and so is excluded by non-observation of new vector bosons at the LEP experiment [112, 290, 291].

6.5.3 Attempt to explain both moments

In an attempt to explain both magnetic moments simultaneously whilst respecting stringent constraints, we set specific values for $M_{Z'}$, M_4^C and $\sin^2 \theta_{14}^L$ that inhabit regions of parameter space in Figures 6.6a, 6.6b and 6.7 that can explain the magnetic moments, and scan through angular mixing parameters as before. The investigated region is summarised in Table 6.4. The choice of Z' mass here is motivated by studying
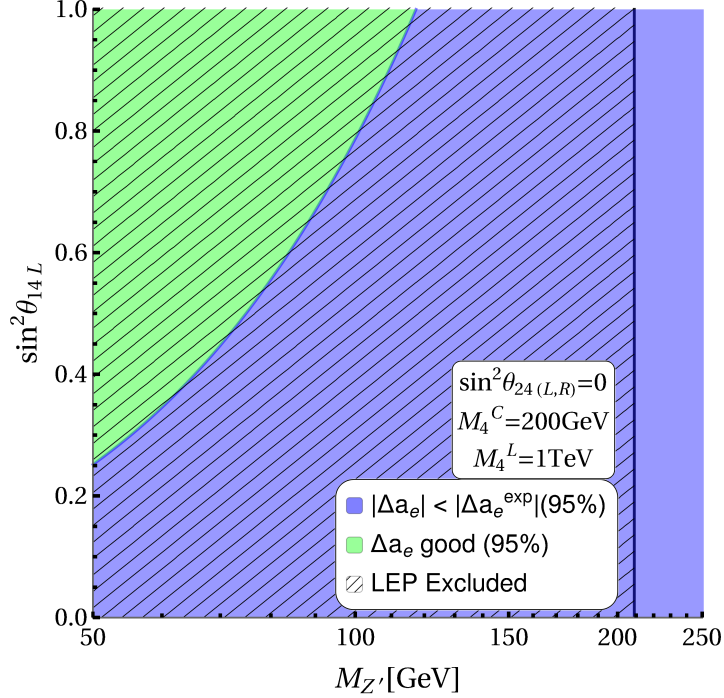
Figure 6.7: Δa_e impact on $\sin^2 \theta_{14L}$, $M_{Z'}$ parameter space with no mixing between muons and vector-like leptons. LEP-II exclusion limit is shown as hashed region.

the regions of Figures 6.6 and 6.7 that admit muon and electron magnetic moment experimental results respectively. This story concludes quite quickly with all points being excluded. The enhancement factor of M_4^C/m_μ in Equation (6.24) is largely responsible for $(g-2)_\mu$ in this scenario, however such a term also gives an unacceptably large contribution to $\mathrm{BR}(\mu \to e\gamma)$ as per Equation (6.22), resulting in a branching fraction far above the experimental limit; the minimum $\mathrm{BR}(\mu \to e\gamma)$ for any parameter points in this scenario is around 10^{-3}, as shown in Table 6.4. Such a situation persists even if $\sin^2 \theta_{14}^L$ is scanned through its entire range, and is unchanged by the choice of M_4^L, and is insensitive to the Z' mass in the case of large M_4^C. We conclude, therefore, that with a large chirality-flipping mass circa 200 GeV, it is not possible to simultaneously satisfy constraints and make predictions consistent with current data. This conclusion is consistent with the analytic arguments of the previous section, where the large contributions coming from large chirality flipping fourth family masses M_4^C were assumed to dominate. We now go beyond this approximation, considering henceforth very small M_4^C.

If one sets M_4^C vanishing, terms proportional to the aforementioned enhancement factor also vanish, eliminating the largest contribution to $\mu \to e\gamma$, as follows from Equation (6.22). Motivated by this reduction in the most restrictive decay the above analysis is repeated with $M_4^C = 0$.

111

Parameter/Observable	Value/Scanned Region
$M_{Z'}$	75 GeV
M_4^C	200 GeV
M_4^L	1000 GeV
$\sin^2\theta_{12L,R}$	0.0
$\sin^2\theta_{14L}$	0.75
$\sin^2\theta_{14R}$	0.0
$\sin^2\theta_{24L,R}$	$10^{-7} \to 1.0$
$\text{BR}(\mu \to e\gamma)$	$10^{-3} \to 1.0$

Table 6.4: Observables and $\text{BR}(\mu \to e\gamma)$ in a parameter space where electron and muon both mix with the vector-like lepton. Attempt to recover both anomalous moments.
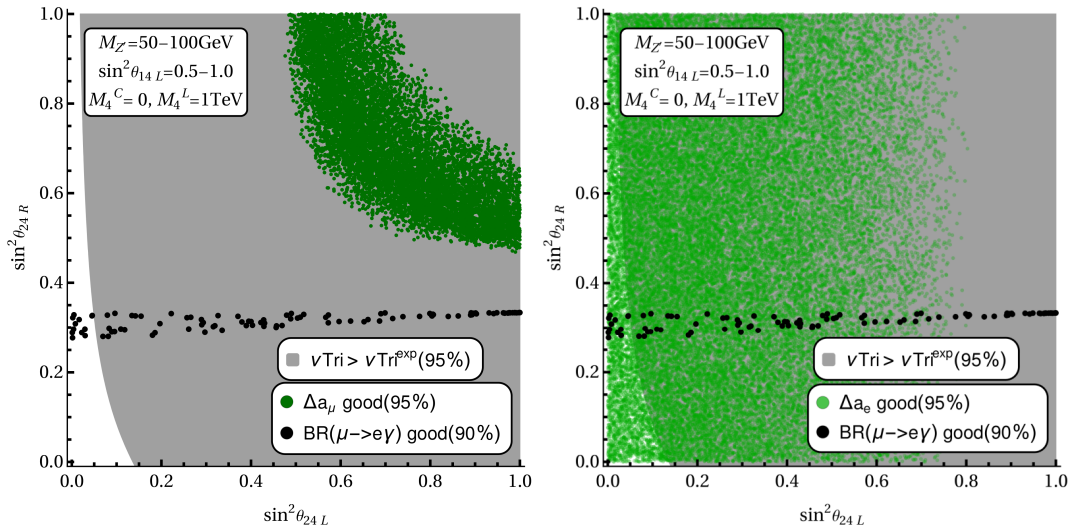
Vanishing M_4^C

If we choose to turn off the chirality-flipping mass of the vector-like leptons, their mass becomes composed entirely of M_4^L. Terms proportional to the enhancement factor M_4^C/m_μ in Equation (6.24) are sacrificed, which makes achieving $(g-2)_\mu$ consistent with the experimental result more challenging. Larger mixing between the muon and vector-like leptons is required, but more freedom exists with respect to $\text{BR}(\mu \to e\gamma)$. We investigated the region of parameter space detailed in Table 6.5, to test its viability. We consider the impact of each constraint separately, then check for overlap of allowed

Parameter	Value/Scanned Region
$M_{Z'}$	$50 \to 100$ GeV
M_4^C	0 GeV
M_4^L	1000 GeV
$\sin^2\theta_{12L,R}$	0.0
$\sin^2\theta_{14L}$	$0.5 \to 1.0$
$\sin^2\theta_{14R}$	0.0
$\sin^2\theta_{24L,R}$	$0.0 \to 1.0$

Table 6.5: Region of parameter space without chirality-flipping mass.

regions. Note that in Figure 6.8, angular parameters *and* the Z' mass are varied simultaneously, hence here we randomly select points and evaluate relevant phenomena. This also explains the spread of parameter points compared to previous figures. Note that the range of $\sin^2\theta_{14}^L$ has been restricted in Tables 6.5 and 6.6 as no points with a sufficiently small $\text{BR}(\mu \to e\gamma)$ could be found with $\sin^2\theta_{14}^L < 0.5$, omitting this region increases the probability of finding optimal points. We also limit the ranges of $M_{Z'}$ in Tables 6.5 and 6.6 as Z' masses much higher than this were found to be incompatible

with $(g-2)_\mu$, and masses much below saturated the bound from $\mu \to e\gamma$. In Figure

(a) Parameter points that resolve Δa_μ and separately points allowed under the $\mu \to e\gamma$ constraint. Fixed parameters are given in the legend. Chirality-flipping mass is set vanishing. All good Δa_μ points are excluded by trident and $\mu \to e\gamma$.

(b) Parameter points that resolve Δa_e and separately points allowed under $\mu \to e\gamma$. Fixed parameters are given in the legend. Chirality-flipping mass is set vanishing. Some good Δa_e points are allowed by trident and $\mu \to e\gamma$.

Figure 6.8: Parameter scan results for $M_4^C = 0$.

6.8a, one can see that, as suspected, larger $\sin^2 \theta_{24L,R}$ mixings are required to obtain a muon $(g-2)_\mu$ consistent with current data. However, there is no overlapped region in Figure 6.8a, and $(g-2)_\mu$ cannot be solved without violating the muon decay constraint, or the shown exclusion for neutrino trident production. On the other hand, Figure 6.8b shows that there are points that resolve the SM's tension with $(g-2)_e$, and are allowed by the strict BR$(\mu \to e\gamma)$ limit and neutrino trident production. The lack of terms with the enhancement factor of M_4^C/m_μ in Equation (6.22) means that points have been found with an acceptable branching fraction of $\mu \to e\gamma$ that was not possible with a large M_4^C.

Note that in both panels of Figure 6.8 the most conservative neutrino trident limit is shown, where we assume that $M_{Z'}$ is fixed at 50GeV. We have also found that there is also no obvious correlation between $M_{Z'}$ and $\sin^2 \theta_{14L}$ for $\mu \to e\gamma$, and points appear to be randomly distributed in this space. Since we have seen that neither large nor vanishing M_4^C are viable, in the next subsection we switch on a small but non-zero M_4^C, to investigate if it may be possible to increase $(g-2)_\mu$ to an acceptable level, without giving an overlarge contribution to the LFV muon decay.

Small M_4^C $\mathcal{O}(m_\mu)$

Here we perform analogous tests to those above but with a small chirality flipping mass, motivated by $(g-2)_\mu$ with the requirement that $\mathrm{BR}(\mu \to e\gamma)$ remains below the experimental limit. Ranges of parameters scanned in this investigation are given in Table 6.6. Figure 6.9 shows points allowed under each separate observable in an

Parameter	Value/Scanned Region
$M_{Z'}$	$50 \to 100$ GeV
M_4^C	$5m_\mu$
$\sin^2 \theta_{14L}$	$0.5 \to 1.0$
$\sin^2 \theta_{14R}$	0.0
$\sin^2 \theta_{24L,R}$	$0.0 \to 1.0$
$\sin^2 \theta_{12L,R}$	0.0

Table 6.6: Parameters for larger scan with small chirality-flipping mass.

analogous parameter space to Figure 6.8, but with $M_4^C = 5m_\mu$. Once more neutrino trident production excludes a large portion of the space under test. It seems that there is overlap between the allowed regions of $(g-2)_\mu$, $(g-2)_e$ and $\mathrm{BR}(\mu \to e\gamma)$. However, upon closer inspection of the parameter points allowed by $\mu \to e\gamma$, those points always yield negative (wrong sign) $(g-2)_\mu$ that is far away from the experimental value, and hence all points are excluded. In Table 6.7, we examine more closely the points that are allowed under the strict $\mu \to e\gamma$ constraint. As vector-like mixing with the muons exists in this space, neutrino trident production is also a consideration, and the constraint of this observable in our space is given in Figure 6.9. All points valid when considering $\mathrm{BR}(\mu \to e\gamma)$ exist with a small $\sin^2 \theta_{24R}$ mixing angle, but can have a wide range of Z' masses and $\sin^2 \theta_{14L}$. We see that for the points in Table 6.7, $(g-2)_e$ prefers regions with small $\sin^2 \theta_{24L}$, similarly to the preferred points under the neutrino trident constraint, given in the same plot as an excluded region derived in the same way as previous results for $M_4^C = 0$. Many of these points are simultaneously consistent with the $\mu \to e\gamma$ limit, and also provide a $(g-2)_e$ consistent with experimental data (denoted in green), whilst a subset of these points do not violate the neutrino trident production limit. From these results, we can conclude that the best points lie in the region of small $\sin^2 \theta_{24L}$ and $\sin^2 \theta_{24R}$, and that such points simultaneously comply with $\mathrm{BR}(\mu \to e\gamma)$, $(g-2)_e$ and neutrino trident. Such candidate points do not allow for resolution of Δa_μ, as they all have negative values for Δa_μ.

Several other values for M_4^C were examined in this work, in the region $5m_\mu < M_4^C < 200$ GeV, including a parameter scan whereby M_4^C was randomly selected between these limits, and these tests yielded similar results to those shown in the last three sections, whereby it was not possible to obtain predictions that were simultaneously consistent
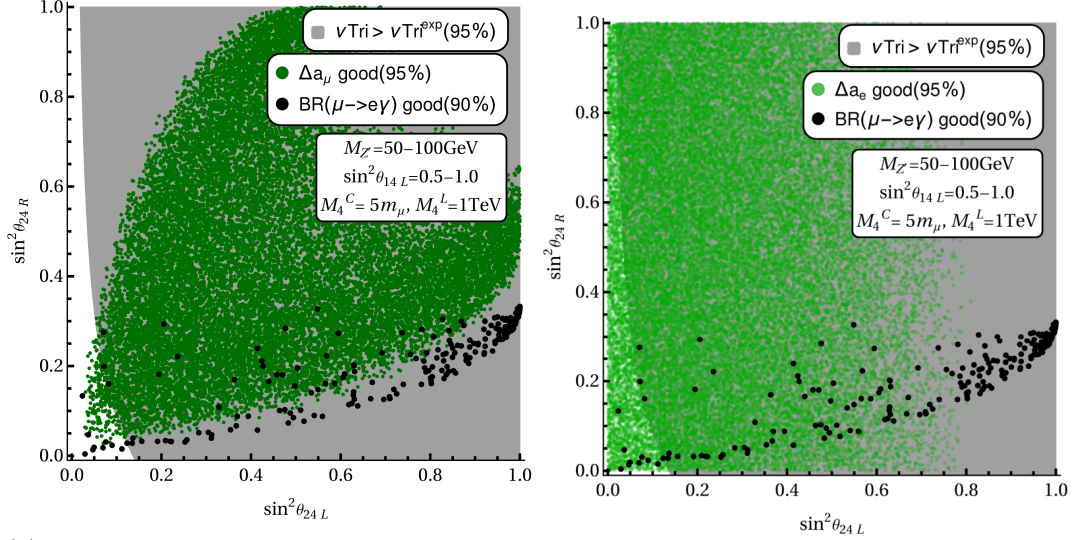
(a) Parameter points that resolve Δa_μ and separately points allowed under the $\mu \to e\gamma$ constraint. Fixed parameters are given in the legend, small-chirality flipping mass. No points shown obey all constraints simultaneously (see text).

(b) Parameter points that resolve Δa_e and separately points allowed under the $\mu \to e\gamma$ constraint. Fixed parameters are given in the legend, small-chirality flipping mass.

Figure 6.9: Parameter scan results for small $M_4^C = 5m_\mu$.

Parameter				Observable		
$M_{Z'}/\mathrm{GeV}$	$\sin^2\theta_{14L}$	$\sin^2\theta_{24L}$	$\sin^2\theta_{24R}$	$\mathrm{BR}(\mu \to e\gamma)$	Δa_e	Δa_μ
69.5	0.61	0.11	0.02	3.25×10^{-13}	-2.15×10^{-13}	-1.80×10^{-10}
68.5	0.80	0.05	0.01	1.69×10^{-13}	-3.32×10^{-13}	-1.63×10^{-10}
91.0	0.99	0.08	0.16	3.34×10^{-13}	-2.41×10^{-13}	-1.19×10^{-9}
63.0	0.99	0.02	0.13	1.38×10^{-13}	-5.390×10^{-13}	-2.03×10^{-9}
65.5	0.78	0.07	0.02	4.94×10^{-14}	-3.43×10^{-13}	-2.36×10^{-10}
64.8	0.78	0.09	0.02	3.61×10^{-13}	-3.46×10^{-13}	-3.19×10^{-10}
77.9	0.85	0.005	0.02	6.13×10^{-14}	-2.77×10^{-13}	-1.77×10^{-10}
91.4	0.81	0.14	0.04	5.80×10^{-14}	-1.73×10^{-13}	-2.71×10^{-10}
97.2	0.86	0.08	0.03	1.07×10^{-13}	-1.73×10^{-13}	-2.71×10^{-10}
76.0	0.63	0.03	0.004	1.72×10^{-13}	-2.01×10^{-13}	-3.97×10^{-11}
56.8	0.96	0.04	0.05	3.77×10^{-14}	-6.22×10^{-13}	-8.36×10^{-10}
78.1	0.99	0.07	0.20	1.84×10^{-14}	-3.32×10^{-13}	-2.04×10^{-9}
89.4	1.0	0.07	0.28	2.95×10^{-13}	-2.56×10^{-13}	-2.25×10^{-9}

Table 6.7: Parameter points that are below the upper bound on $\mathrm{BR}(\mu \to e\gamma)$ for $M_4^C = 5m_\mu$. The points in this table correspond to the black points in Figure 6.9 that are also below the grey neutrino trident exclusion. These points do not conform to the experimental value of $(\Delta a_\mu)_{\mathrm{exp}} = (26.1 \pm 8) \times 10^{-10}$.

with $(g-2)_e$, $(g-2)_\mu$ and BR($\mu \to e\gamma$).

Although we have been able to recover regions of parameter space which can seemingly account for either the muon or electron anomalous magnetic moments, we now return to the earlier discussion of LEP-II constraints that was touched on briefly when considering large chirality flipping masses of $M_4^C = 200$ GeV. In fact, all points in both Figure 6.8 and Figure 6.9 are excluded by LEP data [112, 290–294] due to their small $M_{Z'}$, and large mixing between as required for reproducing electron magnetic moment data. As such, this model is only able to give a full explanation for $(g-2)_\mu$, and not the corresponding electron anomalous magnetic moment. However, it could form a part of the explanation for $(g-2)_e$, perhaps with the addition of new scalar fields.

6.6 Summary

In this chapter, we investigated the anomalous muon and electron magnetic moments within the context of a model with vector-like leptons and Z' gauge bosons. We considered a simple model in which the Z' only has couplings to the electron, muon and their associated neutrinos, arising from mixing with a vector-like fourth family of leptons. This is achieved by assuming that only the vector-like leptons have non-vanishing $U(1)'$ charges and are assumed to only mix with the first and second family of SM charged leptons.

A feature of the analysis is that we distinguish the two sources of mass for the 4th, vector-like family: the chirality-flipping fourth family mass terms M_4^C arising from the Higgs Yukawa couplings and are proportional to the Higgs VEV, and vector-like masses M_4^L which are not protected by any symmetry.

We assumed large chirality-flipping masses $M_4^C \gg m_\mu$, and showed that expressions for $(g-2)_\mu$, $(g-2)_e$ and BR($\mu \to e\gamma$) reduced to a minimal number of terms, all proportional to M_4^C. We constructed an analytic argument which shows that it is not possible to explain the anomalous muon and electron magnetic moments in the Z' model while respecting the bound on BR($\mu \to e\gamma$). We performed a detailed numerical analysis of the parameter space of the model, beginning with large $M_4^C = 200$ GeV, where we showed that it is possible to account for $(g-2)_\mu$ in a region of parameter space where the electron couplings were zero. Similarly, we showed that it is possible to account for $(g-2)_e$ in a region of parameter space where the muon couplings were zero, however, this very region is excluded by constraints from the LEP collider. Keeping $M_4^C = 200$ GeV, we attempted to explain both anomalous magnetic moments by switching on couplings to the electron and muon simultaneously, but it was not possible to do this while and avoid the strict constraint from BR($\mu \to e\gamma$), as expected from analytic arguments.

A regime beyond the previous analytic arguments was investigated by considering very small values of M_4^C. With $M_4^C = 0$, it is not possible to account for $(g-2)_\mu$ without violating bounds from BR($\mu \to e\gamma$) and trident.

We stress that the fermiophobic Z' model is a good candidate to explain $(g-2)_\mu$, consistently with $\mathrm{BR}(\mu \to e\gamma)$, neutrino trident production, and limits from the LEP collider. However to explain the $(g-2)_\mu$ always requires a significant chirality-flipping mass involving the 4th vector-like family of leptons, which can lead to trouble with flavour-violating muon decays.

Does this conclusion apply to all Z' models? While it is impossible to answer this question absolutely, there are reasons why the results presented here could be considered general and indicative of a large class of Z' models. Allowed Z' couplings are free parameters in this approach and so could represent couplings in a large class of Z' models. Furthermore, we present a general analytic argument that provides some insight into our numerical results. We do not require the Z' couple identically to left- and right-handed leptons, and masses for intermediate propagating particles in one-loop diagrams cancel in the final expression for $\mathrm{BR}(\mu \to e\gamma)$ in Equation 6.38. This chapter details the first work that attempts to explain both electron and muon anomalous magnetic moments simultaneously within a Z' model.

Finally, we comment that since there are models in the literature which account for all these observables based on having scalars, it would be interesting to extend the scalar sector of a model such as this. Lepton flavour violating processes could then be used to set constraints on the masses for CP-even and CP-odd heavy neutral scalars, as done previously [269]. However, such a study is beyond the scope of this analysis. The author's hope is the work presented here will inspire models of vector-like leptons that can simultaneously provide solutions for discrepancies between the predicted and observed anomalous magnetic moments of the muon and electron.

Chapter 7

Concluding Remarks

In this thesis, we reviewed the Standard Model and various extensions that try to explain many phenomena that are not included in its description. Follwoing this, several phenomenological analyses were presented that determine some measure of suitability for these theories that have the potential to form part of a complete description of fundamental physics. We close with remarks on these analyses and speculation on how such research could be extended and used in the future.

In Chapter 4, we investigated a minimal Type-I seesaw model known as the Littlest Seesaw by fitting model parameters to experimental neutrino data combined with the baryon asymmetry of the universe, as predicted in such a model by leptogenesis. We employed careful renormalisation group methods to ensure that the theory was correctly handled in a variety of regimes, depending on the scale under test, and ensured that model predictions and experimental data were properly compared at the relevant scales. We found that the model can readily predict neutrino mass and oscillation phenomena, along with a baryon asymmetry with the correct sign. It is remarkable that such a simple model can be used to predict such a variety of phenomena, and the author sincerely hopes that the work presented in this chapter will inspire more work on the Littlest Seesaw and other minimal models of neutrino physics. Upcoming experiments such as DUNE and HyperKamiokande [295] will enable neutrino masses and mixing parameters to be measured much more precisely, and will prove to be a further challenge to the Littlest Seesaw and research presented here.

Following this, in Chapter 5 we investigated flavour violation in the Minimal Supersymmetric Standard Model arising from the breaking of a discrete A_4 symmetry in a flavoured SUSY GUT. Discrete symmetries offer not only an attractive solution to the flavour problem, but through their breaking they may also describe the mass hierarchies and flavour structures seen at low scales. The analysis presented here shows striking hints that flavour structures present at unified scales can have a drastic effect on low-scale flavour physics. Though the structure of quark mixing in the CKM matrix remains untouched, interesting interdependencies are uncovered during the course of the analysis. Correlations in flavour violating parameters at the SUSY scale could

hint that if flavour violation is present in a grand unified theory at high scales, there is an imprint of this at the SUSY scale. This is another avenue by which high-scale physics could show up in experimental data and is an interesting topic to consider. We hope that this work will inform future model building in this area and inspire other unified theories with interesting flavour implications. It is possible that hints of flavour patterns from grand unification will show their faces at the high luminosity run of the LHC (HL-LHC) or in future colliders.

In the final research chapter, Chapter 6, we discuss the possibilities for explaining anomalous magnetic moments of leptons in a model with vector-like fermions and a $U(1)'$ gauge symmetry. Such a model contains an entire family of vector-like fermions, which avoid chiral anomalies in the usual way. Through rigorous statistical analyses, we conclude that such a model can explain the observed muon anomaly Δa_μ with relative ease, through use of loop diagrams that contain heavy vector-like leptons which couple to the SM Higgs and the Z' boson that obtains mass through breaking of the $U(1)'$ symmetry by additional scalars. However, such a model cannot explain both of these anomalies whilst conforming to strict constraints from lepton flavour violating decays and the LEP collider. This model was originally developed to study lepton universality in decays of B mesons, and so future studies of heavy meson decays could have interesting consequences for this theory and its ability to explain lepton magnetic moment anomalies. Furthermore, upcoming results from the $(g-2)_\mu$ experiment at Fermilab [296] could also impact the prospects of such a model. Results presented here may have far-reaching implications for a wider class of Z' models.

To conclude, we hope that this thesis gives an insight into the phenomenology of theories inspired by unification, and provides the reader with a sense of the vital role that statistics and analytical techniques play in the study of theoretical physics. More generally, phenomenology continues to be an interesting subject that is constantly evolving and moving forward with new techniques such as machine learning, providing the community with yet more ways to investigate the viability of theories. We hope that experimental particle physics continues to provide us with more hints beyond the Standard Model and that emerging methods are fully utilised, such that physicists can better probe theories and move toward a complete description of nature at the fundamental level.

Appendix A

Weyl vs. Dirac fermions

There are two primary ways of representing fermion fields in the language of particle physics, known as Weyl notation and Dirac notation [297]. In this appendix, Dirac fermions will always be denoted by ψ and Weyl fields will be exclusively represented by ξ and χ.

A.1   Dirac notation

Dirac fermions must obey the Dirac equation;

$$\overline{\psi}\big(i\slashed{\partial} - m_\psi\big)\psi = 0 \tag{A.1}$$

Where $\slashed{\partial} = \gamma^\mu \partial_\mu$, and γ^μ are the usual 'gamma' matrices which obey the Clifford algebra.

$$\big\{\gamma^\mu, \gamma^\nu\big\} = 2g^{\mu\nu} \tag{A.2}$$

The mass term of a Dirac fermion ψ then becomes apparent from the Dirac equation to be $-m_\psi \overline{\psi}\psi$. To think about handedness of Dirac fields, we will need to project out the chirality from ψ. Projection operators are defined as the following:

$$P_L = \frac{1}{2}\big(1 - \gamma^5\big), \qquad P_R = \frac{1}{2}\big(1 + \gamma^5\big) \tag{A.3}$$

$$\gamma^5 = i\gamma^0 \gamma^1 \gamma^2 \gamma^3 \tag{A.4}$$

One can then break up ψ into its left- and right-handed components:

$$\psi = \psi_L + \psi_R \tag{A.5}$$

$$\psi_L = P_L \psi, \qquad \psi_R = P_R \psi \tag{A.6}$$

In this, the Dirac basis, gamma matrices of the clifford algebra are expressed as per Equation (A.7).

$$\gamma_0 = \begin{pmatrix} \mathbb{I}_2 & 0 \\ 0 & -\mathbb{I}_2 \end{pmatrix}, \; \gamma_k = \begin{pmatrix} 0 & \sigma_k \\ -\sigma_k & 0 \end{pmatrix}, \; \gamma_5 = \begin{pmatrix} 0 & \mathbb{I}_2 \\ \mathbb{I}_2 & 0 \end{pmatrix} \tag{A.7}$$

The Dirac fermion mass term then becomes the following:

$$-m_\psi \overline{\psi}\psi = -m_\psi \left(\overline{\psi_L}\psi_R + \overline{\psi_R}\psi_L \right) \tag{A.8}$$

A.2 Weyl notation

To discuss the concept of Weyl fermions, it is first useful to briefly dissect the Lorentz group algebra. The Lorentz group is a subgroup of the Poincaré group of Minkowski spacetime symmetries, with an algebra of $SO(1,3)$, which is isomorphic to $SU(2) \times SU(2)$. In this language, a left-handed chiral fermion would be a doublet under one of the $SU(2)$s and a singlet under the other, represented by $(\mathbf{2},0)$, and conversely for a right-handed chiral field; $(0,\mathbf{2})$. Both of these left- and right-handed fields are, individually, Weyl fermions. Because a Dirac fermion field transforms like $(\mathbf{2},\mathbf{2})$ under Lorentz group's isomorphism, it is then easy to see that a Dirac fermion can be expressed as a sum of left- and right-handed Weyl fermions:

$$\begin{array}{ccccc} (\mathbf{2},\mathbf{2}) & = & (\mathbf{2},0) & + & (0,\mathbf{2}) \\ \text{Dirac} & = & \text{LH Weyl} & + & \text{RH Weyl} \end{array} \tag{A.9}$$

We can therefore represent Weyl fermions by spinors of two components and Dirac fields using four-component spinors or two Weyl spinors. Note that Weyl fermions still obey the Dirac equation. Denoting a left-handed Weyl fermion as χ and a right-handed Weyl fermion as ξ, we can express a Dirac field in the following way:

$$\psi = \begin{pmatrix} \chi \\ \xi \end{pmatrix}, \qquad \psi_L = P_L\psi = \begin{pmatrix} \chi \\ 0 \end{pmatrix}, \qquad \psi_R = P_R\psi = \begin{pmatrix} 0 \\ \xi \end{pmatrix} \tag{A.10}$$

With reference to the Standard Model, Weyl fermions conjugate under the action of the CP operator, just like Dirac fermions. Under such conjugation (represented by superscript c), the chirality of the field is flipped but the $SU(2)_L$ transformation properties remain the same. For example, χ^c transforms like a right-handed Weyl fermion but is still a doublet under $SU(2)_L$. As such, we can relate the Dirac and Weyl representations

by studying their transformations under charge conjugation:

$$\psi^c = \hat{C}\hat{P}\overline{\psi}^T, \qquad \chi^c = \hat{C}\hat{P}\chi, \qquad \xi^c = \hat{C}\hat{P}\xi \tag{A.11}$$

$$\psi_R^c = \xi^c = (P_R\psi)^c = P_L\psi^c = (\psi^c)_L \tag{A.12}$$

$$\psi_L^c = \chi^c = (P_L\psi)^c = P_R\psi^c = (\psi^c)_R \tag{A.13}$$

In the Weyl, or chiral basis, Clifford algebra matrices are given as the following:

$$\gamma_0 = \begin{pmatrix} 0 & \mathbb{I}_2 \\ \mathbb{I}_2 & 0 \end{pmatrix}, \gamma_k = \begin{pmatrix} 0 & \sigma_k \\ -\sigma_k & 0 \end{pmatrix}, \gamma_5 = \begin{pmatrix} -\mathbb{I}_2 & 0 \\ 0 & \mathbb{I}_2 \end{pmatrix} \tag{A.14}$$

Therefore, with ψ defined as per Equation (A.10), we can express Equation (A.1) for a massless fermion as:

$$i\chi^\dagger\big(\partial_0 - \sigma^k\partial_k\big)\chi + i\xi^\dagger\big(\partial_0 - \sigma^k\partial_k\big)\xi = 0 \tag{A.15}$$

A more detailed description of the differences between Dirac and Weyl fermions can be found in the pedagogical review article by P. Pal [297].

Appendix B

SPheno and the SCKM basis

The CKM basis is the one in which the up- and down-type quark Yukawa matrices are diagonal. The Super-CKM basis (SCKM) is obtained analogously, i.e. the squarks undergo the same rotations as their SM partners. This basis is convenient for phenomenological studies and allows for a consistent expression of flavour violation throughout the literature. The different rotations for the SM quark and lepton fields are:

$$u'_L = V_{u_L} u_L \,, \quad u'_R = V_{u_R} u_R \,, \quad d'_L = V_{d_L} d_L \,, \quad d'_R = V_{d_R} d_R \,,$$
$$e'_L = V_{e_L} e_L \,, \quad e'_R = V_{e_R} e_R \,,$$

(B.1)

where the primed fields are in the flavour basis and the bare fields exist in the basis of diagonal Yukawa couplings. The misalignment between up- and down-type quarks leads to the usual CKM matrix:

$$V_{\mathrm{CKM}} = V_{u_L}^\dagger V_{d_L}$$

(B.2)

In order to account for the change to the SCKM basis, the numerical program `SPheno` assumes diagonal down-type Yukawa matrices. In this case the CKM matrix is the following: $V_{\mathrm{CKM}} = V_{u_L}^\dagger \mathcal{I} = V_{u_L}^\dagger$. In $SU(5)$-like models, the choice of the representations $F = \bar{\mathbf{5}}$ and $T = \mathbf{10}$ forces relationships between Yukawa couplings to hold at the unification scale:

$$y_u = y_u^T \quad \text{and} \quad y_d = y_e^T.$$

(B.3)

As a consequence, we have $V_{u_L} = V_{u_R}$ in this case, meaning both lepton and down-type Yukawas are simultaneously diagonal. For consistency, we then have to perform a systematic CKM rotation for all terms involving V_{u_L} and V_{u_R}. The soft-breaking terms

of the Lagrangian transform as follows when switching to the SCKM basis:

$$
\begin{aligned}
\overline{\widetilde{U}'_{L,R}}\, M_T^2\, \widetilde{U}'_{L,R} &= \overline{\widetilde{U}_{L,R}}\, V_{\text{CKM}}\, M_T^2\, V_{\text{CKM}}^\dagger\, \widetilde{U}_{L,R}\,, \\
\overline{\widetilde{U}'_R}\, A_u \widetilde{U}'_L &= \overline{\widetilde{U}_R}\, V_{\text{CKM}}\, A_u\, V_{\text{CKM}}^\dagger\, \widetilde{U}_L\,, \\
\overline{\widetilde{D}'_{L,R}}\, M_{T,F}^2\, \widetilde{D}'_{L,R} &= \overline{\widetilde{D}_{L,R}}\, M_{T,F}^2\, \widetilde{D}_{L,R}\,, \\
\overline{\widetilde{D}'_R}\, A_d \widetilde{D}'_L &= \overline{\widetilde{D}_R}\, A_d\, \widetilde{D}_L\,, \\
\overline{\widetilde{L}'_L}\, M_{F,T}^2\, \widetilde{L}'_L &= \overline{\widetilde{L}_L}\, M_{F,T}^2\, \widetilde{L}_L\,, \\
\overline{\widetilde{E}'_R}\, M_{F,T}^2\, \widetilde{E}'_R &= \overline{\widetilde{E}_R}\, M_{F,T}^2\, \widetilde{E}_R\,, \\
\overline{\widetilde{E}'_R}\, A_d^T \widetilde{L}'_L &= \overline{\widetilde{E}_R}\, A_d^T\, \widetilde{L}_L\,.
\end{aligned}
\tag{B.4}
$$

Consequently, in the SCKM basis, where the down-type Yukawa matrix is diagonal following the SPheno requirements and assuming the $SU(5)$ relations, the 6×6 soft mass matrices in the MSSM (once trilinear couplings have been taken into account) are

$$
M_{\widetilde{D}}^2 = \begin{pmatrix} M_T^2 & \frac{v_d}{\sqrt{2}} A_D^T \\ \frac{v_d}{\sqrt{2}} A_D & M_F^2 \end{pmatrix}, \qquad
M_{\widetilde{L}}^2 = \begin{pmatrix} M_F^2 & \frac{v_d}{\sqrt{2}} A_D \\ \frac{v_d}{\sqrt{2}} A_D^T & M_T^2 \end{pmatrix},
\tag{B.5}
$$

$$
M_{\widetilde{U}}^2 = \begin{pmatrix} V_{\text{CKM}} M_T^2 V_{\text{CKM}}^\dagger & \frac{v_u}{\sqrt{2}} V_{\text{CKM}} A_U^T V_{\text{CKM}}^\dagger \\ \frac{v_u}{\sqrt{2}} V_{\text{CKM}} A_U V_{\text{CKM}}^\dagger & V_{\text{CKM}} M_T^2 V_{\text{CKM}}^\dagger \end{pmatrix},
$$

up to the D-terms and SM masses. Since SPheno automatically ensures the CKM rotation for the left-left block of $M_{\widetilde{U}}^2$, we enforce the rotation for the other blocks of the up-type squark mass matrix by hand before running SPheno in Chapter 5.

Appendix C

Analytical recasting of lepton flavour predictions

In this appendix, we recast leptonic observables derived in Chapter 6 in terms of leptonic mixing angles. Coupling constants are defined from Equation (6.10) to (6.15) in Section 6.3.

C.1 The branching ratio of $\mu \to e\gamma$

The branching ratio of $\mu \to e\gamma$ in a model with vector-like leptons and an additional $U(1)'$ gauge symmetry is the following:

$$\text{BR}(\mu \to e\gamma) = \frac{\alpha}{1024\pi^4} \frac{m_\mu^5}{M_{Z'}^4 \Gamma_\mu} (|\widetilde{\sigma}_L|^2 + |\widetilde{\sigma}_R|^2) \tag{C.1}$$

The $\widetilde{\sigma}_{L,R}$ are given by:

$$\widetilde{\sigma}_L = \sum_{a=e,\mu,E} \left[(g_L)_{ea}(g_L)_{a\mu} F(x_a) + \frac{m_a}{m_\mu} (g_L)_{ea}(g_R)_{a\mu} G(x_a) \right],$$

$$\widetilde{\sigma}_R = \sum_{a=e,\mu,E} \left[(g_R)_{ea}(g_R)_{a\mu} F(x_a) + \frac{m_a}{m_\mu} (g_R)_{ea}(g_L)_{a\mu} G(x_a) \right], \qquad x_a = \frac{m_a^2}{M_{Z'}^2} \tag{C.2}$$

Expanding the above $\widetilde{\sigma}_{L,R}$ in terms of electron, muon and vector-like couplings, where $(g_L)_{eE}$ represents a coupling between left-handed electrons and a left-handed heavy

lepton from the vector-like family:

$$\widetilde{\sigma}_L = \Big[(g_L)_{ee} (g_L)_{e\mu} F(x_e) + \frac{m_e}{m_\mu} (g_L)_{ee} (g_R)_{e\mu} G(x_e)$$
$$(g_L)_{e\mu} (g_L)_{\mu\mu} F(x_\mu) + \frac{m_\mu}{m_\mu} (g_L)_{e\mu} (g_R)_{\mu\mu} G(x_\mu)$$
$$(g_L)_{eE} (g_L)_{E\mu} F(x_E) + \frac{M_4^C}{m_\mu} (g_L)_{eE} (g_R)_{E\mu} G(x_E) \Big]$$
$$\widetilde{\sigma}_R = \Big[(g_R)_{ee} (g_R)_{e\mu} F(x_e) + \frac{m_e}{m_\mu} (g_R)_{ee} (g_L)_{e\mu} G(x_e)$$
$$(g_R)_{e\mu} (g_R)_{\mu\mu} F(x_\mu) + \frac{m_\mu}{m_\mu} (g_R)_{e\mu} (g_L)_{\mu\mu} G(x_\mu)$$
$$(g_R)_{eE} (g_R)_{E\mu} F(x_E) + \frac{M_4^C}{m_\mu} (g_R)_{eE} (g_L)_{E\mu} G(x_E) \Big]$$

$$(C.3)$$

One important feature in Equation (C.3) is the chirality-flipping mass M_4^C. It then is possible to re-express the coupling constants in each $\widetilde{\sigma}$ as a combination of leptonic

mixing angles by using the Equations (6.10)-(6.15). It was assumed that $g'q_{L4} = 1$.

$$
\begin{aligned}
\widetilde{\sigma}_L = \Big[&\Big(\sin\theta_{12}^L \sin\theta_{24}^L + \cos\theta_{12}^L \cos\theta_{24}^L \sin\theta_{14}^L \Big)^2 \times \\
&\Big(\sin\theta_{12}^L \sin\theta_{24}^L + \cos\theta_{12}^L \cos\theta_{24}^L \sin\theta_{14}^L \Big) \Big(\cos\theta_{12}^L \sin\theta_{24}^L - \cos\theta_{24}^L \sin\theta_{12}^L \sin\theta_{14}^L \Big) F(x_1) \\
&+ \frac{m_1}{m_2} \Big(\sin\theta_{12}^L \sin\theta_{24}^L + \cos\theta_{12}^L \cos\theta_{24}^L \sin\theta_{14}^L \Big)^2 \times \\
&\Big(\sin\theta_{12}^R \sin\theta_{24}^R + \cos\theta_{12}^R \cos\theta_{24}^R \sin\theta_{14}^R \Big) \Big(\cos\theta_{12}^R \sin\theta_{24}^R - \cos\theta_{24}^R \sin\theta_{12}^R \sin\theta_{14}^R \Big) G(x_1) \\
&+ \Big(\sin\theta_{12}^L \sin\theta_{24}^L + \cos\theta_{12}^L \cos\theta_{24}^L \sin\theta_{14}^L \Big) \Big(\cos\theta_{12}^L \sin\theta_{24}^L - \cos\theta_{24}^L \sin\theta_{12}^L \sin\theta_{14}^L \Big) \times \\
&\Big(\cos\theta_{12}^L \sin\theta_{24}^L - \cos\theta_{24}^L \sin\theta_{12}^L \sin\theta_{14}^L \Big)^2 F(x_2) \\
&+ \frac{m_2}{m_2} \Big(\sin\theta_{12}^L \sin\theta_{24}^L + \cos\theta_{12}^L \cos\theta_{24}^L \sin\theta_{14}^L \Big) \Big(\cos\theta_{12}^L \sin\theta_{24}^L - \cos\theta_{24}^L \sin\theta_{12}^L \sin\theta_{14}^L \Big) \times \\
&\Big(\cos\theta_{12}^R \sin\theta_{24}^R - \cos\theta_{24}^R \sin\theta_{12}^R \sin\theta_{14}^R \Big)^2 G(x_2) \\
&+ \cos\theta_{14}^L \cos\theta_{24}^L \Big(\sin\theta_{12}^L \sin\theta_{24}^L + \cos\theta_{12}^L \cos\theta_{24}^L \sin\theta_{14}^L \Big) \times \\
&\cos\theta_{14}^L \cos\theta_{24}^L \Big(\cos\theta_{12}^L \sin\theta_{24}^L - \cos\theta_{24}^L \sin\theta_{12}^L \sin\theta_{14}^L \Big) F(x_4) \\
&+ \frac{M_4^C}{m_2} \cos\theta_{14}^L \cos\theta_{24}^L \Big(\sin\theta_{12}^L \sin\theta_{24}^L + \cos\theta_{12}^L \cos\theta_{24}^L \sin\theta_{14}^L \Big) \times \\
&\cos\theta_{14}^R \cos\theta_{24}^R \Big(\cos\theta_{12}^R \sin\theta_{24}^R - \cos\theta_{24}^R \sin\theta_{12}^R \sin\theta_{14}^R \Big) G(x_4) \Big] \\[1em]
\widetilde{\sigma}_R = \Big[&\Big(\sin\theta_{12}^R \sin\theta_{24}^R + \cos\theta_{12}^R \cos\theta_{24}^R \sin\theta_{14}^R \Big)^2 \times \\
&\Big(\sin\theta_{12}^R \sin\theta_{24}^R + \cos\theta_{12}^R \cos\theta_{24}^R \sin\theta_{14}^R \Big) \Big(\cos\theta_{12}^R \sin\theta_{24}^R - \cos\theta_{24}^R \sin\theta_{12}^R \sin\theta_{14}^R \Big) F(x_1) \\
&+ \frac{m_1}{m_2} \Big(\sin\theta_{12}^R \sin\theta_{24}^R + \cos\theta_{12}^R \cos\theta_{24}^R \sin\theta_{14}^R \Big)^2 \times \\
&\Big(\sin\theta_{12}^L \sin\theta_{24}^L + \cos\theta_{12}^L \cos\theta_{24}^L \sin\theta_{14}^L \Big) \Big(\cos\theta_{12}^L \sin\theta_{24}^L - \cos\theta_{24}^L \sin\theta_{12}^L \sin\theta_{14}^L \Big) G(x_1) \\
&+ \Big(\sin\theta_{12}^R \sin\theta_{24}^R + \cos\theta_{12}^R \cos\theta_{24}^R \sin\theta_{14}^R \Big) \Big(\cos\theta_{12}^R \sin\theta_{24}^R - \cos\theta_{24}^R \sin\theta_{12}^R \sin\theta_{14}^R \Big) \times \\
&\Big(\cos\theta_{12}^R \sin\theta_{24}^R - \cos\theta_{24}^R \sin\theta_{12}^R \sin\theta_{14}^R \Big)^2 F(x_2) \\
&+ \frac{m_2}{m_2} \Big(\sin\theta_{12}^R \sin\theta_{24}^R + \cos\theta_{12}^R \cos\theta_{24}^R \sin\theta_{14}^R \Big) \Big(\cos\theta_{12}^R \sin\theta_{24}^R - \cos\theta_{24}^R \sin\theta_{12}^R \sin\theta_{14}^R \Big) \times \\
&\Big(\cos\theta_{12}^L \sin\theta_{24}^L - \cos\theta_{24}^L \sin\theta_{12}^L \sin\theta_{14}^L \Big)^2 G(x_2) \\
&+ \cos\theta_{14}^R \cos\theta_{24}^R \Big(\sin\theta_{12}^R \sin\theta_{24}^R + \cos\theta_{12}^R \cos\theta_{24}^R \sin\theta_{14}^R \Big) \times \\
&\cos\theta_{14}^R \cos\theta_{24}^R \Big(\cos\theta_{12}^R \sin\theta_{24}^R - \cos\theta_{24}^R \sin\theta_{12}^R \sin\theta_{14}^R \Big) F(x_4) \\
&+ \frac{M_4^C}{m_2} \cos\theta_{14}^R \cos\theta_{24}^R \Big(\sin\theta_{12}^R \sin\theta_{24}^R + \cos\theta_{12}^R \cos\theta_{24}^R \sin\theta_{14}^R \Big) \times \\
&\cos\theta_{14}^L \cos\theta_{24}^L \Big(\cos\theta_{12}^L \sin\theta_{24}^L - \cos\theta_{24}^L \sin\theta_{12}^L \sin\theta_{14}^L \Big) G(x_4) \Big]
\end{aligned}
$$

$$\text{(C.4)}$$

C.2 Muon magnetic moment

The anomalous muon magnetic moment is given by:

$$\Delta a_\mu^{Z'} = -\frac{m_\mu^2}{8\pi^2 M_{Z'}^2} \sum_{a=e,\mu,E} \left[\left(|(g_L)_{\mu a}|^2 + |(g_R)_{\mu a}|^2 \right) F(x_a) + \frac{m_a}{m_\mu} \mathrm{Re}\left[(g_L)_{\mu a} (g_R^*)_{\mu a} \right] G(x_a) \right]$$

$$\text{(C.5)}$$

Expanding the above equation in terms of electron, muon and vector-like lepton couplings yields:

$$
\begin{aligned}
\Delta a_\mu^{Z'} = -\frac{m_\mu^2}{8\pi^2 M_{Z'}^2} \Bigg[&\left(|(g_L)_{\mu e}|^2 + |(g_R)_{\mu e}|^2 \right) F(x_e) + \frac{m_e}{m_\mu} \mathrm{Re}\left[(g_L)_{\mu e} (g_R^*)_{\mu e} \right] G(x_e) \\
+ &\left(|(g_L)_{\mu\mu}|^2 + |(g_R)_{\mu\mu}|^2 \right) F(x_\mu) + \frac{m_\mu}{m_\mu} \mathrm{Re}\left[(g_L)_{\mu\mu} (g_R^*)_{\mu\mu} \right] G(x_\mu) \\
+ &\left(|(g_L)_{\mu E}|^2 + |(g_R)_{\mu E}|^2 \right) F(x_E) + \frac{M_4^C}{m_\mu} \mathrm{Re}\left[(g_L)_{\mu E} (g_R^*)_{\mu E} \right] G(x_E) \Bigg]
\end{aligned}
$$

$$\text{(C.6)}$$

The chirality-flipping mass is used in the last line of equation (C.6) similarly to Equation (C.3). It then is possible to represent Δa_μ in terms of mixing angles.

$$
\begin{aligned}
\Delta a_\mu^{Z'} = -\frac{m_\mu^2}{8\pi^2 M_{Z'}^2} \Bigg[&\bigg(|\left(\sin\theta_{12}^L \sin\theta_{24}^L + \cos\theta_{12}^L \cos\theta_{24}^L \sin\theta_{14}^L \right)\left(\cos\theta_{12}^L \sin\theta_{24}^L - \cos\theta_{24}^L \sin\theta_{12}^L \sin\theta_{14}^L \right)|^2 \\
&+ |\left(\sin\theta_{12}^R \sin\theta_{24}^R + \cos\theta_{12}^R \cos\theta_{24}^R \sin\theta_{14}^R \right)\left(\cos\theta_{12}^R \sin\theta_{24}^R - \cos\theta_{24}^R \sin\theta_{12}^R \sin\theta_{14}^R \right)|^2 \bigg) F(x_1) \\
&+ \frac{m_1}{m_2} \left(\sin\theta_{12}^L \sin\theta_{24}^L + \cos\theta_{12}^L \cos\theta_{24}^L \sin\theta_{14}^L \right)\left(\cos\theta_{12}^L \sin\theta_{24}^L - \cos\theta_{24}^L \sin\theta_{12}^L \sin\theta_{14}^L \right) \\
&\times \left(\sin\theta_{12}^R \sin\theta_{24}^R + \cos\theta_{12}^R \cos\theta_{24}^R \sin\theta_{14}^R \right)\left(\cos\theta_{12}^R \sin\theta_{24}^R - \cos\theta_{24}^R \sin\theta_{12}^R \sin\theta_{14}^R \right) G(x_1) \\
&+ \bigg(|\left(\cos\theta_{12}^L \sin\theta_{24}^L - \cos\theta_{24}^L \sin\theta_{12}^L \sin\theta_{14}^L \right)^2|^2 \\
&+ |\left(\cos\theta_{12}^R \sin\theta_{24}^R - \cos\theta_{24}^R \sin\theta_{12}^R \sin\theta_{14}^R \right)^2|^2 \bigg) F(x_2) \\
&+ \frac{m_2}{m_2} \left(\cos\theta_{12}^L \sin\theta_{24}^L - \cos\theta_{24}^L \sin\theta_{12}^L \sin\theta_{14}^L \right)^2 \left(\cos\theta_{12}^R \sin\theta_{24}^R - \cos\theta_{24}^R \sin\theta_{12}^R \sin\theta_{14}^R \right)^2 G(x_2) \\
&+ \bigg(|\cos\theta_{14}^L \cos\theta_{24}^L \left(\cos\theta_{12}^L \sin\theta_{24}^L - \cos\theta_{24}^L \sin\theta_{12}^L \sin\theta_{14}^L \right)|^2 \\
&+ |\cos\theta_{14}^R \cos\theta_{24}^R \left(\cos\theta_{12}^R \sin\theta_{24}^R - \cos\theta_{24}^R \sin\theta_{12}^R \sin\theta_{14}^R \right)|^2 \bigg) F(x_4) \\
&+ \frac{M_4^C}{m_2} \cos\theta_{14}^L \cos\theta_{24}^L \left(\cos\theta_{12}^L \sin\theta_{24}^L - \cos\theta_{24}^L \sin\theta_{12}^L \sin\theta_{14}^L \right) \\
&\times \cos\theta_{14}^R \cos\theta_{24}^R \left(\cos\theta_{12}^R \sin\theta_{24}^R - \cos\theta_{24}^R \sin\theta_{12}^R \sin\theta_{14}^R \right) G(x_4) \Bigg]
\end{aligned}
$$

$$\text{(C.7)}$$

C.3 Anomalous electron moment

The anomalous electron magnetic moment is given by:

$$\Delta a_e^{Z'} = -\frac{m_e^2}{8\pi^2 M_{Z'}^2} \sum_{a=e,\mu,E} \left[\left(|(g_L)_{ea}|^2 + |(g_R)_{ea}|^2 \right) F(x_a) + \frac{m_a}{m_e} \mathrm{Re}\left[(g_L)_{ea}\, (g_R^*)_{ea} \right] G(x_a) \right]$$

(C.8)

Expanding the above equation in terms of electron, muon and vector-like lepton as previously, the form is

$$\begin{aligned}
\Delta a_e^{Z'} = -\frac{m_e^2}{8\pi^2 M_{Z'}^2} \Bigg[&\left(|(g_L)_{ee}|^2 + |(g_R)_{ee}|^2 \right) F(x_e) + \frac{m_e}{m_e} \mathrm{Re}\left[(g_L)_{ee}\, (g_R^*)_{ee} \right] G(x_e) \\
&+ \left(|(g_L)_{e\mu}|^2 + |(g_R)_{e\mu}|^2 \right) F(x_\mu) + \frac{m_\mu}{m_e} \mathrm{Re}\left[(g_L)_{e\mu}\, (g_R^*)_{e\mu} \right] G(x_\mu) \\
&+ \left(|(g_L)_{eE}|^2 + |(g_R)_{eE}|^2 \right) F(x_E) + \frac{M_4^C}{m_e} \mathrm{Re}\left[(g_L)_{eE}\, (g_R^*)_{eE} \right] G(x_E) \Bigg]
\end{aligned}$$

(C.9)

The chirality-flipping mass is used in the last line of Equation (C.9) similarly to the Equations (C.3) or (C.6). It then is possible to represent Δa_e as a combination of model parameters including leptonic mixing angles, analogously to the muon moment discussed previously.

$$\begin{aligned}
\Delta a_e^{Z'} = -\frac{m_e^2}{8\pi^2 M_{Z'}^2} \Bigg[&\left(|\left(\sin\theta_{12}^L \sin\theta_{24}^L + \cos\theta_{12}^L \cos\theta_{24}^L \sin\theta_{14}^L \right)^2|^2 \right. \\
&+ \left. |\left(\sin\theta_{12}^R \sin\theta_{24}^R + \cos\theta_{12}^R \cos\theta_{24}^R \sin\theta_{14}^R \right)^2|^2 \right) F(x_1) \\
&+ \frac{m_1}{m_1} \left(\sin\theta_{12}^L \sin\theta_{24}^L + \cos\theta_{12}^L \cos\theta_{24}^L \sin\theta_{14}^L \right)^2 \left(\sin\theta_{12}^R \sin\theta_{24}^R + \cos\theta_{12}^R \cos\theta_{24}^R \sin\theta_{14}^R \right)^2 G(x_1) \\
&+ \left(|\left(\sin\theta_{12}^L \sin\theta_{24}^L + \cos\theta_{12}^L \cos\theta_{24}^L \sin\theta_{14}^L \right)\left(\cos\theta_{12}^L \sin\theta_{24}^L - \cos\theta_{24}^L \sin\theta_{12}^L \sin\theta_{14}^L \right)|^2 \right. \\
&+ \left. |\left(\sin\theta_{12}^R \sin\theta_{24}^R + \cos\theta_{12}^R \cos\theta_{24}^R \sin\theta_{14}^R \right)\left(\cos\theta_{12}^R \sin\theta_{24}^R - \cos\theta_{24}^R \sin\theta_{12}^R \sin\theta_{14}^R \right)|^2 \right) F(x_2) \\
&+ \frac{m_2}{m_1} \left(\sin\theta_{12}^L \sin\theta_{24}^L + \cos\theta_{12}^L \cos\theta_{24}^L \sin\theta_{14}^L \right)\left(\cos\theta_{12}^L \sin\theta_{24}^L - \cos\theta_{24}^L \sin\theta_{12}^L \sin\theta_{14}^L \right) \\
&\times \left(\sin\theta_{12}^R \sin\theta_{24}^R + \cos\theta_{12}^R \cos\theta_{24}^R \sin\theta_{14}^R \right)\left(\cos\theta_{12}^R \sin\theta_{24}^R - \cos\theta_{24}^R \sin\theta_{12}^R \sin\theta_{14}^R \right) G(x_2) \\
&+ \left(|\cos\theta_{14}^L \cos\theta_{24}^L \left(\sin\theta_{12}^L \sin\theta_{24}^L + \cos\theta_{12}^L \cos\theta_{24}^L \sin\theta_{14}^L \right)|^2 \right. \\
&+ \left. |\cos\theta_{14}^R \cos\theta_{24}^R \left(\sin\theta_{12}^R \sin\theta_{24}^R + \cos\theta_{12}^R \cos\theta_{24}^R \sin\theta_{14}^R \right)|^2 \right) F(x_4) \\
&+ \frac{M_4^C}{m_1} \cos\theta_{14}^L \cos\theta_{24}^L \left(\sin\theta_{12}^L \sin\theta_{24}^L + \cos\theta_{12}^L \cos\theta_{24}^L \sin\theta_{14}^L \right) \\
&\times \cos\theta_{14}^R \cos\theta_{24}^R \left(\sin\theta_{12}^R \sin\theta_{24}^R + \cos\theta_{12}^R \cos\theta_{24}^R \sin\theta_{14}^R \right) G(x_4) \Bigg]
\end{aligned}$$

(C.10)

C.4 Neutrino trident

The constraint from neutrino trident has a very simple form in terms of mixing angles and masses, when compared to the other observables, as it only depends on the coupling between the heavy Z' and muons.

$$
\begin{aligned}
\frac{(g_L)_{\mu\mu}^2 + (g_L)_{\mu\mu}\,(g_R)_{\mu\mu}}{M_{Z'}^2} = {} & \frac{\left(\cos\theta_{12}^L \sin\theta_{24}^L - \cos\theta_{24}^L \sin\theta_{12}^L \sin\theta_{14}^L \right)^4}{M_{Z'}^2} \\
& + \frac{\left(\cos\theta_{12}^L \sin\theta_{24}^L - \cos\theta_{24}^L \sin\theta_{12}^L \sin\theta_{14}^L \right)^2 \left(\cos\theta_{12}^R \sin\theta_{24}^R - \cos\theta_{24}^R \sin\theta_{12}^R \sin\theta_{14}^R \right)^2}{M_{Z'}^2}
\end{aligned}
$$

$$(C.11)$$

Bibliography

[1] Stephen F. King, Susana Molina Sedgwick, and Samuel J. Rowley. *JHEP* 10 (2018), p. 184. DOI: `10.1007/JHEP10(2018)184`. arXiv: `1808.01005 [hep-ph]`.

[2] Jordan Bernigaud, Björn Herrmann, Stephen F. King, and Samuel J. Rowley. *JHEP* 03 (2019), p. 067. DOI: `10.1007/JHEP03(2019)067`. arXiv: `1812.07463 [hep-ph]`.

[3] A. E. Cárcamo Hernández, S. F. King, H. Lee, and S. J. Rowley (2019). arXiv: `1910.10734 [hep-ph]`.

[4] Georges Aad et al., ATLAS. *Phys. Lett. B* 716 (2012), pp. 1–29. DOI: `10.1016/j.physletb.2012.08.020`. arXiv: `1207.7214 [hep-ex]`.

[5] Serguei Chatrchyan et al., CMS. *Phys. Lett. B* 716 (2012), pp. 30–61. DOI: `10.1016/j.physletb.2012.08.021`. arXiv: `1207.7235 [hep-ex]`.

[6] Sheldon L. Glashow. *Nucl. Phys.* 10 (1959), pp. 107–117. DOI: `10.1016/0029-5582(59)90196-8`.

[7] Steven Weinberg. *Phys. Rev. Lett.* 19 (1967), pp. 1264–1266. DOI: `10.1103/PhysRevLett.19.1264`.

[8] Abdus Salam. *Conf. Proc. C* 680519 (1968), pp. 367–377. DOI: `10.1142/9789812795915\_0034`.

[9] Murray Gell-Mann (Mar. 1961). DOI: `10.2172/4008239`.

[10] Yuval Ne'eman. *Nucl. Phys.* 26 (1961). Ed. by R. Ruffini and Y. Verbin, pp. 222–229. DOI: `10.1016/0029-5582(61)90134-1`.

[11] Murray Gell-Mann. *Phys. Rev.* 125 (1962), pp. 1067–1084. DOI: `10.1103/PhysRev.125.1067`.

[12] Murray Gell-Mann and Yuval Ne'eman (Sept. 1964).

[13] Peter W. Higgs. *Phys. Lett.* 12 (1964), pp. 132–133. DOI: `10.1016/0031-9163(64)91136-9`.

[14] F. Englert and R. Brout. *Phys. Rev. Lett.* 13 (1964). Ed. by J.C. Taylor, pp. 321–323. DOI: `10.1103/PhysRevLett.13.321`.

[15] Peter W. Higgs. *Phys. Rev. Lett.* 13 (1964). Ed. by J.C. Taylor, pp. 508–509. DOI: `10.1103/PhysRevLett.13.508`.

[16] Howard Georgi. *Lie Algebras In Particle Physics: from Isospin To Unified Theories*. Frontiers in Physics. Westview Press, 1999. ISBN: 0738202339.

[17] Heather E. Logan (June 2014). arXiv: `1406.1786 [hep-ph]`.

[18] Jeffrey Goldstone, Abdus Salam, and Steven Weinberg. *Phys. Rev.* 127 (1962), pp. 965–970. DOI: `10.1103/PhysRev.127.965`.

[19] Nicola Cabibbo. *Phys. Rev. Lett.* 10 (1963), pp. 531–533. DOI: `10.1103/PhysRevLett.10.531`.

[20] Makoto Kobayashi and Toshihide Maskawa. *Prog. Theor. Phys.* 49 (1973), pp. 652–657. DOI: `10.1143/PTP.49.652`.

[21] Julian S. Schwinger. *Phys. Rev.* 82 (1951). Ed. by K.A. Milton, pp. 914–927. DOI: `10.1103/PhysRev.82.914`.

[22] Gerhart Luders. *Annals Phys.* 2 (1957), pp. 1–15. DOI: `10.1016/0003-4916(57)90032-5`.

[23] A.D. Sakharov. *Sov.Phys.Usp.* 34.5 (1991), pp. 392–393. DOI: `10.1070/PU1991v034n05ABEH002497`.

[24] Joshua Davies, Florian Herren, Colin Poole, Matthias Steinhauser, and Anders Eller Thomsen. *Phys. Rev. Lett.* 124.7 (2020), p. 071803. DOI: `10.1103/PhysRevLett.124.071803`. arXiv: `1912.07624 [hep-ph]`.

[25] Vera C. Rubin and W. Kent Ford Jr. *The Astrophysical Journal* 159 (1970), p. 379. DOI: `10.1086/150317`.

[26] Vera C. Rubin, W. Kent Ford, and Norbert Thonnard. *The Astrophysical Journal* 238 (1980), pp. 471–487. DOI: `10.1086/158003`.

[27] T. S. van Albada, J. N. Bahcall, K. Begeman, and R. Sancisi. *The Astrophysical Journal* 295 (1985), pp. 305–313. DOI: `10.1086/163375`.

[28] Maxim Markevitch. *ESA Spec. Publ.* 604 (2006), p. 723. arXiv: `astro-ph/0511345`.

[29] Douglas Clowe, Marusa Bradac, Anthony H. Gonzalez, Maxim Markevitch, Scott W. Randall, Christine Jones, and Dennis Zaritsky. *Astrophys. J. Lett.* 648 (2006), pp. L109–L113. DOI: `10.1086/508162`. arXiv: `astro-ph/0608407`.

[30] N. Aghanim et al. (July 2018). DOI: `10.1051/0004-6361/201833910`. arXiv: `1807.06209 [astro-ph.CO]`.

[31] Zhi-zhong Xing. *Int. J. Mod. Phys. A* 29 (2014), p. 1430067. DOI: `10.1142/S0217751X14300671`. arXiv: `1411.2713 [hep-ph]`.

[32] S.F. King. *Prog. Part. Nucl. Phys.* 94 (2017), pp. 217–256. DOI: `10.1016/j.ppnp.2017.01.003`. arXiv: `1701.04413 [hep-ph]`.

[33] Fredrik Björkeroth, Francisco J. de Anda, Stephen F. King, and Elena Perdomo. *JHEP* 10 (2017), p. 148. DOI: `10.1007/JHEP10(2017)148`. arXiv: `1705.01555 [hep-ph]`.

[34] Fredrik Björkeroth, Francisco J. de Anda, Ivo de Medeiros Varzielas, and Stephen F. King. *JHEP* 06 (2015), p. 141. DOI: `10.1007/JHEP06(2015)141`. arXiv: `1503.03306 [hep-ph]`.

[35] Alexander Baur, Hans Peter Nilles, Andreas Trautner, and Patrick K.S. Vaudrevange. *Phys. Lett. B* 795 (2019), pp. 7–14. DOI: `10.1016/j.physletb.2019.03.066`. arXiv: `1901.03251 [hep-th]`.

[36] Stephen P. Martin. "A Supersymmetry primer". *Perspectives on supersymmetry. Vol.2*. Vol. 21. 2010, pp. 1–153. DOI: `10.1142/9789812839657\_0001`. arXiv: `hep-ph/9709356`.

[37] M. Shifman. *Int. J. Mod. Phys. A* 25 (2010). Ed. by Marco Peloso and Arkady Vainshtein, pp. 199–225. DOI: `10.1142/S0217751X10048548`. arXiv: `0907.3074 [hep-ph]`.

[38] Merab Gogberashvili. *Mod. Phys. Lett. A* 14 (1999), pp. 2025–2032. DOI: `10.1142/S021773239900208X`. arXiv: `hep-ph/9904383`.

[39] Ivan Esteban, M.C. Gonzalez-Garcia, Alvaro Hernandez-Cabezudo, Michele Maltoni, and Thomas Schwetz. *JHEP* 01 (2019), p. 106. DOI: `10.1007/JHEP01(2019)106`. arXiv: `1811.05487 [hep-ph]`.

[40] P.A.R. Ade et al. *Astron.Astrophys.* 594 (2016), A13. DOI: `10.1051/0004-6361/201525830`. arXiv: `1502.01589 [astro-ph.CO]`.

[41] Julian S. Schwinger. *Phys. Rev.* 73 (1948), pp. 416–417. DOI: `10.1103/PhysRev.73.416`.

[42] Michel Davier, Andreas Hoecker, Bogdan Malaescu, and Zhiqing Zhang. *Eur. Phys. J. C* 77.12 (2017), p. 827. DOI: `10.1140/epjc/s10052-017-5161-6`. arXiv: `1706.09436 [hep-ph]`.

[43] Alexander Keshavarzi, Daisuke Nomura, and Thomas Teubner. *Phys. Rev. D* 97.11 (2018), p. 114025. DOI: `10.1103/PhysRevD.97.114025`. arXiv: `1802.02995 [hep-ph]`.

[44] Gilberto Colangelo, Martin Hoferichter, and Peter Stoffer. *JHEP* 02 (2019), p. 006. DOI: `10.1007/JHEP02(2019)006`. arXiv: `1810.00007 [hep-ph]`.

[45] Martin Hoferichter, Bai-Long Hoid, and Bastian Kubis. *JHEP* 08 (2019), p. 137. DOI: `10.1007/JHEP08(2019)137`. arXiv: `1907.01556 [hep-ph]`.

[46] M. Davier, A. Hoecker, B. Malaescu, and Z. Zhang. *Eur. Phys. J. C* 80.3 (2020), p. 241. DOI: `10.1140/epjc/s10052-020-7792-2`. arXiv: `1908.00921 [hep-ph]`.

[47] Alexander Keshavarzi, Daisuke Nomura, and Thomas Teubner. *Phys. Rev. D* 101.1 (2020), p. 014029. DOI: `10.1103/PhysRevD.101.014029`. arXiv: `1911.00367 [hep-ph]`.

[48] Alexander Kurz, Tao Liu, Peter Marquard, and Matthias Steinhauser. *Phys. Lett. B* 734 (2014), pp. 144–147. DOI: `10.1016/j.physletb.2014.05.043`. arXiv: `1403.6400 [hep-ph]`.

[49] Kirill Melnikov and Arkady Vainshtein. *Phys. Rev. D* 70 (2004), p. 113006. DOI: `10.1103/PhysRevD.70.113006`. arXiv: `hep-ph/0312226`.

[50] Pere Masjuan and Pablo Sanchez-Puertas. *Phys. Rev. D* 95.5 (2017), p. 054026. DOI: `10.1103/PhysRevD.95.054026`. arXiv: `1701.05829 [hep-ph]`.

[51] Gilberto Colangelo, Martin Hoferichter, Massimiliano Procura, and Peter Stoffer. *JHEP* 04 (2017), p. 161. DOI: `10.1007/JHEP04(2017)161`. arXiv: `1702.07347 [hep-ph]`.

[52] Martin Hoferichter, Bai-Long Hoid, Bastian Kubis, Stefan Leupold, and Sebastian P. Schneider. *JHEP* 10 (2018), p. 141. DOI: `10.1007/JHEP10(2018)141`. arXiv: `1808.04823 [hep-ph]`.

[53] Antoine Gérardin, Harvey B. Meyer, and Andreas Nyffeler. *Phys. Rev. D* 100.3 (2019), p. 034520. DOI: `10.1103/PhysRevD.100.034520`. arXiv: `1903.09471 [hep-lat]`.

[54] Johan Bijnens, Nils Hermansson-Truedsson, and Antonio Rodríguez-Sánchez. *Phys. Lett. B* 798 (2019), p. 134994. DOI: `10.1016/j.physletb.2019.134994`. arXiv: `1908.03331 [hep-ph]`.

[55] Gilberto Colangelo, Martin Hoferichter, Andreas Nyffeler, Massimo Passera, and Peter Stoffer. *Phys. Lett. B* 735 (2014), pp. 90–91. DOI: `10.1016/j.physletb.2014.06.012`. arXiv: `1403.7512 [hep-ph]`.

[56] Gilberto Colangelo, Franziska Hagelstein, Martin Hoferichter, Laetitia Laub, and Peter Stoffer. *JHEP* 03 (2020), p. 101. DOI: `10.1007/JHEP03(2020)101`. arXiv: `1910.13432 [hep-ph]`.

[57] Thomas Blum, Norman Christ, Masashi Hayakawa, Taku Izubuchi, Luchang Jin, Chulwoo Jung, and Christoph Lehner. *Phys. Rev. Lett.* 124.13 (2020), p. 132002. DOI: `10.1103/PhysRevLett.124.132002`. arXiv: `1911.08123 [hep-lat]`.

[58] Andrzej Czarnecki, William J. Marciano, and Arkady Vainshtein. *Phys. Rev. D* 67 (2003). [Erratum: Phys.Rev.D 73, 119901 (2006)], p. 073006. DOI: `10.1103/PhysRevD.67.073006`. arXiv: `hep-ph/0212229`.

[59] C. Gnendiger, D. Stöckinger, and H. Stöckinger-Kim. *Phys. Rev. D* 88 (2013), p. 053005. DOI: `10.1103/PhysRevD.88.053005`. arXiv: `1306.5546 [hep-ph]`.

[60] T. Aoyama et al. (June 2020). arXiv: `2006.04822 [hep-ph]`.

[61] G.W. Bennett et al. *Phys. Rev. D* 73 (2006), p. 072003. DOI: `10.1103/PhysRevD.73.072003`. arXiv: `hep-ex/0602035`.

[62]   Kaoru Hagiwara, Ruofan Liao, Alan D. Martin, Daisuke Nomura, and Thomas Teubner. *J. Phys. G* 38 (2011), p. 085003. DOI: `10.1088/0954-3899/38/8/085003`. arXiv: `1105.3149 [hep-ph]`.

[63]   Michel Davier, Andreas Hoecker, Bogdan Malaescu, and Zhiqing Zhang. *Eur. Phys. J. C* 71 (2011). [Erratum: Eur.Phys.J.C 72, 1874 (2012)], p. 1515. DOI: `10.1140/epjc/s10052-012-1874-8`. arXiv: `1010.4180 [hep-ph]`.

[64]   Takaaki Nomura and Hiroshi Okada. *Phys. Dark Univ.* 26 (2019), p. 100359. DOI: `10.1016/j.dark.2019.100359`. arXiv: `1808.05476 [hep-ph]`.

[65]   Takaaki Nomura and Hiroshi Okada. *Phys. Rev. D* 97.9 (2018), p. 095023. DOI: `10.1103/PhysRevD.97.095023`. arXiv: `1803.04795 [hep-ph]`.

[66]   Richard H. Parker, Chenghui Yu, Weicheng Zhong, Brian Estey, and Holger Müller. *Science* 360 (2018), p. 191. DOI: `10.1126/science.aap7706`. arXiv: `1812.04130 [physics.atom-ph]`.

[67]   S. Laporta and E. Remiddi. *Phys. Lett. B* 379 (1996), pp. 283–291. DOI: `10.1016/0370-2693(96)00439-X`. arXiv: `hep-ph/9602417`.

[68]   Tatsumi Aoyama, Masashi Hayakawa, Toichiro Kinoshita, and Makiko Nio. *Phys. Rev. Lett.* 109 (2012), p. 111807. DOI: `10.1103/PhysRevLett.109.111807`. arXiv: `1205.5368 [hep-ph]`.

[69]   Tatsumi Aoyama, M. Hayakawa, Toichiro Kinoshita, and Makiko Nio. *Phys. Rev. D* 91.3 (2015). [Erratum: Phys.Rev.D 96, 019901 (2017)], p. 033006. DOI: `10.1103/PhysRevD.91.033006`. arXiv: `1412.8284 [hep-ph]`.

[70]   C.P. Burgess. *Ann. Rev. Nucl. Part. Sci.* 57 (2007), pp. 329–362. DOI: `10.1146/annurev.nucl.56.080805.140508`. arXiv: `hep-th/0701053`.

[71]   Stephan Hartmann. *Stud. Hist. Phil. Sci. B* 32 (2001), pp. 267–304. DOI: `10.1016/S1355-2198(01)00005-3`.

[72]   Peter Minkowski. *Phys. Lett. B* 67 (1977), pp. 421–428. DOI: `10.1016/0370-2693(77)90435-X`.

[73]   Tsutomu Yanagida. "Horizontal gauge symmetry and masses of neutrinos". *Proceedings: Workshop on the Unified Theories and the Baryon Number in the Universe: Tsukuba, Japan, February 13-14, 1979*. Vol. 7902131. 1979, pp. 95–99.

[74]   Murray Gell-Mann, Pierre Ramond, and Richard Slansky. "Complex Spinors and Unified Theories". *Supergravity Workshop*. Vol. 790927. 1979, pp. 315–321. arXiv: `1306.4669 [hep-th]`.

[75]   Rabindra N. Mohapatra and Goran Senjanovic. *Phys.Rev.Lett.* 44 (1980), p. 912. DOI: `10.1103/PhysRevLett.44.912`.

[76]   J. Schechter and J.W.F. Valle. *Phys.Rev.D* 22 (1980), p. 2227. DOI: `10.1103/PhysRevD.22.2227`.

[77] M. Magg and C. Wetterich. *Phys. Lett. B* 94 (1980), pp. 61–64. DOI: 10.1016/0370-2693(80)90825-4.

[78] George Lazarides, Q. Shafi, and C. Wetterich. *Nucl. Phys. B* 181 (1981), pp. 287–300. DOI: 10.1016/0550-3213(81)90354-0.

[79] Robert Foot, H. Lew, X.G. He, and Girish C. Joshi. *Z. Phys. C* 44 (1989), p. 441. DOI: 10.1007/BF01415558.

[80] Rabindra N. Mohapatra and Goran Senjanovic. *Phys. Rev. D* 23 (1981), p. 165. DOI: 10.1103/PhysRevD.23.165.

[81] R.N. Mohapatra and J.W.F. Valle. *Phys. Rev. D* 34 (1986), p. 1642. DOI: 10.1103/PhysRevD.34.1642.

[82] R.N. Mohapatra. *Phys. Rev. Lett.* 56 (1986), pp. 561–563. DOI: 10.1103/PhysRevLett.56.561.

[83] M.B. Gavela, T. Hambye, D. Hernandez, and P. Hernandez. *JHEP* 09 (2009), p. 038. DOI: 10.1088/1126-6708/2009/09/038. arXiv: 0906.1461 [hep-ph].

[84] Ettore Majorana. *Nuovo Cim.* 14 (1937), pp. 171–184. DOI: 10.1007/BF02961314.

[85] Ziro Maki, Masami Nakagawa, and Shoichi Sakata. *Prog. Theor. Phys.* 28 (1962), pp. 870–880. DOI: 10.1143/PTP.28.870.

[86] B. Pontecorvo. *Sov. Phys. JETP* 7 (1958), pp. 172–173.

[87] Alexander Lenz. *Adv. High Energy Phys.* 2013 (2013), p. 910275. DOI: 10.1155/2013/910275.

[88] A.M. Baldini et al. *Eur. Phys. J. C* 76.8 (2016), p. 434. DOI: 10.1140/epjc/s10052-016-4271-x. arXiv: 1605.05081 [hep-ex].

[89] Zijie Poh and Stuart Raby. *Phys. Rev. D* 96.1 (2017), p. 015032. DOI: 10.1103/PhysRevD.96.015032. arXiv: 1705.07007 [hep-ph].

[90] Stuart Raby and Andreas Trautner. *Phys. Rev. D* 97.9 (2018), p. 095006. DOI: 10.1103/PhysRevD.97.095006. arXiv: 1712.09360 [hep-ph].

[91] Adam Falkowski, Stephen F. King, Elena Perdomo, and Mathias Pierre. *JHEP* 08 (2018), p. 061. DOI: 10.1007/JHEP08(2018)061. arXiv: 1803.04430 [hep-ph].

[92] Junichiro Kawamura, Stuart Raby, and Andreas Trautner. *Phys. Rev. D* 101.3 (2020), p. 035026. DOI: 10.1103/PhysRevD.101.035026. arXiv: 1911.11075 [hep-ph].

[93] Pierre Ramond. *Phys. Rev. D* 3 (1971), pp. 2415–2418. DOI: 10.1103/PhysRevD.3.2415.

[94] J. Wess and B. Zumino. *Nucl. Phys. B* 70 (1974). Ed. by A. Salam and E. Sezgin, pp. 39–50. DOI: 10.1016/0550-3213(74)90355-1.

[95]   Sidney R. Coleman and J. Mandula. *Phys. Rev.* 159 (1967). Ed. by A. Zichichi, pp. 1251–1256. DOI: 10.1103/PhysRev.159.1251.

[96]   Rudolf Haag, Jan T. Lopuszanski, and Martin Sohnius. *Nucl. Phys. B* 88 (1975), p. 257. DOI: 10.1016/0550-3213(75)90279-5.

[97]   Savas Dimopoulos and Stuart Raby. *Nucl. Phys. B* 192 (1981), pp. 353–368. DOI: 10.1016/0550-3213(81)90430-2.

[98]   Savas Dimopoulos and Howard Georgi. *Nucl. Phys. B* 193 (1981), pp. 150–162. DOI: 10.1016/0550-3213(81)90522-8.

[99]   N. Sakai. *Z. Phys. C* 11 (1981), p. 153. DOI: 10.1007/BF01573998.

[100]   Romesh K. Kaul and Parthasarathi Majumdar. *Nucl. Phys. B* 199 (1982), p. 36. DOI: 10.1016/0550-3213(82)90565-X.

[101]   A. Arbey, M. Battaglia, A. Djouadi, F. Mahmoudi, and J. Quevillon. *Phys. Lett. B* 708 (2012), pp. 162–169. DOI: 10.1016/j.physletb.2012.01.053. arXiv: 1112.3028 [hep-ph].

[102]   Ali H. Chamseddine, Richard L. Arnowitt, and Pran Nath. *Phys. Rev. Lett.* 49 (1982), p. 970. DOI: 10.1103/PhysRevLett.49.970.

[103]   Lawrence J. Hall, V.Alan Kostelecky, and S. Raby. *Nucl. Phys. B* 267 (1986), pp. 415–432. DOI: 10.1016/0550-3213(86)90397-4.

[104]   Gian F. Giudice, Markus A. Luty, Hitoshi Murayama, and Riccardo Rattazzi. *JHEP* 12 (1998), p. 027. DOI: 10.1088/1126-6708/1998/12/027. arXiv: hep-ph/9810442.

[105]   Lisa Randall and Raman Sundrum. *Nucl. Phys. B* 557 (1999), pp. 79–118. DOI: 10.1016/S0550-3213(99)00359-4. arXiv: hep-th/9810155.

[106]   H. Goldberg. *Phys. Rev. Lett.* 50 (1983). Ed. by M.A. Srednicki. [Erratum: Phys.Rev.Lett. 103, 099905 (2009)], p. 1419. DOI: 10.1103/PhysRevLett.50.1419.

[107]   John R. Ellis, J.S. Hagelin, Dimitri V. Nanopoulos, Keith A. Olive, and M. Srednicki. *Nucl. Phys. B* 238 (1984). Ed. by M.A. Srednicki, pp. 453–476. DOI: 10.1016/0550-3213(84)90461-9.

[108]   H. Georgi and S.L. Glashow. *Phys. Rev. Lett.* 32 (1974), pp. 438–441. DOI: 10.1103/PhysRevLett.32.438.

[109]   Jogesh C. Pati and Abdus Salam. *Phys. Rev. D* 10 (1974). [Erratum: Phys.Rev.D 11, 703–703 (1975)], pp. 275–289. DOI: 10.1103/PhysRevD.10.275.

[110]   Howard Georgi. *AIP Conf. Proc.* 23 (1975). Ed. by Hugh C. Carl E. Wolfe Carlson, pp. 575–582. DOI: 10.1063/1.2947450.

[111]   Harald Fritzsch and Peter Minkowski. *Annals Phys.* 93 (1975), pp. 193–266. DOI: 10.1016/0003-4916(75)90211-0.

[112] P.A. Zyla et al. *PTEP* 2020.8 (2020), p. 083C01. DOI: `10.1093/ptep/ptaa104`.

[113] Edited by T. Ohlsson. *Nucl. Phys.* B908 (2016 Special Edition), pp. 1–466. URL: `http://www.sciencedirect.com/science/journal/05503213/908/supp/C`.

[114] Zhi-zhong Xing and Shun Zhou. *Neutrinos in particle physics, astronomy and cosmology.* 2011. ISBN: 9783642175596, 9787308080248.

[115] Stephen F. King. *J. Phys.* G42 (2015), p. 123001. DOI: `10.1088/0954-3899/42/12/123001`. arXiv: `1510.02091 [hep-ph]`.

[116] K. Abe et al. *Phys. Rev. Lett.* 118.15 (2017), p. 151801. DOI: `10.1103/PhysRevLett.118.151801`. arXiv: `1701.00432 [hep-ex]`.

[117] P. Adamson et al. *Phys. Rev. Lett.* 118.15 (2017), p. 151802. DOI: `10.1103/PhysRevLett.118.151802`. arXiv: `1701.05891 [hep-ex]`.

[118] *"Latest Oscillation Results from NOvA"*. Fermilab Joint Experimental-Theoretical Physics (JETP) seminar. 2018.

[119] P. F. de Salas, D. V. Forero, C. A. Ternes, M. Tortola, and J. W. F. Valle. *Phys. Lett.* B782 (2018), pp. 633–640. DOI: `10.1016/j.physletb.2018.06.019`. arXiv: `1708.01186 [hep-ph]`.

[120] Ivan Esteban, M. C. Gonzalez-Garcia, Michele Maltoni, Ivan Martinez-Soler, and Thomas Schwetz. *JHEP* 01 (2017), p. 087. DOI: `10.1007/JHEP01(2017)087`. arXiv: `1611.01514 [hep-ph]`.

[121] S.L. Glashow. "The Future of Elementary Particle Physics". *QUARKS AND LEPTONS. PROCEEDINGS, SUMMER INSTITUTE, CARGESE, FRANCE, JULY 9-29, 1979.* Vol. 61. 1980, p. 687. DOI: `10.1007/978-1-4684-7197-7\_15`.

[122] S.F. King. *Phys.Lett.B* 439 (1998), pp. 350–356. DOI: `10.1016/S0370-2693(98)01055-7`. arXiv: `hep-ph/9806440`.

[123] S.F. King. *Nucl.Phys.B* 576 (2000), pp. 85–105. DOI: `10.1016/S0550-3213(00)00109-7`. arXiv: `hep-ph/9912492`.

[124] S.F. King. *JHEP* 09 (2002), p. 011. DOI: `10.1088/1126-6708/2002/09/011`. arXiv: `hep-ph/0204360`.

[125] P.H. Frampton, S.L. Glashow, and T. Yanagida. *Phys.Lett.B* 548 (2002), pp. 119–121. DOI: `10.1016/S0370-2693(02)02853-8`. arXiv: `hep-ph/0208157`.

[126] M. Fukugita and T. Yanagida. *Phys.Lett.B* 174 (1986), pp. 45–47. DOI: `10.1016/0370-2693(86)91126-3`.

[127] Wan-lei Guo and Zhi-zhong Xing. *Phys.Lett.B* 583 (2004), pp. 163–172. DOI: `10.1016/j.physletb.2003.12.043`. arXiv: `hep-ph/0310326`.

[128] A. Ibarra and Graham G. Ross. *Phys.Lett.B* 591 (2004), pp. 285–296. DOI: `10.1016/j.physletb.2004.04.037`. arXiv: `hep-ph/0312138`.

[129] Jian-wei Mei and Zhi-zhong Xing. *Phys.Rev.D* 69 (2004), p. 073003. DOI: 10. 1103/PhysRevD.69.073003. arXiv: hep-ph/0312167.

[130] Wan-lei Guo, Zhi-zhong Xing, and Shun Zhou. *Int.J.Mod.Phys.E* 16 (2007), pp. 1–50. DOI: 10.1142/S0218301307004898. arXiv: hep-ph/0612033.

[131] S. Antusch, P. Di Bari, D.A. Jones, and S.F. King. *Phys.Rev.D* 86 (2012), p. 023516. DOI: 10.1103/PhysRevD.86.023516. arXiv: 1107.6002 [hep-ph].

[132] Keisuke Harigaya, Masahiro Ibe, and Tsutomu T. Yanagida. *Phys.Rev.D* 86 (2012), p. 013002. DOI: 10.1103/PhysRevD.86.013002. arXiv: 1205.2198 [hep-ph].

[133] Jue Zhang and Shun Zhou. *JHEP* 09 (2015), p. 065. DOI: 10.1007/JHEP09(2015) 065. arXiv: 1505.04858 [hep-ph].

[134] Gustavo C. Branco, M.N. Rebelo, and J.I. Silva-Marcos. *Phys.Lett.B* 633 (2006), pp. 345–354. DOI: 10.1016/j.physletb.2005.11.067. arXiv: hep-ph/0510412.

[135] S.F. King. *JHEP* 08 (2005), p. 105. DOI: 10.1088/1126-6708/2005/08/105. arXiv: hep-ph/0506297.

[136] Stefan Antusch, Stephen F. King, Christoph Luhn, and Martin Spinrath. *Nucl.Phys.B* 856 (2012), pp. 328–341. DOI: 10.1016/j.nuclphysb.2011.11.009. arXiv: 1108.4278 [hep-ph].

[137] Stephen F. King. *JHEP* 07 (2013), p. 137. DOI: 10.1007/JHEP07(2013)137. arXiv: 1304.6264 [hep-ph].

[138] S.F. King. *Phys.Lett.B* 724 (2013), pp. 92–98. DOI: 10.1016/j.physletb.2013. 06.013. arXiv: 1305.4846 [hep-ph].

[139] Stephen F. King. *JHEP* 01 (2014), p. 119. DOI: 10.1007/JHEP01(2014)119. arXiv: 1311.3295 [hep-ph].

[140] Stephen F. King. *JHEP* 08 (2014), p. 130. DOI: 10.1007/JHEP08(2014)130. arXiv: 1406.7005 [hep-ph].

[141] Fredrik Björkeroth and Stephen F. King. *J.Phys.G* 42.12 (2015), p. 125002. DOI: 10.1088/0954-3899/42/12/125002. arXiv: 1412.6996 [hep-ph].

[142] Fredrik Björkeroth, Francisco J. de Anda, Ivo de Medeiros Varzielas, and Stephen F. King. *JHEP* 10 (2015), p. 104. DOI: 10.1007/JHEP10(2015)104. arXiv: 1505.05504 [hep-ph].

[143] Stephen F. King. *JHEP* 02 (2016), p. 085. DOI: 10.1007/JHEP02(2016)085. arXiv: 1512.07531 [hep-ph].

[144] Stephen F. King and Christoph Luhn. *JHEP* 09 (2016), p. 023. DOI: 10.1007/ JHEP09(2016)023. arXiv: 1607.05276 [hep-ph].

[145] Peter Ballett, Stephen F. King, Silvia Pascoli, Nick W. Prouse, and TseChun Wang. *JHEP* 03 (2017), p. 110. DOI: 10.1007/JHEP03(2017)110. arXiv: 1612.01999 [hep-ph].

[146] Gui-Jun Ding, Stephen F. King, and Cai-Chang Li. *JHEP* 12 (2018), p. 003. DOI: 10.1007/JHEP12(2018)003. arXiv: 1807.07538 [hep-ph].

[147] Marco Chianese and Stephen F. King. *JCAP* 09 (2018), p. 027. DOI: 10.1088/1475-7516/2018/09/027. arXiv: 1806.10606 [hep-ph].

[148] Stephen F. King and Celso C. Nishi. *Phys.Lett.B* 785 (2018), pp. 391–398. DOI: 10.1016/j.physletb.2018.08.056. arXiv: 1807.00023 [hep-ph].

[149] Stephen F. King, Jue Zhang, and Shun Zhou. *JHEP* 12 (2016), p. 023. DOI: 10.1007/JHEP12(2016)023. arXiv: 1609.09402 [hep-ph].

[150] Tanja Geib and Stephen F. King. *Phys.Rev.D* 97.7 (2018), p. 075010. DOI: 10.1103/PhysRevD.97.075010. arXiv: 1709.07425 [hep-ph].

[151] Stefan Antusch, Jörn Kersten, Manfred Lindner, Michael Ratz, and Michael Andreas Schmidt. *JHEP* 03 (2005), p. 024. DOI: 10.1088/1126-6708/2005/03/024. arXiv: hep-ph/0501272.

[152] Steven Weinberg. *Phys.Rev.Lett.* 42 (1979), pp. 850–853. DOI: 10.1103/PhysRevLett.42.850.

[153] D. Toussaint, S.B. Treiman, Frank Wilczek, and A. Zee. *Phys.Rev.D* 19 (1979), pp. 1036–1045. DOI: 10.1103/PhysRevD.19.1036.

[154] W. Buchmuller, P. Di Bari, and M. Plumacher. *Annals Phys.* 315 (2005), pp. 305–351. DOI: 10.1016/j.aop.2004.02.003. arXiv: hep-ph/0401240.

[155] A. Abada, S. Davidson, A. Ibarra, F.-X. Josse-Michaux, M. Losada, and A. Riotto. *JHEP* 09 (2006), p. 010. DOI: 10.1088/1126-6708/2006/09/010. arXiv: hep-ph/0605281.

[156] S. Antusch, S.F. King, and A. Riotto. *JCAP* 11 (2006), p. 011. DOI: 10.1088/1475-7516/2006/11/011. arXiv: hep-ph/0609038.

[157] Laura Covi, Esteban Roulet, and Francesco Vissani. *Phys.Lett.B* 384 (1996), pp. 169–174. DOI: 10.1016/0370-2693(96)00817-9. arXiv: hep-ph/9605319.

[158] Steve Blanchet and Pasquale Di Bari. *JCAP* 03 (2007), p. 018. DOI: 10.1088/1475-7516/2007/03/018. arXiv: hep-ph/0607330.

[159] P. S. Bhupal Dev, Pasquale Di Bari, Bjorn Garbrecht, Stéphane Lavignac, Peter Millington, and Daniele Teresi. *Int.J.Mod.Phys.A* 33 (2018), p. 1842001. DOI: 10.1142/S0217751X18420010. arXiv: 1711.02861 [hep-ph].

[160] Steve Blanchet and Pasquale Di Bari. *JCAP* 06 (2006), p. 023. DOI: 10.1088/1475-7516/2006/06/023. arXiv: hep-ph/0603107.

[161]   S.F. King. *Phys.Rev.D* 67 (2003), p. 113010. DOI: 10.1103/PhysRevD.67.113010. arXiv: hep-ph/0211228.

[162]   Monika Blanke, Benjamin Fuks, Iftah Galon, and Gilad Perez. *JHEP* 04 (2016), p. 044. DOI: 10.1007/JHEP04(2016)044. arXiv: 1512.03813 [hep-ph].

[163]   G. Brooijmans et al. "Les Houches 2017: Physics at TeV Colliders New Physics Working Group Report". *Les Houches 2017: Physics at TeV Colliders Standard Model Working Group Report*. 2018. arXiv: 1803.10379 [hep-ph]. URL: http://lss.fnal.gov/archive/2017/conf/fermilab-conf-17-664-ppd.pdf.

[164]   Amit Chakraborty, Motoi Endo, Benjamin Fuks, Björn Herrmann, Mihoko M. Nojiri, Priscilla Pani, and Giacomo Polesello. *Eur. Phys. J.* C78.10 (2018), p. 844. DOI: 10.1140/epjc/s10052-018-6331-x. arXiv: 1808.07488 [hep-ph].

[165]   M. Arana-Catania, S. Heinemeyer, and M.J. Herrero. *Phys. Rev. D* 90.7 (2014), p. 075003. DOI: 10.1103/PhysRevD.90.075003. arXiv: 1405.6960 [hep-ph].

[166]   Kamila Kowalska. *JHEP* 09 (2014), p. 139. DOI: 10.1007/JHEP09(2014)139. arXiv: 1406.0710 [hep-ph].

[167]   Karen De Causmaecker, Benjamin Fuks, Bjoern Herrmann, Farvah Mahmoudi, Ben O'Leary, Werner Porod, Sezen Sekmen, and Nadja Strobbe. *JHEP* 11 (2015), p. 125. DOI: 10.1007/JHEP11(2015)125. arXiv: 1509.05414 [hep-ph].

[168]   D.J.H. Chung, L.L. Everett, G.L. Kane, S.F. King, Joseph D. Lykken, and Lian-Tao Wang. *Phys. Rept.* 407 (2005), pp. 1–203. DOI: 10.1016/j.physrep.2004.08.032. arXiv: hep-ph/0312378.

[169]   A. Bartl, K. Hidaka, K. Hohenwarter-Sodek, T. Kernreiter, W. Majerotto, and W. Porod. *Eur. Phys. J. C* 46 (2006), pp. 783–789. DOI: 10.1140/epjc/s2006-02528-4. arXiv: hep-ph/0510074.

[170]   Giuseppe Bozzi, Benjamin Fuks, Bjorn Herrmann, and Michael Klasen. *Nucl. Phys. B* 787 (2007), pp. 1–54. DOI: 10.1016/j.nuclphysb.2007.05.031. arXiv: 0704.1826 [hep-ph].

[171]   A. Bartl, K. Hidaka, K. Hohenwarter-Sodek, T. Kernreiter, W. Majerotto, and Werner Porod. *Phys. Lett. B* 660 (2008), pp. 228–235. DOI: 10.1016/j.physletb.2007.12.040. arXiv: 0709.1157 [hep-ph].

[172]   F. del Aguila et al. *Eur. Phys. J. C* 57 (2008), pp. 183–308. DOI: 10.1140/epjc/s10052-008-0713-4. arXiv: 0801.1800 [hep-ph].

[173]   Tobias Hurth and Werner Porod. *JHEP* 08 (2009), p. 087. DOI: 10.1088/1126-6708/2009/08/087. arXiv: 0904.4574 [hep-ph].

[174]   A. Bartl, K. Hidaka, K. Hohenwarter-Sodek, T. Kernreiter, W. Majerotto, and W. Porod. *Phys. Lett. B* 679 (2009), pp. 260–266. DOI: 10.1016/j.physletb.2009.07.050. arXiv: 0905.0132 [hep-ph].

[175] Matthias Bruhnke, Bjorn Herrmann, and Werner Porod. *JHEP* 09 (2010), p. 006. DOI: 10.1007/JHEP09(2010)006. arXiv: 1007.2100 [hep-ph].

[176] A. Bartl, H. Eberl, B. Herrmann, K. Hidaka, W. Majerotto, and W. Porod. *Phys. Lett. B* 698 (2011). [Erratum: Phys.Lett.B 700, 390–390 (2011)], pp. 380–388. DOI: 10.1016/j.physletb.2011.01.020. arXiv: 1007.5483 [hep-ph].

[177] A. Bartl, H. Eberl, E. Ginina, B. Herrmann, K. Hidaka, W. Majerotto, and W. Porod. *Phys. Rev. D* 84 (2011), p. 115026. DOI: 10.1103/PhysRevD.84.115026. arXiv: 1107.2775 [hep-ph].

[178] A. Bartl, H. Eberl, E. Ginina, B. Herrmann, K. Hidaka, W. Majerotto, and W. Porod. *Int. J. Mod. Phys. A* 29.07 (2014), p. 1450035. DOI: 10.1142/S0217751X14500353. arXiv: 1212.4688 [hep-ph].

[179] A. Bartl, H. Eberl, E. Ginina, K. Hidaka, and W. Majerotto. *Phys. Rev. D* 91.1 (2015), p. 015007. DOI: 10.1103/PhysRevD.91.015007. arXiv: 1411.2840 [hep-ph].

[180] H. Eberl, E. Ginina, A. Bartl, K. Hidaka, and W. Majerotto. *JHEP* 06 (2016), p. 143. DOI: 10.1007/JHEP06(2016)143. arXiv: 1604.02366 [hep-ph].

[181] Helmut Eberl, Elena Ginina, and Keisho Hidaka. *Eur. Phys. J. C* 77.3 (2017), p. 189. DOI: 10.1140/epjc/s10052-017-4754-4. arXiv: 1702.00348 [hep-ph].

[182] Jordan Bernigaud and Björn Herrmann. *SciPost Phys.* 6.6 (2019), p. 066. DOI: 10.21468/SciPostPhys.6.6.066. arXiv: 1809.04370 [hep-ph].

[183] Vernon Barger, Danny Marfatia, Azar Mustafayev, and Ali Soleimani. *Phys. Rev. D* 80 (2009), p. 076004. DOI: 10.1103/PhysRevD.80.076004. arXiv: 0908.0941 [hep-ph].

[184] Bjorn Herrmann, Michael Klasen, and Quentin Le Boulc'h. *Phys. Rev. D* 84 (2011), p. 095007. DOI: 10.1103/PhysRevD.84.095007. arXiv: 1106.6229 [hep-ph].

[185] Debtosh Choudhury, Raghuveer Garani, and Sudhir K. Vempati. *JHEP* 06 (2012), p. 014. DOI: 10.1007/JHEP06(2012)014. arXiv: 1104.4467 [hep-ph].

[186] Prateek Agrawal, Monika Blanke, and Katrin Gemmler. *JHEP* 10 (2014), p. 072. DOI: 10.1007/JHEP10(2014)072. arXiv: 1405.6709 [hep-ph].

[187] F. Gabbiani and A. Masiero. *Nucl. Phys. B* 322 (1989), pp. 235–254. DOI: 10.1016/0550-3213(89)90492-6.

[188] John S. Hagelin, S. Kelley, and Toshiaki Tanaka. *Nucl. Phys. B* 415 (1994), pp. 293–331. DOI: 10.1016/0550-3213(94)90113-9.

[189] F. Gabbiani, E. Gabrielli, A. Masiero, and L. Silvestrini. *Nucl. Phys. B* 477 (1996), pp. 321–352. DOI: 10.1016/0550-3213(96)00390-2. arXiv: hep-ph/9604387.

[190] Bhaskar Dutta and Yukihiro Mimura. *Phys. Lett. B* 790 (2019), pp. 563–567. DOI: 10.1016/j.physletb.2018.12.070. arXiv: 1811.10209 [hep-ph].

[191] S.F. King and M. Oliveira. *Phys. Rev. D* 60 (1999), p. 035003. DOI: 10.1103/PhysRevD.60.035003. arXiv: hep-ph/9804283.

[192] G. Barenboim, K. Huitu, and M. Raidal. *Phys. Rev. D* 63 (2001), p. 055006. DOI: 10.1103/PhysRevD.63.055006. arXiv: hep-ph/0005159.

[193] Seungwon Baek, Toru Goto, Yasuhiro Okada, and Ken-ichi Okumura. *Phys. Rev. D* 64 (2001), p. 095001. DOI: 10.1103/PhysRevD.64.095001. arXiv: hep-ph/0104146.

[194] T. Blazek and S.F. King. *Nucl. Phys. B* 662 (2003), pp. 359–378. DOI: 10.1016/S0550-3213(03)00297-9. arXiv: hep-ph/0211368.

[195] J.G. Hayes, S.F. King, and I.N.R. Peddie. *Nucl. Phys. B* 739 (2006), pp. 106–119. DOI: 10.1016/j.nuclphysb.2006.01.017. arXiv: hep-ph/0509218.

[196] L. Calibbi, A. Faccia, A. Masiero, and S.K. Vempati. *Phys. Rev. D* 74 (2006), p. 116002. DOI: 10.1103/PhysRevD.74.116002. arXiv: hep-ph/0605139.

[197] S.-G. Kim, N. Maekawa, A. Matsuzaki, K. Sakurai, and T. Yoshikawa. *Phys. Rev. D* 75 (2007), p. 115008. DOI: 10.1103/PhysRevD.75.115008. arXiv: hep-ph/0612370.

[198] Kingman Cheung, Sin Kyu Kang, C.S. Kim, and Jake Lee. *Phys. Lett. B* 652 (2007), pp. 319–324. DOI: 10.1016/j.physletb.2007.06.081. arXiv: hep-ph/0702050.

[199] M. Ciuchini, A. Masiero, L. Silvestrini, S.K. Vempati, and O. Vives. *Phys. Rev. Lett.* 92 (2004), p. 071801. DOI: 10.1103/PhysRevLett.92.071801. arXiv: hep-ph/0307191.

[200] M. Ciuchini, A. Masiero, P. Paradisi, L. Silvestrini, S.K. Vempati, and O. Vives. *Nucl. Phys. B* 783 (2007), pp. 112–142. DOI: 10.1016/j.nuclphysb.2007.05.032. arXiv: hep-ph/0702144.

[201] Stefan Antusch, Stephen F. King, and Michal Malinsky. *JHEP* 06 (2008), p. 068. DOI: 10.1088/1126-6708/2008/06/068. arXiv: 0708.1282 [hep-ph].

[202] Carl H. Albright and Mu-Chun Chen. *Phys. Rev. D* 77 (2008), p. 113010. DOI: 10.1103/PhysRevD.77.113010. arXiv: 0802.4228 [hep-ph].

[203] A. Masiero, P. Paradisi, and R. Petronzio. *JHEP* 11 (2008), p. 042. DOI: 10.1088/1126-6708/2008/11/042. arXiv: 0807.4721 [hep-ph].

[204] Abdelhamid Albaid. *Int. J. Mod. Phys. A* 27 (2012), p. 1250005. DOI: 10.1142/S0217751X12500054. arXiv: 1106.4070 [hep-ph].

[205] Takeo Moroi, Minoru Nagai, and Tsutomu T. Yanagida. *Phys. Lett. B* 728 (2014), pp. 342–346. DOI: 10.1016/j.physletb.2013.11.058. arXiv: 1305.7357 [hep-ph].

[206] Sylvain Fichet, Bjoern Herrmann, and Yannick Stoll. *Phys. Lett. B* 742 (2015), pp. 69–73. DOI: 10.1016/j.physletb.2015.01.013. arXiv: 1403.3397 [hep-ph].

[207] Sylvain Fichet, Björn Herrmann, and Yannick Stoll. *JHEP* 05 (2015), p. 091. DOI: 10.1007/JHEP05(2015)091. arXiv: 1501.05307 [hep-ph].

[208] Alexander S. Belyaev, Steve F. King, and Patrick B. Schaefers. *Phys. Rev. D* 97.11 (2018), p. 115002. DOI: 10.1103/PhysRevD.97.115002. arXiv: 1801.00514 [hep-ph].

[209] Stefan Antusch, Stephen F. King, and Martin Spinrath. *Phys. Rev. D* 87.9 (2013), p. 096018. DOI: 10.1103/PhysRevD.87.096018. arXiv: 1301.6764 [hep-ph].

[210] Maria Dimou, Stephen F. King, and Christoph Luhn. *JHEP* 02 (2016), p. 118. DOI: 10.1007/JHEP02(2016)118. arXiv: 1511.07886 [hep-ph].

[211] Maria Dimou, Stephen F. King, and Christoph Luhn. *Phys. Rev. D* 93.7 (2016), p. 075026. DOI: 10.1103/PhysRevD.93.075026. arXiv: 1512.09063 [hep-ph].

[212] Benjamin D. Callen and Raymond R. Volkas. *Phys. Rev. D* 86 (2012), p. 056007. DOI: 10.1103/PhysRevD.86.056007. arXiv: 1205.3617 [hep-ph].

[213] Iain K. Cooper, Stephen F. King, and Christoph Luhn. *JHEP* 06 (2012), p. 130. DOI: 10.1007/JHEP06(2012)130. arXiv: 1203.1324 [hep-ph].

[214] Iain K. Cooper, Stephen F. King, and Christoph Luhn. *Phys. Lett. B* 690 (2010), pp. 396–402. DOI: 10.1016/j.physletb.2010.05.066. arXiv: 1004.3243 [hep-ph].

[215] C. Patrignani et al. *Chin. Phys. C* 40.10 (2016), p. 100001. DOI: 10.1088/1674-1137/40/10/100001.

[216] Georges Aad et al. *JHEP* 05 (2014), p. 071. DOI: 10.1007/JHEP05(2014)071. arXiv: 1403.5294 [hep-ex].

[217] Paolo Gondolo and Graciela Gelmini. *Nucl. Phys. B* 360 (1991), pp. 145–179. DOI: 10.1016/0550-3213(91)90438-4.

[218] M. Tanabashi et al. *Phys. Rev. D* 98.3 (2018), p. 030001. DOI: 10.1103/PhysRevD.98.030001.

[219] Werner Porod. *Comput. Phys. Commun.* 153 (2003), pp. 275–315. DOI: 10.1016/S0010-4655(03)00222-4. arXiv: hep-ph/0301101.

[220] W. Porod and F. Staub. *Comput. Phys. Commun.* 183 (2012), pp. 2458–2469. DOI: 10.1016/j.cpc.2012.05.021. arXiv: 1104.1573 [hep-ph].

[221] Y. Amhis et al. *Eur. Phys. J. C* 77.12 (2017), p. 895. DOI: 10.1140/epjc/s10052-017-5058-4. arXiv: 1612.07233 [hep-ex].

[222] Luca Di Luzio, Matthew Kirk, and Alexander Lenz. *Phys. Rev. D* 97.9 (2018), p. 095035. DOI: 10.1103/PhysRevD.97.095035. arXiv: 1712.06572 [hep-ph].

[223] Joachim Brod and Martin Gorbahn. *Phys. Rev. Lett.* 108 (2012), p. 121801. DOI: 10.1103/PhysRevLett.108.121801. arXiv: 1108.2036 [hep-ph].

[224] G. Belanger, F. Boudjema, A. Pukhov, and A. Semenov. *Comput. Phys. Commun.* 149 (2002), pp. 103–120. DOI: 10.1016/S0010-4655(02)00596-9. arXiv: hep-ph/0112278.

[225] G. Belanger, F. Boudjema, A. Pukhov, and A. Semenov. *Comput. Phys. Commun.* 174 (2006), pp. 577–604. DOI: 10.1016/j.cpc.2005.12.005. arXiv: hep-ph/0405253.

[226] D. Barducci, G. Belanger, J. Bernon, F. Boudjema, J. Da Silva, S. Kraml, U. Laa, and A. Pukhov. *Comput. Phys. Commun.* 222 (2018), pp. 327–338. DOI: 10.1016/j.cpc.2017.08.028. arXiv: 1606.03834 [hep-ph].

[227] Florian Staub. *Comput. Phys. Commun.* 181 (2010), pp. 1077–1086. DOI: 10.1016/j.cpc.2010.01.011. arXiv: 0909.2863 [hep-ph].

[228] Florian Staub. *Comput. Phys. Commun.* 182 (2011), pp. 808–833. DOI: 10.1016/j.cpc.2010.11.030. arXiv: 1002.0840 [hep-ph].

[229] Florian Staub. *Comput. Phys. Commun.* 185 (2014), pp. 1773–1790. DOI: 10.1016/j.cpc.2014.02.018. arXiv: 1309.7223 [hep-ph].

[230] Werner Porod, Florian Staub, and Avelino Vicente. *Eur. Phys. J. C* 74.8 (2014), p. 2992. DOI: 10.1140/epjc/s10052-014-2992-2. arXiv: 1405.1434 [hep-ph].

[231] B.C. Allanach et al. *Comput. Phys. Commun.* 180 (2009), pp. 8–25. DOI: 10.1016/j.cpc.2008.08.004. arXiv: 0801.0045 [hep-ph].

[232] Sebastien Descotes-Genon, Joaquim Matias, and Javier Virto. *Phys. Rev. D* 88 (2013), p. 074002. DOI: 10.1103/PhysRevD.88.074002. arXiv: 1307.5683 [hep-ph].

[233] Wolfgang Altmannshofer and David M. Straub. *Eur. Phys. J. C* 73 (2013), p. 2646. DOI: 10.1140/epjc/s10052-013-2646-9. arXiv: 1308.1501 [hep-ph].

[234] Diptimoy Ghosh, Marco Nardecchia, and S.A. Renner. *JHEP* 12 (2014), p. 131. DOI: 10.1007/JHEP12(2014)131. arXiv: 1408.4097 [hep-ph].

[235] Roel Aaij et al. *Phys. Rev. Lett.* 122.19 (2019), p. 191801. DOI: 10.1103/PhysRevLett.122.191801. arXiv: 1903.09252 [hep-ex].

[236] *"Search for new physics with $b \to s\ell^+\ell^-$ decays at LHCb"*. CERN LHC seminar. 2017. URL: https://cds.cern.ch/record/2260258.

[237] Gudrun Hiller and Ivan Nisandzic. *Phys. Rev. D* 96.3 (2017), p. 035003. DOI: 10.1103/PhysRevD.96.035003. arXiv: 1704.05444 [hep-ph].

[238] Marco Ciuchini, Antonio M. Coutinho, Marco Fedele, Enrico Franco, Ayan Paul, Luca Silvestrini, and Mauro Valli. *Eur. Phys. J. C* 77.10 (2017), p. 688. DOI: 10.1140/epjc/s10052-017-5270-2. arXiv: 1704.05447 [hep-ph].

[239] Li-Sheng Geng, Benjamín Grinstein, Sebastian Jäger, Jorge Martin Camalich, Xiu-Lei Ren, and Rui-Xiang Shi. *Phys. Rev. D* 96.9 (2017), p. 093006. DOI: 10.1103/PhysRevD.96.093006. arXiv: 1704.05446 [hep-ph].

[240] Bernat Capdevila, Andreas Crivellin, Sébastien Descotes-Genon, Joaquim Matias, and Javier Virto. *JHEP* 01 (2018), p. 093. DOI: 10.1007/JHEP01(2018)093. arXiv: 1704.05340 [hep-ph].

[241] Diptimoy Ghosh. *Eur. Phys. J. C* 77.10 (2017), p. 694. DOI: 10.1140/epjc/s10052-017-5282-y. arXiv: 1704.06240 [hep-ph].

[242] Marco Ciuchini, António M. Coutinho, Marco Fedele, Enrico Franco, Ayan Paul, Luca Silvestrini, and Mauro Valli. *Eur. Phys. J. C* 79.8 (2019), p. 719. DOI: 10.1140/epjc/s10052-019-7210-9. arXiv: 1903.09632 [hep-ph].

[243] Debjyoti Bardhan, Pritibhajan Byakti, and Diptimoy Ghosh. *Phys. Lett. B* 773 (2017), pp. 505–512. DOI: 10.1016/j.physletb.2017.08.062. arXiv: 1705.09305 [hep-ph].

[244] Sheldon L. Glashow, Diego Guadagnoli, and Kenneth Lane. *Phys. Rev. Lett.* 114 (2015), p. 091801. DOI: 10.1103/PhysRevLett.114.091801. arXiv: 1411.0565 [hep-ph].

[245] Guido D'Amico, Marco Nardecchia, Paolo Panci, Francesco Sannino, Alessandro Strumia, Riccardo Torre, and Alfredo Urbano. *JHEP* 09 (2017), p. 010. DOI: 10.1007/JHEP09(2017)010. arXiv: 1704.05438 [hep-ph].

[246] Jason Aebischer, Wolfgang Altmannshofer, Diego Guadagnoli, Méril Reboud, Peter Stangl, and David M. Straub. *Eur. Phys. J. C* 80.3 (2020), p. 252. DOI: 10.1140/epjc/s10052-020-7817-x. arXiv: 1903.10434 [hep-ph].

[247] Sébastien Descotes-Genon, Lars Hofer, Joaquim Matias, and Javier Virto. *JHEP* 06 (2016), p. 092. DOI: 10.1007/JHEP06(2016)092. arXiv: 1510.04239 [hep-ph].

[248] Andreas Crivellin, Lars Hofer, Joaquim Matias, Ulrich Nierste, Stefan Pokorski, and Janusz Rosiek. *Phys. Rev. D* 92.5 (2015), p. 054013. DOI: 10.1103/PhysRevD.92.054013. arXiv: 1504.07928 [hep-ph].

[249] Avelino Vicente. *Adv. High Energy Phys.* 2018 (2018), p. 3905848. DOI: 10.1155/2018/3905848. arXiv: 1803.04703 [hep-ph].

[250] Andreas Crivellin, Giancarlo D'Ambrosio, and Julian Heeck. *Phys. Rev. D* 91.7 (2015), p. 075006. DOI: 10.1103/PhysRevD.91.075006. arXiv: 1503.03477 [hep-ph].

[251] Cesar Bonilla, Tanmoy Modak, Rahul Srivastava, and Jose W. F. Valle. *Phys. Rev. D* 98.9 (2018), p. 095002. DOI: 10.1103/PhysRevD.98.095002. arXiv: 1705.00915 [hep-ph].

[252] Nima Assad, Bartosz Fornal, and Benjamin Grinstein. *Phys. Lett. B* 777 (2018), pp. 324–331. DOI: 10.1016/j.physletb.2017.12.042. arXiv: 1708.06350 [hep-ph].

[253] Stephen F. King. *JHEP* 08 (2017), p. 019. DOI: 10.1007/JHEP08(2017)019. arXiv: 1706.06100 [hep-ph].

[254] Miguel Crispim Romao, Stephen F. King, and George K. Leontaris. *Phys. Lett. B* 782 (2018), pp. 353–361. DOI: 10.1016/j.physletb.2018.05.057. arXiv: 1710.02349 [hep-ph].

[255] Stefan Antusch, Christian Hohl, Steve F. King, and Vasja Susic. *Nucl. Phys. B* 934 (2018), pp. 578–605. DOI: 10.1016/j.nuclphysb.2018.07.022. arXiv: 1712.05366 [hep-ph].

[256] P. Ko, Takaaki Nomura, and Hiroshi Okada. *Phys. Lett. B* 772 (2017), pp. 547–552. DOI: 10.1016/j.physletb.2017.07.021. arXiv: 1701.05788 [hep-ph].

[257] Stephen F. King. *JHEP* 09 (2018), p. 069. DOI: 10.1007/JHEP09(2018)069. arXiv: 1806.06780 [hep-ph].

[258] Basabendu Barman, Debasish Borah, Lopamudra Mukherjee, and Soumitra Nandi. *Phys. Rev. D* 100.11 (2019), p. 115010. DOI: 10.1103/PhysRevD.100.115010. arXiv: 1808.06639 [hep-ph].

[259] A.E. Cárcamo Hernández and Stephen F. King. *Phys. Rev. D* 99.9 (2019), p. 095003. DOI: 10.1103/PhysRevD.99.095003. arXiv: 1803.07367 [hep-ph].

[260] Ivo de Medeiros Varzielas and Stephen F. King. *JHEP* 11 (2018), p. 100. DOI: 10.1007/JHEP11(2018)100. arXiv: 1807.06023 [hep-ph].

[261] Paulina Rocha-Moran and Avelino Vicente. *Phys. Rev. D* 99.3 (2019), p. 035016. DOI: 10.1103/PhysRevD.99.035016. arXiv: 1810.02135 [hep-ph].

[262] Quan-Yi Hu, Xin-Qiang Li, and Ya-Dong Yang. *Eur. Phys. J. C* 79.3 (2019), p. 264. DOI: 10.1140/epjc/s10052-019-6766-8. arXiv: 1810.04939 [hep-ph].

[263] Marcela Carena, Eugenio Megías, Mariano Quíros, and Carlos Wagner. *JHEP* 12 (2018), p. 043. DOI: 10.1007/JHEP12(2018)043. arXiv: 1809.01107 [hep-ph].

[264] K.S. Babu, Bhaskar Dutta, and Rabindra N. Mohapatra. *JHEP* 01 (2019), p. 168. DOI: 10.1007/JHEP01(2019)168. arXiv: 1811.04496 [hep-ph].

[265] B.C. Allanach and Joe Davighi. *JHEP* 12 (2018), p. 075. DOI: 10.1007/JHEP12(2018)075. arXiv: 1809.01158 [hep-ph].

[266] Bartosz Fornal, Sri Aditya Gadam, and Benjamin Grinstein. *Phys. Rev. D* 99.5 (2019), p. 055025. DOI: 10.1103/PhysRevD.99.055025. arXiv: 1812.01603 [hep-ph].

[267] Ufuk Aydemir, Djordje Minic, Chen Sun, and Tatsu Takeuchi. *JHEP* 09 (2018), p. 117. DOI: 10.1007/JHEP09(2018)117. arXiv: 1804.05844 [hep-ph].

[268] A.E. Cárcamo Hernández, Sergey Kovalenko, Roman Pasechnik, and Ivan Schmidt. *JHEP* 06 (2019), p. 056. DOI: 10.1007/JHEP06(2019)056. arXiv: 1901.02764 [hep-ph].

[269] A.E. Cárcamo Hernández, Sergey Kovalenko, Roman Pasechnik, and Ivan Schmidt. *Eur. Phys. J. C* 79.7 (2019), p. 610. DOI: 10.1140/epjc/s10052-019-7101-0. arXiv: 1901.09552 [hep-ph].

[270] Ufuk Aydemir, Tanumoy Mandal, and Subhadip Mitra. *Phys. Rev. D* 101.1 (2020), p. 015011. DOI: 10.1103/PhysRevD.101.015011. arXiv: 1902.08108 [hep-ph].

[271] Andreas Crivellin, Martin Hoferichter, and Philipp Schmidt-Wellenburg. *Phys. Rev. D* 98.11 (2018), p. 113002. DOI: 10.1103/PhysRevD.98.113002. arXiv: 1807.11484 [hep-ph].

[272] G.F. Giudice, P. Paradisi, and M. Passera. *JHEP* 11 (2012), p. 113. DOI: 10.1007/JHEP11(2012)113. arXiv: 1208.6583 [hep-ph].

[273] Hooman Davoudiasl and William J. Marciano. *Phys. Rev. D* 98.7 (2018), p. 075011. DOI: 10.1103/PhysRevD.98.075011. arXiv: 1806.10252 [hep-ph].

[274] Jia Liu, Carlos E.M. Wagner, and Xiao-Ping Wang. *JHEP* 03 (2019), p. 008. DOI: 10.1007/JHEP03(2019)008. arXiv: 1810.11028 [hep-ph].

[275] Martin Bauer, Matthias Neubert, Sophie Renner, Marvin Schnubel, and Andrea Thamm (July 2019). arXiv: 1908.00008 [hep-ph].

[276] Xiao-Fang Han, Tianjun Li, Lei Wang, and Yang Zhang. *Phys. Rev. D* 99.9 (2019), p. 095034. DOI: 10.1103/PhysRevD.99.095034. arXiv: 1812.02449 [hep-ph].

[277] Marcin Badziak and Kazuki Sakurai. *JHEP* 10 (2019), p. 024. DOI: 10.1007/JHEP10(2019)024. arXiv: 1908.03607 [hep-ph].

[278] Motoi Endo and Wen Yin. *JHEP* 08 (2019), p. 122. DOI: 10.1007/JHEP08(2019)122. arXiv: 1906.08768 [hep-ph].

[279] Thomas Appelquist, Maurizio Piai, and Robert Shrock. *Phys. Lett. B* 593 (2004), pp. 175–180. DOI: 10.1016/j.physletb.2004.04.062. arXiv: hep-ph/0401114.

[280] Ben Allanach, Farinaldo S. Queiroz, Alessandro Strumia, and Sichun Sun. *Phys. Rev. D* 93.5 (2016). [Erratum: Phys.Rev.D 95, 119902 (2017)], p. 055045. DOI: 10.1103/PhysRevD.93.055045. arXiv: 1511.07447 [hep-ph].

[281] Junichiro Kawamura, Stuart Raby, and Andreas Trautner. *Phys. Rev. D* 100.5 (2019), p. 055030. DOI: 10.1103/PhysRevD.100.055030. arXiv: 1906.11297 [hep-ph].

[282] Manfred Lindner, Moritz Platscher, and Farinaldo S. Queiroz. *Phys. Rept.* 731 (2018), pp. 1–82. DOI: 10.1016/j.physrep.2017.12.001. arXiv: 1610.06587 [hep-ph].

[283] Lorenzo Calibbi and Giovanni Signorelli. *Riv. Nuovo Cim.* 41.2 (2018), pp. 71–174. DOI: 10.1393/ncr/i2018-10144-0. arXiv: 1709.00294 [hep-ph].

[284] L. Lavoura. *Eur. Phys. J. C* 29 (2003), pp. 191–195. DOI: 10.1140/epjc/s2003-01212-7. arXiv: hep-ph/0302221.

[285] Cheng-Wei Chiang, Yi-Fan Lin, and Jusak Tandean. *JHEP* 11 (2011), p. 083. DOI: 10.1007/JHEP11(2011)083. arXiv: 1108.3969 [hep-ph].

[286] D. Geiregat et al. *Phys. Lett. B* 245 (1990), pp. 271–275. DOI: 10.1016/0370-2693(90)90146-W.

[287] S.R. Mishra et al. *Phys. Rev. Lett.* 66 (1991), pp. 3117–3120. DOI: 10.1103/PhysRevLett.66.3117.

[288] Wolfgang Altmannshofer, Stefania Gori, Maxim Pospelov, and Itay Yavin. *Phys. Rev. Lett.* 113 (2014), p. 091801. DOI: 10.1103/PhysRevLett.113.091801. arXiv: 1406.2332 [hep-ph].

[289] Adam Falkowski, Martín González-Alonso, and Kin Mimouni. *JHEP* 08 (2017), p. 123. DOI: 10.1007/JHEP08(2017)123. arXiv: 1706.03783 [hep-ph].

[290] J. Alcaraz et al. (Dec. 2006). arXiv: hep-ex/0612034.

[291] Paul Langacker. *Rev. Mod. Phys.* 81 (2009), pp. 1199–1228. DOI: 10.1103/RevModPhys.81.1199. arXiv: 0801.1345 [hep-ph].

[292] Marcela Carena, Alejandro Daleo, Bogdan A. Dobrescu, and Timothy M.P. Tait. *Phys. Rev. D* 70 (2004), p. 093009. DOI: 10.1103/PhysRevD.70.093009. arXiv: hep-ph/0408098.

[293] G. Abbiendi et al. *Eur. Phys. J. C* 6 (1999), pp. 1–18. DOI: 10.1007/s100529801027. arXiv: hep-ex/9808023.

[294] S. Schael et al. *Phys. Rept.* 532 (2013), pp. 119–244. DOI: 10.1016/j.physrep.2013.07.004. arXiv: 1302.3415 [hep-ex].

[295] Peter Ballett, Stephen F. King, Silvia Pascoli, Nick W. Prouse, and TseChun Wang. *Phys. Rev. D* 96.3 (2017), p. 033003. DOI: 10.1103/PhysRevD.96.033003. arXiv: 1612.07275 [hep-ph].

[296] J.L. Holzbauer. *J. Phys. Conf. Ser.* 770.1 (2016). Ed. by Marco Bozzo, David S. Armstrong, Patrizia Cenci, Kevin Giovanetti, Cristina Lazzeroni, Janis McKenna, Philip Rubin, Elton S. Smith, Nick Solomey, and Igor Strakowsky, p. 012038. DOI: 10.1088/1742-6596/770/1/012038. arXiv: 1610.10069 [physics.ins-det].

[297] Palash B. Pal. *Am. J. Phys.* 79 (2011), pp. 485–498. DOI: 10.1119/1.3549729. arXiv: 1006.1718 [hep-ph].